eman ta zabal zazu

Universidad del País Vasco

Euskal Herriko Unibertsitatea

DOCTORAL THESIS

Pharmacological characterization of prostaglandin E_2 EP receptors in the rodent brain: functional studies in locus coeruleus neurons and the preBötzinger complex

Thesis for doctoral degree by Amaia Nazabal Gaztañaga

Leioa, 2019

This Doctoral Thesis has been carried out thanks to a predoctoral fellowship (Formación de Personal Investigador, 2015-2018) from the Basque Government.

AGRADECIMIENTOS / ACKNOWLEDGEMENTS

En primer lugar, me gustaría mostrar mi agradecimiento a mis directores de tesis Aitziber Mendiguren y Joseba Pineda por acogerme en el laboratorio y por guiarme por el metódico y laborioso camino de la ciencia. En definitiva, sin ellos no habría sido posible esta tesis.

También me gustaría agradecer esta tesis a mis compañeros de laboratorio Erik Aostri por enseñarme algo nuevo cada día y a Irati Rodilla por transmitirme entusiasmo y constancia. Txetxu Soga por enseñarme pacientemente la técnica y Patricia Pablos por ayudarme con mis dudas y amenizar la hora del café.

Thanks to Eric Herlenius for pushing forward a little bit the limits, forcing me into excellence. Also, thanks to all the group for allowing me to be part of it. In particular to Antoine Honoré for all the support with the analysis and the really fun times. You made Sweden home. Thanks to David Forsberg, for being always willing to help, and bringing joy and veganism into the lab. Finally, thanks to the rest of the everyday group: Wiktor Phillips, Naify Ramadan, Jan Philipp Reising, and Yuri Shvarev and to the temporary ones.

Thanks to all on the formerly 9th floor, without you; Elena di Martino, Monique Havermans or Martin Becker to name a few, it wouldn't have been the same. In particular, thanks to Cecilia Dominguez for being the best social glue and fika organizer. I would also like to remember Lea Ballenberger for being a ray of sunshine in the cold Stockholm.

No me gustaría olvidarme de mis compañeras de carrera Oihana, Sara y María. Muchas gracias por los grandes momentos dentro y fuera del aula. Por la motivación y los buenos momentos a lo largo de todos estos años de formación que han precedido al doctorado y se han continuado con él.

Por supuesto, me gustaría agradecer a todas aquellas personas que me han acompañado e inspirado a lo largo de este viaje: Nora, Lara, Jon y Gema. Gracias por estar a mi lado y animarme para seguir adelante. Gracias por el sosiego emocional interrumpido a carcajadas.

Por último, muchas gracias a mi familia. A mis padres, Begoña y José Ángel por el amor y apoyo incondicional. Gracias por la comprensión y por haberme constituido como persona. Gracias Laxmi, por todo lo que me has enseñado, Lucas por ser como un hermano y al pequeño Egan por ser el futuro de la familia. Gracias también al resto de la familia por el cariño recibido.

*"*Hope is not the conviction that something will turn out well, but the certainty that something makes sense, regardless of how it turns out*"*

Vaclav Havel, 1990

"A lab of one's own"

Adapted from Virginia Woolf

A mi familia

ABSTRACT

BACKGROUND AND PURPOSE

Prostaglandin E_2 (PGE_2) is an inflammatory mediator synthesized by the brain constitutive cyclooxygenase (COX) enzyme, whose activity is blocked by the nonsteroidal anti-inflammatory drugs (NSAIDs). PGE_2 binds to G protein-coupled EP1-4 receptors (EP1 to G_q, EP2 and EP4 to G_s, and EP3 to $G_{i/o}$). Activation of EP receptors by PGE_2 has been shown to modulate the synaptic transmission and neuronal activity in various brain regions, such as in the hippocampus, the hypothalamus, and the periaqueductal grey. One of the areas that expresses EP2, EP3, and EP4 receptors is the LC, the main noradrenergic nucleus in the brain, which is involved in the regulation of the sleep-wake cycle, arousal, cognition, pain, and reward behavior. To date, the role of EP receptors in regulating the neuronal activity of LC noradrenergic cells has not been elucidated. Therefore, our main aim was to pharmacologically characterize the EP2, EP3, and EP4 receptors in the rat LC by recording the firing activity of LC cells by electrophysiological techniques *in vitro*. We also studied the interaction between the prostanoid and the opioid systems by live time-lapse calcium imaging in the mice preBötzinger complex (preBötC), the central inspiratory pattern generator. It has been shown that preBötC inspiratory neurons express μ-opioid receptors (MOR) and respond to PGE_2. Thus, administration of PGE_2 increases the frequency of sighs and induces gasps under hypoxic circumstances, while opioid receptor agonists produce respiratory depression through their action in the preBötC. However, the possible interaction between both systems to induce major respiratory disturbances remains to be studied.

EXPERIMENTAL APPROACH

In the first, second, and third studies, we characterized the effects of EP2, EP3, and EP4 receptor agonists by single-unit extracellular electrophysiological techniques in rat brain slices of the LC. For this purpose, we perfused agonists of EP receptors in the absence and presence of selective EP receptor antagonists or different modulators of EP receptor signaling mechanisms. In the fourth study, we tested the effect of PGE_2 and the MOR agonist DAMGO and their combination by live time-lapse calcium imaging on preBötC organotypic slices from both wild-type mice (WT) and mice lacking the EP3 receptor ($Ptger3^{-/-}$).

KEY RESULTS

STUDY I

The EP3 receptor agonist sulprostone (0.15 nM – 1.28 μM), the endogenous PGE_2 (0.31 nM – 10.2 μM), and the PGE_1 analogue misoprostol (0.31 nM – 2.56 μM) inhibited the firing rate of LC neurons in a concentration-dependent manner (EC_{50}=15 nM, 51 nM, and 110 nM, respectively). The EP3 receptor antagonist L-798,106 (10 μM), but not the EP2 (PF-04418948, 10 μM) or EP4 (L-161,982, 10 μM) receptor antagonists, caused a more than 8-fold rightward shift in the concentration-effect curves for the EP3 receptor agonists. The sulprostone-induced effect was attenuated by the $G_{i/o}$-protein blocker pertussis toxin (PTX, 500 ng ml^{-1}) and the inhibitors of inwardly rectifying potassium channels (GIRK) $BaCl_2$ (300 μM) and SCH-23390 (15 μM).

STUDY II

The EP2 receptor agonist butaprost (0.01-10 μM) and the prostacyclin (PGI_2) analog treprostinil (0.03-10 μM) increased the firing rate of LC neurons in a concentration-dependent manner (EC_{50}=0.45 μM and 0.54 μM; Emax=74.3% and 81.3%; respectively). The selective EP2 receptor antagonist PF-04418948 (10 nM), but not the EP3 (L-798,106, 10 nM) or EP4 (L-161,982, 10 nM) receptor antagonists, hindered the excitatory effect of butaprost and treprostinil. Furthermore, extracellular sodium replacement and a $G_{\beta\gamma}$ blocker (gallein, 20 μM) prevented the butaprost-induced increase in the firing activity of LC cells. However, the excitatory effect caused by butaprost was not reduced by a PKA activator (8-Br-cAMP, 1 mM) or a PKA inhibitor (H-89, 10 μM). This effect was not modified by synaptic blockade or by inhibitors of the $G_{\alpha s}$ subunits (NF449, 10 μM), hyperpolarization-activated cyclic nucleotide-gated (HCN) channels (ZD7288, 30 μM), transient receptor potential (TRP) channels (2-APB, 30 μM), and Kir6.2 channels (glibenclamide 3 μM).

STUDY III

The EP4 receptor agonists rivenprost (0.01 nM – 1 μM) and TCS 2510 (0.20 nM – 2 μM) increased the firing rate of LC cells in a concentration-dependent manner (EC_{50}=1.43 nM and 18.0 nM; Emax=83.7% and 98.4%; respectively). The selective EP4 receptor antagonist L-161,982 (30 and 300 nM) hindered the excitatory effect caused by rivenprost and TCS 2510, whereas the EP2 (PF-04418948, 300 nM) or EP3 (L-798,106, 300 nM) receptor antagonists did not reduce it. Furthermore, extracellular sodium replacement and a $G_{\alpha s}$ blocker (NF449, 10 μM) prevented the rivenprost-induced stimulation of neuronal activity. However, the excitatory

effect caused by rivenprost was not attenuated by a PKA activator (8-Br-cAMP, 1 mM) or a PKA inhibitor (H-89, 10 μM), nor was it reduced by a phosphatidylinositol 3-kinase (PI3K) blocker (wortmannin, 100 nM), a PKC inhibitor (chelerythrine, 10 μM) or a $G_{\beta\gamma}$ signaling blocker (gallein, 20 μM). Furthermore, previous administration of the EP2 receptor agonist butaprost (1 μM) did not occlude the excitatory effect caused by rivenprost, suggesting that EP2 and EP4 receptors may not share the same signaling pathway to stimulate LC neurons.

STUDY IV

DAMGO (0.5 and 5 μM) or PGE_2 (10 and 100 nM) reduced the Ca^{2+} transient frequency of the whole cell population and respiratory neurons of the preBötC in WT. Notably, in $Ptger3^{-/-}$ mice, the inhibitory effect of PGE_2 on Ca^{2+} transient frequency was absent, and the effect caused by DAMGO (5 μM) was delayed on time comparing to WT mice. This result suggests an interaction between the prostanoid and the opioid systems. Moreover, application of DAMGO in the presence of PGE_2 did not further reduce the Ca^{2+} oscillatory activity, which suggests that they probably share a common signaling pathway. Indeed, the phosphodiesterase 4 blocker rolipram (5 μM) and the GIRK channel blocker SCH-23390 (15 μM) prevented both DAMGO- and PGE_2-induced reduction in Ca^{2+} oscillatory activity, suggesting a mutual dependency on the cAMP pathway and GIRK channels. Finally, both DAMGO and PGE_2 reduced the cellular connectivity and synchronicity and increased the segregation into local cell clusters. The effects of DAMGO on the network connectivity and topology were abolished by rolipram and SCH-23390, whereas the effect of PGE_2 was partially hindered by rolipram.

CONCLUSIONS AND IMPLICATIONS

Firing activity of LC neurons is regulated in an inhibitory manner by EP3 receptors, presumably by a $G_{i/o}$ protein and GIRK-mediated mechanism. In addition, activation of EP2 or EP4 receptors may excite LC noradrenergic neurons through a $G_{\beta\gamma}$ and $G_{\alpha s}$-dependent regulation of sodium currents. On the other hand, PGE_2 inhibits the preBötC cellular activity and interferes with the opioid-induced respiratory depression. Given the role of the LC and the preBötC in the regulation of nociception and its affective component, as well as in the induction of fever, anxious states, and the inspiratory pattern, the presence of the prostanoid system in these brain areas may constitute a suitable target for the treatment of neuropsychiatric or breathing disorders triggered or mediated by neuroinflammatory mediators.

LIST OF ABBREVIATIONS

5-HT	Serotonin
5-SP	Spinal trigeminal nucleus
AA	Arachidonic acid
aCSF	Artificial cerebrospinal fluid
ADHD	Attention-deficit/hyperactivity disorder
Amy	Amygdala
ANOVA	Analysis of variance
AP	Area postrema
BBB	Blood brain barrier
BF	Basal forebrain
BNST	Bed nucleus of the stria terminalis
cAMP	Cyclic adenosine monophosphate
Cb	Cerebellum
Cdh9	Cadherin 9
CeA	Central amygdala
ChAT	Choline acetyltransferase
CL	Central medial thalamus
CNS	Central nervous system
COX-1	Cyclooxygenase 1
COX-2	Cyclooxygenase 2
cPGES	Cytosolic PGE synthase
CREB	cAMP response-element binding
CSF	Cerebrospinal fluid
Ctx	Cortex

DAMGO	[D-Ala2, N-Me-Phe4, Gly5-ol]-enkephalin
DBH	Dopamine-β-hydroxylase
Dbx1	Developing brain homeobox 1 protein
DIV	Days i*n vitro*
DMH	Dorsomedial hypothalamus
DMSO	Dimethylsulphoxide
DRG	Dorsal root ganglion
FR	Firing rate
GABA	Gamma-aminobutyric acid
GIRK	$G_{i/o}$ protein-coupled inwardly rectifying potassium channels
GlyT2	Glycine transporter 2
GPCR	G-protein Coupled Receptor
HCN	Hyperpolarization-activated Cyclic Nucleotide-gated Channel
Hi	Hippocampus
HIV	Human immunodeficiency virus
Hy	Hypothalamus
IC	Inferior colliculus
i.c.v.	Intracerebroventricular
IL-1β	Interleukin 1β
IO	Inferior olivary complex
i.p.	intraperitoneal
IRN	Intermediate reticular nucleus
KF	Kölliker-Fuse nucleus
KOR	κ-opioid receptor
LC	Locus coeruleus

LH	Lateral hypothalamus
LPBr	Lateral parabrachial nucleus
LPGi	Nucleus lateral paragigantocellularis
LPO	Lateral preoptic area
LPS	Lipopolysaccharide
LRN or LRt	Lateral reticular nucleus
MDL	Medial dorsal thalamus
Me5	Mesencephalic trigeminal nucleus
MnPO	Median preoptic nucleus of the hypothalamus
MOR	μ-opioid receptor
mPGES-1	Microsomal Prostaglandin E Synthase 1
MRN	Midbrain reticular nucleus
NA	Noradrenaline
NAd	Nucleus ambiguus
Na_v	Voltage-gated sodium channels
NK1R	Neurokinin 1 Receptor
NSAID	Nonsteroidal anti-inflammatory drug
NTS	Nucleus of the solitary tract
OAT	Organic anion transporter
PaF	Parafascicular thalamus
PAG	Periaqueductal gray matter
PB	Parabrachial nucleus
pF	Parafacial nucleus
pFRG/RTN	Parafacial Respiratory Group/Retrotrapezoid Nucleus
PLA_2	Phospholipase A_2

PGD_2	Prostaglandin D_2
PGE_2	Prostaglandin E_2
PGES	PGE synthase
$PGF_{2\alpha}$	Prostaglandin $F_{2\alpha}$
PGH_2	Prostaglandin H_2
PGI_2	Prostacyclin
PGRN/GRN	Paragigantocellular/gigantocellular nucleus
PGT	Prostaglandin transporter
PI3K	Phosphatidylinositol 3-kinase
PiCo	Post inspiratory complex
PKA	Protein kinase A
PKC	Protein kinase C
Pn	Ventral pontine nucleus
POA	Preoptic area
preBötC	preBötzinger Complex
PRG	Pontine respiratory group
PrH	Nucleus prepositus hypoglossi
PRN	Pontine reticular nucleus
Ptger3	EP3 receptor gene
RO	Raphé obscurus
ROI	Region of Interest
RVLM	Rostral ventrolateral medulla
SC	Superior colliculus
SEM	Standard error of the mean
SIDS	Sudden infant death syndrome

SO	Superior olivary complex
SP	Substance P
SST	Somatostatin
SVN	Spinal vestibular nucleus
TH	Tyrosine hydroxylase
Th	Thalamus
TMR-SP	Tetramethylrhodamine-conjugated substance P
TNFα	Tumor necrosis factor α
TTX	Tetrodotoxin
TXA_2	Thromboxane A_2
V	Motor nucleus of the trigeminal nerve
V4	Fourth ventricle
VIIn	Facial nucleus
VIP	Vasoactive intestinal peptide
VRC	Ventral respiratory column
VRG	Ventral respiratory group
VTA	Ventral tegmental area
XII	Hypoglossal motor nucleus
ZI	Zona Incerta
$\Delta F/F_0$	Normalized average fluorescence intensity
γ	Small-world parameter
λ	Mean shortest path length
σ	Mean clustering coefficient

CONTENTS

1 INTRODUCTION

Prostaglandins are associated with the immune system, as they are released in response to harmful stimuli and constitute the main immune messenger across the blood-brain barrier (BBB)[1]. Furthermore, common painkillers exert an anti-inflammatory effect by blocking the synthesis of prostaglandins. However, several pieces of evidence broaden the role of prostaglandins as brain mediators under non-inflammatory conditions, considering they are found constitutively present in the brain[2] and integrate a part of the glial-neuronal signaling[3,4]. Additionally, prostaglandins modulate the neuronal activity[5], which raises the question of whether they are key mediators within the central nervous system (CNS).

1.1 PROSTANOIDS

Prostanoids, as a subclass of eicosanoids, are lipid compounds involved in many physiological and pathophysiological processes, including vasodilation, reproduction, and inflammation[6]. They are comprised by the prostaglandins, prostacyclins (PGI_2), and thromboxanes (TX; such as the TXA_2) (Figure 1.1). Prostaglandins were first isolated in 1935 from the prostate gland and seminal fluid by M.W. Goldblatt and U.S. von Euler[7]. The most widely synthesized prostaglandin in mammals is the prostaglandin E_2 (PGE_2)[8,9], although other types, such as the prostaglandin D_2 (PGD_2) or prostaglandin $F_{2\alpha}$ ($PGF_{2\alpha}$) also have important physiological roles.

1.1.1 Synthesis, transport, and metabolism

Prostanoids are synthesized and immediately released, without being stored[10]. Then, they work in an autocrine or paracrine manner[11], in part limited by their short half-life[12]. For these reasons, the content of PGE_2 is determined by its synthetic and degradative enzymatic activity[11].

PGE_2 is synthesized from membrane phospholipids, which are converted into arachidonic acid (AA) by the phospholipase A_2 (PLA_2) enzyme. Then, the AA can be transformed by the cyclooxygenase enzyme (COX) into an unstable precursor of prostanoids; the prostaglandin H_2 (PGH_2). Finally, PGH_2 is converted into PGE_2 and other prostaglandins by the PGE synthase (PGES)[13].

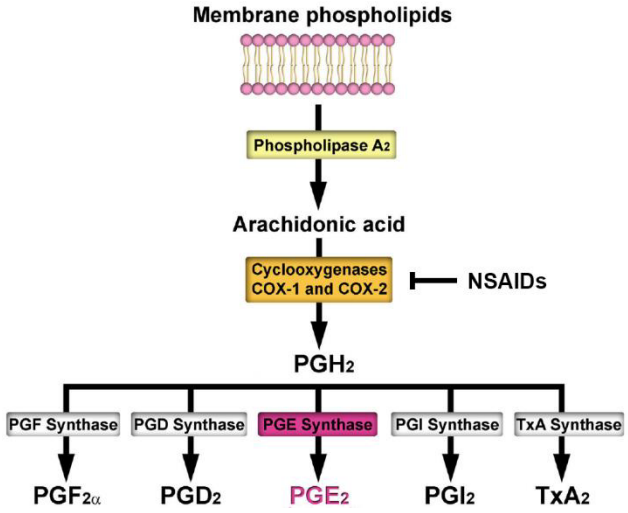

Figure 1.1. Illustrative drawing of PGE_2 synthesis from membrane phospholipids[14]. NSAIDs block the synthesis of prostanoids.

The rate-limiting enzyme for the synthesis of prostaglandins is the COX enzyme, which enzymatic activity is blocked by common painkillers or nonsteroidal anti-inflammatory drugs (NSAIDs), such as ibuprofen or naproxen (Figure 1.1). There are mainly two COX subtypes, COX-1 and COX-2, although a third subtype COX-3 has been described as a splice variant of the COX-1[15]. All the subtypes are constitutively present in the CNS[16,17], although the COX-2 is considered to be an inducible enzyme in the rest of the body. Specifically, COX-2 has been found active in the spinal cord[18–20], locus coeruleus (LC)[21], paraventricular hypothalamic nucleus[22], hippocampus, and cerebral cortex[10,23]. At the cellular level, COX-1 is mainly expressed in microglia and endothelial cells, while COX-2 is localized in postsynaptic dendrites and excitatory terminals[24]. PGE_2 is primarily synthesized by the COX-2, as shown by a reduction in brain PGE_2 concentration due to selective COX-2 blockers[25,26] or mice lacking COX-2[27]. In fact, mice lacking COX-1 show higher concentration of PGE_2 due to a compensatory upregulation of COX-2[28]. Therefore, these data indicate that COX-2 is involved in the synthesis of PGE_2 on basal conditions.

As abovementioned, other enzymes take part in the synthesis of PGE_2, including the PLA_2 and the PGES. The former is expressed predominantly in neurons of the medulla oblongata, pons and epiphysis, and glial cells of the choroid plexus[29]. It is localized in dendritic spines[30], and when released to the extracellular medium, it can promote the transcellular generation of PGE_2 by the neighboring cells[31]. On the other hand, the PGES isozymes are classified into cytosolic (cPGES) and microsomal PGES (mPGES-1 and mPGES-2). In basal conditions, brain constitutive mPGES is found in endothelial cells, astrocytes and choroid plexus[32]. However, upon immune stimulation, mPGES-1 and COX-2 coexpression is upregulated in the

vasculature[22,32,33], and as a consequence, the production of PGE_2 increases almost immediately[33–35]. Thus, inflammatory signals, including the cytokines interleukin IL-1β[36–38] and tumor necrosis factor α (TNFα)[39], are the principal inducers of the PGE_2 formation. Endogenous synthesis of PGE_2 can also be stimulated upon regular synaptic activity[10], as seen after administration of a 5-$HT_{2A/2C}$ receptor agonist in the LC[40] or a CB1 receptor agonist in the hippocampus[41].

Once synthesized in the cytoplasm, PGE_2 becomes anionic at physiologic pH, so it needs to be actively transported by the prostaglandin transporter (PGT)[42,43] and organic anion transporter (OAT)[44]. This active transport mechanism is also responsible for the clearance of PGE_2, which half-life is 3.4 min in the cerebrospinal fluid (CSF)[12] and 16.3 min in the cerebral cortex[45]. PGE_2 undergoes a final elimination by the cytoplasmic prostaglandin 15 dehydrogenase[46], whose activity in the choroid plexus is very low at adult stages[47]. Therefore, it seems likely that PGE_2 crosses the BBB in its intact form through the specific transporters and then undergoes peripheral metabolism[45], mostly in liver and lungs[47].

1.1.2 Prostanoid receptors: distribution and signaling transduction pathways

PGE_2 targets eicosanoid prostanoid (EP) receptors, which are members of the G protein-coupled receptor superfamily principally located on the cell membrane[48], although they have also been found in the cytoplasm and perinuclear regions[49–52]. Upon ligand binding, the G protein forms a complex with the receptor, which conformational change dissociates the G_α subunit from the $G_{\beta\gamma}$ dimer. Both G_α and $G_{\beta\gamma}$ can activate downstream proteins to amplify the signal transduction[53]. Four subtypes of G protein-coupled EP receptors have been cloned so far: EP1, EP2, EP3, and EP4.

In the brain, EP1 receptor mRNA expression is almost restricted to Purkinje cells of the cerebellum, whereas one of the lowest expression levels in the brain is found in the brainstem[54]. EP1 receptor couples to G_q protein, and its activation leads to an influx of extracellular calcium[55]. However, coupling to $G_{i/o}$ as a secondary pathway has also been proposed[56].

In situ hybridization signal for EP2 mRNA is predominantly found in the hippocampus, amygdala, and hypothalamus. By contrast, in the brainstem, the signal for EP2 mRNA is scarcely present and almost exclusively found in the LC, where it shows a moderate signal[57]. EP2 receptor couples to G_s protein and its stimulation results in an adenylate cyclase activation and increase of cAMP concentration (Figure 1.2)[58], which in turn activates the protein kinase A (PKA) and/or the hyperpolarization-activated, cyclic nucleotide-gated cationic (HCN)

channels[59]. Phylogenetically, the EP2 receptor shows higher homology with the PGI_2-IP and PGD_2-DP_1 receptors than with other EP receptors, such as the EP4 receptor (Figure 1.2)[60] with which it only shares the 31% of the amino acid identity[61].

EP3 mRNA expression is widely shown across the CNS[62]. In particular, an intense mRNA signal is found in the median preoptic nucleus of the hypothalamus, substantia nigra, LC, raphe nuclei, nucleus of the solitary tract (NTS), and ventrolateral medulla[62–64]. In these regions, such as the LC, inflammatory signals like IL-1β do not further upregulate the EP3 expression[63], since it is already prominent. The EP3 receptor has a neuronal preference[62,65,66], even though cultured glial cells also show some expression[67] possibly in response to excitotoxicity[68]. Apart from the cellular membrane, the EP3 receptor has been detected at the nuclear level in cerebral endothelial cells, which activation induces the transcription of the endothelial nitric oxide synthase[50,51]. Furthermore, several splicing isoforms (EP3α, EP3β, and EP3γ) have been described in mice, rats, and humans[69–74], with the EP3α isoform being the most prominently expressed[69,75]. EP3 receptors mainly couple to $G_{i/o}$ protein, but since the splicing isoforms differ in the C-terminal[69,72], coupling to the G protein and constitutive activity can vary. Indeed, EP3α and EP3γ have constitutive activity in receptor overexpressing cultured cells (Figure 1.2)[76,77] and EP3γ can also couple to G_s[78].

EP4 mRNA signal is most abundant in the supraoptic nucleus, followed by the posterior hypothalamus, the LC and the cerebellum, and to a lesser extent in the dorsal raphe and NTS[57]. These areas are activated in response to an acute inflammatory insult, as demonstrated by higher c-Fos immunoreactivity, which suggests that the EP4 receptor signaling is involved[57]. In contrast to the EP2 receptor, the EP4 has a long C-tail that allows its desensitization and recycling (Figure 1.2)[79,80]. EP4 receptor mainly couples to G_s protein, which activation by an agonist leads to cAMP formation[61]. However, an additional $G_{i/o}$ protein-dependent pathway has been described, with the subsequent involvement of the phosphatidylinositol 3-kinase (PI3K) (Figure 1.2) in cultured cells[81] and neurons[82].

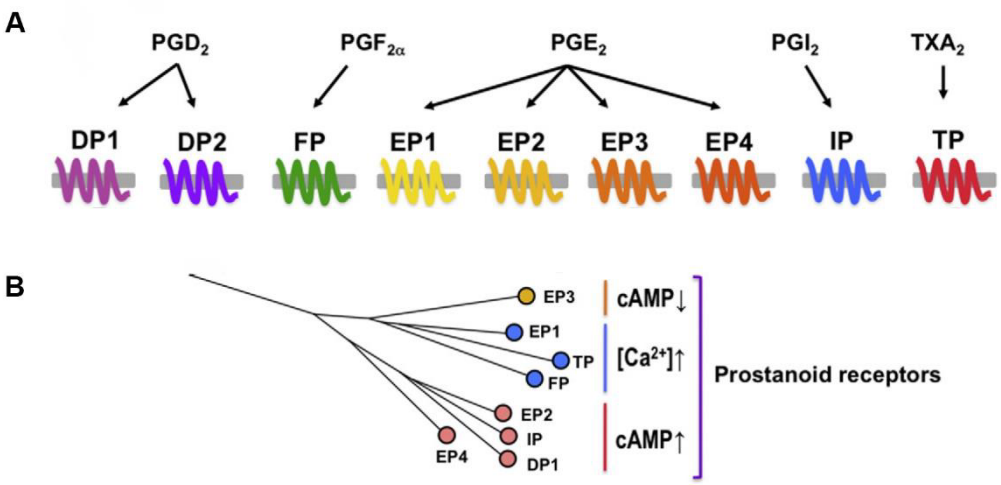

C

Subtype	Isoform	G protein	Signaling	Desensitization	Constitutive activity
EP2		G_s	cAMP ↑	No	
EP4		G_s (G_i)	cAMP ↑, PI3K	Yes	
EP1		G_q (G_i)	Ca^{2+} ↑	–	
EP3	EP3α	G_i, G_{12}	cAMP ↓, IP_3/Ca^{2+} ↑, Rho	Yes	++
	EP3β	G_i, G_{12}	cAMP ↓, IP_3/Ca^{2+} ↑, Rho	No	–
	EP3γ	G_i, G_s	cAMP ↓, cAMP ↑, IP_3/Ca^{2+} ↑	–	+

Figure 1.2. A) Different types of prostanoids and their specific receptors. B) Phylogenetic tree of prostanoid receptors[60]. C) PGE_2-EP receptors and their associated G-protein coupling, signaling transduction, desensitization ability, and constitutive activity[61].

1.1.3 Physiological and pathophysiological roles of the prostanoid system

The prostanoid system serves as a mediator in the inflammatory response to toxic compounds or traumatic injuries. In the first instance, the toxicity derives from either biological or xenobiotic substances; including drugs, microorganisms, and health conditions (e.g., ischemia or Alzheimer's disease). In the second instance, traumatic injuries promote the release of prostaglandins that might compromise the well-being by producing pain.

Some drugs and toxic compounds such as fluoxetin[83], amphetamines[84], alcohol[85] or carrageenan[11] may produce an inflammatory state, also in the brain. In response to either pro-inflammatory drugs or threatening pathogens, like those containing the component of the bacterial wall lipopolysaccharide (LPS), immune cells respond by releasing a cascade of signaling molecules. These include the cytokines IL-1β, IL-6 or TNF-α, and prostaglandins, which serve to attract other cells to the site of inflammation by vasodilation or to spread the signal throughout the body[6,86]. The cytokines, however, are too bulky and hydrophilic to cross the BBB, so they promote prostaglandin entrance[87] or prostaglandin synthesis in the brain vascular cells[22] and CSF[88]. Once PGE_2 is synthesized, its local release adjacent to hypothalamic neurons[89,90] can trigger inflammatory fever by binding to EP3 receptors (Figure 1.3)[5,91,92].

Therefore, prostaglandins are lipid inflammatory mediators that coordinate the immune-to-brain signaling[1].

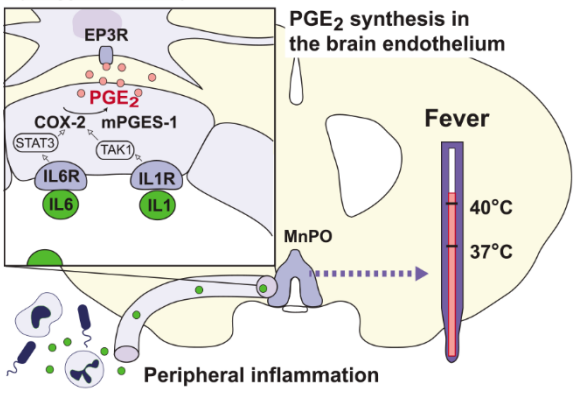

Figure 1.3. Representation of how peripheral inflammation can trigger fever by PGE_2 synthesis in endothelial cells of the brain that are close to the median preoptic nucleus of the hypothalamus (MnPO)[92].

Prostaglandins are closely related to blood vessels, not only because they can be synthesized in the endothelium in response to inflammatory signals, but also because PGE_2 has a role in neurovascular coupling. Neurons synthesize and release PGE_2 upon neuronal activation to adapt the supply of O_2 and glucose from blood vessels by EP2 and EP4-dependent vasodilation[23]. As a consequence, signaling via the EP2 receptor could have neuroprotective effects in cerebral ischemia[93]. Conversely, activation of EP3 receptors has deleterious effects in stroke and excitotoxicity[94] due to vasoconstriction, and it further increases the blood pressure by its action in the rostral ventrolateral medulla (RVLM)[95] and hypothalamic paraventricular nucleus[96]. Likewise, inhibitory EP3 receptors hinder the breathing pattern generation[97] and the response to hypoxic events[98], leading to sighs and gasps, particularly in neonates (Table 1.1)[99].

With regard to additional pathophysiological events in the brain, PGE_2 has been linked to psychiatric and neurologic disorders. Depression and inflammation are closely related as depressed patients have higher levels of plasmatic cytokines[6]. Furthermore, LPS-induced PGE_2 synthesis leads to a depressive-like behavior[100], and thereby, COX-2 inhibitors can be effective against depression[6]. In addition, PGE_2 may be involved in many neurologic disorders as showed by the increased levels of PGE_2 in CSF (Table 1.1). Patients of Alzheimer's disease have higher COX-2 mRNA levels in the brain[16] and higher PGE_2 levels in CSF compared to controls (Table 1.1)[101]. Furthermore, PGE_2 impairs the long-term hippocampal plasticity[102] and increases the expression of the β-amyloid precursor protein, which deposition is thought to contribute to Alzheimer's neuropathology[103].

Disease	PGE_2 levels in CSF
Alzheimer's disease	Increased by 5 fold in early Alzheimer's disease but declined with progressive cognitive impairment
Amyotrophic lateral sclerosis	Increased by 2 to 10 fold
Creutzfeldt-Jakob disease	Increased by 6 fold in patients with sporadic, familial forms or variant Creutzfeldt-Jakob disease
Ischemic stroke	Increased by 2 fold during initial 72 h
HIV-associated dementia	Increased by 40% in all HIV-seropositive patients and positively correlated with the degree of cognitive impairment
Hypoxic-ischemic encephalopathy	Increased PGE_2 metabolite in newborns with hypoxic-ischemic encephalopathy and positively correlated with severity and outcome

Table 1.1. PGE_2 levels in CSF from human patients with neurologic diseases compared to controls (Adapted from [101,104]).

Regarding nociception, PGE_2 contributes to hyperalgesia and allodynia (increased pain perception to both noxious and non-noxious stimuli, respectively). This sensitization is observed after both peripheral and central activation of EP receptors. Thus, intraplantar administration of PGE_2 results in hyperalgesia[105] at least due to EP4 receptor activation[106]. Under inflammatory conditions, the EP4 receptor is upregulated in the dorsal root ganglion (DRG)[107], ultimately promoting the excitatory nociceptive signal transmission[80,82]. By contrast, this EP4-dependent sensitization can be counteracted by DRG EP3 receptor activation[108]. Concerning central activation of EP receptors, spinal intrathecal administration of PGE_2 produces hyperalgesia[109,110] and allodynia[111] via an EP2 receptor-dependent blockade of glycinergic inhibitory transmission in the spinal cord[112]. Furthermore, selective activation of EP1, EP2, and EP3 receptors in the periaqueductal gray matter (PAG) decreases the nociceptive threshold *in vivo*[113–115], which should contribute to the pain sensitization.

1.2 BRAINSTEM

The brainstem, located in the caudal part of the brain, is the most primitive part of the CNS[116] and composed of the midbrain, the pons, and the medulla oblongata. It coordinates many primary and autonomic functions. For example, the LC regulates nociception, wakefulness, and arousal states, among others. It was not until the time of the French revolution that those vital functions of the brainstem became apparent, including breathing[117]. The respiratory rhythm, necessary to supply the organism with O_2, is generated by the preBötzinger complex (preBötC), but it is finely tuned by chemosensitive areas or emotional states[118]. Although both the LC and preBötC differ in morphology, they share numerous features. For instance, both express pain-related receptors (substance P-NK, PGE_2-EP3) and μ-opioid receptors (MOR)[97,119–121] and are involved in the regulation of breathing. Furthermore, both regions are anatomically connected. Thus, LC neurons receive excitatory afferents from the preBötC[122,123] and may provide excitatory input to the respiratory rhythm generator[124–126].

1.2.1 Locus coeruleus

1.2.1.1 Anatomy of the LC

The LC (A6) is the richest noradrenaline (NA)-containing nucleus in the CNS and the main site for NA synthesis[116]. It is a pontine nucleus first described by Reil in 1809, although its name was proposed by Wenzel and Wenzel in 1812[127], meaning "blue spot" in Latin as this was the nucleus in fresh tissue. The color is caused by the polymerization of NA into melanin[128]. The LC is located bilaterally on the lateral border of the 4th ventricle, surrounded by the mesencephalic nucleus of the trigeminal nerve (Me5) and the medial parabrachial nucleus (MPN) (Figure 1.4)[129]. Rostro-caudally, the LC measures around 480 μm and contains between 1600 and 2000 neurons in rodents[116,129].

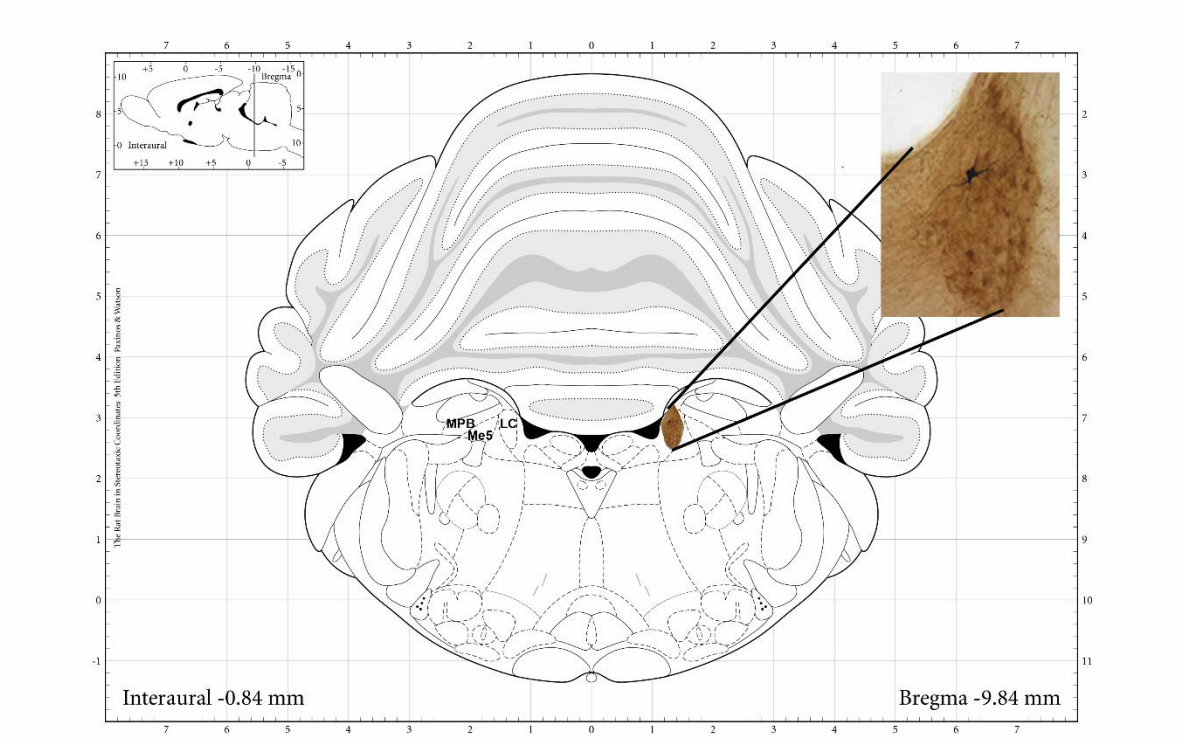

Figure 1.4. Coronal view of the rat brain showing the location of the LC near the 4th ventricle. A zoomed area shows a NA neuron filled with biocytin. The dark area (TH immunoreactivity) delineates the LC (Adapted from [130,131]).

The vast majority of the neurons are noradrenergic and contain tyrosine hydroxylase (TH), defining a compact and homogeneous nucleus[116]. Despite its uniformity, the cells within the nucleus display some degree of specialization. First, two types of NA neurons can be distinguished by staining with Nissl and for dopamine-β-hydroxylase (DBH): large multipolar and small fusiform cells, with the latter composing of about the 25% of the neurons, predominantly found in the dorsal part of the LC (Figure 1.5)[129,132]. Second, a subset of NA neurons co-releases either galanin or neuropeptide Y (Figure 1.5)[133], although vasopressin, corticotropin-releasing factor, enkephalin, and tachykinin peptides can also be found. Third, LC neurons projecting to the prefrontal cortex show higher firing rate (FR), and higher expression of voltage-gated sodium channels (Na_v) and ionotropic glutamate receptors (Figure 1.5) than those projecting to the motor cortex[134]. Finally, the differences are expressed in behavioral tests, as specific activation of LC neurons projecting to the prefrontal cortex results in anxiety, whereas activation of LC neurons projecting to the spinal cord leads to antinociception[135,136]. Apart from neurons, the LC contains glial cells, which can be electrotonically coupled to neurons[137] or modulate the neuronal discharge by gliotransmitters, such as L-lactate[138].

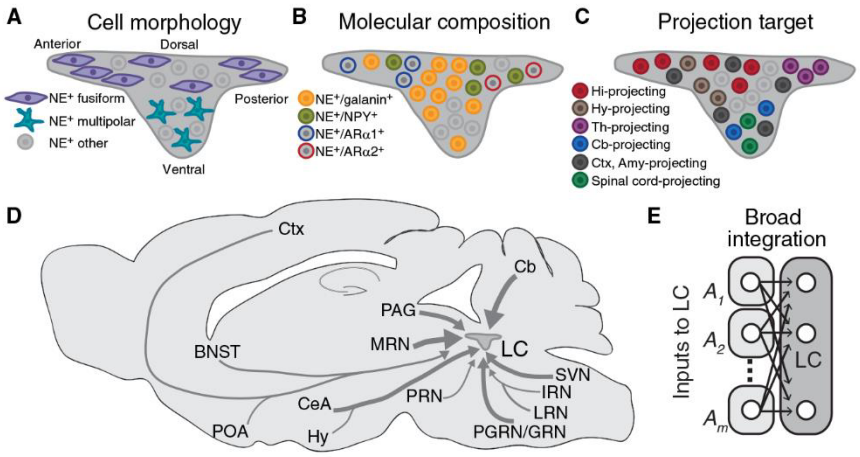

Figure 1.5. Schematic representation of LC neuronal specialization in terms of morphology (A), receptor expression (B), and projection target (C). (D) A simplified sagittal view of the anatomical inputs to the LC. (E) Integration of several inputs from different brain regions in the LC[133]. (See abbreviation list for further details).

a) Afferent projections to the LC

A single LC-NA neuron receives input from 9-15 different brain areas[133] (Figure 1.5). The main brain regions projecting to the LC are the nucleus prepositus hypoglossi (PrH) and the nucleus lateral paragigantocellularis (LPGi), both in the rostral medulla[139], which send GABAergic or glutamatergic inputs, respectively. The LC also receives inputs from areas involved in cardiorespiratory control and autonomic functions, including the rostral ventrolateral medulla, NTS, parafacial respiratory group/retrotrapezoid nucleus (pFRG/RTN) and preBötC[122]. In particular, the preBötC contains a neuronal subpopulation that excites NA neurons in the LC[123]. Other areas sending projections to the LC are the noradrenergic A5 nucleus, the Kölliker-Fuse nucleus, and the contralateral LC, together with the serotonergic dorsal raphe and the GABAergic pericoeruleus area in the pons[122,140]. Similarly, the PAG and the dopaminergic ventral tegmental area (VTA) in the midbrain also connect with the LC (Figure 1.5)[141].

b) Efferent projections from the LC

LC neurons are the major source of NA in the CNS[142], so they send projections to virtually all brain regions, except the basal ganglia[143] (Figure 1.6). Moreover, the neocortex and the hippocampus receive NA inputs exclusively from the LC[144]. As a consequence of this innervation to different brain areas, LC contributes to memory formation[145], modulates different behaviors, and coordinates responses to stress and arousal[146] (Figure 1.6). For example, upon NA release from the LC, α1 and β1 adrenoceptor activation in cholinergic

neurons of the cortex promotes an awakening state, and meanwhile, α2 adrenoceptor inhibits the activity of GABAergic neurons (Figure 1.6). Thus, they have an overall awakening output on the cortex[133].

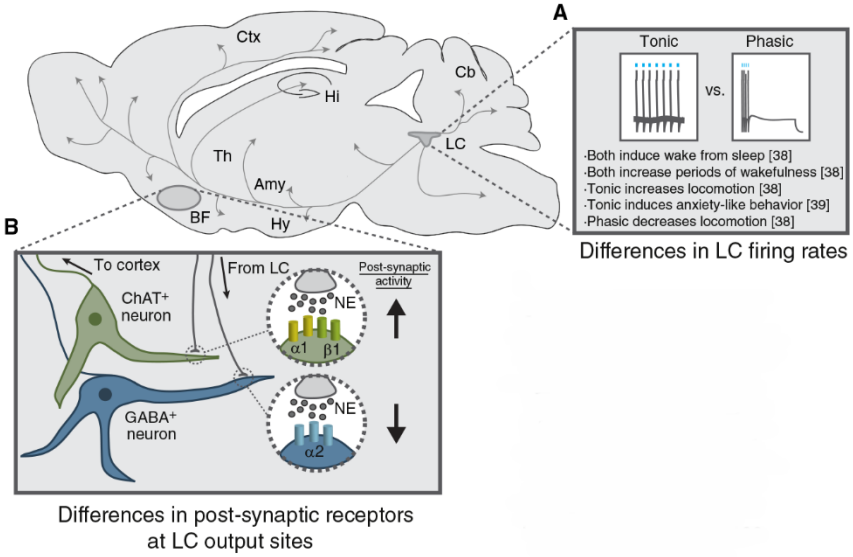

Figure 1.6. LC neurons send broad innervation to virtually the whole brain. (A) Tonic and phasic firing modes differentially modulate behavior. (B) Differences in receptor expression at targeted neurons determine the final action of NA[133].

1.2.1.2 Physiology of the LC: intrinsic properties and regulation of NA cells

LC neurons fire spontaneous action potentials ranging from 0.5 to 5 Hz *in vitro*[147], and up to 7 Hz *in vivo*[148]. Electrophysiologically, LC neurons are characterized by a resting membrane potential of -55 to -65 mV, a threshold for spike generation of -55 mV[147], a slow, broad action potential waveform (1-2 ms), and a quiescence period after generation of burst discharges[144].

A remarkable characteristic of LC neurons is the pacemaker activity, which implies that in the absence of any stimulus or synaptic activity, they discharge spontaneous action potentials[149] followed by interspike intervals. Such intervals consist of an afterhyperpolarization and a slow depolarization[147], involving voltage-dependent Na^+ and K^+ currents in neonatal mice[150,151] and an additional calcium-activated potassium channel in adult rats[152,153]. The pacemaker activity is also controlled by cAMP concentration and PKA activation[149]. Furthermore, LC neurons show pacemaker synchronous activity (i.e., electrotonic coupling), subject to developmental changes[154] and attributed to gap junctions in pericoerulear neuronal dendrites[155], and between neurons and glia[137]. This synchronous activity may contribute to harmonizing the activity of

the entire nucleus in response to sensory inputs[156]. However, when the electrotonic coupling is weak, the synchrony depends basically on the firing frequency[157].

LC neurons discharge in tonic and phasic modes. The former is regular, and the latter is composed of a brief burst followed by an inhibition[133] (Figure 1.6). Importantly, a change in the firing mode anticipates the behavioral response[144]. Thereby, stimulation of both tonic and phasic modes increase wakefulness, but only the tonic mode stimulates locomotion and anxiety-like behavior[133,146]. In contrast, the phasic mode is associated with focused attention[144]. LC discharge activity is linearly correlated with the release of NA[144]. For instance, cAMP-mediated increase in the neuronal activity[158] leads to an equivalent enhancement of the NA efflux[159] and cortical excitability in just a few milliseconds[160].

Neurotransmitters can modify the spontaneous neuronal LC activity. First, the quantal somatodendritic release of NA from the LC leads to neuronal hyperpolarization by α_2 autoreceptors that open $G_{i/o}$ protein-coupled inwardly rectifying potassium channels (GIRK), which serves as a negative feedback[161–164]. Akin to the α_2 adrenoceptor, NA cells are modulated by $G_{i/o}$ protein-coupled MOR, which activation results in a decrease of a cAMP-dependent Na^+ current[158], and a $G_{\beta\gamma}$-dependent opening of GIRK channels[165–167]. Other inhibitory inputs to the LC are mediated by activation of specific receptors for the neurotransmitters GABA[168] or serotonin[169], along with the neuropeptides galanin, neuropeptide Y, and somatostatin[170]. In sharp contrast, neuronal stimulation can be driven by glutamate, which binds to ionotropic NMDA or non-NMDA receptors or, to a lesser extent, to metabotropic receptors[171]. Additional excitatory effects on the neuronal activity can be driven by the vasoactive intestinal peptide (VIP), which binds to VPAC receptors and activates an inward sodium current via cAMP/PKA[172,173]. Further excitatory responses can be triggered by binding of cannabinoids[174], imidazolines[175], orexins[176], thyrotropin-releasing hormone[177], substance P (SP), and corticotropin-releasing factor[170] to specific membrane receptors. Finally, gliotransmitters such as ATP or L-lactate can also promote neuronal excitability[138,178].

In addition to synaptic neurotransmitters, LC cells can respond to specific trophic factors present in the CSF (neurotrophic nerve growth factor) due to its convenient location on the dorsolateral wall of the 4th ventricle[179] or to LPS administered both intraperitoneally (i.p.)[180] or locally in the CNS. Hence, when LPS is microinjected into the LC, a prolonged excitation is observed, which is dependent on IL-1[181] and mPGES-1[182]. In addition, LPS upregulates mRNA expression of IL-1β, TNFα[183], and microglial COX-2[184]. Moreover, when the IL-1 receptor

antagonist is microinjected into the LC, the neuronal activity decreases[185], suggesting a possible tonic excitation and a role for cytokines in LC neuronal signaling.

1.2.1.3 Functional implications and pathophysiological aspects of the LC-NA system

Anatomical and physiological properties of LC neurons determine the performance of the entire system. The LC finely tune brain functions, and its dysregulation may play a key role in many pathophysiological conditions.

a) *Sleep cycle and arousal*. Optogenetic photostimulation of LC neurons induces cortical excitability and, thus, sleep-to-wake transition[146]. During sleep, on the contrary, LC activity stops due to tonic GABAergic inhibition[186]. Alteration of the noradrenergic neurotransmission could lead to sleep disorders. For instance, in pain-related sleep disorders (e.g., sciatic nerve ligation) increased cortical levels of NA and enhancement of wakefulness have been observed[187].

b) *Attention*. LC neuronal discharge in phasic mode improves attentional shift to the target stimuli[188], whereas its optogenetic silencing impairs the cognitive flexibility due to poorer attentional shift[189]. In addition, alteration of the cAMP/CREB signaling pathway in the LC produces attention-deficit/hyperactivity disorder (ADHD)-resembling symptoms[190].

c) *Anxiety*. Excessive activity of LC neurons projecting to the prefrontal cortex[136] and amygdala[191] results in anxiety-like behavior. This effect is mediated by the β receptor, and for this reason, its pharmacological blockade mitigates anxiety symptoms[192].

d) *Nociception*. The LC constitutes a part of the descending modulatory pathway. Thus, stimulation of spinally projecting LC neurons produces antinociception to a thermal stimulus[135,136], to a peripheral inflammatory hyperalgesia[193,194], and to a hind paw pinch[195] through spinal α_2 adrenoceptors[196]. On the other hand, persistent inflammatory pain increases the release of endogenous opioids, which downregulates MOR in LC neurons[197].

e) *Learning and memory*. LC neurons send widespread projections to learning-involved areas, some of which require the β adrenoceptor for memory consolidation[143] and a proper microglial function[198]. Hence, LC neuronal activation enhances hippocampal

memory persistence, particularly in response to novel[199] and aversive stimuli[200]. In contrast, during Alzheimer disease, the loss of up to 50% of LC neurons[201] makes the human LC to shrink in volume[202]. Subsequently, hippocampal microglia is blunted, and thereby, it fails to clear amyloid-β deposition[198].

f) *Autonomic functions*. LC promotes sympathetic activity and diminishes parasympathetic activity by innervating preganglionic neurons[145,203]. These effects result in higher blood pressure[138], heart rate increase[203], pupil dilation, and reduction in salivation[145].

g) *Body temperature*. Lesioning the LC completely blocks the development of LPS- and PGE_2-induced fever[204]. Furthermore, LC neurons respond to thermal stimuli[205] and LPS-induced fever with the apparent involvement of the serotonergic 5-HT_{2A} receptor[206] and nitric oxide (NO)[207]. The latter is also thought to play a role in the hypoxia-induced hypothermia and hyperventilation[208].

h) *Breathing control*. The LC constitutes one of the putative central chemosensory brainstem nuclei, along with the pFRG/RTN, NTS, and LPGi[209]. LC neurons respond not only to peripheral chemoreceptor stimulation[210] but also directly to hypercapnia. The rise of CO_2 levels increases the firing rate of LC neurons by closing the GIRK channels[211] and opening the L-type calcium channels[212] and TRP channels[213]. The gap-junctions are also believed to be involved since their blockade impair the LC chemosensitivity[214]. Thus, LC lesion blunts the response to hypercapnia[215]. Most LC neurons fire synchronously with the respiratory rhythm[216], and thereby, increased activity of LC neurons results in an increase of breathing frequency[124] via the α_1 adrenoceptor[217]. In fact, NA has an overall excitatory effect on the breathing behavior[126] because it excites the pFRG/RTN[218] and the inspiratory-generator preBötC[219], whereas it depresses the Bötzinger complex (BötC)-inspiratory inhibition[220]. Moreover, the LC is necessary for the maturation of the brainstem respiratory network[221] as the LC chemosensitivity index is higher in neonates[222]. Thus, dysfunctional LC performance has been associated with respiratory depression[217,222], Rett syndrome, and sudden infant death syndrome (SIDS)[127,168,223]. Furthermore, in Parkinson's disease, the central chemosensitivity may depend on the LC, rather than on the pFRG/RTN due to its deterioration[224].

i) *Inflammation*. The LC is vulnerable to inflammation. First, single i.p. injection of LPS increases NA content in the LC[225] and c-fos immunoreactivity[182,226], which is greatly reduced in mPGES1$^{-/-}$ mice[182]. In contrast, chronic LPS exposure produces a loss of NA cells in the LC[227,228] and an increase of IL-1β levels in the brainstem[228]. Furthermore, NA has a potent anti-inflammatory effect on astrocytes and microglia, which leads to a decrease in cytokine signaling and an increase in brain-derived neurotrophic factor[198,229,230]. Accordingly, degeneration of LC-NA neurons potentiates LPS-induced astrocytosis[231,232].

j) *Opiate tolerance and withdrawal*. Acute opioid administration inhibits LC neuronal activity[158], which turns into an excitatory effect upon chronic exposure[233] due to cellular tolerance[234]. Furthermore, this increased activity of LC neurons is partly responsible for the opioid withdrawal syndrome[156], which is attenuated with an EP3 receptor agonist[120], suggesting a role for the prostanoid system in the LC-mediated opioid withdrawal signs.

1.2.2 PreBötzinger complex

1.2.2.1 Anatomy of the preBötC

The preBötzinger complex (preBötC) is a cluster of neurons located in the ventrolateral medulla oblongata that contains the kernel for breathing rhythmogenesis[235]. Several reasons support the involvement of the preBötC in driving the inspiratory breathing. First, optogenetic excitation of preBötC neurons increases the respiratory frequency[236], whereas unilateral lesion *in vivo* induces a sigh behavior and bilateral loss of preBötC neurons produces erratic breathing and pathological responses to changes in O_2 concentration[237]. Second, the oscillatory activity is maintained in slices, where the preBötC population activity can simulate eupneic and sigh patterns[238]. Furthermore, inspiratory neurons discharge in phase with the rhythmic motor output measured on the hypoglossal XII nerve[239] and laser ablation of these inspiratory neurons impair breathing rhythm in slices[240]. In conclusion, the preBötC is both necessary and sufficient for generating the respiratory rhythm[241].

The preBötC lies within the rostral ventrolateral medulla (RVLM)[242] and its core is located 0.43 mm (between 0.35 - 0.5 mm) posterior to the caudal border of the VII motor nucleus in neonatal mice (Figure 1.7)[243] immediately ventral to the nucleus ambiguus[244]. The preBötC constitutes a part of the ventral respiratory group, along with the Bötzinger complex and the rostral and caudal part of the ventral respiratory group, which in turn, comprises the ventral respiratory column (VRC) in conjunction with the pFRG/RTN (Figure 1.7)[245].

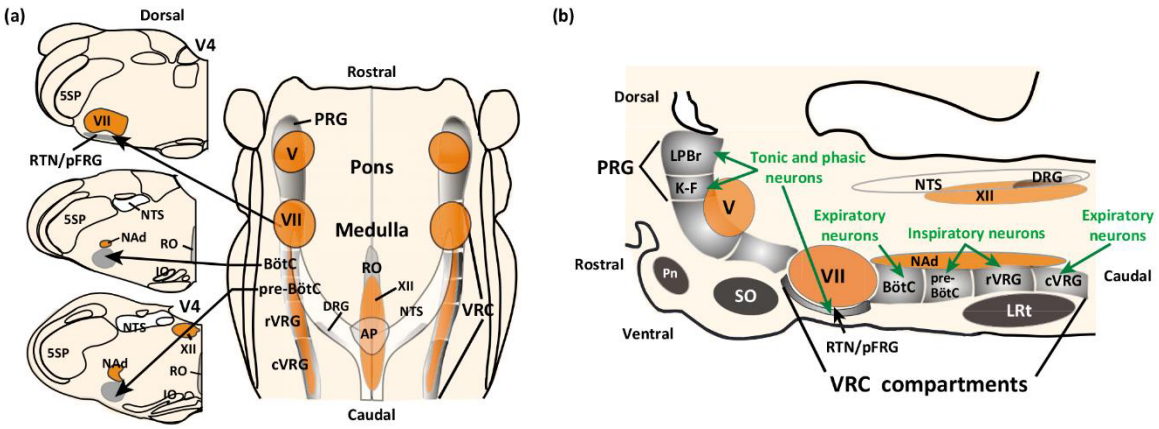

Figure 1.7. Outline of the breathing brainstem anatomy in coronal slices (a; left), in horizontal view (a; right) and parasagittal section (b)[245]. (See abbreviation list for further details).

The preBötC is a highly heterogeneous region, broadly composed of glial cells, and glycinergic, GABAergic, and glutamatergic neurons[239]. Since no motoneurons are present, the neuronal population is composed of interneurons[246] that derive from Dbx1-expressing

progenitors[247], which are only apparent during embryonic development[248]. Among neurons, only 15% of the glutamatergic neurons show intrinsic oscillatory bursting[239], and their selective laser ablation precludes the breathing rhythm in slices[240]. Additionally, these glutamatergic neurons express SP-NK1 receptor and somatostatin-SST receptors[121,247,249,250], whereas most GABAergic cells fail to express the NK1 receptor[121]. NK1 receptor located at postsynaptic sites is prevailing in the preBötC[121,251]. Thus, markers for NK receptors are frequently used to identify and localize the preBötC[119]. SP terminals innervating the preBötC assemble excitatory synapses[251], and accordingly, SP administration increases the neuronal burst frequency via NK1 receptor[252]. In addition to the NK receptor, some rhythmogenic glutamatergic neurons express MOR[119,253]. Thus, opioid administration into the preBötC abolishes the breathing rhythm, causing respiratory depression[253,254]. Therefore, the preBötC has been considered essential for the opioid-induced respiratory depression[255].

a) Afferent projections to the preBötC

PreBötC NK1R$^+$ neurons are innervated by excitatory glutamatergic[256] and inhibitory GABAergic or glycinergic inputs[257]. Some glutamatergic afferents originate in the pFRG/RTN[258], and some have shown to form SP and enkephalin-mediated synapses[251]. Enkephalin terminals are thought to come from the RVLM or NTS [251]. On the other hand, GABAergic SST$^+$ arising from the NTS and parabrachial nuclei[250] send inhibitory inputs to the preBötC, together with the expiratory Bötzinger complex (BötC), which inhibits the inspiratory function of the preBötC during expiration (Figure 1.8)[245].

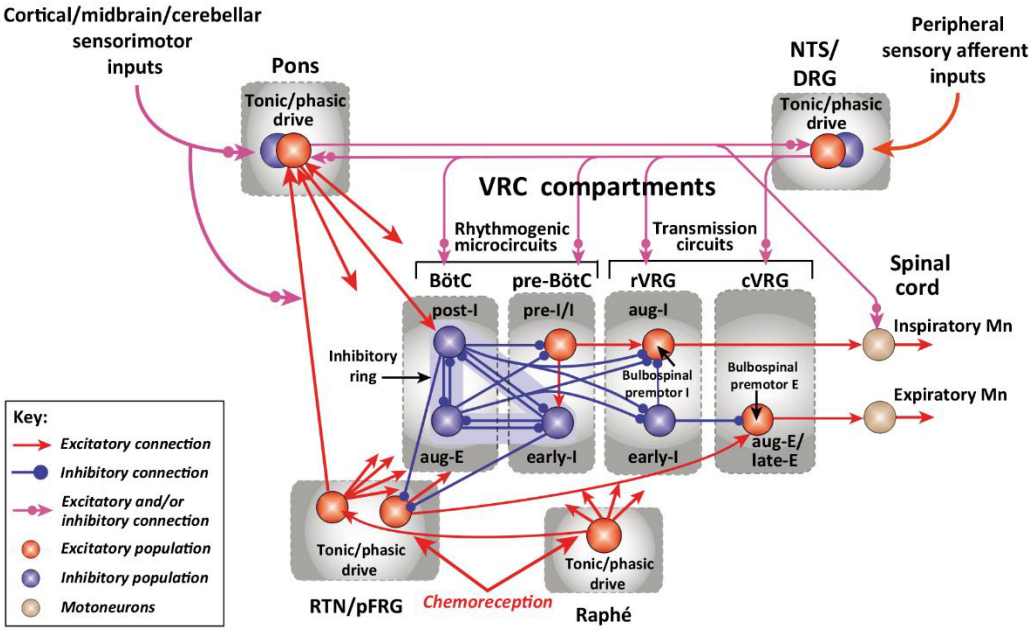

Figure 1.8. A general overview of the complex connectivity among regions of the breathing brainstem that generate inspiratory output[245].

c) Efferent projections from the preBötC

Both excitatory SST$^+$ and inhibitory glycinergic neurons in the preBötC send parallel projections to the same brain regions involved in breathing modulation: the contralateral preBötC, BötC, ventral respiratory column, pFRG/RTN, NTS, Kölliker-Fuse, PAG[259,260] and post-inspiratory complex (PiCo)[261] (Figure 1.9). Interestingly, a few suprapontine regions are innervated by the preBötC, including the thalamus, lateral and dorsomedial hypothalamus, and lateral preoptic area, suggesting a role for breathing in higher-order functions[260]. Moreover, a subset of excitatory neurons, expressing both cadherin-9 and Dbx1 (Cdh9$^+$/Dbx1$^+$), send projections to the LC (Figure 1.9), and its selective ablation leads to calm behaviors[123]. The synchronized activity of both sides of the preBötC[246,262] and the hypoglossal XII motor output[239,263] (Figure 1.10) is attributable to the commissural innervation[239], which shapes the inspiratory rhythm[240].

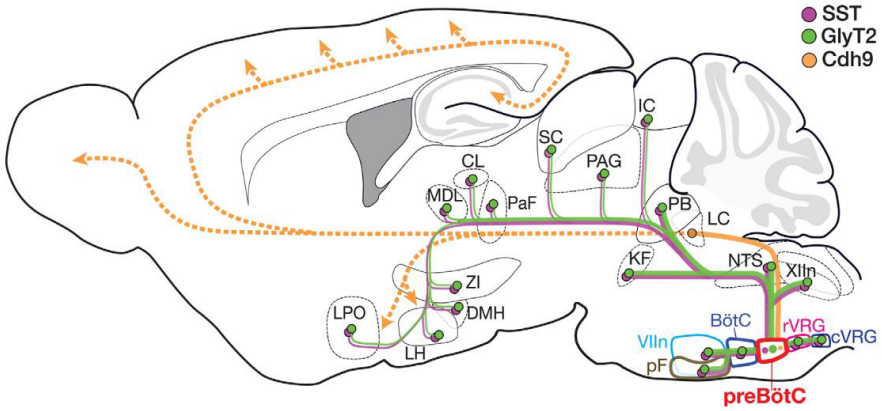

Figure 1.9. Anatomical sagittal scheme for the parallel excitatory and inhibitory efferences arising from the preBötC. Note the excitatory Cdh9 connexion between the preBötC and the LC[260]. (See abbreviation list for further details).

1.2.2.2 Physiology of the preBötC: intrinsic properties and physiological regulation

The preBötC primary function is to generate the breathing pattern[260], as confirmed by the disrupted breathing and apneas following preBötC neuronal ablation both *in vivo* and *in vitro*[240,264,265]. Furthermore, more than 80% of neurons and glial cells in the preBötC fire in synchrony with the inspiratory phase of breathing[239,241] (Figure 1.10), and accordingly, both optogenetic photostimulation[236] or inhibition[266] modifies the rhythm. Finally, activation of

astrocytes within the preBötC anticipates the neuronal inspiratory burst[246,267], so that both neurons and astrocytes are functionally coupled[268].

The majority of the respiratory neurons in the preBötC are inspiratory (80%) (Figure 1.10), implying that they fire in phase with the preBötC population[269,270]. However, 5% of the neuronal population in the preBötC are inhibited during inspiration, and those are expiratory neurons (Figure 1.10). In addition, the preBötC contains post-inspiratory neurons that are also inhibited during inspiration but experience a post-inspiratory rebound[269]. Finally, 11% of the population are non-respiratory neurons that fire tonically regardless of the inspiratory activity[269] (Figure 1.10).

Among the inspiratory neurons, 24% have pacemaker activity, defined as maintained rhythmic burst after synaptic blockade[271]. The pacemaker activity is mainly dependent on a persistent sodium current, and to a lesser extent to a calcium-activated non-specific cation current, which is also sensitive to hypoxia[271]. Nevertheless, pacemaker activity should not be a binary classification, there is instead, a spectrum of firing patterns[272].

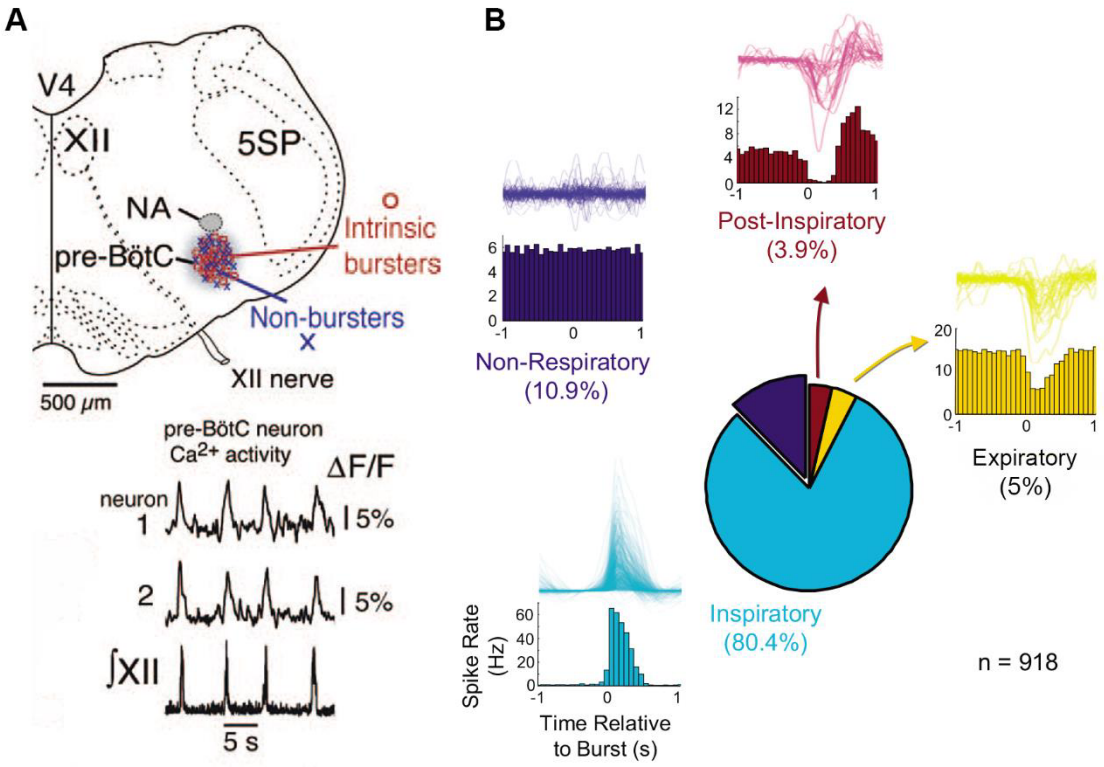

Figure 1.10. (A) Reconstruction of a preBötC-containing slice with the electrophysiological characteristics of its neurons. The left image at the bottom represents examples of Ca^{2+} imaging traces for two neurons and synchronous inspiratory activity recorded on the hypoglossal nerve root (∫XII) (Adapted from [273]). (B) Different neuronal subtypes in the preBötC and their representative histograms of activity[269].

Despite the cellular diversity of the preBötC[270], the synchronicity and connectivity among different cells are thought to play a fundamental role in constituting the neuronal "group pacemaker"[262,274]. Ultimately, in order to harmonize the rhythm of both sides of the preBötC[246,262], the network rhythmogenesis depends on a non-NMDA synaptic transmission[241,262] together with the electrical coupling[270,275]. Furthermore, preBötC neurons organize into clusters[276] interconnected by hubs and resembling the small-world topology[97] (Figure 1.11), by which neighboring cells in a network are connected with a regular pattern and some random rewiring[277,278]. These networks are defined by the parameters mean clustering coefficient (σ) and shortest path length (λ), where σ is the number of nodes that are also neighbors of each other and λ is the minimum number of nodes that must be passed to travel from one node to another (Figure 1.11). As a consequence of this neural circuit, the signal of a few neurons is amplified into a burst of a whole population[279] and finally transmitted to the XII motoneurons by electrical coupling[275].

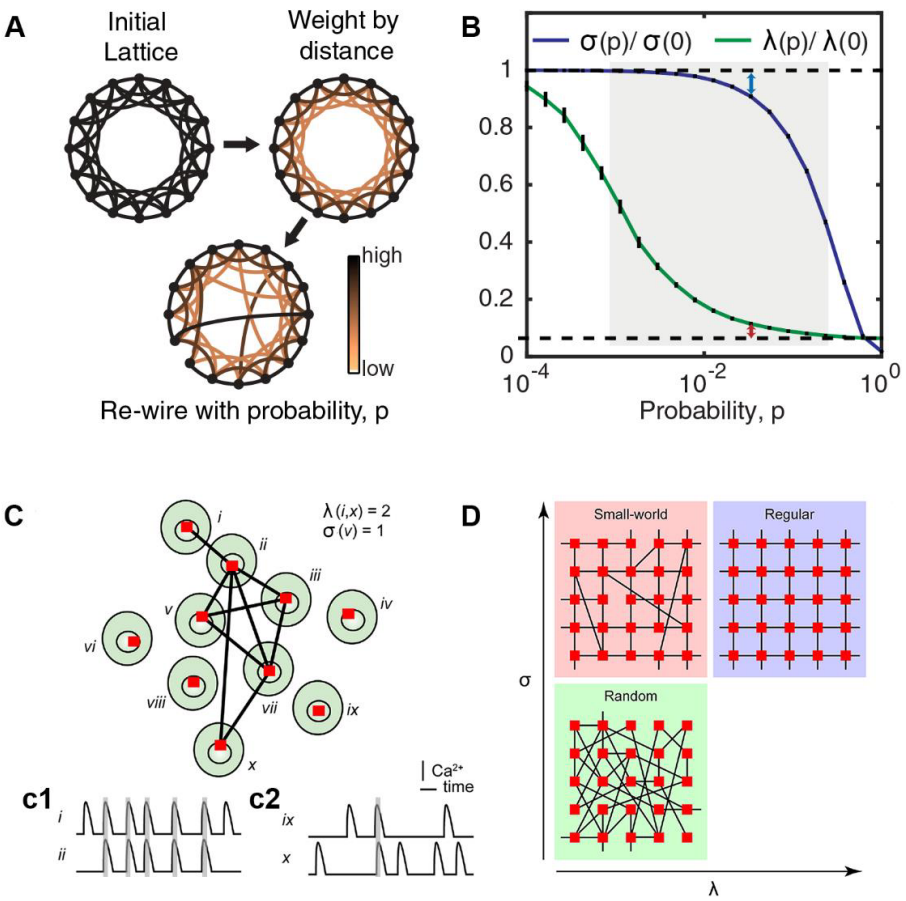

Figure 1.11. (A) Representation of a regular ring lattice by which all nodes or hubs are connected by edges. Distance weight shows a higher strength of close edges, and progressive random rewire creates a small-world network. (B) σ and λ as a function of the rewiring probability (p) (adapted from [280]). C) Illustration of ten cells, in which some cells are connected due to a high correlation coefficient (c1) defined by their synchronous activity,

compared to low correlated cells (c2). (D) The small-world network combines features of both regular and random networks, with high σ and short λ. A decrease in the σ implies increased randomness of the network (adapted from [278]).

The generation of the respiratory rhythm is thought to be driven by the alternation of activity between the inspiratory (preBötC) and the expiratory (pFRG/RTN) function[281] (Figure 1.8). At rest, however, the expiration is passive[282], so a triple oscillator theory has been proposed[272], by which the ventilation is induced due to the inspiratory activity of the preBötC and the post-inspiratory of the PiCo[261]. In contrast, the pFRG/RTN only generates active expiration to induce ventilatory movements[282] in the event of high metabolism[272], hypercapnia[4,97], or the absence of preBötC activity[282].

1.2.2.3 Physiological and pathophysiological aspects of preBötC

The preBötC is capable of reacting to hypoxia[283] in order to adapt the inspiration to the need for O_2. The preBötC activity *in vitro* shows a population burst, and an additional pattern resembling sighs[238], so it may be plausible that the preBötC generates different respiratory patterns[118]. Then, during hypoxic events, the preBötC reacts by increasing the frequency of sighs[238], which have essential functions, as they expand the lungs, induce arousal, and reshape the breathing network[118].

The preBötC is sensible to inflammation, as PGE_2 increases the frequency of sighs, induces gasps under hypoxic conditions[99], and increased the apnea frequency[38], through inhibitory EP3 receptors[97]. Furthermore, babies with severe hypoxic-ischemic encephalopathy have higher PGE_2 metabolite levels in CSF[104], and sudden infant death syndrome victims show structural and functional alterations of the preBötC[284].

Also, the preBötC has been defined as crucial in the opioid-induced respiratory depression[254,255]. NK1 receptor-expressing neurons in the preBötC respond to opioids[119,254] via MOR[285], which activation produces a $G_{i/o}$-protein-dependent[286] decrease of cAMP production[287,288] and opening of GIRK channels[289,290]. As a result, the breathing rhythm decreases[253], and that could have severe consequences[291]. Neonates can be particularly sensitive to opioid-induced respiratory depression as their brainstem has high MOR binding density[292]. MOR signaling is also involved in analgesia, so the analgesic effect cannot be isolated from the respiratory depression[293,294]. Moreover, after chronic opioid treatment, it is easier to develop tolerance (i.e., loss of pharmacologic response) to opioid-induced analgesia than to the respiratory depression[295,296]. Thus, tolerance culminates in dose escalation and ultimately in opioid-related adverse effects.

2 HYPOTHESIS AND OBJECTIVES

Prostaglandins, as inflammatory molecules spreading across the BBB[1], are released in response to blood inflammatory signals in the vicinity of the neurons, where they can modulate the neuronal activity[5]. First, prostaglandins stimulate the nociceptive transmission by increasing the excitability of nociceptive[112,297–299] and spinal neurons[300] or by further decreasing the nociceptive threshold in the PAG[115,301], and ultimately promoting hyperalgesia[109] and allodynia[111]. Secondly, fever is triggered by the activation of EP3 receptors, which inhibits median preoptic neurons[5] and disinhibits the thermogenic pathway (for review see Blomqvist and Engblom[92]). Finally, prostaglandins regulate autonomic functions by increasing the neuronal activity of the NTS[302], control the release of oxytocin and vasopressin by exciting supraoptic neurons through EP4 receptors[303], or modify the synaptic transmission in the neocortex via EP3 or in the hippocampus via presynaptic EP2 receptors[26,304,305]. Moreover, PGE_2 may serve as a gliotransmitter to activate hypothalamic neuroendocrine neurons[3] and the respiratory network[4,97]. Hence, prostaglandins might act as lipid signaling molecules between brain cells. In summary, prostaglandins can modulate neuronal discharge activity in different brain areas[3,26,302–304,306,307], including those involved in inflammation and nociception[5,92,115,305].

The LC, the main noradrenergic nucleus in the brain, is susceptible to inflammation. First, LPS or PGE_2 produce fever via a pathway that includes the LC, as the thermogenic response to these signals is reduced in LC-lesioned rats[204]. Second, LPS administration produces neuroadaptive effects in the LC, including a strong rise in c-fos immunoreactivity[180,182], loss of TH immunoreactivity[227,228], increased expression of IL-1β and TNF-α[183,308], and increased NA content[225]. Third, microinjection of IL-1β, TNF-α, and LPS modifies the LC firing activity[181,185] and ultimately leading to activation of the LC descending pathways and reduction in the development of hyperalgesia[193,194], since NA has antinociceptive[193,194] and anti-inflammatory actions[229,309]. Accordingly, LC-NA neurons synthesize anti-inflammatory mediators[310], and its deterioration during stress[311] or Alzheimer's disease[202] can aggravate the inflammatory response and increase amyloid-β deposition[198,232]. Thus, suggesting that the LC plays a role in neurodegenerative diseases[145,312], as shown in a Parkinson's disease model, where the LC reestablishes the chemosensitivity to hypercapnia due to the impaired function of the main central chemoreceptor RTN[224].

Notably, LC neurons are not only sensitive to inflammation in general but to prostaglandins in particular. First, LC neurons possess the enzymatic machinery necessary to synthesize prostaglandins; including constitutive COX-2, and $mPGES_1$[21,182]. Thus, NSAIDs, by blocking the synthesis of prostanoids, attenuate the activation of LC neurons in response to nociception and inflammation[180,313,314]. Second, the EP2, EP3, and EP4 receptor mRNA is found in the LC by *in situ* hybridization[57,62,63,120] and the EP3 receptor protein by immunoreactivity[64] and double immunofluorescence[65]. Furthermore, it is likely that during inflammatory conditions, there is a bias towards the EP4 receptor signaling in catecholaminergic neurons[57]. Third, EP3 receptor activation in the LC reduces c-fos mRNA and opioid-withdrawal syndrome[120,315]. Additionally, presynaptic EP3 receptors mediate the inhibition of NA release in the main projection areas of the LC, including the cortex, hippocampus, and hypothalamus[316–320].

Taken together, this evidence suggests an interaction between the prostaglandin system and the LC concerning inflammation, nociception, fever, and neurodegeneration. To date, however, the role of EP receptors in the regulation of the LC neuronal activity has not been studied.

On the other hand, the release of endogenous opioids counteracts the effect of nociceptive signals[321]. Due to their potent analgesic effect, opioids are widely used in the clinic, with the major drawback of producing potentially lethal respiratory depression[291] and dependence[322]. The main target of opioids in the respiratory brainstem is the inspiratory pattern generator preBötC, which is considered essential in the opioid-induced respiratory rate depression[254,255]. Furthermore, preBötC inspiratory neurons express MOR[119,254] and κ-opioid receptor (KOR) RNA[248]. Thus, opioids act postsynaptically on preBötC neurons by decreasing the inspiratory frequency in slices[119], but producing a quantal slowing in *en bloc* or *in vivo* preparations, due to the complex configuration of the breathing brainstem[323]. The underlying mechanism involves a $G_{i/o}$ protein-dependent[286] opening of GIRK channels[290] and decrease of cAMP formation[287,288] leading to neuronal hyperpolarization[119].

Apart from being inflammatory messengers, the prostaglandins produce respiratory depression by interfering with the breathing rhythm generation[324], as demonstrated by the fact that i.c.v. administration of PGE_2 leads to irregular breathing and apneas[98,325] via the EP3 receptor[38]. Furthermore, PGE_2 metabolite concentration in neonatal CSF correlates positively with asphyxia and the outcome of hypoxic-ischemic encephalopathy[104]. Additionally, in the preBötC, the brainstem central pattern generator, PGE_2 lowers the calcium transient frequency

of the network[97] and increases the sigh frequency and gasp tendency[99]. However, the possible synergy between PGE_2 and opioids to induce major respiratory disruption, e.g., during infections and surgery, remains to be elucidated.

In sum, the global aim of this study was to characterize the effect of prostanoid agonists on the LC neuronal activity and to elucidate its underlying mechanism. Furthermore, we aimed to study the interaction between the prostaglandin and opioid systems in the inspiratory pattern generator preBötC. The specific objectives of the present study were:

I. To characterize the functional role of the prostaglandin E_2 EP3 receptors in the rat LC by single-unit extracellular recording *in vitro*. For this purpose, we studied the effect of various EP3 receptor agonists on the spontaneous firing activity of NA cells, and we evaluated the underlying signaling mechanism in the LC.

II. To determine the role of the EP2 receptors in the rat LC by single-unit extracellular recording *in vitro*. Accordingly, the effect of EP2 receptor agonists and different blockers of the signaling mechanism were tested on the spontaneous firing activity of LC cells.

III. To investigate the function of EP4 receptors in the rat LC by single-unit extracellular recordings *in vitro*. For this reason, the effect of EP4 receptor agonists and signaling inhibitors were examined.

IV. To study the interaction between the effect of PGE_2 and opioids on the Ca^{2+} transient frequency and cellular connectome of the inspiratory pattern generator preBötC in neonatal mice by time-lapse calcium imaging on brainstem organotypic slice cultures.

3 MATERIALS AND METHODS

3.1 MATERIALS

3.1.1 Animals

Adult male Sprague-Dawley rats (200-300 g) bred in the animal facility of the University of the Basque Country were used for the electrophysiological experiments. The animals were kept under controlled environmental conditions (22 ºC, 12-h light/dark cycle, humidity of 65 – 70%) and with food and water *ad libitum*.

For calcium imaging studies, postnatal day 3 – 4 (P3 – P4) C57BL/6J mice were used as wild type (WT). Additionally, a knockout mouse strain (B6.E14Tg2a-Ptger3^{tm1Unc}) was derived from the WT by deleting the EP3 receptor gene (Ptger3). Phenotypically, the Ptger3$^{-/-}$ mice have higher body weight and increased nocturnal activity[326].

All experimental procedures were conducted in accordance with the Directive 2010/63/EU of the European Parliament and of the Council of 22 September 2010 on the protection of animals used for scientific purposes and with the institutional guidelines for animals used in research (Animal Care and Use Committee of the University of the Basque Country or Sweden). All the efforts were made to minimize animal suffering and to reduce the number of animals used according to the Three Rs: Replace, Reduce, and Refine.

3.1.2 Drugs and reagents

Drugs and reagents used in this thesis are shown in alphabetical order in Table 3.1.

Table 3.1. Employed drugs and reagents:

DRUG / REAGENT	PROFILE / PHARMACOLOGICAL ACTIVITY	PROVIDER	SOLVENT	FINAL CONCEN-TRATION / DOSE	APPLI-CATION TIME
2-APB (2-di(phenyl)boranyloxyethanamine)	Non-selective TRP channel blocker	Tocris	DMSO	30 µM	10 min
8-Bromo-cAMP	cAMP permeable analog, PKA activator	Enzo life sciences	H_2O	1 mM	8 min

$BaCl_2$	Non-selective GIRK channel blocker	Sigma-Aldrich	H_2O	300 µM	15 min
Butaprost free acid	EP2>>EP3>EP4 agonist	Cayman chemical	methyl acetate	10 nM – 10 µM (3x)	10 – 15 min
Chelerythrine chloride	Cell-permeable PKC inhibitor	Tocris	H_2O	10 µM	30 min
Chloral hydrate	Anesthetic	Sigma-Aldrich	NaCl 0.9%	400 mg kg^{-1}	
CNQX (6-cyano-7-notroquinoxaline-2, 3-dione)	AMPA/kainate receptor antagonist (non-NMDA iGluR)	Tocris	H_2O	30 µM	10 min
DAMGO (2-Ala-4-mephe-5-gly-enkephalin)	MOR agonist	Sigma-Aldrich	H_2O	0.5 – 5 µM	5 – 15 min
d-AP5 (d-(–)-2-amin-5-phosponopentanoic acid)	NMDA receptor antagonist	Tocris	H_2O	100 µM	10 min
Fluo-8 AM	Green fluorescent dye for Ca^{2+}	AAT Bioquest	Pluronic acid 1% (DMSO)	10 µM	30 min
GABA	GABA receptors agonist	Sigma-Aldrich	H_2O	1 mM	1 min
Gallein	Inhibitor of G-protein βγ signaling	Tocris	DMSO	20 µM	120 min
Glibenclamide	Kir6.2 //ATP-sensitive inwardly rectifying K+ channel blocker	Tocris	DMSO	3 µM	15 min
H-89	PKA inhibitor	Tocris	H_2O	10 µM	20 min
L-161,982	EP4>>EP3>>EP2 antagonist	Tocris	DMSO	3 nM – 10 µM	30 min
L-798,106	EP3>>EP4>EP2 antagonist	Tocris	DMSO	10 nM – 10 µM	30 min
ME ([Met]-Enkephalin)	MOR agonist	Bachem	H_2O	0.8 µM	1 min
Misoprostol free acid	EP3>EP4≥EP2 agonist	Cayman chemical	methyl acetate	0.31 nM – 2.56 µM (2x)	1 min
Naloxone hydrochloride dihydrate	Opioid receptors antagonist	Sigma-Aldrich	H_2O	5 µM	10 min
NF449	$G_{\alpha s}$ subunit blocker	Tocris	H_2O	10 µM	30 min

Pertussis toxin	Bacterial toxin that catalyzes ADP-ribosylation of G-proteins G_i, G_o and G_t	Tocris	H_2O	500 ng ml^{-1}	overnight (18 h)
PF-04418948	EP2>>EP3>EP4 antagonist	Tocris	DMSO	3 nM – 10 µM	30 min
PGE_2	EP3≥EP4>EP2>EP1 agonist	Tocris / Sigma Aldrich	DMSO or absolute ethanol	0.31 nM – 10.2 µM (2x)	1-5 min
Picrotoxin	$GABA_A$ and glycine receptor blocker	Sigma-Aldrich	aCSF	100 µM	10 min
Rivenprost (Ono-4819)	EP4>EP3 (partial)>EP2 agonist	Cayman chemical	methyl acetate	0.01 nM – 1 µM (3x)	10 min
Rolipram	PDE4 inhibitor	Sigma-Aldrich	DMSO	5 µM	10 min
RS-MCPG (RS-methyl-4-carboxyphenylglycine)	Non-selective mGluR antagonist	Tocris	aCSF	500 µM	10 min
SCH-23390	Selective Kir3.2/GIRK2 gating inhibitor	Tocris / Sigma Aldrich	H_2O	15 µM	30 min
Sulprostone	EP3>EP1 agonist	Cayman chemical	methyl acetate	1.25 nM – 1.28 µM (2x)	1 min
TCS 2510	EP4>>EP1=EP2=EP3 agonist	Tocris	absolute ethanol	0.20 nM – 2 µM (3x)	10 min
TMR-SP (tetramethylrhodamine-conjugated Substance P)	NK1R fluorescent agonist	Biomol	H_2O	3 µM	10 min
Treprostinil	DP1=EP2>IP>EP1>EP4 agonist	Tocris	DMSO	30 nM – 10 µM (3x)	10 – 15 min
TRIS (Trizma HCl)	Buffer	Sigma-Aldrich	H_2O	104 mM	5 min
VIP	Neuropeptide agonist of VIP and PACAP receptors	Bachem	H_2O	500 nM	5 min
Wortmannin	PI3K inhibitor	Tocris	DMSO	100 nM	20 min
ZD7288	HCN channel blocker	Tocris	H_2O	30 µM	20 min

Most drugs were prepared as stock solutions in miliQ water and stored at -20 ºC until the day of the experiment, when they were finally diluted in artificial cerebrospinal fluid (aCSF). Some other drugs were dissolved in DMSO (Table 3.1) to a final concentration in the perfusion fluid <0.1%, which does not affect the firing activity of LC neurons *in vitro*[327]. Except for PGE_2 and treprostinil, all the EP agonists were purchased pre-dissolved in the corresponding solvent according to Table 3.1, and the final concentration of the solvents in the perfusion fluid was <0.03%. The composition of the aCSF for the electrophysiological studies was (in mM): NaCl 130, KCl 3, NaH_2PO_4 1.25, glucose 10, $NaHCO_3$ 20, $CaCl_2$ 2, $MgSO_4$ 2 saturated with 95% O_2/ 5% CO_2 for a final pH of ~7.34. In some experiments, 80% of the NaCl was equiosmolarly substituted for trizma hydrochloride (TRIS) to a final concentration of NaCl 26 mM[328,329]. For the calcium imaging study, PGE_2 was dissolved in absolute ethanol, and a slightly different aCSF was used (in mM); NaCl 124, KCl 3, NaH_2PO_4 1.1, glucose 10, $NaHCO_3$ 26, $CaCl_2$ 2, $MgSO_4$ 2 and also saturated with 95% O_2/ 5% CO_2.

3.2 METHODS

3.2.1 Electrophysiological procedures

3.2.1.1 Brain slice preparation

Rats were anesthetized with chloral hydrate (400 mg kg^{-1}, i.p.) and decapitated. The brain was rapidly extracted after decapitation and placed in an ice-cold aCSF (4ºC), where NaCl was substituted by sucrose (252 mM) to improve neuronal viability[330]. Coronal brainstem sections of 500-600 μm thickness containing the LC were cut using a vibratome (FHC Inc. USA) with a Valet blade (World Precision Instruments, Inc. USA). The facial nerve and the IV ventricle were used for anatomical references. The slices were allowed to recover from the slicing for 60-90 min in a glass beaker covered with a lid and bubbled with 95% O_2/ 5% CO_2. After the recovery period, the slices were transferred into a custom-made modified Haas-type interface chamber, including a polypropylene mesh covered with cellulose paper (Sigma-Aldrich Química, Spain) and lens paper (Olympus Optical Spain S.A. Spain) on which the tissue was placed. The slice was continuously perfused with oxygenated aCSF at a flow rate of 1.5 ml min^{-1}. Drugs dissolved in aCSF were applied by a polyethylene tube system manually controlled by three-way valves.

3.2.1.2 Uni-extracellular recording technique

Single-unit extracellular recordings of LC neurons were made as previously described [331].

- *Recording electrode preparation*. The recording electrode, an Omegadot glass micropipette, was prepared with a horizontal pipette puller (Sutter Instruments Co., USA). The micropipette tip was shaped by adjusting the parameters of heat and speed of the puller. Then, the electrode was filled with sodium chloride (50 mM) using a Yale spinal needle (0.5 x 90 mm, 25 G, Beckton Dickinson S.A., Spain) coupled to a Sartorious cellulose filter (0.20 μm, Filtros Anoia S.A., Spain). Once filled, the tip was broken to a diameter of 2 – 5 μM for a final resistance of 3 – 5 MΩ.

- *Recording of uni-extracellular electrical activity of LC neurons.* The electrode was positioned, under a binocular microscope (C011, Olympus Optical Spain, S.A., Spain), into the recording area, i.e., the LC. This nucleus was visually identified as a dark oval area on the lateral borders of the central gray and the IV ventricle, anterior to the *genu* of the facial nerve. The electrode was lowered at 4 μm intervals using a micropositioner (6000-ULN, Burleigh Instruments, Canada). Noradrenergic cells were identified by their spontaneous and regular discharge activity, slow firing rate, and long-lasting biphasic positive-negative waveforms[153]. As illustrated in Figure 3.1, the extracellular signal was filtered through a high-input impedance headstage (HS-2A, Axon Instruments, USA) and amplified (x 10) together with a pre-amplifier (Axoclamp-2A, Axon Instruments, USA). Then, the signal was further filtered and amplified by a high input impedance amplifier (Cibertec S.A., Spain). After that, an oscilloscope (Hameg Instruments, Germany) and an audio-analyzer (Cybertec S.A., Spain) were used to monitor the signal. Individual (single-unit) neuronal spikes were isolated from the background noise with a window discriminator (Cibertec S.A., Spain) and finally, the firing rate was analyzed by a PC-based custom-made software (HFCP®, Cibertec S.A., Spain), which generated consecutive histogram bars representing the accumulated number of spikes in 10 s. To maintain the slice at a physiological temperature (33-34 ºC), a thermoregulatory system was used (Cybertec S.A., Spain). All the extracellular set-up was connected to a ground wire to avoid electrical interference.

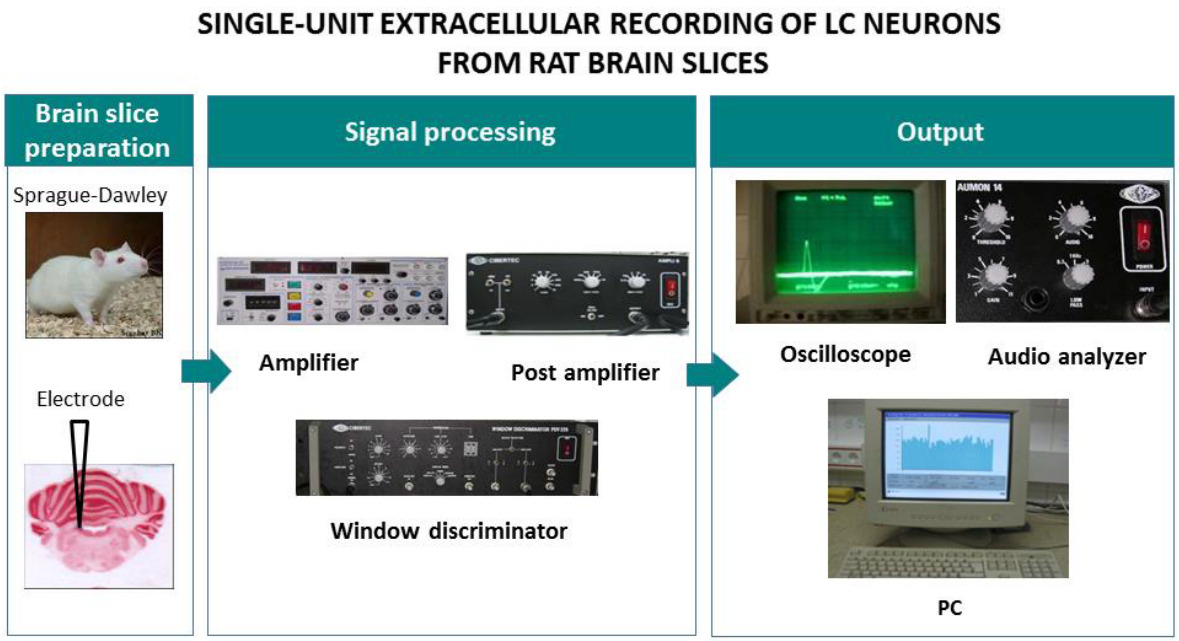

Figure 3.1. Scheme for electrophysiological signal processing and recording.

3.2.2 Calcium time-lapse imaging in organotypic slice cultures

3.2.2.1 Organotypic slice cultures preparation

Organotypic slice cultures containing the preBötC were used for study IV. One of the advantages of employing organotypic slice cultures is the flattening of the tissue, without changing the cytoarchitecture, which leads to improved optical conditions increasing calcium time-lapse imaging performance[97,252]. The brainstem organotypic cultures were obtained from P2-P5 mice pups, which further provide optimal imaging conditions, due to less glial coverage than in adult slices[332]. As previously described elsewhere[97], pups were decapitated and the brain was dissected in a dissection medium (55% Dulbecco's modified Eagle's medium, 0.3% glucose, 1% HEPES buffer and 1% penicillin-streptomycin). The brain was sectioned into 300 µm-thick transverse slices by using a McIlwain Tissue Chopper (Ted Pella, Inc., Redding, CA, USA). Slices were selected based on anatomical descriptions of previous reports[243,333] and washed by moving them to brain slice medium (55% Dulbecco's modified Eagle's medium, 32.5% Hank's balanced salt solution, 0.3% glucose, 10% fetal bovine serum, 1% HEPES buffer and 1% Antibiotic-Antimycotic [Invitrogen, UK]). Subsequently, they were carefully placed on insert membranes (Millicell Culture Plate Inserts; Millipore, Billerica, MA, USA), which had been coated with poly-L-lysine (0.3 ml; 0.1 mg ml^{-1}, Sigma-Aldrich, St. Louis, USA) and ultimately inserted into six-well plates. Finally, brain slice medium (1 ml) was placed underneath the membrane, allowing the slices to be on the liquid/gas interphase to permit a

correct oxygenation[334] by the Stoppini method[335]. The slice cultures were kept in an incubator (37˚C, 5% CO_2), and the medium was changed every second day. The brainstem slices were kept for 7 – 21 days *in vitro* (DIV) before live imaging experiments.

3.2.2.2 Calcium time-lapse imaging

For Ca^{2+} imaging, Fluo-8 AM (AAT Bioquest, Inc., USA) was added to a solution of pluronic acid 1% in DMSO (Invitrogen, UK). The final concentration in aCSF was 10 µM. In order to localize the preBötC, tetramethylrhodamine-conjugated substance P (TMR-SP; Biomol, Oakdale, NY, USA) was used at a final concentration of 3 µM in aCSF. The TMR-SP solution was placed on top of the brainstem slice and was incubated for 10 min (37˚C, 5% CO_2 atmosphere). The TMR-SP solution was then replaced with 1 ml of the 10 µM Fluo-8 solution, which was in turn incubated for 30 min (37˚C, 5% CO_2). Before imaging, the slice was washed with aCSF for 1-5 min (37˚C, 5% CO_2). During time-lapse imaging, slices were kept in an open chamber perfused with aCSF (1.5 ml min^{-1}) by a peristaltic pump. A Chamlide Inline Heater (Live Cell instruments, Seoul, Korea, cat no. IL-H-10) was used to set the temperature to 32ºC and a Chamlide AC-PU chamber (Live Cell instruments, Seoul, Korea, cat no. ACPU25) for perfusion. The aCSF was constantly bubbled with 5% CO_2 and 95% O_2. Images were captured by using a Zeiss AxioExaminer D1 microscope equipped with 20x and 40x water immersion objectives (N.A. 1.0), a Photometrics Evolve EMCCD-camera and filter sets 38HE (Zeiss) and et560/hq605 (Chroma, Bellows Falls, VT, USA). For live imaging, a frame interval of 0.5 s was used. Exposure time was set to 100 ms. Testing drugs were dissolved in aCSF prior to application and added to the chamber by using a continuous flow system. When the effect of SCH-23390 was tested, it was added to the Fluo-8 solution for the 30-minute incubation. For each experiment, a baseline period with aCSF (5 min) was followed by drug application. The drug concentrations employed in this investigation are in accordance with those used in previous studies in slices[97,99,336,337].

Table 3.3. Summary of the studies, regions, and techniques used in this thesis.

Studies	Region	Technique	Animals	Slices
I-III	Locus coeruleus	Extracellular electrophysiology	Sprague-Dawley adult rats	Acute
IV	preBötzinger complex	Calcium time lapse imaging	C57BL/6J and Ptger3$^{-/-}$ neonate mice	Organotypic cultures

3.2.3 Pharmacological procedures

3.2.3.1 Pharmacological characterization of EP3 receptors in rat LC neurons

To study the effect of EP3 receptor agonists on the firing rate of LC neurons, we perfused increasing concentrations of the EP1/EP3 receptor agonist sulprostone (0.31 nM – 1.28 μM, 2x), PGE_2 (0.31 nM – 10.2 μM, 2x) or the PGE_1 analog misoprostol (0.31 nM – 2.56 μM, 2x). Concentrations were based on previous studies in brain slices[318,338]. Each concentration of the EP receptor agonists was perfused for enough time to reach the maximal effect (1 min).

To identify the subtype of EP receptor involved in the effect of sulprostone, PGE_2, and misoprostol, concentration-effect curves for these agonists were performed in the presence of different EP receptor-selective antagonists. First, for sulprostone, the EP2 receptor antagonist PF-04418948 (3 and 10 μM), the EP3 receptor antagonist L-798,106 (3 and 10 μM), and the EP4 receptor antagonist L-161,982 (3 and 10 μM) were used at the concentrations previously reported[339]. Next, for PGE_2 and misoprostol, the EP3 receptor antagonist L-798,106 at 10 μM was used, along with a combination of the aforementioned EP2 and EP4 receptor antagonists at 10 μM. All the antagonists were perfused for 30 min before performing the concentration-effect curves for the EP receptor agonists.

Based on its pharmacological profile, sulprostone was selected to further characterize the molecular mechanism underlying EP3 receptor activation. To study the involvement of $G_{i/o}$ proteins, concentration-effect curves for sulprostone were made after overnight incubation of the slices with the irreversible inhibitor of $G_{i/o}$ proteins pertussis toxin (PTX, 500 ng ml^{-1}, 18 h) in an oxygenating glass beaker at room temperature, in line with preceding studies[340]. In order to verify that PTX had effectively blocked the $G_{i/o}$ protein, the effect of the $G_{i/o}$-coupled MOR agonist ME was tested. Thus, only cells with a reduced inhibitory effect of ME (<80%) were considered to perform the concentration-effect curves for sulprostone. In those cells, proper drug perfusion was assessed with GABA (1 mM, 1 min)

To confirm the involvement of GIRK channels, which are described to be activated by $G_{i/o}$ proteins[166], concentration-effect curves for sulprostone were performed in the presence of the GIRK blocker $BaCl_2$ (300 μM, 15 min) or the selective GIRK2 gating inhibitor SCH-23390 (15 μM, 30 min) at the concentrations previously used[211,336].

3.2.3.2 Pharmacological characterization of EP2 receptors in rat LC neurons

To characterize the effect of EP2 receptor agonists in LC neurons, we perfused increasing concentrations of the EP2 receptor agonist butaprost free acid (10 nM – 10 μM, 3x) and the synthetic PGI_2 analog treprostinil, which has a high affinity for the EP2 receptor (30 nM – 10 μM, 3x), based on other studies[93]. Each concentration of the EP2 receptor agonists was perfused for at least 10 min. To verify the specificity of the agonists for the EP2 receptor, the EP2 receptor antagonist PF-04418948 (3 and 10 nM) was used according to preceding reports[341–343]. A combination of the EP3 receptor antagonist L-798,106 (10 nM) and the EP4 receptor antagonist L-161,982 (10 nM) was also used to study the selectivity of the EP2 receptor agonists for the EP3 and EP4 receptors. All the antagonists employed were perfused for 30 min before performing the concentration-effect curves for the EP2 receptor agonists.

Butaprost was used for subsequent characterization of the molecular mechanism involved in EP2 receptor activation. A mechanism described for excitatory responses of LC neurons consists of a cAMP/PKA-induced opening of a non-selective cation current[327]. Then, to investigate the involvement of sodium current in the butaprost-mediated effect, a low sodium-containing aCSF was prepared by replacing 80% of the NaCl equiosmolarly with Trizma hydrochloride/base (TRIS), and then the effect of butaprost was tested[329]. To further describe the involvement of sodium currents, we checked whether the transient receptor potential (TRP) ion channels[213] might contribute to butaprost effect by using the nonselective TRP blocker 2-APB (30 μM, 10 min). Finally, to discard the activation of other channels that may mediate excitatory effects in the LC neurons[344], we examined the effect of butaprost in the presence of the ATP-sensitive potassium channel (Kir6.2) specific blocker glibenclamide (3 μM, 15 min).

To test whether the sodium current was induced by a rise in the cAMP levels and the resultant activation of the PKA, we performed an occlusion experiment with the non-hydrolyzable cell-permeable cAMP analog 8-Br-cAMP (1 mM, 8 min)[173]. Thus, in case the EP2 receptor activation depends on the cAMP/PKA pathway, administration of a saturating concentration of 8-Br-cAMP would occlude the subsequent effect of butaprost. In addition, the cAMP/PKA-dependency was further determined by testing butaprost in the presence of the PKA inhibitor H-89 (10 μM, 20 min)[345] or the HCN channel blocker ZD7288 (30 μM, 20 min)[346].

Then, we evaluated the possible activation of ion channels in a cAMP/PKA-independent manner. For this purpose, we tested whether the $G_{\alpha s}$ protein would intermediate in the effect of butaprost by application of the blocker of the $G_{\alpha s}$-dependent signaling NF449 (10 μM, 30

min)[347]. In these assays, VIP (0.5 μM, 5 min) administration was used as a positive control to confirm that NF449 was effectively blocking the $G_{\alpha s}$ protein, as previously reported in LC neurons[172]. Finally, to assess the involvement of the $G_{\beta\gamma}$ subunits, the effect of butaprost was tested in slices previously incubated with gallein (20 μM) in an aluminum foil-covered glass beaker for 120 min[348].

In order to study the involvement of presynaptic mechanisms in the effect caused by EP2 receptor activation, butaprost was applied in the presence of the $GABA_A$ channel blocker picrotoxin (100 μM), the non-NMDA ionotropic glutamate receptor antagonist CNQX (30 μM), the NMDA receptor antagonist d-AP5 (100 μM), and the non-selective metabotropic glutamate receptor antagonist RS-MCPG (500 μM)[349,350]. All mentioned drugs were bath perfused for at least 10 min before and during testing the effect of butaprost.

3.2.3.3 Pharmacological characterization of EP4 receptors in rat LC neurons

To characterize the effect of EP4 receptor agonists in LC neurons, we perfused increasing concentrations of the EP4 receptor agonist rivenprost (0.01 nM – 1 μM, 3x) and TCS 2510 (0.20 nM – 2 μM, 3x) for at least 8 min each concentration, based on previous studies[351]. To pinpoint the EP receptor involved in the observed effect upon rivenprost administration, the EP4 receptor antagonist L-161,982 (3, 30, and 300 nM), the EP2 receptor antagonist PF-04418948 (300 nM), and the EP3 receptor antagonist L-798,106 (300 nM) were used. All the antagonists were perfused for 30 min before performing the concentration-effect curves for the EP4 agonists.

To investigate the molecular mechanism involved in EP4 receptor activation, we used a similar approach to the pharmacological characterization of the EP2 receptor (see section 3.2.3.2 for further details). First, low-sodium aCSF (TRIS 80%) and the TRP channel blocker 2-APB (30 μM, 10 min) were employed to test the involvement of sodium currents. Secondly, 8-Br-cAMP (1 mM, 8 min) and H-89 (10 μM, 20 min) were used to study the connection with the cAMP/PKA pathway.

Considering the similarities between the effects of EP2 and EP4 receptor activation, we performed an occlusion experiment in the presence of a submaximal concentration of butaprost (1 μM, 15 min) to examine the possible convergence of both signaling pathways.

In addition, the effect of rivenprost was tested in the presence of the $G_{\alpha s}$ blocker NF449 (10 μM, 30 min) or the $G_{\beta\gamma}$ blocker gallein (20 μM, 120 min) to further characterize the G-protein subunits involved (see section 3.2.3.2 for further details).

Finally, since the EP4 receptor has been described to couple to the PI3K and PKC signaling pathways[81,352,353], the PI3K inhibitor wortmannin (100 nM, 20 min) and the cell-permeable PKC inhibitor chelerythrine (10 μM, 30 min) were used at previously tested concentrations[354,355].

Except otherwise stated, all mentioned drugs were bath perfused for at least 10 min before and during testing the effect of rivenprost.

Table 3.2. Prostanoid receptor binding profiles for the employed agonists and antagonists. Specific binding was determined using displacement radioligand binding to HEK cell membranes expressing the EP receptors. The values represent the inhibition constant (Ki) in nM, whereas those with an asterisk (*) represent the IC_{50}.

			Ki (nM)					
			EP1	**EP2**	**EP3**	**EP4**	**DP1**	**Reference**
EP receptor	Agonists	PGE_2	22	6.8	0.9	1.1	119	356
		Sulprostone	94	>100000	0.7	43600		356
		Misoprostol	11935	34	7.9	23		357
		Butaprost	38700	65	11815	15700		356
		Treprostinil	212	3.6	2505	826	4.4	358
		Rivenprost	10000	620	56	0.7		359
		TCS 2510	>13000	>13000	>13000	1.2		360
	Antagonists	PF-04418948	>10000*	16*	>10000*	>33300*		341
		L-798,106	>8400	>9200	0.2	>3200		361
		L-161,982	61000	58000	7000	32		362

3.2.3.4 Influence of PGE_2 on opioid-induced respiratory depression

For the study IV, we hypothesized that the PGE_2-induced irregular breathing would enhance the opioid-induced respiratory depression to cause major breathing disruption. In order to characterize the possible influence of PGE_2 on opioid-induced respiratory depression, PGE_2 at 10 and 100 nM was used along with the MOR agonist DAMGO at 0.5 and 5 μM. To verify

that the effect of DAMGO was caused by the activation of MOR, the opioid receptor antagonist naloxone (5 μM, 10 min) was used. In addition, the implication of GIRK channels was studied by incubation with the GIRK2 gating inhibitor SCH-23390 (15 μM, 30 min). Finally, the involvement of the cAMP pathway was determined by the administration of rolipram (5 μM, 10 min), an inhibitor of the cAMP degradative enzyme phosphodiesterase 4 (PDE4), at the concentrations previously used[288].

3.2.4 Data analysis and statistics

3.2.4.1 Electrophysiology

In electrophysiological experiments, the neuronal firing rate (FR) was collected in 10 s bin frequency histograms, where each bar represents the accumulated neuronal discharges in 10 seconds (spikes 10 s^{-1}). The inhibitory effect of [Met]enkephalin (ME, 0.8 μM, 1 min) was used as a control for the perfusion system (Figure 3.2), and to test the efficacy of some blockers that would presumably inhibit the effect of ME, such as the pertussis toxin, barium or SCH-23390. The effect of prostanoid agonists could not be washed out easily. Thus, the effect (E) was calculated as the percentage of reduction/increase of firing rate from the baseline, according to the following equation:

$$E(\%) = \frac{FR_{pre} - FR_{post}}{FR_{basal}} \cdot 100$$

Where:

- E is the inhibitory/excitatory effect of the drug in percentage.
- FR_{basal} is the average firing rate for 60 s at the beginning of the recording or immediately before the prostanoid receptor agonist administration.
- FR_{pre} is the average firing rate for 60 s immediately before drug application.
- FR_{post} is the average firing rate after drug application, with the time of calculation depending on the kinetics of the drug effect as follows:
    - For ME application: average firing rate for 90 s, ruling out the first 40 s after switching to the drug solution (dead volume) (see Figure 3.2).
    - For EP3 receptor agonists: average firing rate for 60 s, ruling out the first 60 s after switching to the drug solution (dead volume) (see Figure 3.2).
    - For GABA application: average firing rate for the time of complete inhibition.

- For the EP2 and EP4 receptor agonists: average firing rate for 60 s, once it reached a plateau of firing rate (see Figure 3.3).

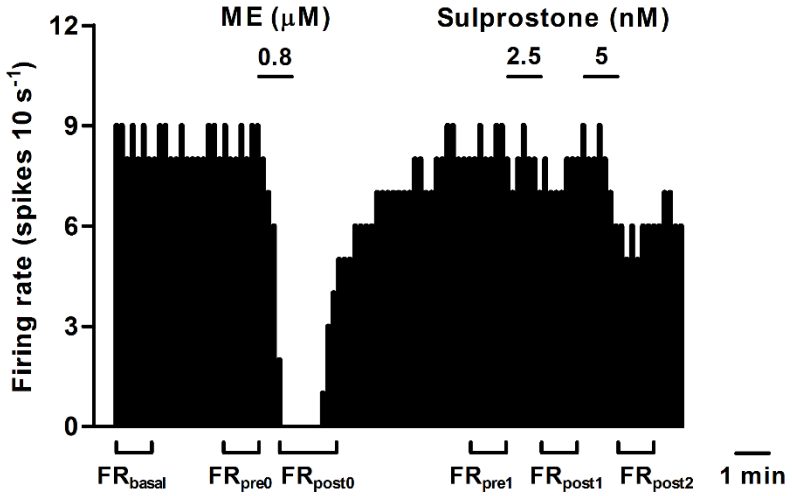

Figure 3.2. Representative example of the firing rate of an LC neuron showing the inhibitory effect of ME (0.8 μM) and sulprostone (2.5 and 5 nM). The vertical bars are the number of spikes accumulated every 10 s, whereas the horizontal lines represent the period of drug application.

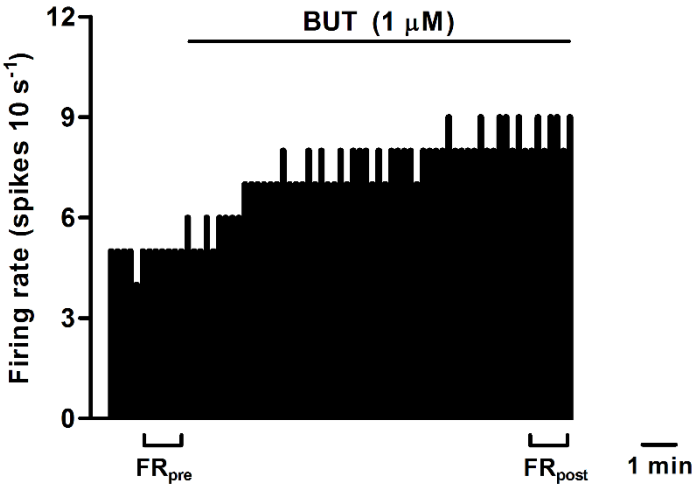

Figure 3.3. Representative example of the firing rate of an LC neuron showing the excitatory effect of butaprost (BUT, 1 μM), where the vertical bars are the number of spikes accumulated every 10 s, and the horizontal line represents the period of drug application.

To construct concentration-effect curves for the EP receptor agonists, increasing concentrations of the agonist were perfused (2 – 3x), until the maximal effect was reached. Individual experiments in each group were then fitted into a logistic three-parameter equation:

$$E = \frac{Emax}{1 + \left(\frac{EC_{50}}{A}\right)^{n}} \cdot 100$$

Where:

- E is the effect induced by each concentration of the agonist.
- A is the concentration of the agonist (nM or μM).
- E_{max} is the maximal effect (constrained to 100% in the case of the inhibitory effects, as no further inhibition could be recorded after the complete silencing of the neuron).
- EC_{50} is the concentration of the agonist needed to elicit a 50% of the maximal effect.
- *n* is the slope factor of the concentration-effect curve.

EC_{50} values from individual experiments were finally converted to negative logarithm values (pEC_{50}, M) to adjust them to a normal Gaussian distribution[363] for further statistical analysis.

Competitive antagonists compete with the agonist for the same binding site on the receptor and are their respective concentration and affinity which determines the prevalence of one or another. Ideally, increasing the concentration of the agonist would favor its action and the maximal effect will be reached. In a semi-logarithmic representation of the concentration-effect curve, the presence of a competitive antagonist produces a parallel rightward shift in the concentration-effect curve for the agonist (Figure 3.4), indicating that a higher concentration of the agonist is required to obtain the same amount of effect. Supposing that the maximal effect is not reached in the presence of the antagonist under equilibrium conditions, the antagonist most likely behaves in a non-competitive manner (Figure 3.5).

In addition to the concentration, the antagonist affinity value (pK_B) dictates the outcome of the agonist-antagonist interaction. The pK_B is the negative logarithm of the equilibrium dissociation constant of the antagonist-receptor complex (K_B). When the antagonist causes a twofold shift in the concentration-effect curve for the agonist, the pK_B is usually referred to as pA_2 (see below). A few methods could be used to determine the pK_B of a given antagonist. The most common one, the Gaddum/Schild, compares the whole curve shift. Additionally, if

more than three concentrations of the antagonist were employed, the EC_{50} displacement could be expressed graphically as the Schild plot, where the slope must be equal to one for competitive antagonists (Figure 3.4). If that is not the case, then a non-competitive binding could be assumed, and the affinity value could be derived by plotting double equieffective concentrations of the agonist in the absence and presence of the antagonist, in the so-called Gaddum method (Figure 3.5).

In the first case, the Gaddum/Schild equation allows the global fitting of the curves[364]. In this method, control experiments in the absence of the antagonist were averaged into a theoretical curve, which was compared to each individual experimental curve obtained in the presence of the antagonist.

$$Response = Bottom + \frac{(Top - Bottom)}{1 + \{10^{Log\,EC50}[1 + ([B]/10^{-pA_2})^S]/[A]\}^n}$$

Where:

- Top and Bottom is the highest and lowest asymptote of the curves.
- $logEC_{50}$ is the logarithm of EC_{50} in the absence of the antagonist.
- n is the slope.
- S is the Schild slope, which was constrained to one.
- [B] is the concentration of antagonist.
- pA_2 is the negative logarithm of the [B] that produces a 2-fold shift in the agonist EC_{50} by a factor of 2. When less than three different concentrations of the antagonist were employed, the term pA_2 was substituted by pK_B.

pK_B values for individual experiments were then grouped by the concentration of the antagonist, where a mean was extracted and compared statistically. Considering the pK_B values should not depend on the concentration of the antagonist, the pK_B values can then be pooled and averaged to yield a mean pK_B[365]. However, when differences among the pK_B values were found depending on the antagonist concentration (Table 3.3), the Schild analysis was used as an additional pK_B estimation.

The Schild analysis is based on the dextral displacement caused by the competitive antagonist in the concentration-effect curve for the agonist, which defines a concentration ratio (CR) as the ratio of equieffective agonist concentrations (Figure 3.4).

$$log(CR - 1) = log[B] - logK\mathrm{B}$$

Where:

- [B] is the concentration of the antagonist (in M).
- K_B is the equilibrium dissociation constant of an antagonist from the receptor (in M).

From the equation, it could be deduced that when the antagonist doubles the EC_{50} of the concentration-effect curve for a given agonist (CR = 2) (Figure 3.4), then log[B] would equal $logK_B$. Therefore, the pA_2 is the negative logarithm of the antagonist concentration that causes a 2-fold shift in the concentration-effect curve for the agonist. The linear relationship between log (CR – 1) and log[B] could be drawn in a Schild plot (Figure 3.4), where the pA_2 is the intercept of the *x*-axis when the ordinate value is zero (Figure 3.4). One of the advantages of the pA_2 is that it is independent of the agonist concentration[366].

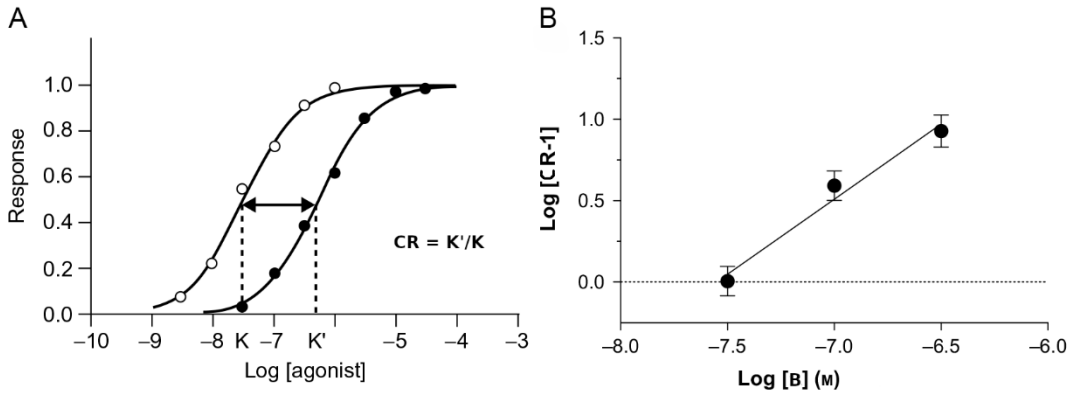

Figure 3.4. A) Simulated concentration-response curves showing the effect of an agonist in the absence (○) and presence (●) of an antagonist. The rightward shift implies that a concentration of the agonist needed to reach the EC_{50} (K) is higher in the presence of an antagonist (K'). Further, a concentration ratio (CR) could be established as the ratio of equieffective agonist concentrations[367]. B) Example of a Schild plot extracted from the literature[368]. In order to consider that an antagonist is competitive, the slope must not differ from unity.

Table 3.3. Methods employed to analyze the pK_B and comparison of the yielded pK_B values obtained with the different methods.

Receptor characte-rization	Standard agonist	EP receptor antagonist	Concen-tration	Gaddum/Schild method	Schild method	Gaddum or double equieffective concentrations
EP3	Sulprostone	+ L-798,106	3 µM	5.61 ± 0.15	-	-
			10 µM	5.93 ± 0.12	-	-
	Misoprostol	+ L-798,106	10 µM	5.91 ± 0.14	-	-
	PGE_2	+ L-798,106	10 µM	6.26 ± 0.05*	-	-
EP2	Butaprost	+ PF-04418948	3 nM	8.45 ± 0.18	-	-
			10 nM	8.34 ± 0.25	-	-
	Treprostinil	+ PF-04418948	10 nM	-	-	8.34 (95% CI: 8.29 – 8.38)
EP4	Rivenprost	+ L-161,982	3 nM	8.84 ± 0.13	8.69 (95% CI: 15.96 – 7.92) slope: 0.39 (95% CI: 0.05 – 0.72)	-
			30 nM	7.94 ± 0.24†		-
			300 nM	7.40 ± 0.08†		-
	TCS 2510	+ L-161,982	300 nM	-	-	7.69 (95% CI: 7.61 – 7.76)

Values are expressed as mean ± SEM or 95% CI. *$P < 0.05$ when compared to the pK_B values obtained with sulprostone or misoprostol as the standard agonist (one-way ANOVA followed by a Bonferroni's *post hoc* test). †$P < 0.05$ when compared to the pK_B values obtained with the different concentrations of the antagonist (one-way ANOVA followed by a Bonferroni's *post hoc* test).

On the other hand, when the Schild slope differs from unity, the generated pA_2 cannot be considered an estimate of the pK_B. Thus, either the system had not reached the equilibrium conditions, or the antagonists are non-competitive. In both cases, the maximal effect can decrease. However, in the presence of a non-competitive antagonist, high receptor reserve (very efficacious agonists that only need a fraction of the total receptor population to elicit the maximal response) may result in a parallel shift of the concentration-effect curve with no depression in the Emax[367,369]. In the case of non-competitive antagonists, the affinity measurement was obtained from the Gaddum method by plotting double equieffective concentrations of the agonist in the absence (ordinates) and presence (abscissae) of the antagonist (Figure 3.5). The concentrations were extracted from the theoretical concentration-effect curves for the agonist. Then, the equilibrium dissociation constant is calculated by:

$$K_B = [B]/(slope - 1)$$

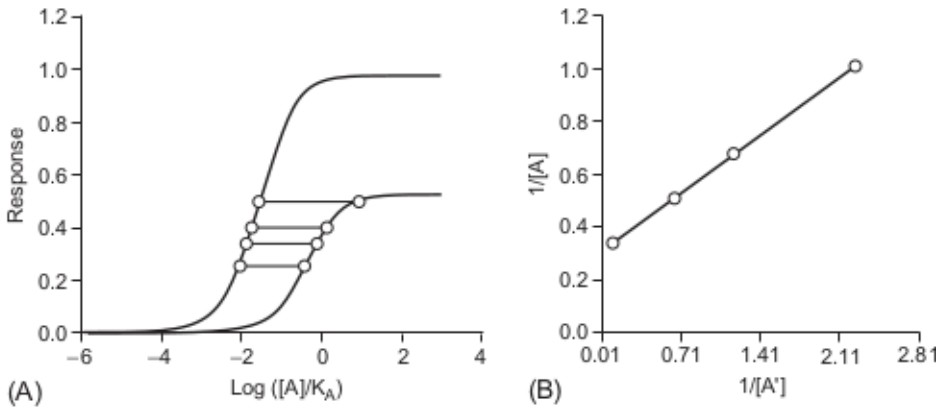

Figure 3.5. A) Concentration-effect curve for an agonist in the absence and presence of a non-competitive antagonist, which causes a decrease in the agonist maximal effect. B) Double reciprocal plot of equieffective concentrations in the presence and absence of a non-competitive antagonist.

Statistical analysis was performed by the software GraphPad Prism (5.01 for Windows), SPSS statistics (22.0.0.1 for Windows) and Microsoft Excel 2016 (16.0.4639.1000 for Windows). Data were expressed as the mean ± standard error of the mean (SEM) of *n* number of experiments. For statistical evaluation, a paired Student's t-test was used when the effects before and after the drug application were compared within the same cell or an unpaired Student's t-test when two independent groups were compared. Comparison among more than two experimental conditions was made by one-way analysis of variance (ANOVA) followed by a Dunnett's *post hoc* test or Bonferroni's Multiple Comparison test only if *F* achieved the

necessary level of statistical significance (i.e., $P < 0.05$) and there was no significant variance inhomogeneity. Dunnett's method is used for comparison with a control group and Bonferroni's test for comparison among all the groups. The threshold for considering statistical significance was set at $P = 0.05$, and only one level of probability was reported.

3.2.4.2 Calcium Time Lapse Imaging

Ca^{2+} imaging time traces were analyzed with a recently published method[278,370]. Regions of interest (ROI) were marked for all cells based on the standard deviation of fluorescence intensity over time, using a semiautomatic, adapted ImageJ script kindly provided by Dr. John Hayes (The College of William and Mary, Williamsburg, VA, USA, http://physimage.sourceforge.net/). For each frame, the mean intensity value within each ROI was measured using ImageJ, along with their coordinates. Then, the fluorescence signals were normalized to baseline values. Synchronized activity between cells was measured by the Pearson correlation with a custom-made script in MATLAB (version 9.2.0.538062 R2017a; MathWorks, Natick, MA, USA) and by the mic2net toolbox[278] (version 6.12; MathWorks). The calculated pair-wise correlation coefficients resulted in a correlation matrix that was converted to an adjacency matrix by applying a cut-off level. The cut-off level was selected by calculating the mean of the 99th percentile of correlation coefficients for a set of experiments with scrambled signals. Scrambling was performed by randomly translating all traces in the time-domain. The network structure was visualized by plotting a line between pairs of cells, where the color of the lines was proportionate to the correlation coefficient. The degree of connections within a network (connectivity) was defined as the number of cell pairs with a correlation coefficient larger than the cut-off value divided by the total number of cell pairs. PreBötC cells are organized in a small-world structure[97] formed by hubs or nodes connected in clusters and allowing high connectivity efficiency with a minimal connection cost[371]. The information travels from one node to another, so that the parameter mean shortest path length (λ) could be defined as the minimum number of nodes that must be passed in between. In addition, the mean clustering coefficient (σ) is the number of neighbors of a node that are also neighbors of each other. Finally, as the small-world parameter (γ) equals σ/λ[278] these networks are defined by short distance λ and high σ (For further details see figure 1.11 in the introduction section). The parameters were calculated by using the MATLAB BGL library (http://www.mathworks.com/matlabcentral/fileexchange/10922) and compared to the corresponding randomized networks. For each ROI a baseline fluorescence was determined (F0), which was used to normalize the change in fluorescence as $\Delta F/F0$, where $\Delta F=F1-F0$,

being F1 is the specific fluorescence intensity at a specific time point, and F0 is the average intensity of 30 s before and after F1. A previously published toolbox was used for the frequency analysis of time traces by the Fourier transform[372]. Data were further processed in GraphPad Prism 5.01 (GraphPad Software, Inc., USA) to create the figures.

Since the preBötC is constituted by a heterogeneous population of cells and some of them were found insensitive to DAMGO[283], the cells were sorted out into two groups depending on their behavior within the first 5 minutes of drug application. The behavior was defined as either decreased or increased Ca^{2+} oscillation frequency compared to control. This analysis allowed the proportion of cells that were affected by the drug in a certain way to be calculated. Then, the behavior of single cells could be followed.

Experiments were excluded based on the following criteria: low dye loading, the total number of cells per slice less than 20, standard deviation (SD) at the control period higher than the 50% of the mean frequency, and peaks of maximum amplitude in the Fourier transform of calcium oscillation signal above 200 mHz.

For statistical evaluation, a paired Student's t-test was used when the effects before and after the drug application were compared within the same cell or an unpaired Student's t-test when two independent groups were compared. Comparisons among more than two experimental conditions by one-way analysis of variance (ANOVA) followed by a Dunnett's *post hoc* for comparison with a control group and only if F achieved the necessary level of statistical significance (i.e., $P < 0.05$) and there was no significant variance inhomogeneity. All calculations for the statistical tests were conducted with Microsoft Excel 2016 (16.0.4639.1000 for Windows), LibreOffice Calc (6.0.7.3 for Ubuntu), and GraphPad Prism (5.01 for Windows). In all cases, $P < 0.05$ was considered statistically significant. Data are presented as mean ± SD.

4 RESULTS

4.1 STUDY I – INHIBITION OF RAT LOCUS COERULEUS NEURONS VIA PROSTAGLANDIN E_2 EP3 RECEPTOR: PHARMACOLOGICAL CHARACTERIZATION *IN VITRO*

The results of this study are going to be submitted to the British Journal of Pharmacology. The written version of the manuscript has been attached in the section of accompanying manuscripts.

Effect of the EP3 receptor agonist sulprostone on the firing rate of LC neurons

EP3 receptors are expressed in catecholaminergic neurons of the brain, including the LC[65]. To investigate the effect of EP3 receptor activation on the firing rate of LC neurons, we performed concentration-effect curves for sulprostone, an EP3 receptor agonist that shows more than 300-fold higher affinity for the EP3 receptor than for the EP1 receptor[357]. Increasing concentrations of sulprostone (1.25 – 320 nM, 2x, 1 min each) inhibited the neuronal activity of LC cells in a concentration-dependent manner with an EC_{50} value of 14.8 nM (Figures 4.1A and C; Table 4.1). Complete inhibition of the firing rate of noradrenergic cells was achieved at the highest concentration of sulprostone used (20 – 320 nM) and persisted for 265 ± 53 s on average (n = 9).

In order to study the EP receptor involved in the sulprostone-induced inhibitory effect, concentration-effect curves for sulprostone (0.15 nM – 1.28 μM) were performed in the presence of the EP3 receptor antagonist (L-798,106), the EP2 receptor antagonist (PF-04418948) or the EP4 receptor antagonist (L-161,982) at 3 and 10 μM. Perfusion with L-798,106 (3 μM) for 30 min did not change the firing rate of LC neurons, but reduced the steepness of the concentration-effect curve for sulprostone (Figure 4.1C; Table 4.1). Moreover, a higher concentration of L-798,106 (10 μM, 10 min) reduced by 17.7 ± 3.8 % the firing rate of LC neurons (n = 6, $P < 0.05$ compared to baseline) and shifted by 8 fold to the right the concentration-effect curve for sulprostone (Figures 4.1B and C; Table 4.1). The apparent affinity of L-798,106 for the EP3 receptor (pK_B) was calculated to be 5.77 ± 0.10 (n = 12).

In contrast, the EP2 receptor antagonist PF-04418948 (3 μM) failed to cause significant changes in the firing rate or any rightward shift in the concentration-effect curve for sulprostone (Figure 4.2B; Table 4.1). Indeed, unexpectedly, the highest concentration of PF-04418938 (10 μM) produced a 4-fold leftward shift in the concentration-effect curve for sulprostone (Figures 4.2A and B; Table 4.1). Similar to the EP2 receptor antagonist, perfusion with the EP4 receptor antagonist L-161,982 (3 and 10 μM) failed to change the firing rate or to shift to the right the concentration-effect curve for sulprostone (Figures 4.2C and D; Table 4.1). Altogether, these results indicate that the inhibitory effect of sulprostone on the firing rate of LC neurons is mainly mediated by the EP3 receptor.

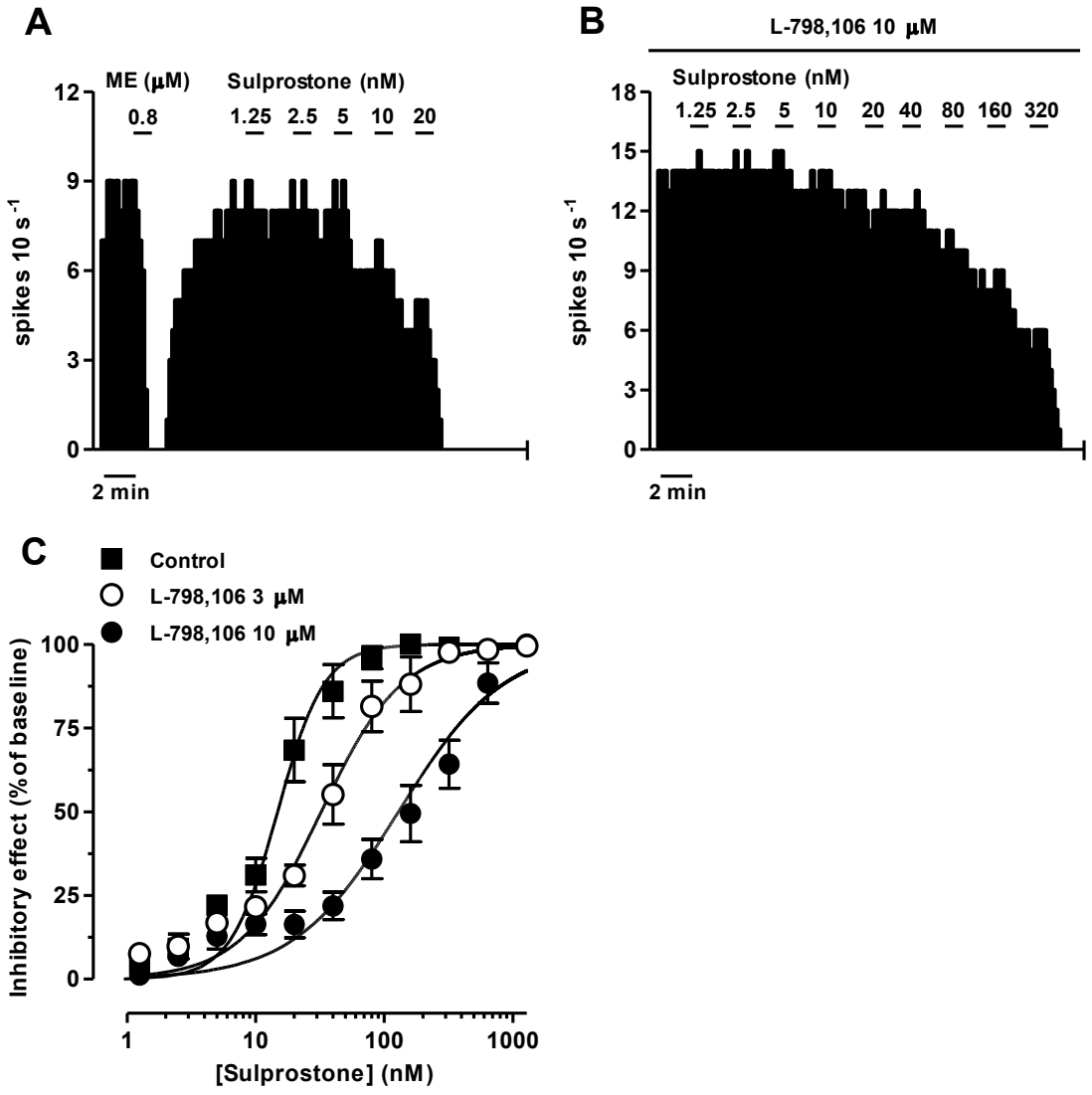

Figure 4.1. Effect of the EP3 receptor agonist sulprostone on the firing rate of LC neurons in the absence or presence of the EP3 receptor antagonist L-798,106. **(A, B)** Representative examples of firing rate recordings of two LC neurons showing the effect of increasing concentrations of sulprostone in the absence **(A)** and presence of L-798,106 (10 μM) **(B)**. The vertical lines represent the number of spikes recorded every 10 s and the

horizontal bars the period of drug application. **(C)** Concentration-effect curves for sulprostone in control (filled squares) and in the presence of L-798,106 (3 μM, open circles or 10 μM, filled circles). The horizontal axis shows the sulprostone concentration on a semi-logarithmic scale. The vertical axis expresses the reduction in firing rate of LC neurons as the percentage of the baseline. Data points are the mean ± SEM at each sulprostone concentration obtained from *n* number of experiments. The lines through the data are the theoretical curves in each group constructed from the mean of the individual concentration-effect curve parameters, as estimated by nonlinear regressions. Note that the concentration-effect curve for sulprostone is shifted to the right by the EP3 receptor antagonist.

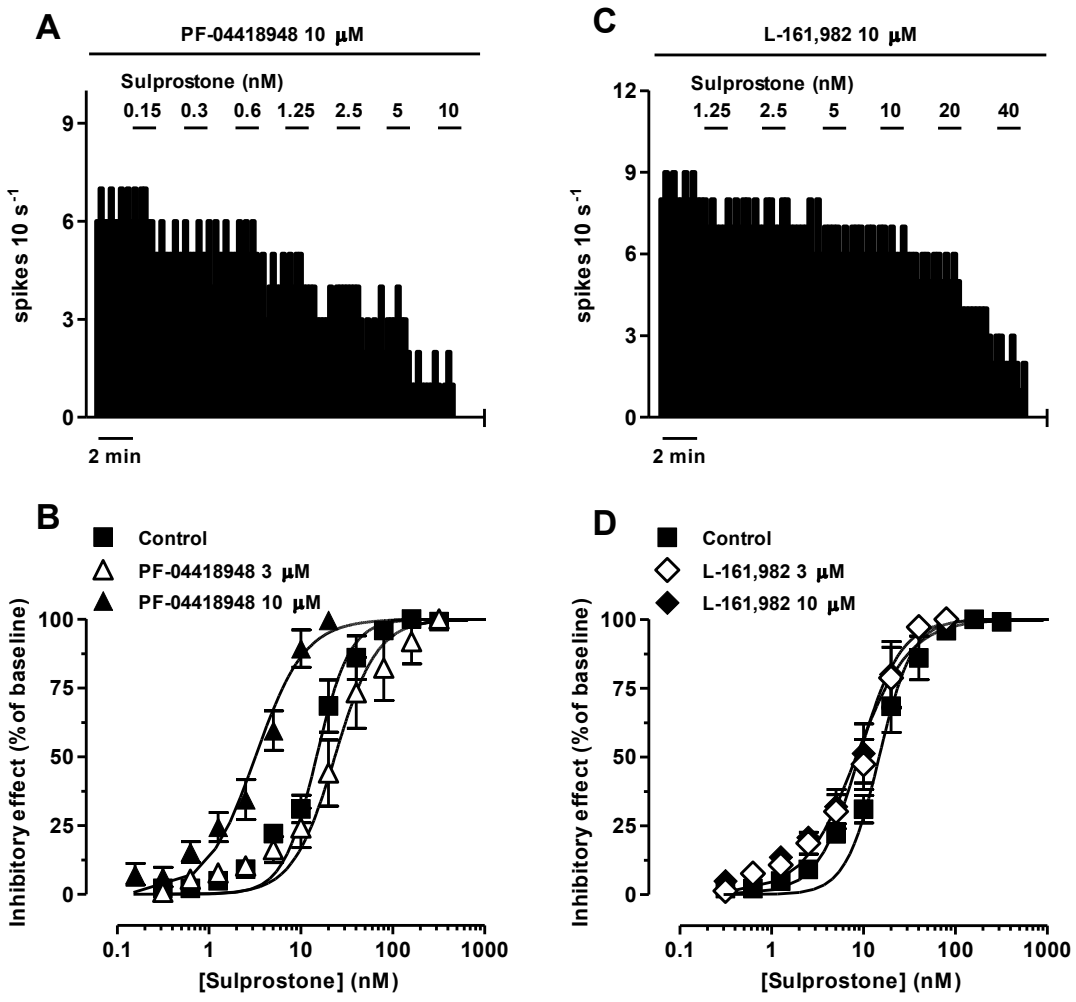

Figure 4.2. Effect of the EP3 receptor agonist sulprostone on the firing rate of LC neurons in the presence of the EP2 receptor antagonist PF-04418948 or the EP4 receptor antagonist L-161,982. **(A, B)** Representative examples of firing rate recordings of two LC neurons showing the effect of increasing concentrations of sulprostone in the presence of PF-04418948 (10 μM) **(A)** or L-161,982 (10 μM) **(B)**. **(C, D)** Concentration-effect curves for sulprostone in control (filled squares) and in the presence of PF-04418948 (3 μM, open triangles or 10 μM, filled triangles) **(C)** or L-161,982 (3 μM, open diamonds or 10 μM, filled diamonds) **(D)**. The horizontal axis shows the sulprostone concentration on a semi-logarithmic scale. The vertical axis expresses the reduction in firing rate of LC neurons as the percentage of the baseline. Data points are the mean ± SEM at

each sulprostone concentration obtained from *n* number of experiments. The lines through the data are the theoretical curves in each group constructed from the mean of the individual concentration-effect curve parameters, as estimated by nonlinear regressions.

Table 4.1. Basal firing rate and concentration-effect curve parameters for the inhibitory action of the EP3 receptor agonist sulprostone on LC neurons in the absence (control) or in the presence of the EP3 (L-798,106), EP2 (PF-04418948), and EP4 (L-161,982) receptor antagonists.

			Concentration-effect curves[1]			
Drugs	Concentration	Basal firing rate (Hz)	pEC_{50} (M)	(EC_{50}, nM)	Slope factor	*n*
Sulprostone						
Control		0.84 ± 0.07	7.83 ± 0.08	(14.8)	2.39 ± 0.37	9
+ L-798,106	3 µM	0.64 ± 0.11	7.49 ± 0.09	(32.4)	1.39 ± 0.16*	6
	10 µM	0.87 ± 0.22	6.89 ± 0.11*	(128)	1.07 ± 0.12*	6
+ PF-04418948	3 µM	0.66 ± 0.11	7.63 ± 0.15	(23.5)	1.89 ± 0.14	6
	10 µM	0.58 ± 0.08	8.49 ± 0.10*	(3.25)	1.61 ± 0.21	5
+ L-161,982	3 µM	0.64 ± 0.11	8.05 ± 0.11	(8.93)	1.92 ± 0.36	5
	10 µM	0.71 ± 0.12	8.08 ± 0.11	(8.34)	1.49 ± 0.11	5

[1]Values are expressed as mean ± SEM obtained by nonlinear regression of *n* cells. Maximal effect values were 100% in all cases. pEC_{50} is the negative logarithm of the concentration needed to elicit 50% of the maximal effect. *$P < 0.05$ when compared to the control group (one-way ANOVA followed by a Dunnett's *post hoc* test).

Effect of PGE_2 and the PGE_1 analog misoprostol on the firing rate of LC neurons

To study whether the endogenous PGE_2 and the PGE_1 synthetic analog misoprostol mimic the inhibitory effect observed with sulprostone on the firing rate of LC cells, we performed concentration-effect curves for PGE_2 and misoprostol. PGE_2 (0.31 nM – 1.28 μM, 2x, 1 min each) concentration-dependently inhibited the firing rate of LC neurons with the EC_{50} being 110 nM (Figures 4.3A and C; Table 4.2). Likewise, misoprostol (0.31 – 320 nM, 2x, 1 min each) inhibited the neuronal activity of LC cells with an EC_{50} of 50.7 nM (Figures 4.4A and C; Table 4.2).

Perfusion with the EP3 receptor antagonist L-798,106 (10 μM) displaced by 19 and 9 fold, respectively, to the right the concentration-effect curves for PGE_2 (0.31 nM – 10.2 μM) and misoprostol (0.31 nM – 2.56 μM) (both $n = 5$, $P < 0.05$; Figures 4.3B and C, 4.4B and C; Table 4.2). When PGE_2 was used as the standard agonist, the pK_B value for L-798,106 was higher ($pK_B = 6.26 \pm 0.05$; $n = 5$, $P < 0.05$, one-way ANOVA followed by Bonferroni's Multiple Comparison test) than that with sulprostone (see above). However, the pK_B value estimated for L-798,106 with misoprostol ($pK_B = 5.91 \pm 0.14$; $n = 5$, $P > 0.05$) was not different from that obtained with sulprostone. On the other hand, administration of a combination of the EP2 receptor antagonist PF-04418948 (10 μM) and the EP4 receptor antagonist L-161,982 (10 μM) caused a more than 6-fold leftward shift in the concentration-effect curve for PGE_2 ($n = 5$, $P < 0.05$; Figure 4.3C; Table 4.2). However, both antagonists in combination did not produce any shift in the concentration-effect curve for misoprostol (Figures 4.4C; Table 4.2). Finally, none of these antagonists changed the slope of the concentration-effect curves. As a whole, these results suggest that the endogenous ligand PGE_2 and the PGE_1 analog misoprostol inhibit the activity of LC neurons, preferentially through the EP3 receptor. In addition, administration of the EP2 and EP4 receptor antagonists apparently potentiate the inhibitory effect of PGE_2.

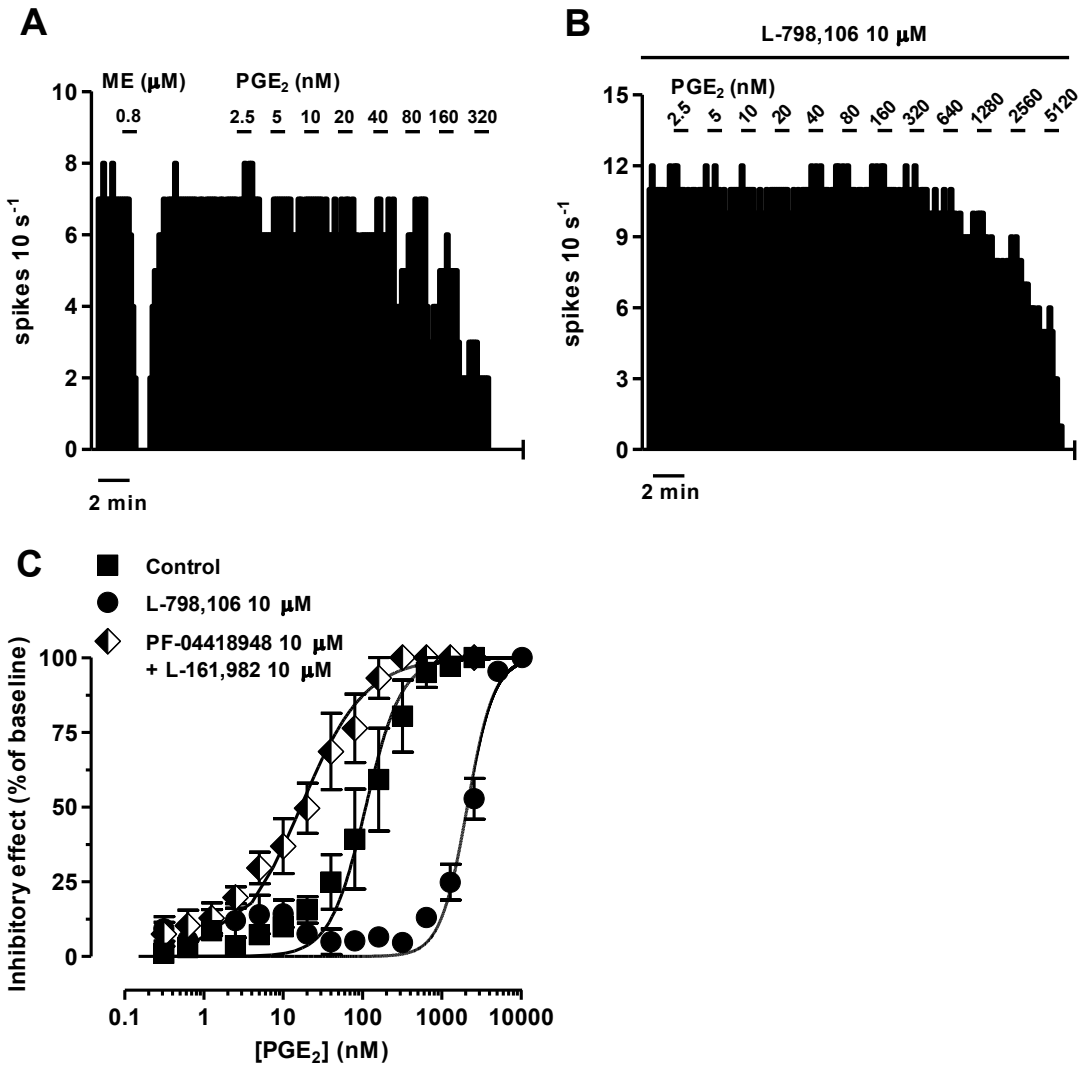

Figure 4.3. Effect of PGE_2 on the firing rate of LC neurons in the absence or presence of the EP3 receptor antagonist L-798,106 or a combination of the EP2 receptor antagonist PF-04418948 and the EP4 receptor antagonist L-161,982. **(A, B)** Representative examples of firing rate recordings of two LC neurons showing the effect of increasing concentrations of PGE_2 in the absence **(A)** and presence of L-798,106 (10 μM) **(B)**. The vertical lines represent the number of spikes recorded every 10 s and the horizontal bars the period of drug application. **(C)** Concentration-effect curves for PGE_2 in control (filled squares) and in the presence of L-798,106 (10 μM, filled circles) or PF-04418948 and L-161,982 (10 μM each, half-filled diamonds). The horizontal axis shows the PGE_2 concentration on a semi-logarithmic scale. The vertical axis expresses the reduction in firing rate of LC neurons as the percentage of the baseline. Data points are the mean ± SEM at each PGE_2 concentration obtained from *n* number of experiments. The lines through the data are the theoretical curves in each group constructed from the mean of the individual concentration-effect curve parameters, as estimated by nonlinear regressions. Note that the concentration-effect curve for PGE_2 is shifted to the right by the EP3 receptor antagonist and to the left by the EP2 and EP4 receptor antagonists.

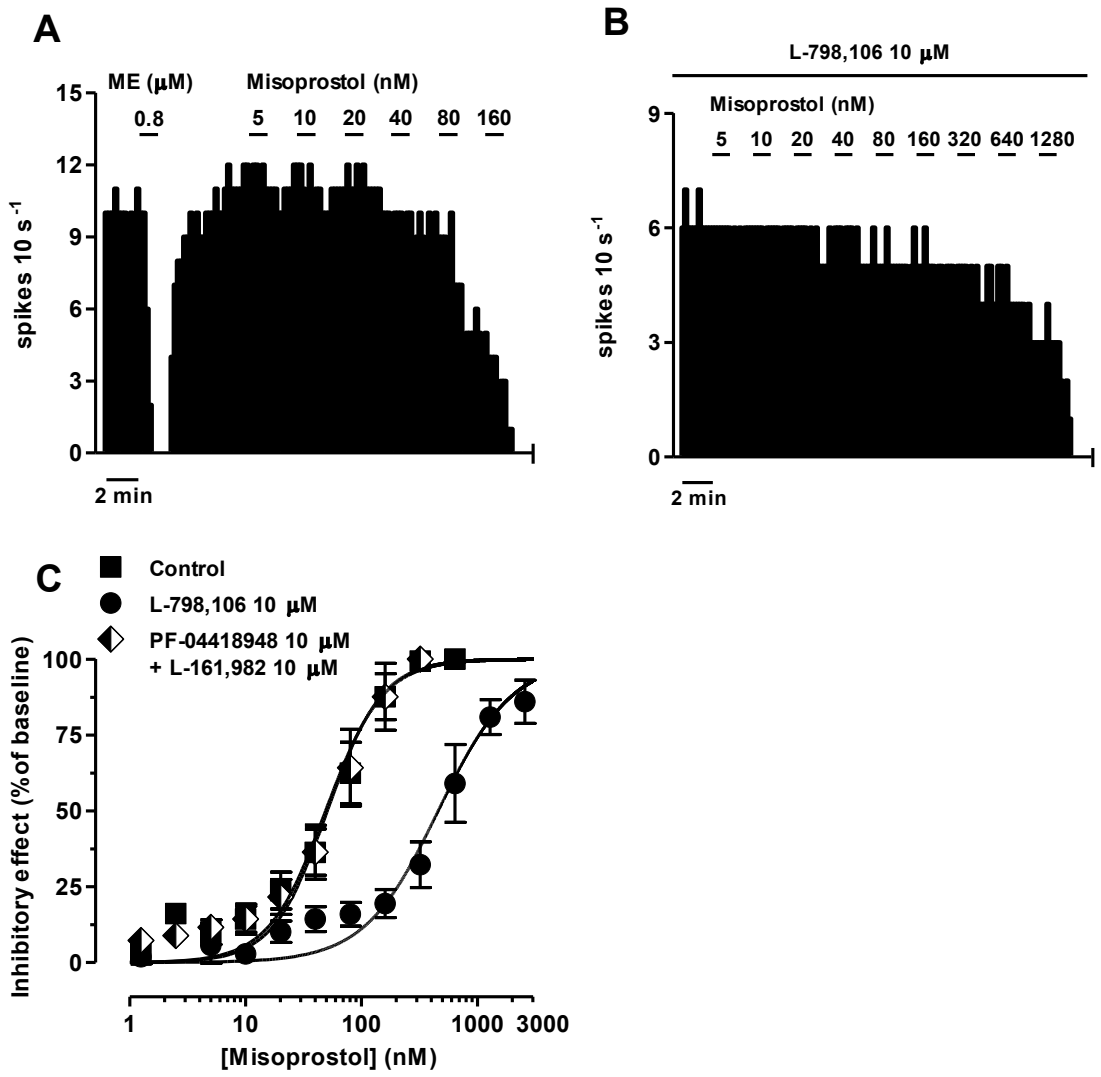

Figure 4.4. Effect of misoprostol on the firing rate of LC neurons in the absence or presence of the EP3 receptor antagonist L-798,106 or a combination of the EP2 receptor antagonist PF-04418948 and the EP4 receptor antagonist L-161,982. **(A, B)** Representative examples of firing rate recordings of two LC neurons showing the effect of increasing concentrations of misoprostol in the absence **(A)** and presence of L-798,106 (10 μM) **(B)**. The vertical lines represent the number of spikes recorded every 10 s and the horizontal bars the period of drug application. **(C)** Concentration-effect curves for misoprostol in control (filled squares) and in the presence of L-798,106 (10 μM, filled circles) or PF-04418948 and L-161,982 (10 μM each, half-filled diamonds). The horizontal axis shows the misoprostol concentration on a semi-logarithmic scale. The vertical axis expresses the reduction in firing rate of LC neurons as the percentage of the baseline. Data points are the mean ± SEM at each misoprostol concentration obtained from *n* number of experiments. The lines through the data are the theoretical curves in each group constructed from the mean of the individual concentration-effect curve parameters, as estimated by nonlinear regressions. Note that the concentration-effect curve for misoprostol is shifted to the right by the EP3 receptor antagonist.

Table 4.2. Basal firing rate and concentration-effect curve parameters for the inhibitory action of the EP3 receptor agonists PGE_2 and misoprostol on LC neurons in the absence (control) or in the presence of the EP3 (L-798,106) or a combination of the EP2 (PF-04418948) and EP4 (L-161,982) receptor antagonists.

			Concentration-effect curves[1]			
Drugs	Concentration	Basal firing rate (Hz)	pEC_{50} (M)	(EC_{50}, nM)	Slope factor	*n*
PGE_2						
Control		0.76 ± 0.10	6.96 ± 0.20	(110)	1.92 ± 0.36	5
+ L-798,106	10 µM	0.87 ± 0.14	5.68 ± 0.05*	(2098)	2.55 ± 0.47	5
+ PF-04418948 L-161,982	10 µM 10 µM	0.83 ± 0.24	7.78 ± 0.19*	(16.6)	1.07 ± 0.06	5
Misoprostol						
Control		0.80 ± 0.12	7.30 ± 0.13	(50.7)	1.85 ± 0.30	5
+ L-798,106	10 µM	0.67 ± 0.11	6.34 ± 0.12*	(455)	1.36 ± 0.28	5
+ PF-04418948 L-161,982	10 µM 10 µM	0.72 ± 0.11	7.31 ± 0.12	(49.5)	1.76 ± 0.33	5

[1]Values are expressed as mean ± SEM obtained by nonlinear regression of *n* cells. Maximal effect values were 100% in all cases. pEC_{50} is the negative logarithm of the concentration needed to elicit 50% of the maximal effect. *$P < 0.05$, when compared to their respective control group (one-way ANOVA followed by a Dunnett's *post hoc* test).

Molecular mechanisms involved in the effect of EP3 receptor agonists on the firing rate of LC neurons

The EP3 receptor has been shown to be coupled to $G_{i/o}$ protein[373] and GIRK channels[374]. Thus, to identify the molecular mechanisms involved in the EP3 receptor-mediated inhibition of firing rate of LC cells, we performed concentration-effect curves for sulprostone (0.31 nM – 1.28 µM, 2x) in slices incubated for 18 h with the irreversible $G_{i/o}$ protein blocker pertussis toxin (PTX, 500 ng ml^{-1}). In order to confirm that PTX had effectively blocked the $G_{i/o}$ protein, only cells with a reduced inhibitory response (inhibition <80% of basal firing rate) to the $G_{i/o}$-coupled MOR agonist ME (0.8 µM, 1 min) were selected to perform the concentration-effect curves for sulprostone. Moreover, proper drug perfusion was tested with GABA (1 mM, 1 min), which has been shown to fully inhibit the firing rate through $GABA_A$ ionotropic receptors. Thus, overnight treatment of the slices with PTX shifted by 6 fold to the right the concentration-effect curve for sulprostone (n = 5, P < 0.05), without affecting the maximal response or the basal firing rate (Figures 4.5A, D; Table 4.3).

To study the involvement of GIRK channels, we performed concentration-effect curves for sulprostone (0.31 nM – 2.56 µM, 2x) in the presence of the non-selective GIRK channel blocker $BaCl_2$ or the selective GIRK2 gating inhibitor SCH-23390. Since ME-induced inhibitory effect depends on the opening of GIRK channels, ME (0.8 µM, 1 min) was previously applied in the presence of the GIRK channel blockers to confirm the blockade action. Thus, GIRK channel blockade with Ba^{2+} (300 µM, 15 min) and SCH-23390 (15 µM, 30 min) reduced the inhibitory effect of ME by 29.6 ± 6.3% (n = 5, P < 0.05; Figure 4.5B) and by 25.2 ± 8.6% (n = 5, P < 0.05; Figure 4.5C), respectively, as previously described[158,375]. Bath perfusion with $BaCl_2$ (300 µM, 15 min) increased the firing rate of LC neurons by 42.6 ± 13.1% (n = 5, P < 0.05 compared to baseline) and shifted by 3 fold to the right the concentration-effect curve for sulprostone (n = 5, P < 0.05; Figures 4.5B, D; Table 4.3). Likewise, bath administration of SCH-23390 (15 µM, 30 min) increased the firing activity of LC neurons by 144 ± 57% (n = 5, P < 0.05 compared to baseline) and shifted by 2 fold to the right the concentration-effect curve for sulprostone (n = 5, P < 0.05; Figures 4.5C, D; Table 4.3). $BaCl_2$ and SCH-23390 slightly reduced the maximal effect of sulprostone, but these changes did not reach statistical significances (Table 4.3). These results suggest that EP3 receptor activation inhibits the LC neuronal activity through activation of $G_{i/o}$ proteins and GIRK channels.

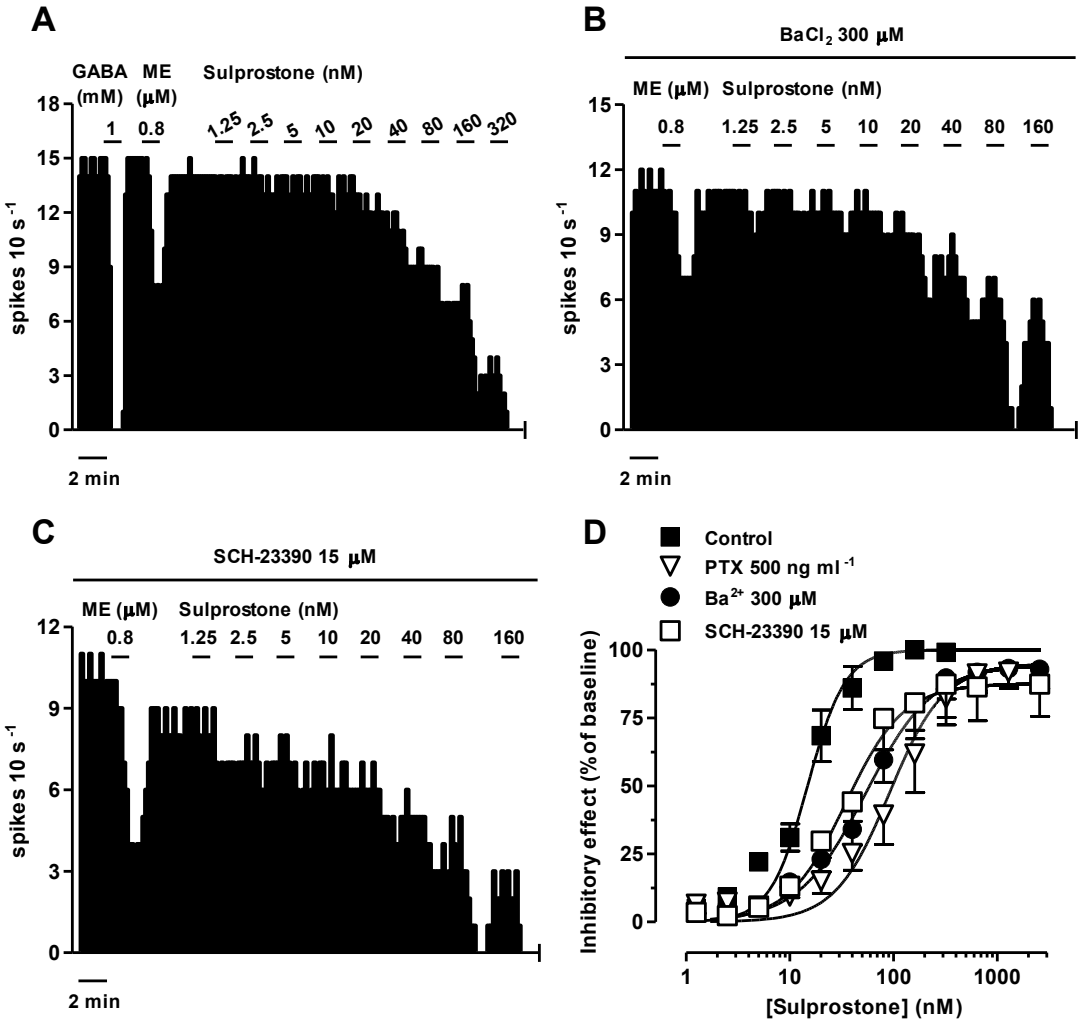

Figure 4.5. Effect of sulprostone on the firing rate of LC neurons after overnight treatment of the slices with the $G_{i/o}$ inhibitor pertussis toxin (PTX) or in the presence of the GIRK blockers Ba^{2+} or SCH-23390. Representative examples of firing rate recordings of three LC neurons showing the effect of increasing concentrations of sulprostone after overnight treatment with PTX (500 ng ml^{-1}) **(A)** or in the presence of $BaCl_2$ (300 μM) **(B)** or SCH-23390 (15 μM) **(C)**. The vertical lines represent the number of spikes recorded every 10 s and the horizontal bars the period of drug application. Note that the effect of ME (0.8 μM) is reduced compared to control (see Figure 4.1) while the inhibitory effect of GABA (1 mM) is maintained (A). **(D)** Concentration-effect curves for sulprostone in control (filled squares) or after overnight treatment with PTX (500 ng ml^{-1}, open triangles) or in the presence of Ba^{2+} (300 μM, filled circles) or SCH-23390 (15 μM, open squares). The vertical axis expresses the reduction in firing rate of LC as the percentage of the baseline. Data points are the mean ± SEM at each sulprostone concentration obtained from *n* number of experiments. The lines through the data are the theoretical curves in each group constructed from the mean of the individual concentration-effect curve parameters, as estimated by nonlinear regressions. Note that the concentration-effect curve for sulprostone is shifted to the right by PTX, Ba^{2+}, and SCH-23390.

Table 4.3. Basal firing rate and concentration-effect curve parameters for the inhibitory action of sulprostone on LC neurons in the absence (control) or in the presence of PTX, $BaCl_2$, and SCH-23390.

			Concentration-effect curves[1]				
Drugs	Concentration	Basal firing rate (Hz)	Emax (%)	pEC_{50} (M)	(EC_{50}, nM)	Slope factor	*n*
Sulprostone							
Control		0.84 ± 0.07	100	7.83 ± 0.08	(14.8)	2.39 ± 0.37	9
+ PTX	500 ng ml^{-1}	1.12 ± 0.18	94.9	7.04 ± 0.15*	(90.9)	1.65 ± 0.28	5
+ $BaCl_2$	300 µM	1.03 ± 0.13	94.6	7.27 ± 0.09*	(53.7)	1.37 ± 0.18	5
+ SCH-23390	15 µM	1.37 ± 0.28	87.5	7.46 ± 0.05*	(34.6)	1.56 ± 0.17	5

[1]Values are expressed as mean ± SEM obtained by nonlinear regression of *n* cells. Emax is the maximal inhibitory effect, and pEC_{50} is the negative logarithm of the concentration needed to elicit 50% of the Emax. *$P < 0.05$ when compared to the control group (one-way ANOVA followed by a Dunnett's *post hoc* test).

4.2 STUDY II – PHARMACOLOGICAL CHARACTERIZATION OF PROSTANOID EP2 RECEPTOR IN RAT LOCUS COERULEUS NEURONS *IN VITRO*

The results of this study are going to be submitted to the British Journal of Pharmacology. The written version of the manuscript has been attached in the section of accompanying manuscripts.

Effect of the EP2 receptor agonist butaprost on the firing rate of LC neurons

In the brainstem, the EP2 receptor is expressed almost exclusively in the LC[57], but its functional role remains unknown. To investigate the effect of EP2 receptor activation on the firing rate of LC neurons, we performed concentration-effect curves for the EP2 receptor agonist butaprost (10 nM – 10 μM). Administration of increasing concentrations of butaprost (10 nM – 10 μM, 3x, 15 min each) increased the firing rate of LC neurons (from 0.85 ± 0.09 Hz to 1.38 ± 0.11 Hz; $n = 8$, $P < 0.05$) in a concentration-dependent manner with an EC_{50} value of 0.45 μM (Figures 4.6A and C; Table 4.4).

To elucidate which EP receptor was mediating the excitatory effect observed with butaprost, we constructed concentration-effect curves for this EP2 receptor agonist in the presence of the EP2 receptor antagonist PF-04418948 (3 and 10 nM) or a combination of the EP3 receptor antagonist L-798,106 (10 nM) and the EP4 receptor antagonist L-161,982 (10 nM). Bath application of PF-04418948 (3 and 10 nM) for 30 min did not change the firing rate, but the highest concentration (10 nM) shifted by 6 fold ($n = 6$, $P < 0.05$) to the right the concentration-effect curve for butaprost without affecting the maximal effect significantly (Figures 4.6B and C; Table 4.4). The calculated affinity for the EP2 receptor antagonist (pK_B) was 8.39 ± 0.16 ($n = 11$). On the other hand, perfusion with a combination of L-798,106 and L-161,982 (10 nM each) for 30 min did not change the firing activity or shift to the right the concentration-effect curve for butaprost (Figures 4.7A and B; Table 4.4). There was a trend for the Emax to be higher after the combination of L-798,106 and L-161,982, but this increase was not significant (Figure 4.7B; Table 4.4). Altogether, these results suggest that butaprost increased the LC neuronal activity via activation of the EP2 receptor.

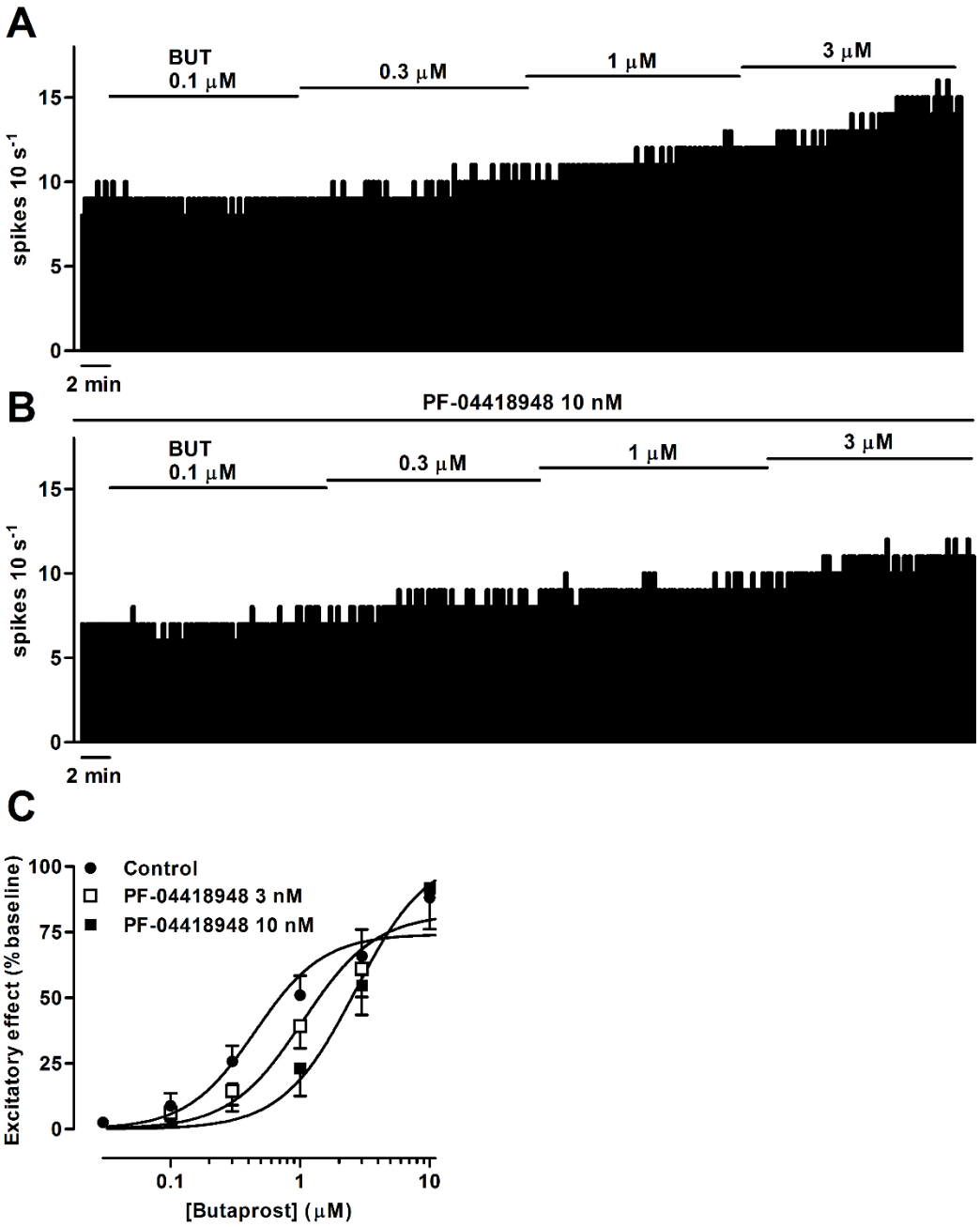

Figure 4.6. Effect of the EP2 receptor agonist butaprost on the firing rate of LC neurons in the absence or presence of the EP2 receptor antagonist PF-04418948. **(A, B)** Representative examples of firing rate recordings of LC neurons showing the effect of increasing concentrations of butaprost in the absence **(A)** and presence of PF-04418948 (10 nM) **(B)**. The vertical lines represent the number of spikes recorded every 10 s and the horizontal bars the period of drug application. **(C)** Concentration-effect curves for butaprost in control (filled circles) and in the presence of PF-04418948 (3 nM, open squares or 10 nM, filled squares). The horizontal axis shows the butaprost concentration on a semi-logarithmic scale. The vertical axis expresses the increase in firing rate of LC neurons as the percentage of the baseline. Data points are the mean ± SEM at each butaprost concentration obtained from *n* number of experiments (see Table 4.4). The lines through the data are the theoretical curves in each group constructed from the mean of the individual concentration-effect curve parameters, as estimated by nonlinear regressions. Note that the concentration-effect curve for butaprost is shifted to the right by the EP2 receptor antagonist.

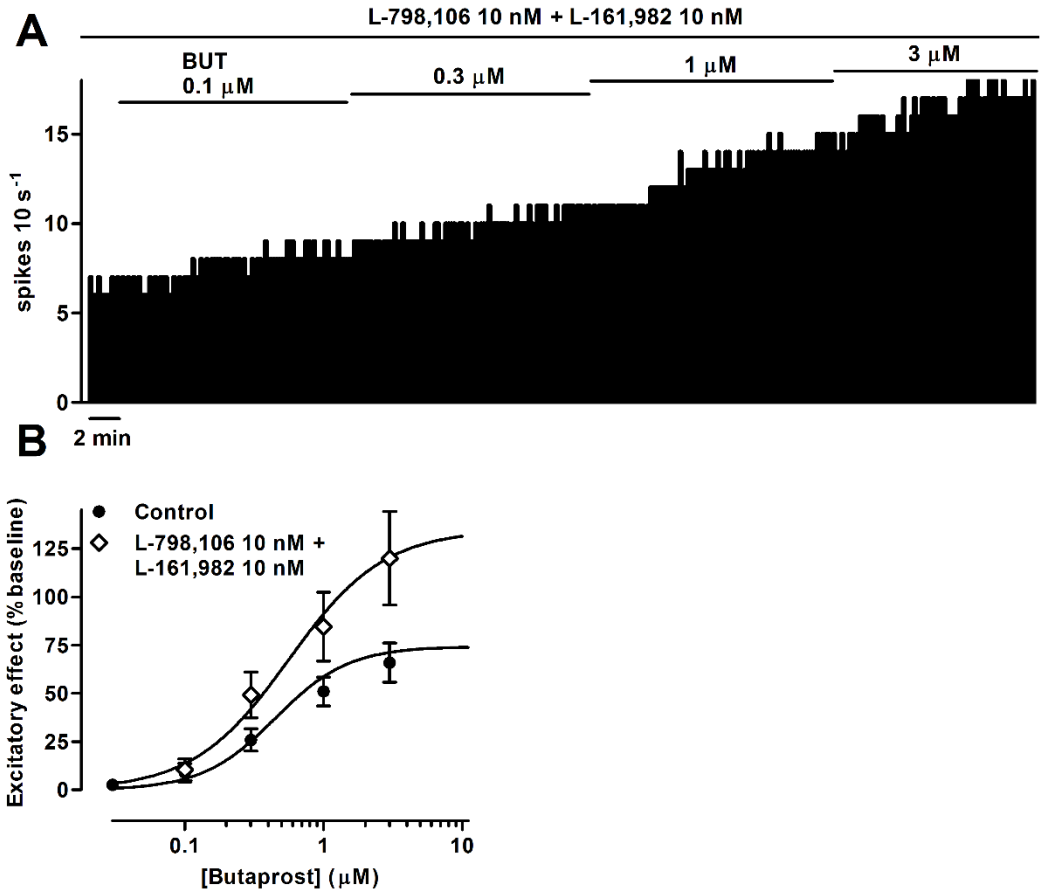

Figure 4.7. Effect of the EP2 receptor agonist butaprost on the firing rate of LC neurons in the presence of a combination of the EP3 receptor antagonist L-798,106 and EP4 receptor antagonist L-161,982. **(A)** Representative example of the firing rate recording of an LC neuron showing the effect of increasing concentrations of butaprost in the presence of L-798,106 and L-161,982 (10 nM each). The vertical lines represent the number of spikes recorded every 10 s and the horizontal bars the period of drug application. **(B)** Concentration-effect curves for butaprost in control (filled circles) and in the presence of L-798,106 and L-161,982 (10 nM each, open diamonds). The horizontal axis shows the butaprost concentration on a semi-logarithmic scale. The vertical axis expresses the increase in firing rate of LC neurons as the percentage of the baseline. Data points are the mean ± SEM at each butaprost concentration obtained from *n* number of experiments (see Table 4.4). The lines through the data are the theoretical curves in each group constructed from the mean of the individual concentration-effect curve parameters, as estimated by nonlinear regressions.

Table 4.4. Basal firing rate and concentration-effect curve parameters for the excitatory action of the EP2 receptor agonists butaprost and treprostinil on LC neurons in the absence (control) or in the presence of the EP2 (PF-04418948) or a combination of the EP3 (L-798,106) and EP4 (L-161,982) receptor antagonists.

			Concentration-effect curves[1]				
Drugs	Concentration	Basal firing rate (Hz)	Emax (%)	pEC_{50} (M)	(EC_{50}, μM)	Slope factor	*n*
Butaprost							
Control		0.85 ± 0.09	74.3 ± 11.6	6.35 ± 0.10	(0.45)	1.65 ± 0.41	8
+ PF-04418948	3 nM	0.87 ± 0.12	82.1 ± 18.4	5.98 ± 0.15	(1.05)	1.55 ± 0.30	5
	10 nM	0.73 ± 0.08	105 ± 15	5.57 ± 0.08*	(2.67)	1.55 ± 0.41	6
+ L-798,106	10 nM						
L-161,982	10 nM	0.67 ± 0.11	135 ± 29	6.25 ± 0.07	(0.56)	1.27 ± 0.14	5
Treprostinil							
Control		0.68 ± 0.07	81.3 ± 6.5	6.27 ± 0.15	(0.54)	0.95 ± 0.12	6
+ PF-04418948	10 nM	0.78 ± 0.13	42.8 ± 8.1*	6.55 ± 0.19	(0.28)	1.29 ± 0.34	6
+ L-798,106	10 nM						
L-161,982	10 nM	0.80 ± 0.12	144 ± 8*	6.34 ± 0.12	(0.46)	1.20 ± 0.09	5

[1]Values are expressed as mean ± SEM obtained by nonlinear regression of *n* cells. Emax is the maximal excitatory effect, and pEC_{50} is the negative logarithm of the concentration needed to elicit 50% of the Emax. *$P < 0.05$ when compared to their respective control group (one-way ANOVA followed by a Dunnett's *post hoc* test).

Effect of the PGI_2 analog treprostinil on the firing rate of LC neurons

To further study the effect of EP2 receptor activation in the LC, we used the PGI_2 analog treprostinil, a clinically relevant drug that shows high affinity for the EP2 receptor in binding studies[358]. Thus, administration of increasing concentrations of treprostinil (30 nM – 10 μM, 3x, 15 min each concentration) induced an excitatory effect on the firing rate of LC neurons in a concentration-dependent manner (from 0.68 ± 0.07 Hz to 1.22 ± 0.17 Hz; $n = 6$, $P < 0.05$). The EC_{50} value for the concentration-effect curve for treprostinil was 0.54 μM (Figures 4.8A and C; Table 4.4).

Considering that treprostinil has a high affinity for other prostanoid receptors, we assessed whether the observed excitatory response was produced by the activation of the EP2 receptor by using the specific EP2 (PF-04418948), EP3 (L-798,106), or EP4 (L-161,982) receptor antagonists at 10 nM. Perfusion with PF-04418948 (10 nM) for 30 min did not modify the firing rate or the EC_{50} of the concentration-effect curve for treprostinil. However, the EP2 receptor antagonist decreased by 47.4% the Emax value of the concentration-effect curve for treprostinil ($n = 6$, $P < 0.05$; Figures 4.8B and C; Table 4.4). Given the apparent non-competitive binding, the affinity value of PF-04418948 for the EP2 receptor was calculated from the double reciprocal plot of equieffective agonist concentrations in the presence and absence of the antagonist[369]. Thus, the estimated pK_B for PF-04418948 using treprostinil as an agonist was 8.34 (95% CI: 8.29 – 8.38). In addition, bath application of a combination of L-798,106 and L-161,982 did not produce any rightward shift but increased the Emax value of the concentration-effect curve for treprostinil by 77.7% ($n = 5$, $P < 0.05$; Figures 4.9A and B; Table 4.4). Thus, these results suggest that the treprostinil-induced stimulation of LC neuronal firing rate is caused, at least in part, by activation of the EP2 receptor.

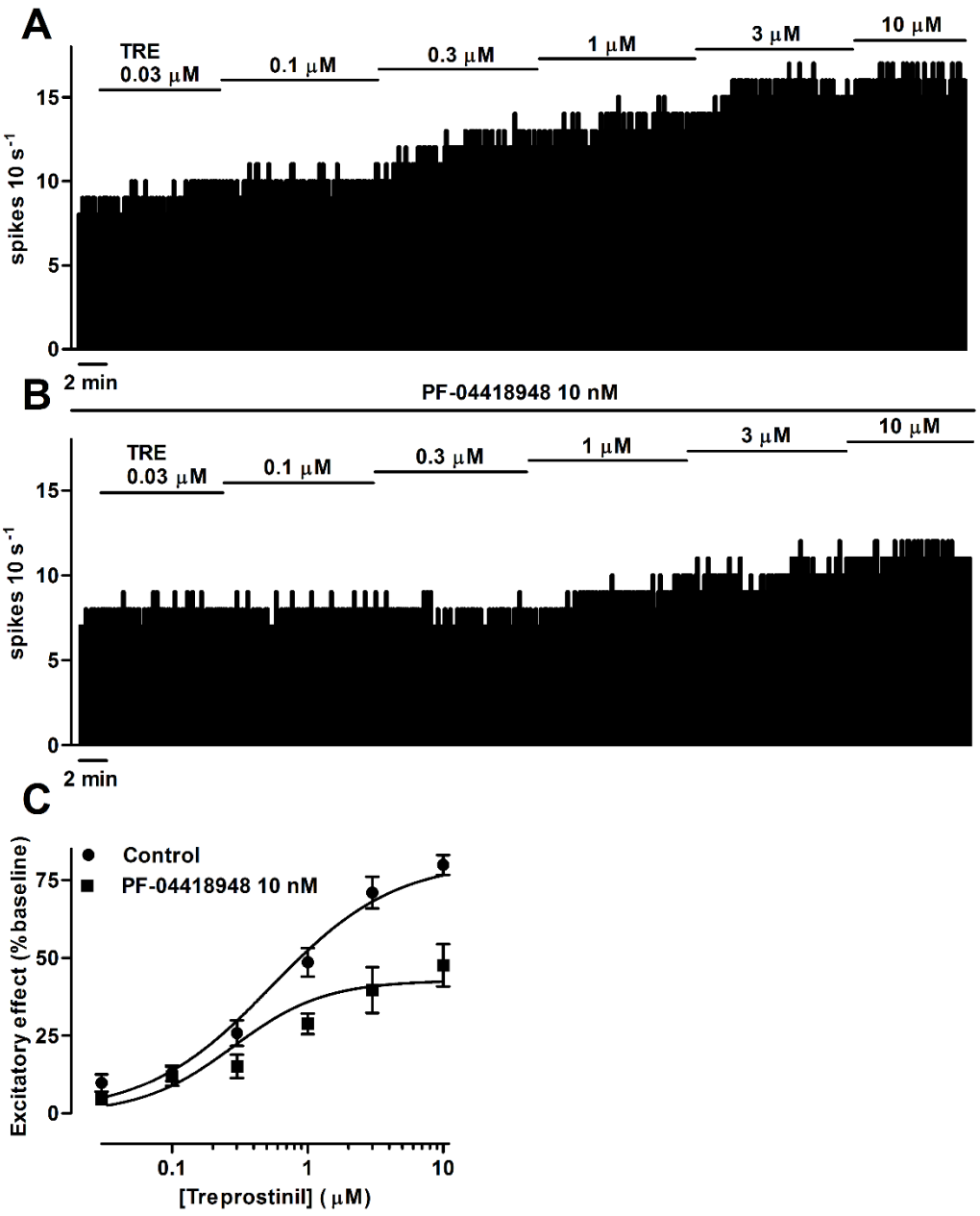

Figure 4.8. Effect of the EP2 receptor agonist treprostinil on the firing rate of LC neurons in the absence or presence of the EP2 receptor antagonist PF-04418948. **(A, B)** Representative examples of firing rate recordings of two LC neurons showing the effect of increasing concentrations of treprostinil in the absence **(A)** and presence of PF-04418948 (10 nM) **(B)**. The vertical lines represent the number of spikes recorded every 10 s and the horizontal bars the period of drug application. **(C)** Concentration-effect curves for treprostinil in control (filled circles) and in the presence of PF-04418948 (10 nM, filled squares). The horizontal axis shows the treprostinil concentration on a semi-logarithmic scale. The vertical axis expresses the increase in firing rate of LC neurons as the percentage of the baseline. Data points are the mean ± SEM at each treprostinil concentration obtained from *n* number of experiments (see Table 4.4). The lines through the data are the theoretical curves in each group constructed from the mean of the individual concentration-effect curve parameters, as estimated by nonlinear regressions. Note that the Emax of treprostinil decreases in the presence of the EP2 receptor antagonist.

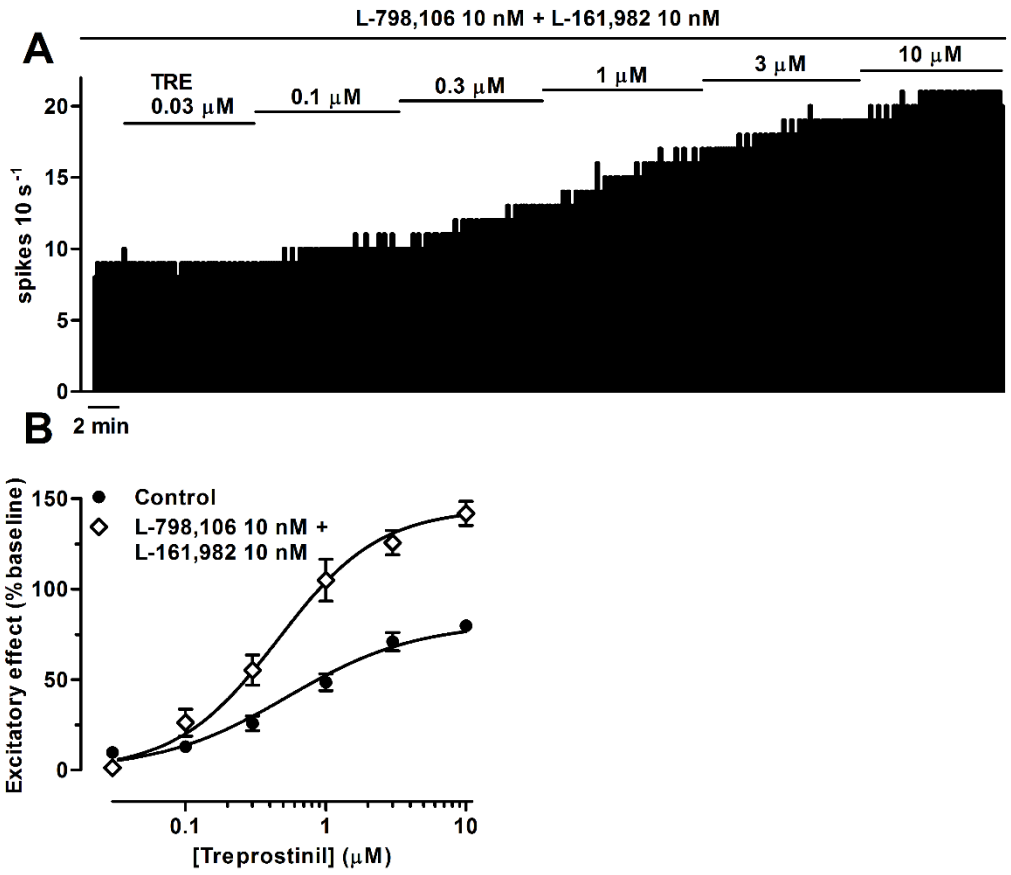

Figure 4.9. Effect of the EP2 receptor agonist treprostinil on the firing rate of LC neurons in the presence of a combination of the EP3 receptor antagonist L-798,106 and the EP4 receptor antagonist L-161,982. **(A)** Representative example of the firing rate recording of an LC neuron showing the effect of increasing concentrations of treprostinil in the presence of L-798,106 and L-161,982 (10 nM each). The vertical lines represent the number of spikes recorded every 10 s and the horizontal bars the period of drug application. **(C)** Concentration-effect curves for treprostinil in control (filled circles) and in the presence of L-798,106 and L-161,982 (10 nM each, open diamonds). The horizontal axis shows the treprostinil concentration on a semi-logarithmic scale. The vertical axis expresses the increase in firing rate of LC neurons as the percentage of the baseline. Data points are the mean ± SEM at each treprostinil concentration obtained from *n* number of experiments (see Table 4.4). The lines through the data are the theoretical curves in each group constructed from the mean of the individual concentration-effect curve parameters, as estimated by nonlinear regressions.

Study of cationic currents and cAMP/PKA signaling pathway involvement in EP2 receptor activation in LC neurons

It is known that PGE_2 increases a sodium current via activation of the EP2 receptor in neurons from different CNS areas such as the cerebellum[376] or the spinal dorsal horn[300]. In the LC, NA cells are stimulated by a cAMP/PKA-induced inward sodium current[327]. Therefore, to test the putative involvement of sodium current in the butaprost-induced stimulation of LC cells, we used a low sodium-containing aCSF, in which 80% of the sodium had been replaced by TRIS[328,329]. Switching from the regular aCSF to a low-sodium aCSF (TRIS 80%) reduced the spontaneous activity of LC neurons by 66.5 ± 2.3% (from 1.11 ± 0.34 to 0.35 ± 0.11; n = 7, $P < 0.05$; Figure 4.10A) and completely blocked the excitation caused by butaprost (1 μM) (n = 7, $P < 0.05$ *vs.* control; Figures 4.10A and B). This suggests that the excitatory effect of the EP2 receptor agonist butaprost is dependent on a sodium current. Next, to further describe the ion channel responsible for this sodium current, we tested whether the cation-permeable transient receptor potential (TRP) channel could be involved in the butaprost-induced effect. This family of channels has been reported to participate in the hypercapnic response of the LC[213]. Perfusion with the non-selective TRP channel blocker 2-APB (30 μM) reduced the LC cell firing rate by 40.2 ± 4.9% (from 0.76 ± 0.09 to 0.46 ± 0.07, n = 5, $P < 0.05$), but did not block the excitatory effect caused by butaprost (1 μM) (Figure 4.10C). Thus, the TRP channels do not appear to mediate the sodium current induced by the EP2 receptor agonist butaprost. Excitatory effects on the LC cell firing activity have also been reported to be elicited by the inhibitory ATP-sensitive K^+ channels (the Kir6.2)[344]. Therefore, we tested the Kir6.2 channel blocker glibenclamide (3 μM), which administration for 15 min failed to affect the excitatory response induced by butaprost (1 μM) (n = 5, $P > 0.05$ *vs*. control; Figure 4.10C). This suggests that the ATP-dependent K^+ channels are not involved in the excitatory effect of EP2 receptor activation on LC neurons.

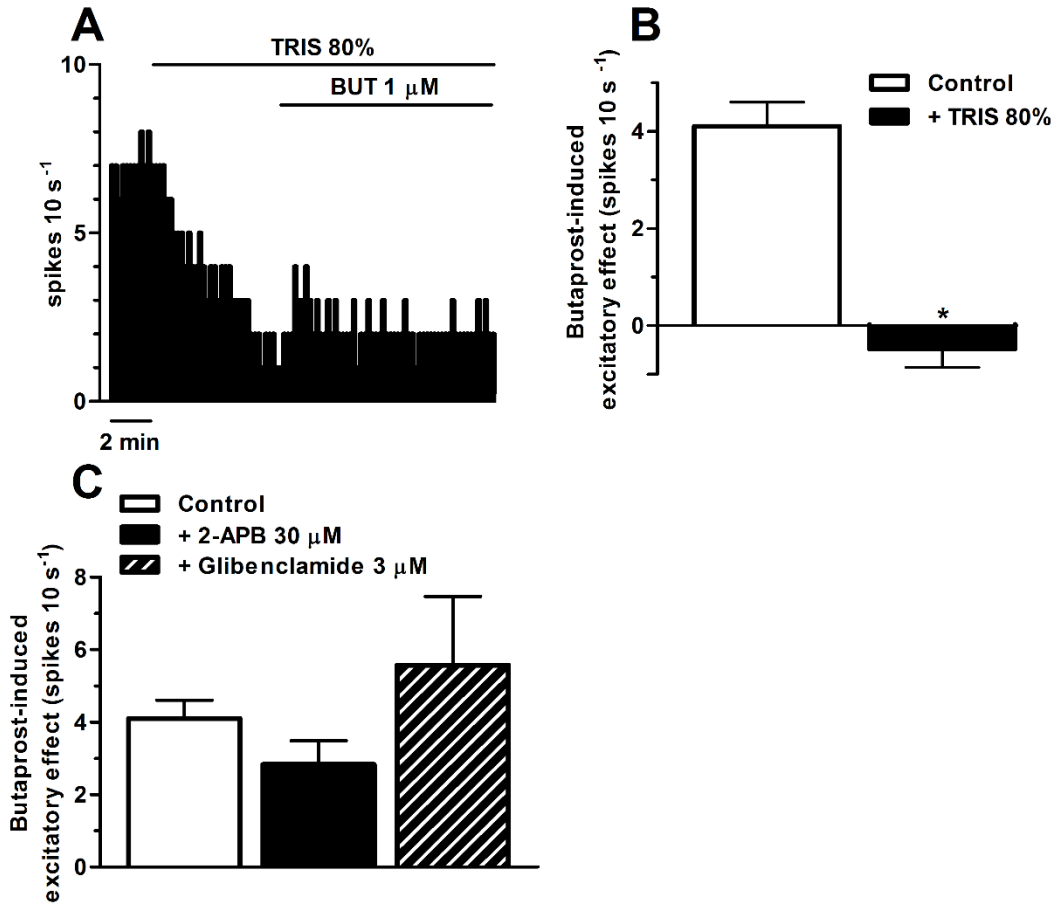

Figure 4.10. Effect of cationic current blockers on the butaprost-induced excitatory effect on LC neurons. **(A)** Representative example of the firing rate recording of an LC neuron showing the effect of butaprost (1 μM, 15 min) in the presence of low-sodium aCSF (TRIS 80%, 5 min). The vertical lines represent the number of spikes recorded every 10 s and the horizontal bars the period of drug application. Note that TRIS 80% abolishes the stimulatory effect of butaprost. **(B, C)** Bar graphs showing the excitatory effect of butaprost (1 μM, 15 min) as the increase in the number of spikes per 10 s in the absence (control) and in the presence of TRIS 80% (n = 7) **(B)** or 2-APB (30 μM, black bar) or glibenclamide (3 μM, hatched bar) (both n = 5) **(C)**. Bars are the mean ± SEM of n experiments. *P < 0.05 when compared to the control group (unpaired Student's t-test).

Then, to test whether the butaprost-induced activation of a sodium current is mediated by the cAMP/PKA pathway, we used 8-Br-cAMP (1 mM), a non-hydrolyzable cell-permeable cAMP analog that activates the PKA[377] and sodium currents[327]. In the case that activation of the EP2 receptor by butaprost depended on the cAMP/PKA pathway, prior administration of a saturating concentration of 8-Br-cAMP would occlude the excitatory effect of butaprost. As expected from previous reports[327], perfusion with 8-Br-cAMP (1 mM) for 8 min produced a 2-fold increase in the firing activity of LC neurons (from 0.71 ± 0.06 Hz to 1.40 ± 0.14 Hz;

$n = 5$, $P < 0.05$) (Figures 4.11A and B). However, administration of butaprost (1 μM, 15 min) in the presence of 8-Br-cAMP further increased the firing activity of LC cells (from 1.40 ± 0.14 Hz to 1.97 ± 0.18 Hz; $n = 5$, $P < 0.05$) (Figures 4.11A and B), which suggests that the effect of butaprost was not occluded by 8-Br-cAMP. Therefore, the excitatory effect of the EP2 receptor agonist does not seem to depend on the cAMP/PKA pathway. To confirm it, we studied the effect of butaprost in the presence of the PKA inhibitor H-89. Bath application of H-89 (10 μM) for 20 min increased the LC firing rate by 18.0 ± 5.5% (from 0.87 ± 0.11 Hz to 1.02 ± 0.14 Hz; $n = 5$, $P < 0.05$). However, H-89 did not change the parameters of the concentration-effect curve for butaprost (0.3 – 3 μM, 3x). Thus, the Emax value in the presence of H-89 was 86.3 ± 7.1% and the pEC_{50} was 6.19 ± 0.07 (EC_{50}=0.64 μM; Figure 4.11C), not different from those obtained in control ($n = 5$, $P > 0.05$; see Table 4.4). Hence, these data rule out the implication of the PKA in the excitatory effect of butaprost. On the other hand, a cationic current has been reported to be activated directly by increased levels of cAMP[299,378] or the $G_{\beta\gamma}$ subunits[379] via activation of HCN channels without the involvement of PKA. In fact, HCN channels play a functional role in some responses of LC cells[378] and to PGE_2 in other CNS[307] and peripherical neurons[380]. Then, to analyze whether the HCN channels may be involved in the stimulatory effect of butaprost, we perfused the EP2 receptor agonist in the presence of the HCN blocker ZD7288. Perfusion of ZD7288 (30 μM) for 20 min increased the spontaneous firing rate of LC neurons by 77.0 ± 14.1% (from 0.70 ± 0.09 Hz to 1.20 ± 0.09 Hz; $n = 5$, $P < 0.05$). However, the HCN blocker did not change the concentration-effect curve for butaprost (0.3 – 3 μM, 3x) (Emax = 64.4 ± 17.1%, pEC_{50} = 6.40 ± 0.06, and EC_{50} = 0.40 μM; $n = 5$, $P > 0.05$ *vs.* control; see Table 4.4) (Figure 4.11C). Thus, the EP2 receptor activation does not seem to regulate LC neurons through the cAMP/PKA signaling pathway or the HCN channels.

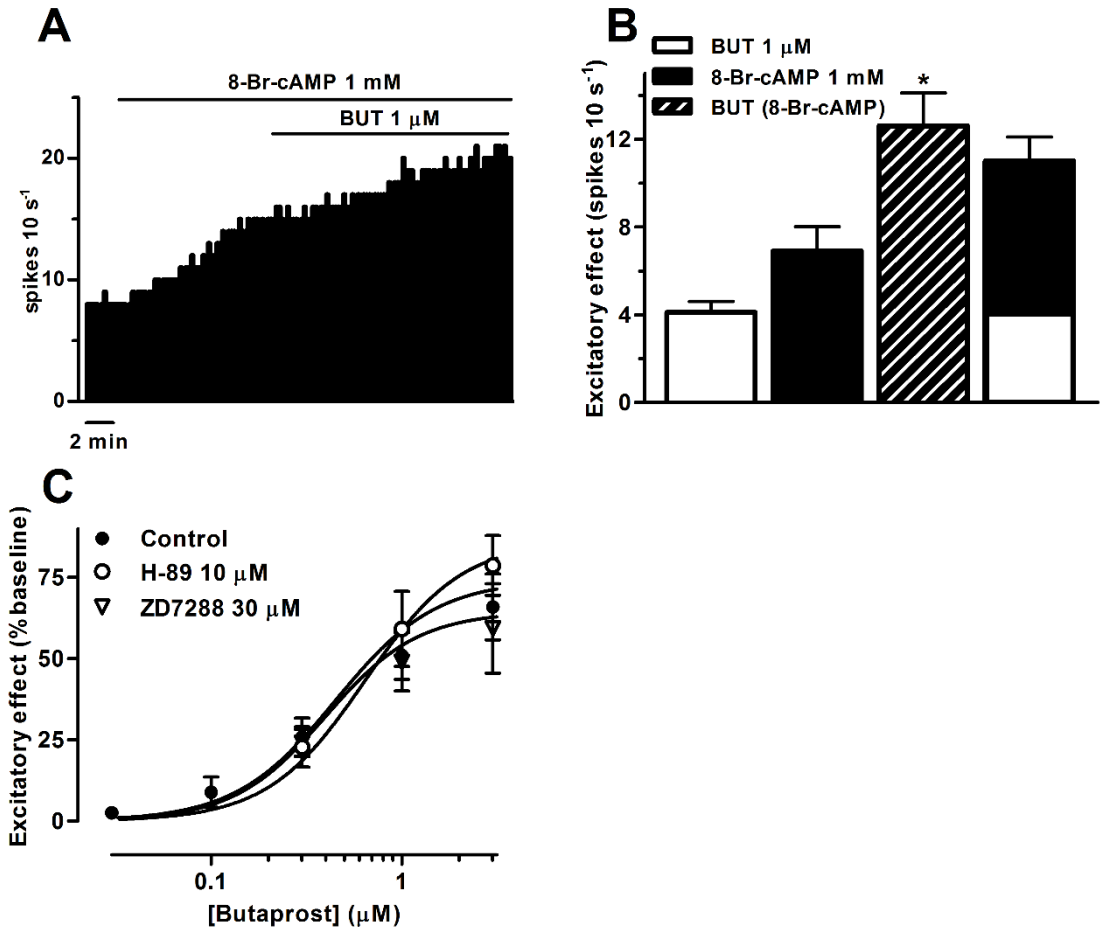

Figure 4.11. Effect of blocking the cAMP/PKA pathway and HCN channels on the butaprost-induced excitatory effect on LC neurons. **(A)** Representative example of the firing rate recording of an LC neuron showing the effect of butaprost (1 μM, 15 min) in the presence of 8-Br-cAMP (1 mM, 8 min). The vertical lines represent the number of spikes recorded every 10 s and the horizontal bars the period of drug application. Note that 8-Br-cAMP increases the spontaneous discharge of the LC neuron and that butaprost produce an additional stimulatory effect. **(B)** Bar graph showing the increase in the number of spikes per 10 s caused by butaprost (1 μM, white bar), 8-Br-cAMP (1 mM, black bar), butaprost in the presence of 8-Br-cAMP (hatched bar), and the arithmetic sum of the effects of butaprost and 8-Br-cAMP (black and white bar). Application of butaprost in the presence of 8-Br-cAMP further increased the excitatory effect caused by 8-Br-cAMP (paired Student's t-test). Note that application of 8-Br-cAMP does not occlude the excitatory response to butaprost since no difference was found between the effect of butaprost in the presence of 8-Br-cAMP and the sum of effects (unpaired Student's t-test). Bars are the mean ± SEM of *n* experiments. **(C)** Concentration-effect curves for butaprost in control (filled circles, $n = 8$) and in the presence of the PKA inhibitor H-89 (10 μM, open circles) or the HCN channel blocker ZD7288 (30 μM, open triangles). The horizontal axis shows the butaprost concentration on a semi-logarithmic scale. The vertical axis expresses the increase in firing rate of LC neurons as the percentage of the baseline. Data points are the mean ± SEM at each butaprost concentration obtained from *n* number of experiments ($n = 5$ in all experimental groups). The lines through the data are the theoretical curves in each group constructed from the mean of the individual concentration-effect curve parameters, as estimated by nonlinear regressions.

Study of the involvement of $G_{\alpha s}$ and $G_{\beta\gamma}$ subunits and presynaptic mechanisms on EP2 receptor activation in LC neurons

The EP2 receptor has been described to couple to G_s protein[58]. Therefore, we addressed whether the $G_{\alpha s}$ and $G_{\beta\gamma}$ subunits would be involved in the stimulatory effect of butaprost. For this purpose, we used the $G_{\alpha s}$-dependent signaling inhibitor NF449[347] and the $G_{\beta\gamma}$-dependent signaling inhibitor gallein. Administration of NF449 (10 μM) for 30 min did not modify the spontaneous firing activity of LC neurons. To verify that NF449 was effectively blocking the $G_{\alpha s}$ subunit, we used VIP (0.5 μM) as a positive control, given that VIP excites LC neurons via G_s-dependent activation of a sodium current[172]. Perfusion of VIP (0.5 μM, 5 min) increased the firing rate by 82.5 ± 16.6% (from 0.69 ± 0.09 Hz to 1.24 ± 0.16 Hz; n = 5, $P < 0.05$; Figure 4.12A). In the presence of NF449, the VIP-induced excitatory effect was reduced by 53% (n = 5, $P < 0.05$ *vs*. control; Figure 4.12A), which indicates that NF449 was readily blocking the $G_{\alpha s}$-dependent signaling. However, unlike VIP, the excitatory effect of butaprost (1 μM) was not modified in the presence of NF449 (n = 6, $P > 0.05$ *vs*. control; Figure 4.12A). This result indicates that the effect of butaprost on LC neurons does not appear to require the $G_{\alpha s}$ signaling proteins. On the other hand, slice incubation with the $G_{\beta\gamma}$-signaling inhibitor gallein (20 μM, 120 min) reduced the basal firing rate of LC neurons compared to baseline in controls before the administration of butaprost (0.85 ± 0.09 Hz in controls *vs*. 0.47 ± 0.10 Hz after gallein incubation; n = 7, $P < 0.05$) and reduced to nearly the half the excitatory effect of butaprost (1 μM) (n = 7, $P < 0.05$ *vs*. control; Figure 4.12B). In light of these results, the $G_{\beta\gamma}$ subunits may be involved in the excitatory effect induced by the EP2 receptor agonist butaprost on LC neurons.

Finally, to investigate whether a presynaptic mechanism could be involved in the excitatory effect of butaprost on the LC, we blocked the main inhibitory and excitatory receptors regulating the firing rate of LC cells: GABA and glutamate receptors. Perfusion with a combination of the $GABA_A$ channel blocker picrotoxin (100 μM), the non-NMDA receptor antagonist CNQX (30 μM), the NMDA receptor antagonist d-AP5 (100 μM), and the metabotropic receptor antagonist RS-MCPG (500 μM) increased the activity of NA cells by 110 ± 14.3% (from 0.69 ± 0.10 Hz to 1.41 ± 0.14 Hz; n = 6, $P < 0.05$), as previously described[349]. However, blockade of presynaptic mechanisms did not reduce the excitation caused by butaprost (1 μM) but further potentiated it (n = 6, $P < 0.05$; Figure 4.12C). Thus,

these results suggest that the butaprost-induced excitatory effect on LC neurons is not caused by presynaptic EP2 receptors.

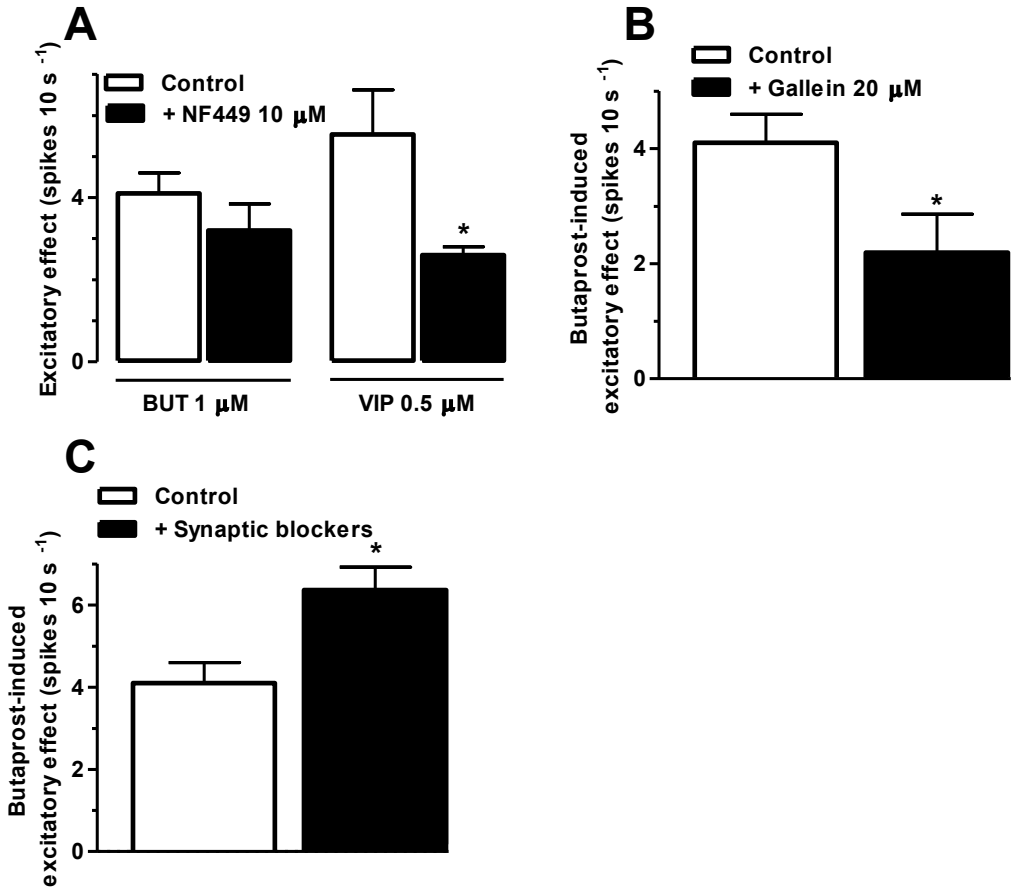

Figure 4.12. Effect of blocking the $G_{\alpha s}$ and $G_{\beta\gamma}$-dependent signaling and the presynaptic afferences on the butaprost-induced excitatory effect on LC neurons. **(A, B)** Bar graphs showing the excitatory effect of butaprost (1 µM, 15 min) as the increase in the number of spikes per 10 s in the absence (control, $n = 8$) and in the presence of NF449 (10 µM, 30 min, $n = 6$) **(A)** or gallein (20 µM, 120 min, $n = 7$) **(B)**. VIP (0.5 µM, 5 min) was used as a positive control to demonstrate that NF449 was effectively blocking the $G_{\alpha s}$ subunits (both $n = 5$). **(C)** Bar graph showing the excitatory effect of butaprost in control (white bar) and after the administration of the synaptic blockers: Picrotoxin (100 µM), CNQX (30 µM), d-AP5 (100 µM), and RS-MCPG (500 µM) for 10 min ($n = 6$). Bars are the mean ± SEM of n experiments. *$P < 0.05$ when compared to their respective control group (unpaired Student's t-test).

4.3 STUDY III – PHARMACOLOGICAL CHARACTERIZATION OF PROSTANOID EP4 RECEPTOR IN RAT LOCUS COERULEUS NEURONS *IN VITRO*

The results of this study are going to be submitted to the British Journal of Pharmacology. The written version of the manuscript has been attached in the section of accompanying manuscripts.

Effect of the EP4 receptor agonists rivenprost and TCS 2510 on the firing rate of LC neurons

In situ hybridization studies have shown mRNA expression for the EP4 receptor in the LC[57]. Moreover, c-fos immunoreactivity is increased in response to a systemic pro-inflammatory cytokine in brain areas expressing the EP4 receptor, including the LC[57]. To study the role of the EP4 receptor in the regulation of the firing rate of LC neurons, we performed concentration-effect curves for the EP4 receptor agonists rivenprost and TCS 2510. Increasing concentrations of rivenprost (0.01 – 100 nM, 3x, 10 min each) increased the firing rate of LC cells (from 0.70 ± 0.09 Hz to 1.14 ± 0.13 Hz; $n = 6$, $P < 0.05$) with an EC_{50} value of 1.4 nM and Emax of 83.7 ± 13.3% (Figures 4.13A and C; Table 4.5).

To determine the EP receptor involved in the rivenprost-induced excitatory effect, the specific EP4 receptor antagonist L-161,982 (3, 30 and 300 nM), the EP2 receptor antagonist PF-04418948 (300 nM), and the EP3 receptor antagonist L-798,106 (300 nM) were used. Bath application of L-161,982 (3, 30, and 300 nM, 30 min) did not change the firing rate of LC cells but 30 nM and 300 nM produced a 4-fold and 8-fold shift in the concentration-effect curve for rivenprost, respectively ($n = 5$, $P < 0.05$ for both 30 and 300 nM; Figures 4.13B and C; Table 4.5). On the other hand, perfusion with PF-04418948 (300 nM) and L-798,106 (300 nM) did not change the firing rate and failed to shift the concentration-effect curve for rivenprost (Figures 4.14A and B; Table 4.5). These results suggest that the excitatory effect of rivenprost was mediated by EP4 receptor activation.

The antagonist affinity of L-161,982 for the EP4 receptor (pK_B) was estimated to be 8.06 ± 0.18 (mean ± SEM, $n = 14$) when calculated with the Gaddum/Schild equation and assumed a Schild slope of unity[381]. However, the calculated pK_B values were variable depending on the concentration of L-161,982 employed, resulting in a higher pK_B value with 3 nM in comparison with 30 or 300 nM (8.84 ± 0.13 for 3 nM different from 7.94 ± 0.24 for 30 nM or 7.40 ± 0.08 for 300 nM; $n = 5$, $P < 0.05$, one-way ANOVA followed by Bonferroni's Multiple Comparison

Test). Therefore, we performed the Schild plot analysis and the resultant pA_2 was 8.69 (95% CI: 15.96-7.92) with a Schild slope of 0.39 (95% CI: 0.05-0.72) different from unity ($n = 5$, $P < 0.05$) (Figure 4.13D). This means that, despite the rightward shift of the concentration-effect curve for rivenprost by L-161,982 (Figure 4.13C), the Schild slope was found different from 1, which suggest a non-competitive condition for L-161,982 (see discussion).

On the other hand, administration of the structurally different EP4 receptor agonist TCS 2510 (0.20 nM – 2 μM, 3x, 10 min each) increased the firing rate of LC cells (from 0.71 ± 0.08 to 1.55 ± 0.12 Hz; $n = 6$, $P < 0.05$), with an EC_{50} value of 18.0 nM and Emax of 98.4 ± 8.1% (Figures 4.15A and C; Table 4.5). Administration of the EP4 receptor antagonist L-161,982 (300 nM) for 30 min decreased the maximal effect by 38% ($n = 5$, $P < 0.05$) and increased the slope steepness by 2 fold ($n = 5$, $P < 0.05$) (Figures 4.15B and C; Table 4.5), suggesting that the excitatory effect caused by TCS 2510 is mediated by EP4 receptor activation. Considering that the Emax reduction for TCS 2510 by L-161,982 may support the non-competitive behavior of the antagonist, we plotted double equieffective concentrations of TCS 2510 in the absence and presence of L-161,982 (300 nM) by the Gaddum method[369], which yielded a pK_B yielded of 7.69 (95% CI: 7.61 – 7.76). Overall, these results indicate that the activation of EP4 receptors by the selective agonists rivenprost and TCS 2510 stimulated LC neuronal activity *in vitro*.

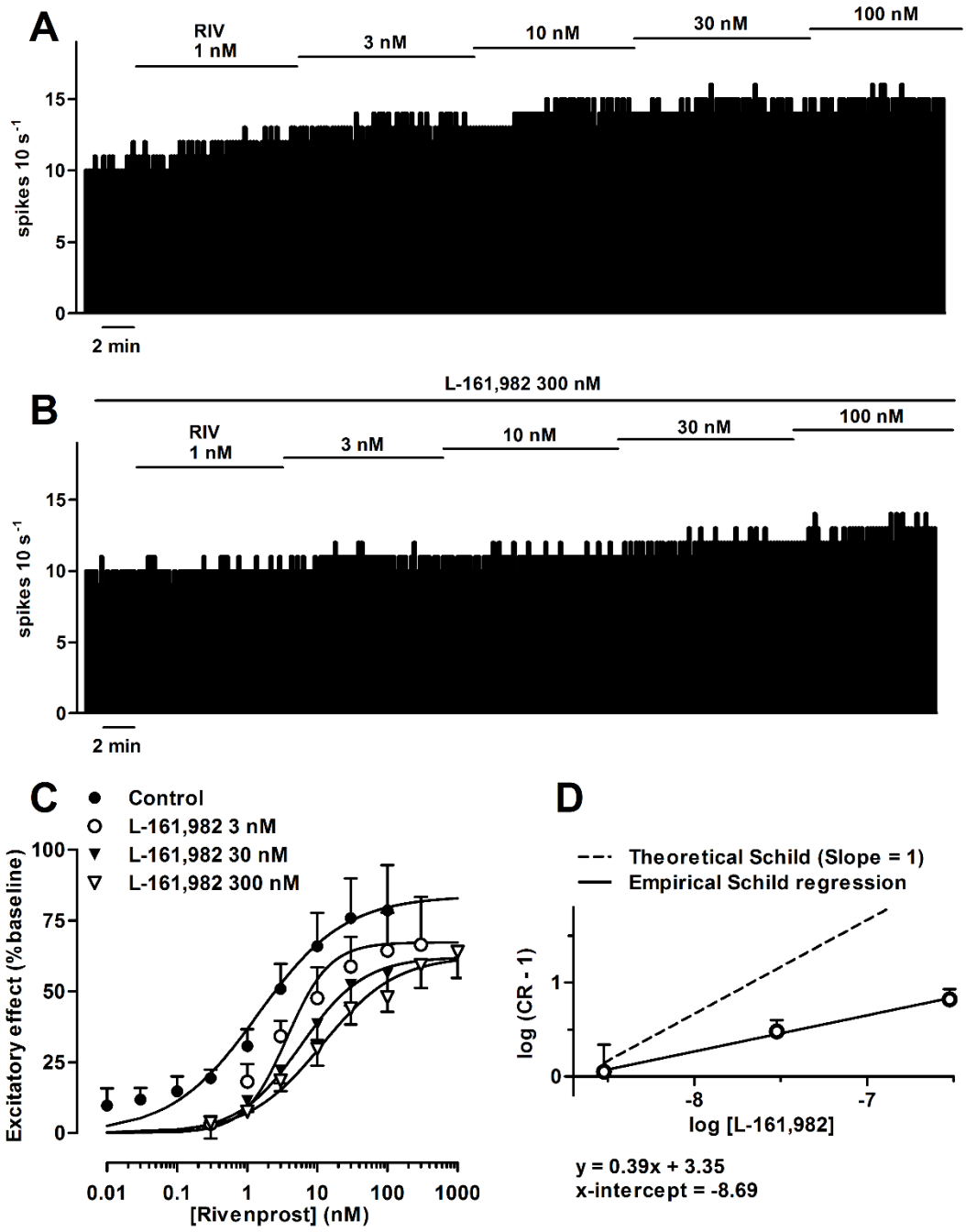

Figure 4.13. Effect of the EP4 receptor agonist rivenprost on the firing rate of LC neurons in the absence or presence of the EP4 receptor antagonist L-161,982. **(A, B)** Representative examples of firing rate recordings of two LC neurons showing the effect of increasing concentrations of rivenprost in the absence **(A)** and presence of L-161,982 (300 nM) **(B)**. The vertical lines represent the number of spikes recorded every 10 s and the horizontal bars the period of drug application. **(C)** Concentration-effect curves for rivenprost in control (filled circles) and in the presence of L-161,982 (3 nM, open circles; 30 nM, full triangles; and 300 nM, open triangles). The horizontal axis shows the rivenprost concentration on a semi-logarithmic scale. The vertical axis expresses the increase in firing rate of LC neurons as the percentage of the baseline. Data points are the mean ± SEM at each rivenprost concentration obtained from *n* number of experiments (see Table 4.5). The lines through the data are the theoretical

curves in each group constructed from the mean of the individual concentration-effect curve parameters, as estimated by nonlinear regressions. Note that the concentration-effect curve for rivenprost is shifted to the right by the EP4 receptor antagonist. **(D)** Schild plot for the three concentrations of L-161,982 obtained in the presence of rivenprost. The concentration ratio (CR) calculated from the EC_{50} of rivenprost in the presence of the antagonist divided by the EC_{50} of the agonist alone. The slope for the regression line was different from unity (0.39; 95% confidence limits between 0.05 and 0.72, and the correlation coefficient $r^2 = 0.996$).

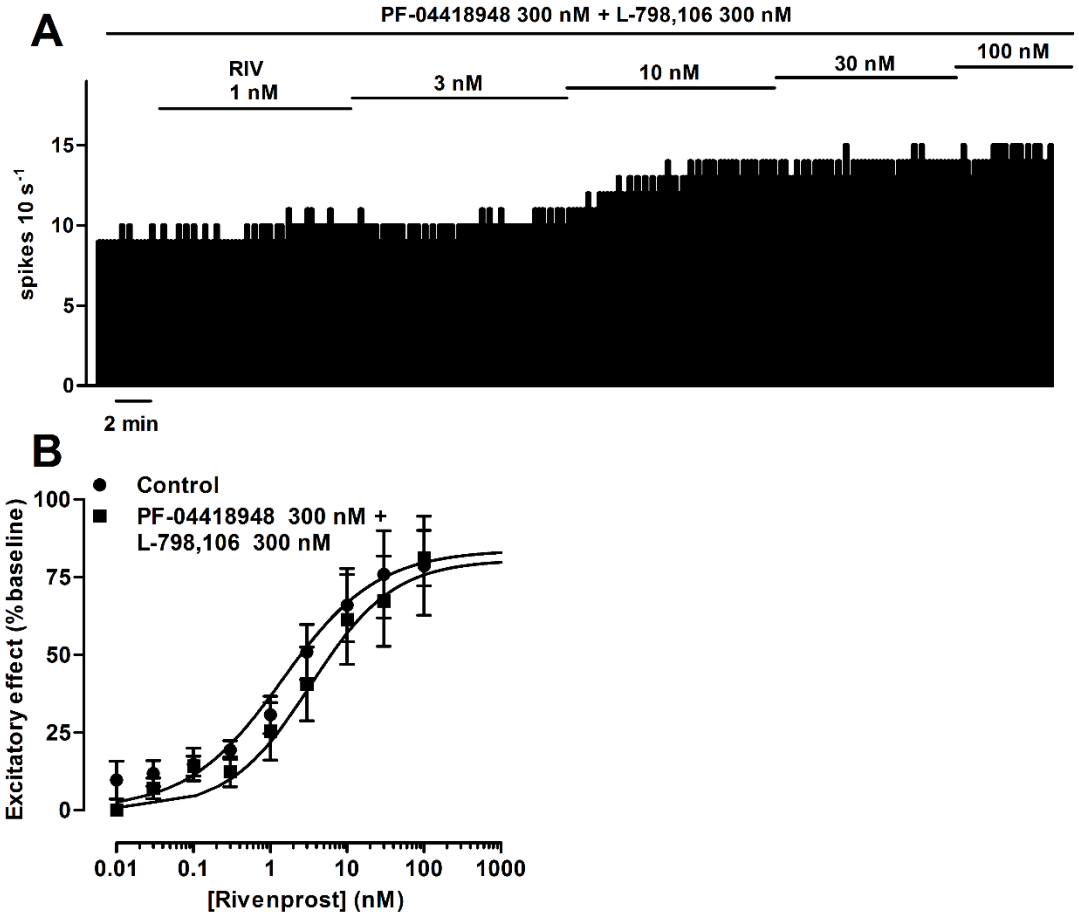

Figure 4.14. Effect of the EP4 receptor agonist rivenprost on the firing rate of LC neurons in the absence or presence of a combination of the EP2 receptor antagonist PF-04418948 and EP3 receptor antagonist L-798,106. **(A)** Representative example of the firing rate recording of an LC neuron showing the effect of increasing concentrations of rivenprost in the presence of PF-04418948 and L-798,106 (300 nM each). The vertical lines represent the number of spikes recorded every 10 s and the horizontal bars the period of drug application. **(B)** Concentration-effect curves for rivenprost in control (filled circles) and in the presence of PF-04418948 and L-798,106 (300 nM each, filled squares). The horizontal axis shows the rivenprost concentration on a semi-logarithmic scale. The vertical axis expresses the increase in firing rate of LC neurons as the percentage of the baseline. Data points are the mean ± SEM at each rivenprost concentration obtained from *n* number of experiments (see Table 4.5). The lines through the data are the theoretical curves in each group constructed from the mean of the individual concentration-effect curve parameters, as estimated by nonlinear regressions.

Table 4.5. Basal firing rate and concentration-effect curve parameters for the excitatory action of the EP4 receptor agonists rivenprost and TCS 2510 on LC neurons in the absence (control) or in the presence of the EP4 (L-161,982) or a combination of the EP2 (PF-04418948) and EP3 (L-798,106) receptor antagonists.

			Concentration-effect curves[1]				
Drugs	Concentration	Basal firing rate (Hz)	Emax (%)	pEC_{50} (M)	(EC_{50}, nM)	Slope factor	*n*
Rivenprost							
Control		0.70 ± 0.09	83.7 ± 13.3	8.84 ± 0.10	(1.43)	0.70 ± 0.17	6
+ L-161,982	3 nM	0.80 ± 0.12	67.3 ± 14.2	8.43 ± 0.13	(3.72)	1.43 ± 0.43	5
	30 nM	0.70 ± 0.07	62.2 ± 5.0	8.23 ± 0.08*	(5.92)	0.97 ± 0.15	5
	300 nM	0.82 ± 0.05	62.5 ± 7.5	7.93 ± 0.12*	(11.8)	0.83 ± 0.10	5
+ L-798,106	300 nM						
PF-04418948	300 nM	0.75 ± 0.09	80.6 ± 13.0	8.47 ± 0.16	(3.38)	0.81 ± 0.11	5
TCS 2510							
Control		0.78 ± 0.07	98.4 ± 8.1	7.74 ± 0.19	(18.0)	0.67 ± 0.05	6
+ L-161,982	300 nM	0.94 ± 0.08	61.0 ± 6.9*	7.43 ± 0.11	(37.5)	1.29 ± 0.25*	5

[1]Values are expressed as mean ± SEM obtained by nonlinear regression of *n* cells. Emax is the maximal excitatory effect, and pEC_{50} is the negative logarithm of the concentration needed to elicit a 50% of the Emax. *$P < 0.05$ when compared to the control group of rivenprost (one-way ANOVA followed by a Dunnett's *post hoc* test) or TCS 2510, respectively (unpaired Student's t-test).

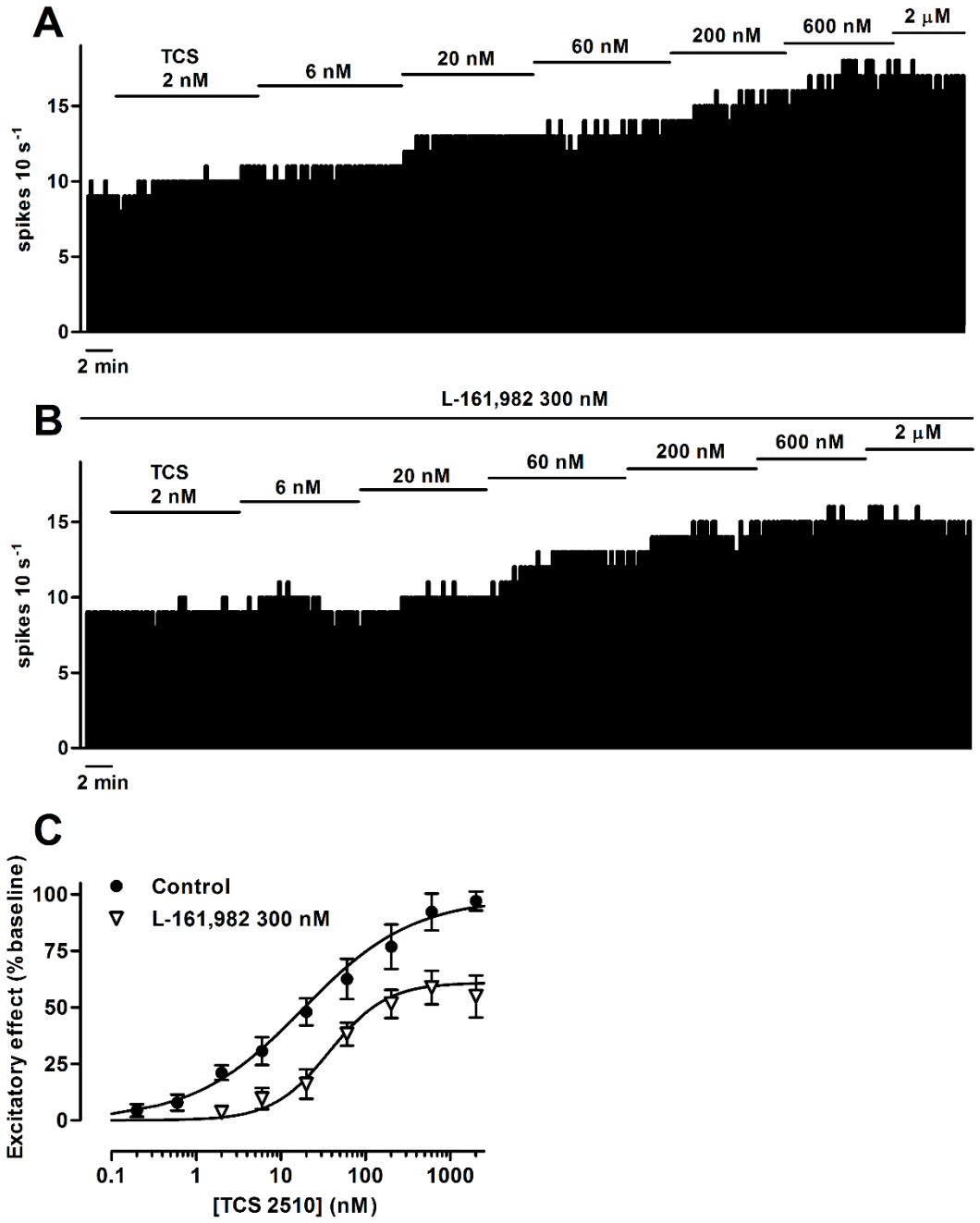

Figure 4.15. Effect of the EP4 receptor agonist TCS 2510 on the firing rate of LC neurons in the absence or presence of the EP4 receptor antagonist L-161,982. **(A, B)** Representative examples of firing rate recordings of two LC neurons showing the effect of increasing concentrations of TCS 2510 in the absence **(A)** and presence of L-161,982 (300 nM) **(B)**. The vertical lines represent the number of spikes recorded every 10 s and the horizontal bars the period of drug application. **(C)** Concentration-effect curves for TCS 2510 in control (filled circles) and in the presence of L-161,982 (300 nM, open triangles). The horizontal axis shows the TCS 2510 concentration on a semi-logarithmic scale. The vertical axis expresses the increase in firing rate of LC neurons as the percentage of the baseline. Data points are the mean ± SEM at each TCS 2510 concentration obtained from *n* number of experiments (see Table 4.5). The lines through the data are the theoretical curves in each group constructed from the mean of the individual concentration-effect curve parameters, as estimated by nonlinear regressions. Note that the Emax of TCS 2510 decreases in the presence of the EP4 receptor antagonist.

Study of cationic currents and cAMP/PKA signaling pathway involvement in EP4 receptor activation in LC neurons

In cerebellar neurons, PGE_2 has been described to elicit a sodium current via activation of G_s-coupled EP4 receptors and in a cAMP/PKA-mediated pathway[376]. In the LC, activation of the cAMP/PKA pathway is known to drive the spontaneous pacemaker activity[149,382] through the opening of an inward sodium current[327]. Therefore, to test the involvement of sodium current in the excitatory effect of rivenprost, we used a low sodium-containing aCSF, in which the 80% of the sodium had been replaced by TRIS (TRIS 80%)[328,329]. Perfusion with TRIS 80% reduced the spontaneous activity of LC neurons by 63.6 ± 2.6% (from 0.92 ± 0.31 to 0.34 ± 0.08; $n = 6$, $P < 0.05$) and completely blocked the excitatory effect caused by rivenprost (30 nM) ($n = 6$, $P < 0.05$; Figures 4.16A and B). This result implies that the excitatory effect of the EP4 receptor agonist rivenprost is dependent on a sodium current. Next, to characterize the molecular substrate for this sodium current, we checked whether the cation-permeable transient receptor potential (TRP) channel was involved. PGE_2 has been reported to increase the activity of these channels in EP4 receptor-expressing cells[383]. Administration of the non-selective TRP channel blocker 2-APB (30 μM) reduced the LC cell firing activity by 41.7 ± 6.1% (from 0.74 ± 0.09 Hz to 0.45 ± 0.11 Hz; $n = 5$, $P < 0.05$) but it failed to alter the excitatory effect induced by rivenprost (30 nM) (Figure 4.16B). Therefore, the TRP channels do not appear to mediate the sodium current induced by the EP4 receptor agonist rivenprost.

Next, to test whether the cAMP/PKA pathway is involved in the EP4 receptor agonist effect, we perfused rivenprost in the presence of 8-Br-cAMP, a non-hydrolyzable cell-permeable cAMP analog that activates the PKA enzyme[377]. Thus, if rivenprost exerted its effect through the cAMP cascade, prior administration of a saturating concentration of 8-Br-cAMP would occlude the excitatory effect induced by rivenprost. As expected from previous reports[327] (see study II), PKA activation with 8-Br-cAMP (1 mM, 8 min) increased by 2 fold the firing rate of LC neurons (from 0.73 ± 0.06 Hz to 1.42 ± 0.12 Hz; $n = 5$, $P < 0.05$) (Figure 4.16C). However, administration of rivenprost (30 nM, 10 min) in the presence of 8-Br-cAMP further increased the firing activity of LC cells (from 1.42 ± 0.12 Hz to 2.02 ± 0.13 Hz; $n = 5$, $P < 0.05$) (Figure 4.16C), which suggests that the effect of rivenprost was not occluded by 8-Br-cAMP. Therefore, the excitatory effect of the EP4 receptor agonist does not apparently depend on the cAMP/PKA pathway. To further test this hypothesis, we studied the effect of

rivenprost (30 nM) in the presence of the PKA inhibitor H-89 (10 μM). Bath application of H-89 (10 μM) for 20 min increased the LC firing rate by 8.99 ± 3.36% (from 0.62 ± 0.06 Hz to 0.68 ± 0.08 Hz; n = 5, P < 0.05). However, H-89 did not change the magnitude of rivenprost-induced excitation (Figure 4.16D). Hence, these data indicate that the effect of the EP4 receptor agonist rivenprost on the LC is dependent on a sodium current but independent of the cAMP/PKA pathway.

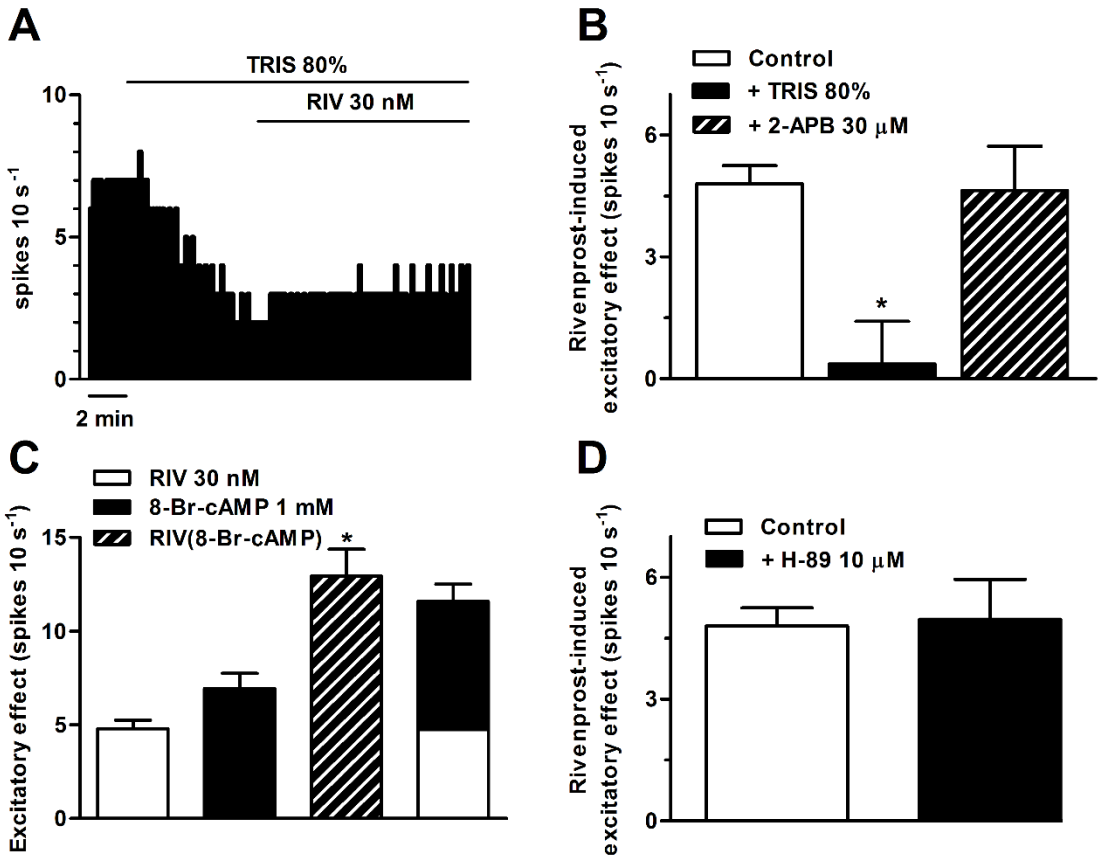

Figure 4.16. Effect of blocking a sodium current and the cAMP/PKA pathway on the rivenprost-induced excitatory effect on LC neurons. **(A)** Representative example of the firing rate recording of an LC neuron showing the effect of rivenprost (30 nM, 10 min) in the presence of low-sodium aCSF (TRIS 80%, 5 min). The vertical lines represent the number of spikes recorded every 10 s and the horizontal bars the period of drug application. Note that TRIS 80% abolishes the stimulatory effect of rivenprost. **(B)** Bar graph showing the increase in the number of spikes per 10 s caused by rivenprost (30 nM) in the absence (control, n = 6) and in the presence of TRIS 80% (black bar, n = 6) or 2-APB (30 μM, hatched bar, n = 5). **(C)** Bar graph showing the increase in the number of spikes per 10 s by rivenprost (30 nM, white bar, n = 6), 8-Br-cAMP (1 mM, black bar, n = 5), rivenprost in the presence of 8-Br-cAMP (hatched bar, n = 5), and the arithmetic sum of the effects of rivenprost and 8-Br-cAMP (black and white bar). Application of rivenprost in the presence of 8-Br-cAMP further increased the excitatory effect caused by 8-Br-cAMP (paired Student's t-test). Note that 8-Br-cAMP does not occlude the excitatory response to rivenprost since no difference was found between the effect of rivenprost in the presence of 8-Br-cAMP and the arithmetic sum of effects (unpaired Student's t-test). **(D)** Bar

graph showing the excitatory effect of rivenprost (30 nM, $n = 6$) in the presence of the PKA inhibitor H-89 (10 µM, $n = 5$) compared to control. Bars are the mean ± SEM of n experiments. *$P < 0.05$ when compared to the control group (unpaired Student's t-test).

We have previously shown that the effect of the EP2 receptor agonist butaprost is also dependent on a sodium current but independent of the cAMP/PKA pathway (see Study II). Therefore, we studied whether the administration of butaprost at a submaximal concentration would occlude the following stimulatory effect of rivenprost. As previously described, administration of butaprost (1 µM, 15 min) increased the firing rate of LC neurons by 61.4 ± 9.7% (from 0.74 ± 0.10 Hz to 1.19 ± 0.17 Hz; $n = 5$, $P < 0.05$) (Figures 4.17A and B). However, in the presence of butaprost, rivenprost (30 nM) further increased the LC cell firing activity (from 1.19 ± 0.17 Hz to 1.51 ± 0.22 Hz; $n = 5$, $P < 0.05$) (Figures 4.17A and B), indicating that the excitatory effect of rivenprost was not occluded by butaprost. These data suggest that the EP2 and EP4 receptors do not share the same signaling pathway to excite the activity of LC neurons.

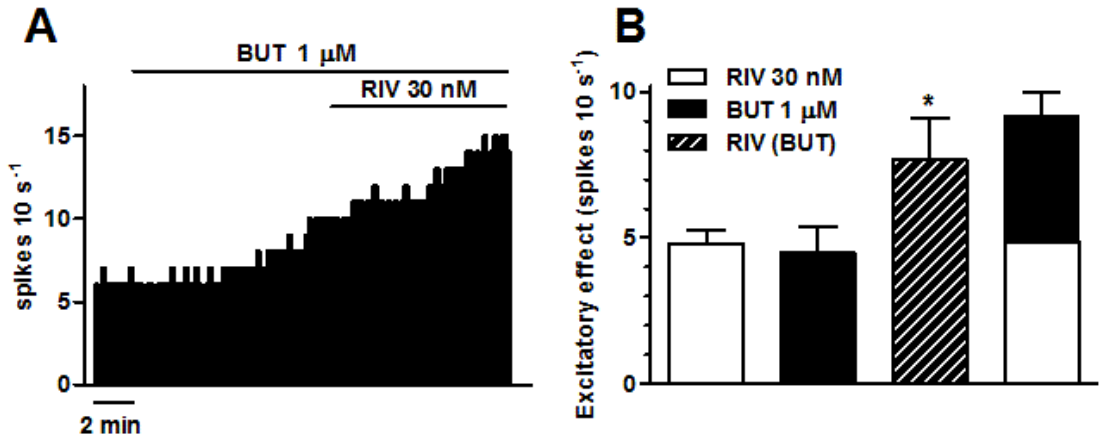

Figure 4.17. Effect of butaprost on the rivenprost-induced excitatory effect on LC neurons. **(A)** Representative example of the firing rate recording of an LC neuron showing the effect of rivenprost (30 nM, 10 min) in the presence of butaprost (1 µM, 15 min). The vertical lines represent the number of spikes recorded every 10 s and the horizontal bars the period of drug application. **(B)** Bar graph showing the increase in the number of spikes per 10 s caused by rivenprost (30 nM, white bar, $n = 6$), butaprost (1 µM, black bar, $n = 5$), rivenprost in the presence of butaprost (hatched bar, $n = 5$), and the arithmetic sum of the effects of rivenprost and butaprost (black and white bar). Application of rivenprost in the presence of butaprost further increased the excitatory effect caused by butaprost (paired Student's t-test). Note that application of butaprost does not occlude the excitatory response to rivenprost since no difference was found between the effect of rivenprost in the presence of butaprost and the arithmetic sum of effects (unpaired Student's t-test). Bars are the mean ± SEM of n experiments.

Study of the involvement of $G_{\alpha s}$ and $G_{\beta\gamma}$ subunits, and PI3K and PKC signaling mechanisms in EP4 receptor activation in LC neurons

The EP4 receptor is described to be coupled to G_s protein in cerebellar neurons[376]. In order to study whether the $G_{\alpha s}$ protein mediated the effect of rivenprost on the LC, we used the specific $G_{\alpha s}$-dependent signaling inhibitor NF449. Administration of NF449 (10 μM) for 20 min did not change the firing activity of LC neurons, but blunted by 42.1% the excitatory effect induced by rivenprost (30 nM) ($n = 6$, $P < 0.05$ *vs*. control; Figures 4.18A and B), suggesting that the effect of rivenprost was mediated by the $G_{\alpha s}$ protein. In addition, we studied the involvement of the $G_{\beta\gamma}$ subunits by testing the effect of rivenprost in the presence of the selective inhibitor gallein. Bath incubation with gallein (20 μM) for 120 min did not change the rivenprost-induced excitation ($n = 5$, $P > 0.05$ *vs*. control; Figure 4.18A). These results indicate that the $G_{\beta\gamma}$ subunits are not involved in the excitatory effect of rivenprost on LC cells.

In addition to $G_{\alpha s}$ protein, the EP4 receptor has been described to be coupled to the PI3K signaling pathway in cultured cells[81,352] and microglia[384]. Furthermore, PI3K signaling is needed for the leptin-induced excitatory effect in hypothalamic neurons[355]. Therefore, we tested the effect of rivenprost in the presence of the PI3K inhibitor wortmannin. Administration of wortmannin (100 nM) for 20 min did not change the spontaneous activity of LC cells and failed to block the excitatory effect of rivenprost (30 nM), suggesting that the stimulatory effect of rivenprost was not mediated by the PI3K. In fact, in the presence of wortmannin, the effect of rivenprost was increased by 58.3% ($n = 5$, $P < 0.05$ *vs*. control; Figure 4.18C). On the other hand, PKC activity is required for the PGE_2-induced modulation of sodium currents in sensory neurons[385] and the PGE_2-induced hypernociception *in vivo*[386]. Therefore, we examined the involvement of PKC by testing the effect of rivenprost in the presence of the PKC inhibitor chelerythrine. Bath perfusion of chelerythrine (10 μM) for 30 min did not change the firing activity of LC neurons and failed to prevent the increase in excitability of LC neurons caused by rivenprost (30 nM). Furthermore, the rivenprost-induced excitatory effect was increased by 2 fold in the presence of chelerythrine ($n = 5$, $P < 0.05$ *vs*. control; Figure 4.18C). In light of this result, the PKC does not seem to mediate the rivenprost-induced excitation. In summary, the excitatory effect observed upon EP4 receptor activation seems to be mediated by the $G_{\alpha s}$ subunits, whereas the $G_{\beta\gamma}$ subunits and the PK3K and PKC signaling pathways are not apparently involved.

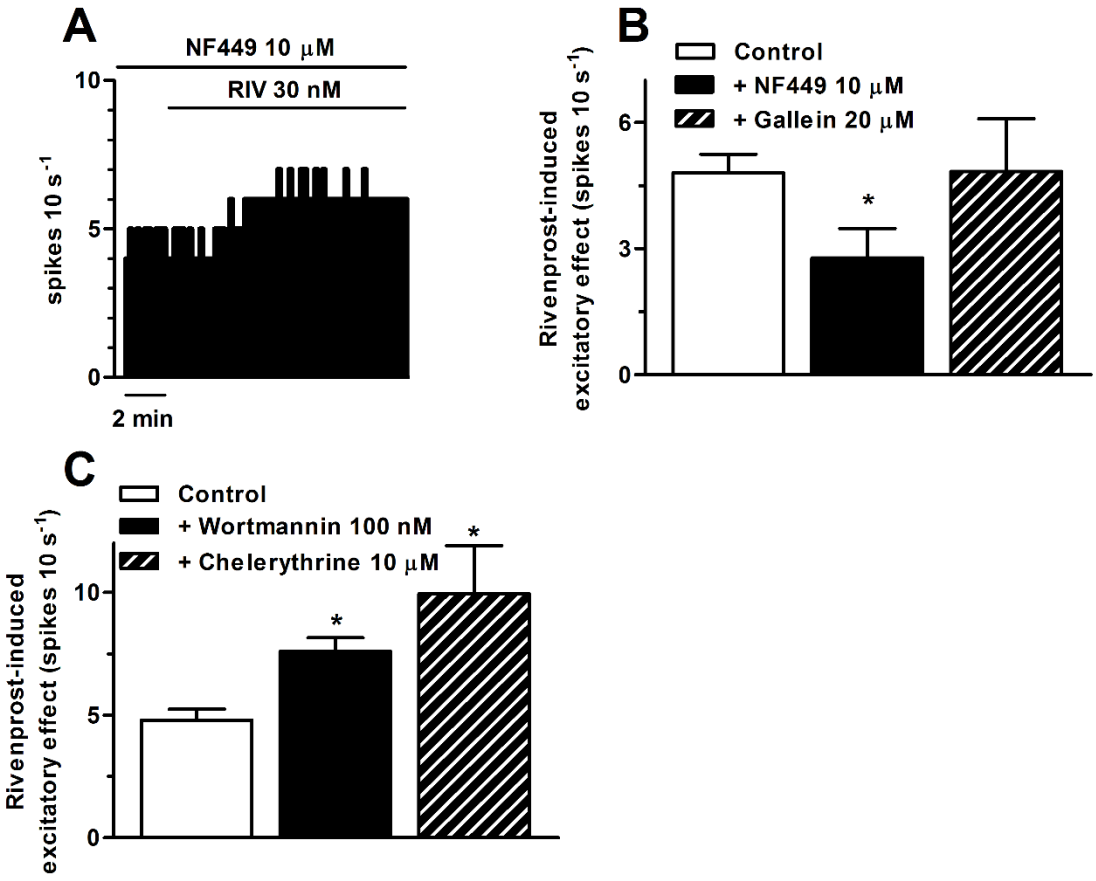

Figure 4.18. Effect of blocking the $G_{\alpha s}$ and $G_{\beta\gamma}$-dependent signaling, and the PI3K and PKC enzymes on the rivenprost-induced excitatory effect on LC neurons. **(A)** Representative example of the firing rate recording of an LC neuron showing the effect of rivenprost (30 nM, 10 min) in the presence of NF449 (10 μM, 20 min). The vertical lines represent the number of spikes recorded every 10 s and the horizontal bars the period of drug application. Note that NF449 hinders the stimulatory effect of rivenprost. **(B, C)** Bar graphs showing the increase in the number of spikes per 10 s caused by rivenprost (30 nM, 10 min) in the absence (control, $n = 6$) or in the presence of NF449 (10 μM, black bar, $n = 6$) or gallein (20 μM, hatched bar, $n = 5$) **(B)** or the PI3K inhibitor wortmannin (100 nM, black bar, $n = 5$) or the PKC inhibitor chelerythrine (10 μM, hatched bar, $n = 5$) **(C)**. Bars are the mean ± SEM of n experiments. *$P < 0.05$ when compared to the control group (unpaired Student's t-test).

4.4 STUDY IV – INTERACTION BETWEEN OPIOIDS AND PROSTAGLANDIN E_2 IN THE INSPIRATION-GENERATING PREBÖTZINGER COMPLEX

The results of this study are going to be submitted to The Journal of Physiology. The written version of the manuscript has been attached in the section of accompanying manuscripts.

Effect of the MOR agonist DAMGO on the cellular activity and network connectivity of the preBötC in vitro

The rhythmic cellular activity of the preBötC is directly related to the respiratory frequency[236], so its neuronal hyperpolarization can lead to apneas *in vivo*[265]. Moreover, it is considered indispensable for the opioid-induced respiratory depression[255], as the majority of the $NK1R^+$ cells (i.e., respiratory neurons) in the preBötC co-express MOR[119]. Therefore, to determine the effect of opioids in preBötC cells *in vitro*, we applied the high-affinity MOR agonist DAMGO (0.5 – 5 μM) for 15 min to organotypic slices and measured Ca^{2+} fluctuations. DAMGO (0.5 μM) did not modify the Ca^{2+} transient amplitude or frequency at any time ($n = 7$) but the highest concentration of DAMGO (5 μM) reduced by 17.2 ± 7.8% the relative amplitude and by 21.7 ± 6.8% the frequency of Ca^{2+} transients within 5 min ($n = 7$, $P < 0.05$ compared to baseline; Figures 4.19A, B, C, and D, Table 4.6). Furthermore, within the first 5 min of recording, the effect of the highest concentration of DAMGO (5 μM) was greater than that of DAMGO 0.5 μM ($n = 7$, $P < 0.05$ compared to DAMGO 0.5 μM; Figures 4.19B and C) and more cells were inhibited (75.3 ± 11.0% *vs.* 46.9 ± 14.5%, respectively; $n = 7$ each, $P < 0.05$; Figure 4.19D). The inhibitory effect of DAMGO (5 μM) persisted throughout the experiment (15 min) (Figures 4.19B and C) showing a small recovery in the Ca^{2+} oscillatory frequency during the last 5 min of application ($n = 7$, $P < 0.05$ when compared to the previous 5 min period; Figure 4.19C), possibly due to MOR desensitization[387]. Furthermore, $NK1R^+$ neurons showed a similar inhibition in the Ca^{2+} transient relative amplitude and frequency to the whole cell population (Figure 4.19A, Table 4.6), and possibly suggesting that the effect on respiratory neurons might define the behavior of the whole network. In light of these results, the opioid agonist DAMGO reduced the Ca^{2+} oscillatory activity of respiratory neurons in preBötC organotypic cultures.

During an inflammatory state or at birth, there is an endogenous release of PGE_2[388], which has been shown to increase the frequency of gasps and sighs at low concentrations[99] via activation

of the $G_{i/o}$-coupled EP3 receptor in the preBötC[97]. Furthermore, a mutual dependency on the cAMP pathway has been suggested for both opioids and prostanoids[324]. Thus, to study the possible interaction between the prostanoid and the opioid systems, we analyzed the effect of DAMGO in mice genetically modified to lack the PGE_2-EP3 receptor ($Ptger3^{-/-}$) and compared them to wild-type mice (WT). Administration of DAMGO (5 μM) in $Ptger3^{-/-}$ mice did not inhibit Ca^{2+} transient amplitude and produced a delayed effect on the oscillatory frequency, as it did not change within the first 10 min, and required 15 min to inhibit to the same extent than WT mice did within 5 min (17.0 ± 13.4% reduction within 15 min in $Ptger3^{-/-}$ mice; $n = 8$, $P < 0.05$ compared to baseline; Figures 4.19B and C). This result means that the DAMGO-induced reduction in Ca^{2+} transient frequency was more gradual in mice lacking the EP3 receptor, but equal in magnitude as in WT mice. Furthermore, this trend held for respiratory neurons, which showed a decrease in Ca^{2+} signaling frequency only within 15 min of DAMGO (5 μM) administration. Thus, showing that the modification in Ca^{2+} transient amplitude induced by DAMGO (5 μM) was hindered in $Ptger3^{-/-}$. Overall, this delayed effect of opioids in mice lacking the EP3 receptor suggests an interaction between the opioid and the prostanoid systems.

PreBötC pacemaker neurons have synchronized activity mediated by gap junctions and excitatory synaptic interactions[262,275]. This synchronized activity between interconnected cells is crucial for driving the inspiratory output[262]. According to the algorithm employed, two cells are defined as connected if their correlation coefficient exceeds the set cut-off[278]. Administration of DAMGO (5 μM) reduced the mean correlation above cut-off values in WT mice (from 0.74 ± 0.06 to 0.59 ± 0.07; $n = 7$, $P < 0.05$; Figure 4.19E) thus suggesting a reduced interconnectivity among cells. Furthermore, DAMGO (5 μM) administration reduced the number of correlations per active cell (from 33 ± 21 to 6 ± 3; $n = 7$, $P < 0.05$), suggesting a reduced functional coupling. Likewise, $Ptger3^{-/-}$ mice displayed similar reductions in the mean correlation above cut-off (from 0.86 ± 0.04 to 0.67 ± 0.10; $n = 8$, $P < 0.05$) and the number of correlations per active cell (from 61 ± 35 to 28 ± 18; $n = 8$, $P < 0.05$) upon DAMGO (5 μM) application. These results suggest that the opioid receptor agonist DAMGO reduced the network synchronization of preBötC cells in organotypic slices and that this effect was not altered in mice lacking the EP3 receptor.

Synchronized bursting activity depends on the network topology[389] and preBötC neurons organize into clusters interconnected by hubs resembling the small-world architecture[97,276]. Thereby, neighboring cells in a network are wired with a few migratory outputs that reduce the

average path length between nodes[277,278], and thus providing efficient transmission of information[371]. These networks are defined by the parameters: mean clustering coefficient (σ), mean shortest path length (λ), and small-world parameter (γ= σ/λ). DAMGO (0.5 – 5 μM) increased the σ within 5 min in WT mice (n = 7, both $P < 0.05$ compared to baseline; Figure 4.19F) and then it returned to baseline, suggesting increased segregation into clusters and tendency towards local connections during the first 5 min. Similarly, DAMGO (0.5 – 5 μM) increased the γ parameter (n = 7, both $P < 0.05$ compared to baseline; Figure 4.19F), indicating an enhancement of small-world features. Furthermore, the highest concentration of DAMGO (5 μM) increased λ by 11.8 ± 6.7% (n = 7, $P < 0.05$ compared to baseline; Figure 4.19F) and produced a higher increase in σ and γ than with DAMGO (0.5 μM) (n = 7, both $P < 0.05$; Figure 4.19F). Likewise, DAMGO (5 μM) increased σ and γ in Ptger3$^{-/-}$ mice within the same period (5 min) (Figure 4.19F) and did not change any further afterward. However, the DAMGO-induced effect on σ and γ was lower in Ptger3$^{-/-}$ than in WT mice (σ by 71.7% and γ by 75.5%; n = 8, both $P < 0.05$ compared to WT; Figure 4.19F). This result suggests that the effect of DAMGO on the network parameters may be hindered in mice lacking the EP3 receptor. Overall, these data insinuate that DAMGO reduced the synchronicity of the network by promoting segregation and local connections within a cluster with a reduction in the outgoing information.

Finally, to ascertain whether the observed effects induced by DAMGO were mediated by MOR activation, we tested the effect of DAMGO (5 μM) in the presence of the MOR antagonist naloxone. Administration of naloxone (5 μM) for 10 min did not change the Ca^{2+} signaling activity but completely abolished the DAMGO-induced reduction in Ca^{2+} transient frequency or relative amplitude in the whole network and respiratory neurons ($P < 0.05$ compared to control in the absence of naloxone; Table 4.6). Furthermore, naloxone blocked the DAMGO-induced modifications of the network parameters and connectivity. These results suggest that MOR activation mediates the inhibitory effect induced by DAMGO in preBötC cellular activity and connectivity *in vitro*.

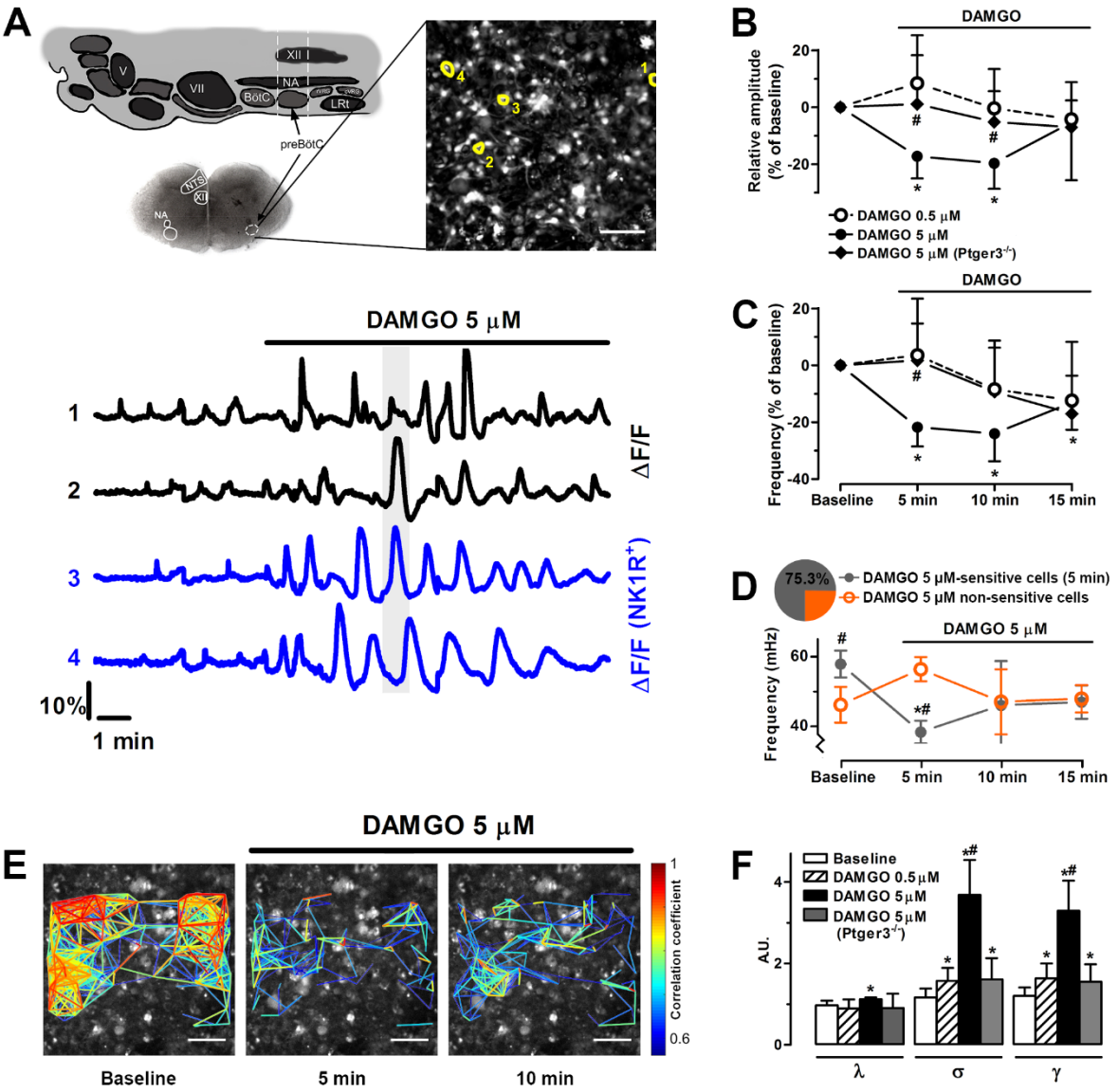

Figure 4.19. DAMGO modulates preBötC network activity and connectivity. **(A)** Localization of the preBötC in a sagittal drawing of the brainstem and in the coronal slice, which also contains the nucleus ambiguus (NA), the nucleus tractus solitarius (NTS), and the nucleus hypoglossus (XII) (Adapted from [97]). Effect of DAMGO (5 µM) administration on representative Ca^{2+} traces as $\Delta F/F_0$ from regular cells (black; #1 and 2) and $NK1R^+$ cells (respiratory neurons; #3 and 4 in blue) and their localization in a single frame of the Ca^{2+} signaling recording from a WT mouse (top right). **(B)** Inhibitory effect of DAMGO (0.5 – 5 µM) on Ca^{2+} transient relative amplitude and frequency **(C)** as a percentage of the baseline value in WT (circles) and $Ptger3^{-/-}$ (diamonds). **(D)** Cells that showed a decrease in Ca^{2+} transient frequency within 5 min of DAMGO (5 µM) administration as a percentage (gray filled circles) and their subsequent behavior over time, in comparison with the non-sensitive cells. Note that sensitive cells displayed a higher baseline frequency. **(E)** Graphical depiction of the network structure on top of NK1R-labelled cells. Each line represents the correlation coefficient above the set cut-off for the cell pairs, and warmer colors are a stronger correlation between the cells connected by the line. Administration of DAMGO (5 µM) decreased the number of correlated cells and the correlation coefficient. **(F)** Network parameter values revealing a small-world topology during baseline and upon DAMGO (0.5 – 5 µM) administration in WT and $Ptger3^{-/-}$ mice. Note that the highest concentration of DAMGO caused more effect than the lowest. Data are presented as means

± SD. * $P < 0.05$ compared to baseline (paired Student's t-test) and # $P < 0.05$ when compared among groups (paired Student's t-test in D and ANOVA followed by a Dunnett's *post hoc* test in the rest). A.U.: arbitrary units. Scale bars: 100 µm.

Table 4.6. Inhibitory effect of DAMGO (5 µM) within 5 min on the Ca^{2+} transient frequency and amplitude of preBötC cells (network) and respiratory neurons ($NK1R^{+}$) *in vitro* in the absence and presence of naloxone (5 µM). N: number of slices, n: number of cells. Data are presented as mean ± SD. *$P < 0.05$ when compared to their respective baseline values. Note that the effect on the respiratory networks resembled the effect of the whole network.

			Relative amplitude ($\Delta F/F_0$)		**Mean frequency (mHz)**	
	Cells	Sample size	Baseline	+DAMGO (5 µM)	Baseline	+DAMGO (5 µM)
Control	network	N=7, n=977	31.1 ± 3.0	25.6 ± 1.2*	55.6 ± 3.6	43.3 ± 2.9*
	$NK1R^{+}$	N=7, n= 110	32.6 ± 6.4	25.4 ± 1.9*	54.8 ± 3.9	43.1 ± 2.5*
Naloxone (5 µM)	network	N=8, n=1300	31.1 ± 3.9	30.7 ± 5.2	56.0 ± 7.3	54.7 ± 5.9
	$NK1R^{+}$	N=6, n=95	30.3 ± 4.4	29.3 ± 6.8	55.4 ± 7.5	50.3 ± 9.3

Effect of PGE_2 and its interaction with DAMGO on the cellular activity and network connectivity of the preBötC in vitro

Prostaglandins have been reported to inhibit the inspiratory nerve discharge in brainstem-spinal cord preparations[324] and to increase the frequency of sighs *in vivo*[97]. This effect may be particularly threatening in neonates, as high levels of PGE_2 metabolite in neonatal cerebrospinal fluid has been associated with severe perinatal asphyxia[104]. Furthermore, activation of EP3 receptors in the preBötC has been shown to decrease the Ca^{2+} transient frequency[97]. Here, we aimed to understand whether prostaglandins and opioids may interact to produce major respiratory depression. Thus, we examined the effect of PGE_2 in preBötC organotypic cultures and then tested the effect of DAMGO in the presence of PGE_2. Administration of PGE_2 (10 – 100 nM) for 5 min did not modify the relative Ca^{2+} transient amplitude but reduced the Ca^{2+} transient frequency in WT mice (n = 12 and n = 10, respectively, both $P < 0.05$ compared to baseline; Table 4.7; Figures 4.20A and B). This PGE_2-induced inhibitory effect was not observed in $Ptger3^{-/-}$ mice (n = 9 and n = 10, respectively, both $P < 0.05$ compared to WT; Table 4.7; Figure 4.20A), which suggests that EP3 receptor activation mediates the inhibition of network activity caused by PGE_2 in the preBötC *in vitro*, as already described[97]. Further, the effect of the highest concentration of PGE_2 (100 nM) was greater than that of PGE_2 (10 nM) (n = 10 and n = 12, respectively, $P < 0.05$; Table 4.7; Figures 4.20A and B) and more cells were inhibited (72.3 ± 8.5% *vs*. 58.3 ± 13.8%; n = 10 and n = 12,

respectively, $P < 0.05$; Figure 4.20B). Notably, during PGE_2 (100 nM) administration, the Ca^{2+} transient frequency reduction in $NK1R^+$ cells was similar to the whole cell population (Table 4.7), thus suggesting that preBötC respiratory neurons were sensitive to PGE_2, in accordance with previous studies[97].

Next, we assessed the possible interaction between opioids and prostaglandins by applying DAMGO in the presence of PGE_2. Thus, the lowest concentration of DAMGO (0.5 μM) in the presence of PGE_2 (10 nM) did not further change Ca^{2+} transient amplitude or frequency (from 53.5 ± 5.8 mHz to 51.8 ± 5.1 mHz in WT, before and after DAMGO administration; $n = 12$, $P > 0.05$ compared to the frequency during PGE_2 administration; Figures 4.20A and B). Similarly, bath perfusion with the highest concentration of DAMGO (5 μM) in the presence of PGE_2 (100 nM) did not further inhibit the Ca^{2+} transient frequency, but decreased the amplitude of the whole network and $NK1^+$ cells ($n = 10$, $P < 0.05$ compared to baseline; Table 4.7, Figures 4.20A and B). Furthermore, the DAMGO-induced reduction in Ca^{2+} transient frequency was smaller in the presence of PGE_2 than in the absence in WT but not in $Ptger3^{-/-}$ ($P < 0.05$ compared to controls in the absence of PGE_2), which suggest that the inhibitory effect of DAMGO was prevented by prior administration of PGE_2 in an EP3 receptor-dependent manner. Overall, these data indicate that the onset of PGE_2-induced inhibitory effect on Ca^{2+} oscillatory activity prevented any further reduction caused by DAMGO. Thus, EP3 receptor activation apparently occluded the effect of DAMGO and therefore, both EP3 and MOR receptor activation seems to share a similar signaling pathway, as elsewhere mentioned[324].

Table 4.7. Inhibitory effect of PGE_2 (100 nM) within 5 min on the Ca^{2+} transient frequency of preBötC cells (network) and respiratory neurons ($NK1R^+$) *in vitro* and effect of subsequent DAMGO (5 μM) administration in the presence of PGE_2 (100 nM). N: number of slices, n: number of cells. Data are presented as mean ± SD. * $P < 0.05$ when compared to their respective baseline values. Note that the effect on the respiratory networks resembled the effect of the whole network and that the inhibitory effect of PGE_2 was absent in slices from $Ptger3^{-/-}$ mice.

			Mean frequency (mHz)		
	Cells	Sample size	Baseline	+ PGE_2 (100 nM)	+ DAMGO (5 μM)
WT	network	N=10, n=1460	59.9 ± 5.2	48.2 ± 6.1*	50.9 ± 7.4*
	$NK1R^+$	N=8, n= 43	59.2 ± 7.4	51.6 ± 8.6*	52.6 ± 5.7
$Ptger3^{-/-}$	network	N=10, n=1938	55.1 ± 5.3	50.9 ± 9.5	47.8 ± 5.1*
	$NK1R^+$	N=9, n=288	53.8 ± 6.8	53.5 ± 15.1	46.6 ± 5.6*

Analysis of the network Ca^{2+} activity revealed that PGE_2 (10 nM) did not modify any parameter, but PGE_2 (100 nM) decreased the mean correlation above cut-off values in WT (from 0.74 ± 0.13 to 0.62 ± 0.10; n = 10, $P < 0.05$ compared to baseline; Figure 4.20C) and Ptger3$^{-/-}$ mice (from 0.77 ± 0.14 to 0.59 ± 0.15; n = 10, $P > 0.05$ compared to WT). These results suggest a decreased network synchronicity induced by PGE_2, which was not apparently mediated by the EP3 receptor. However, PGE_2 (100 nM) reduced the number of correlations per active cell in WT (from 36 ± 16 to 21 ± 17; n = 10, $P < 0.05$ compared to baseline) but not in Ptger3$^{-/-}$ mice, which implies that EP3 receptor activation may reduce the functional interconnectivity among cells. Overall, these data indicate that PGE_2 reduces the network connectivity and synchronicity of preBötC cells and that this effect may be partly mediated by EP3 receptor activation.

Intriguingly, DAMGO (5 μM) in the presence of PGE_2 (100 nM) increased the mean correlation above cut-off values (from 0.62 ± 0.10 to 0.82 ± 0.09; n = 10, $P < 0.05$ compared to the decrease observed during PGE_2 administration; Figure 4.20C) in WT but not in Ptger3$^{-/-}$ mice. Additionally, DAMGO (5 μM) administration in the presence of PGE_2 (100 nM) reversed the number of correlations per active cell to baseline conditions (from 21 ± 17 to 34 ± 26; n = 10, $P < 0.05$ compared to the decrease observed during PGE_2 administration) in WT but not in Ptger3$^{-/-}$ mice. These data suggest that DAMGO in the presence of PGE_2 increased the cellular activity synchronization, which was exactly the opposite behavior than in the absence of PGE_2 (see above). These could be due to an inhibitory effect of DAMGO on a broader number of cells, and then a network resynchronization (see discussion).

Finally, regarding the small-world topology, PGE_2 (100 nM) increased σ and γ in WT mice (n = 10, $P < 0.05$ compared to baseline; Figure 4.20D), suggesting segregation into stronger local connections and small-worldness. On the other hand, this effect was not observed in Ptger3$^{-/-}$ mice or with the lowest concentration of PGE_2 (10 nM) (n = 12, $P > 0.05$ compared to baseline; Figure 4.20D). Thus, suggesting that activation of EP3 receptors mediated the increase of segregation and small-world properties caused by PGE_2 application. In addition, subsequent administration of DAMGO (0.5 – 5 μM) in the presence of PGE_2 (10 – 100 nM) did not change any further the network parameters in WT (n = 10, $P < 0.05$ compared to baseline; Figure 4.20D) and Ptger3$^{-/-}$ mice. This result suggests that activation of EP3 receptors mediated by PGE_2 occluded the following modification of the small-world network features caused by DAMGO.

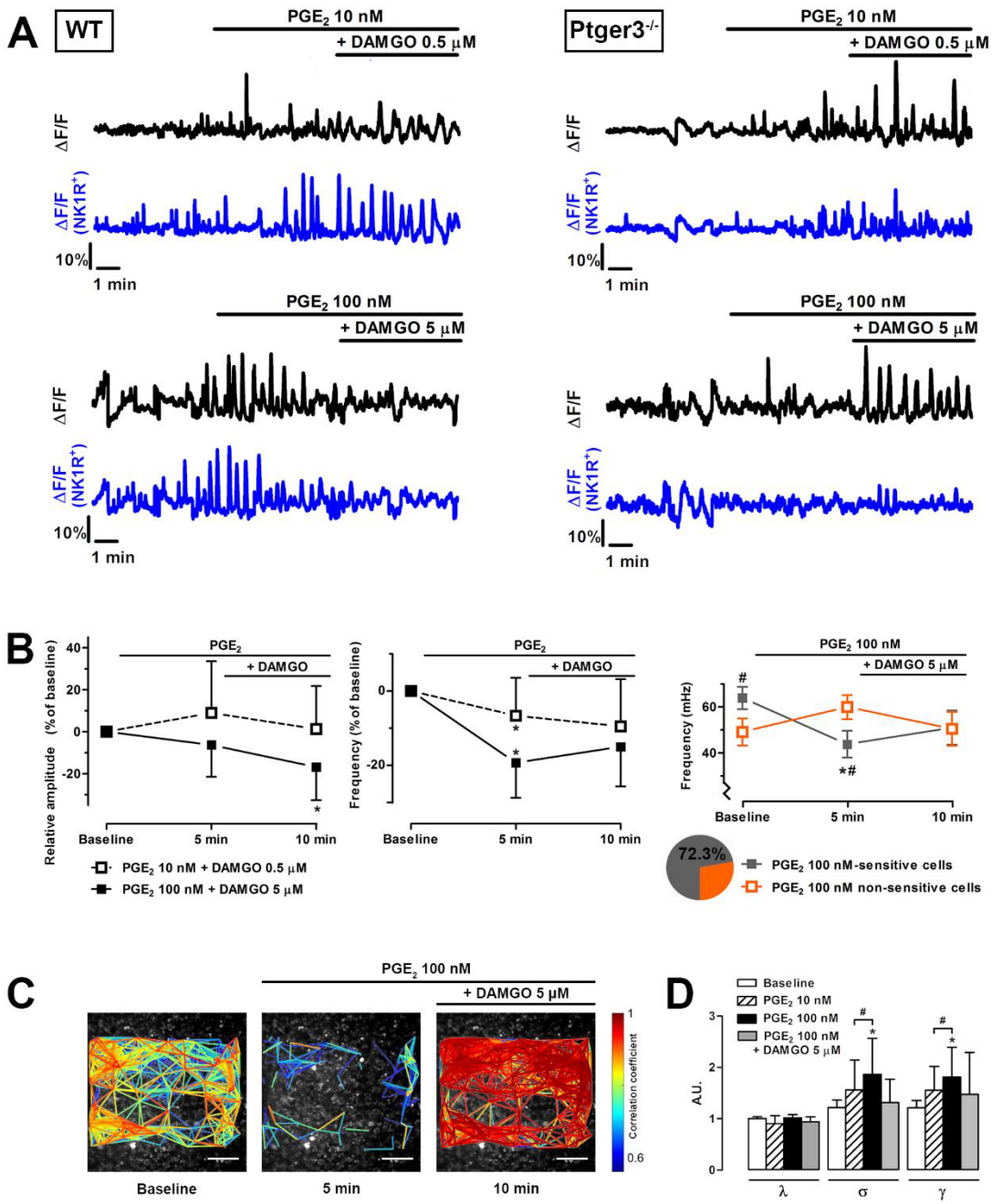

Figure 4.20. PGE_2 (10 – 100 nM) reduces preBötC network activity and connectivity in WT but not in Ptger3$^{-/-}$ mice and occludes the subsequent inhibitory effect induced by DAMGO (0.5 – 5 μM). **(A)** Representative Ca^{2+} traces as $\Delta F/F_0$ from regular cells (top black) and $NK1R^+$ cells (respiratory neurons, bottom blue) in WT (left) and Ptger3$^{-/-}$ mice (right). **(B)** Effect of PGE_2 (10 and 100 nM) and DAMGO (0.5 and 5 μM) administration on Ca^{2+} transient amplitude (left) and frequency (center) as a percentage of the baseline value in WT. Note that DAMGO in the presence of PGE_2 did not produce a further inhibitory effect on the Ca^{2+} transient frequency. At the right: cells that showed a decrease in Ca^{2+} transient frequency within 5 min of PGE_2 (100 nM) administration as a percentage (gray filled circles) and their subsequent behavior over time, in comparison with the non-sensitive cells. Note that PGE_2-sensitive cells displayed a higher baseline frequency and that DAMGO administration did not change the Ca^{2+} transient frequency in those cells, but decreased that of the PGE_2 non-sensitive cells. **(C)** Graphical depiction of the network structure on top of NK1R-labelled cells. Each line represents the correlation coefficient above the set cut-off for the cell pairs, and warmer colors are a stronger correlation between the cells connected

by the line. Administration of PGE_2 (100 nM) decreased the number of correlated cells and the correlation coefficient in WT mice, and this effect was reversed by DAMGO (5 μM). **(F)** Network parameter values revealing a small-world topology during baseline and upon PGE_2 (10 – 100 M) administration in WT. Note that the highest concentration of PGE_2 produced a greater effect. Subsequent administration of DAMGO (5 μM) in the presence of PGE_2 (100 nM) did not change the network parameters any further. Data are presented as means ± SD. * $P <$ 0.05 compared to baseline (paired Student's t-test) and # $P < 0.05$ when compared among groups (paired Student's t-test in A and unpaired in D). A.U.: arbitrary units. Scale bars: 100 μm.

Involvement of the cAMP/PKA pathway in the inhibitory effect caused by PGE_2 and DAMGO on the cellular activity and network connectivity of the preBötC in vitro

Both MOR and EP3 receptor activation has been described to couple to $G_{i/o}$ protein[286,373], which is known to decrease the production of cAMP. Further, a previous study made in isolated brainstem-spinal cord preparations has reported that pharmacological elevation of cAMP levels reversed the PGE_1- and opioid-induced inhibition of the respiratory nerve discharge[324]. To assess whether the proposed common mechanism converges on the cAMP pathway in the preBötC, we utilized the phosphodiesterase 4 (PDE4) inhibitor rolipram (5 μM), which potentially increases cAMP pathway signaling by blocking cAMP degradation. Then, we tested the effect of DAMGO (5 μM) and PGE_2 (100 nM) in the presence of rolipram. Bath perfusion of rolipram (5 μM) for 10 min increased relative Ca^{2+} transient amplitude within the first 5 min ($n = 8$, $P < 0.05$ compared to baseline), returning back to baseline levels after these 5 min (Figures 4.21A and B) and decreased the Ca^{2+} transient frequency within 10 min ($n = 8$, $P <$ 0.05 compared to baseline; Table 4.8, Figures 4.21A and B). On the other hand, upon rolipram administration, respiratory neurons showed a similar tendency in the Ca^{2+} oscillatory activity than the whole network, but it did not reach statistical significance ($P > 0.05$ compared to baseline; Table 4.8, Figure 4.21B). Given that a low number of slices were dyed for the NK1R in this group (Table 4.8), we pooled the $NK1R^+$ data of rolipram administration from before PGE_2 and DAMGO to test whether the respiratory neurons would reflect the response observed in the whole network. Thus, pooling the $NK1R^+$ data resulted in significant changes in Ca^{2+} transient relative amplitude within 5 min (from 26.5 ± 3.8 to 30.6 ± 4.4; $n = 12$, $P < 0.05$ compared to baseline) and frequency within 10 min (from 57.7 ± 6.0 to 51.1 ± 7.2; $n = 12$, $P <$ 0.05 compared to baseline). This result indicates that blocking the degradation of cAMP increased the relative Ca^{2+} transient amplitude, but decreased the Ca^{2+} transient frequency of preBötC cells and respiratory neurons *in vitro*.

Next, we tested the effect of DAMGO after these modifications in Ca^{2+} oscillatory relative amplitude and frequency induced by rolipram. Administration of rolipram (5 μM) completely blocked the DAMGO (5 μM)-induced changes in Ca^{2+} transient relative amplitude and frequency in the whole network ($n = 8$, $P < 0.05$ compared to control in the absence of rolipram, Table 4.8; Figures 4.21A, B, and C) and $NK1R^+$ cells ($n = 5$, $P < 0.05$ compared to control in the absence of rolipram) (Figures 4.21A and B; Table 4.8). These results indicate that the cAMP pathway may have a role in the inhibitory effect caused by DAMGO in the cellular activity of the respiratory network and respiratory neurons of the preBötC.

Likewise, rolipram (5 μM) prevented the reduction in Ca^{2+} transient frequency induced by PGE_2 (100 nM) in the whole network ($P < 0.05$ compared to control in the absence of rolipram; Table 4.8, Figures 4.21A, B, and C). Further, this blockade was also observed in respiratory neurons, which did not display any further decrease in the Ca^{2+} transient frequency upon PGE_2 administration ($P > 0.05$ compared to the previous 5 min period in the presence of rolipram; Table 4.8; Figure 4.21B). However, this effect was not different from $NK1R^+$ cells in controls ($P > 0.05$ compared to control in the absence of rolipram). These results indicate that inhibition of the cAMP degradation reverted the modification in the respiratory network activity induced by PGE_2, but not that observed in respiratory neurons. Overall, these data suggest that the levels of cAMP may modulate the respiratory depression observed with opioids and prostaglandins, as previously suggested[324], and thus, that the cAMP pathway may be the endpoint of the presumed common signaling mechanism.

Table 4.8. Inhibitory effect of rolipram (5 μM) within 10 min on the Ca^{2+} transient frequency of preBötC cells (network) and respiratory neurons ($NK1R^+$) *in vitro* and effect of subsequent DAMGO (5 μM) or PGE_2 (100 nM) administration in the presence of rolipram (5 μM). N: number of slices, n: number of cells. Data are presented as mean ± SD. * $P < 0.05$ when compared to their respective baseline values. N.S.: not significant when the group of DAMGO or PGE_2 was compared to the previous 5 min period in the presence of rolipram. Note that once rolipram had decreased the Ca^{2+} transient frequency, neither DAMGO nor PGE_2 induced any further modification.

			Mean frequency (mHz)			
	Cells	Sample size	Baseline	+ rolipram (5 μM)	+ DAMGO or PGE_2	
DAMGO	network	N=8, n=1943	57.3 ± 4.6	52.8 ± 3.1*	50.9 ± 2.7*	N.S.
(5 μM)	$NK1R^+$	N=5, n= 78	52.2 ± 3.7	46.3 ± 4.6	49.2 ± 5.4	N.S.
PGE_2	network	N=8, n=1796	57.3 ± 3.1	53.3 ± 3.4*	52.0 ± 5.2*	N.S.
(100 nM)	$NK1R^+$	N=7, n=98	61.6 ± 3.6	53.7 ± 6.8*	50.0 ± 7.0*	N.S.

Regarding the network circuitry, administration of rolipram (5 μM) reduced the mean correlation above cut-off within 10 min (from 0.74 ± 0.04 to 0.65 ± 0.08; n = 8, $P < 0.05$ compared to baseline; Figure 4.21D) and hindered the DAMGO (5 μM)-induced modification in the mean correlation above cut-off (from 0.65 ± 0.08 to 0.68 ± 0.06; n = 8, $P < 0.05$ compared to control in the absence of rolipram; Figure 4.21D). These results suggest that rolipram may reduce the interconnectivity among cells but prevented that caused by DAMGO. Furthermore, rolipram administration did not change the number of correlations per active cell but blocked the reduction caused by DAMGO (from 14 ± 14 to 12 ± 15; n = 8, $P > 0.05$ compared to baseline before DAMGO). However, this effect was not different from that observed under control conditions (n = 8, $P > 0.05$ compared to control in the absence of rolipram), possibly due to the high variability. These data suggest that inhibition of cAMP degradation partially hampered the effect of DAMGO on the network configuration. Furthermore, administration of rolipram (5 μM) for 10 min did not modify σ, γ or λ, but abolished the DAMGO-induced changes in small-world features (n = 8, $P < 0.05$ compared to control in the absence of rolipram; Figure 4.21E). Thus, these results suggest that the cAMP pathway seems to mediate the decrease in network synchronicity and connectivity caused by DAMGO in the preBötC.

Furthermore, bath perfusion of rolipram (5 μM) reduced the mean correlation above cut-off within 10 min (from 0.80 ± 0.06 to 0.71 ± 0.11; n = 8, $P < 0.05$ compared to baseline; Figure 4.21D) and blocked the reduction in the mean correlation above cut-off induced by PGE_2 (100 nM) (from 0.71 ± 0.11 to 0.68 ± 0.11; n = 8, $P < 0.05$ compared to control in the absence of rolipram; Figure 4.21D). Additionally, PGE_2 in the presence of rolipram did not alter the number of correlations per active cell (from 12 ± 13 to 5 ± 5; n = 8, $P > 0.05$ compared to baseline before PGE_2) but this effect was not different from that observed under control conditions (n = 8, $P > 0.05$ compared to control in the absence of rolipram). These data suggest that the cAMP pathway seems to be partially involved in the effect of PGE_2 on the network configuration. Further, PGE_2 (100 nM) in the presence of rolipram did not change σ or γ (n = 8, $P > 0.05$ compared to baseline before PGE_2; Figure 4.21E). However, this effect was not different from that observed in controls (n = 8, $P > 0.05$ compared to control in the absence of rolipram), possibly due to the high variability. Thus, these data reveal that blockade of cAMP degradation with rolipram hindered the inhibitory effect of PGE_2 on Ca^{2+} transient frequency and network synchronicity, but it did not seem to intervene in the small-world topology modification caused by PGE_2. As a whole, the cAMP pathway seemed to be involved in both MOR and EP3 receptor activation in the preBötC organotypic cultures.

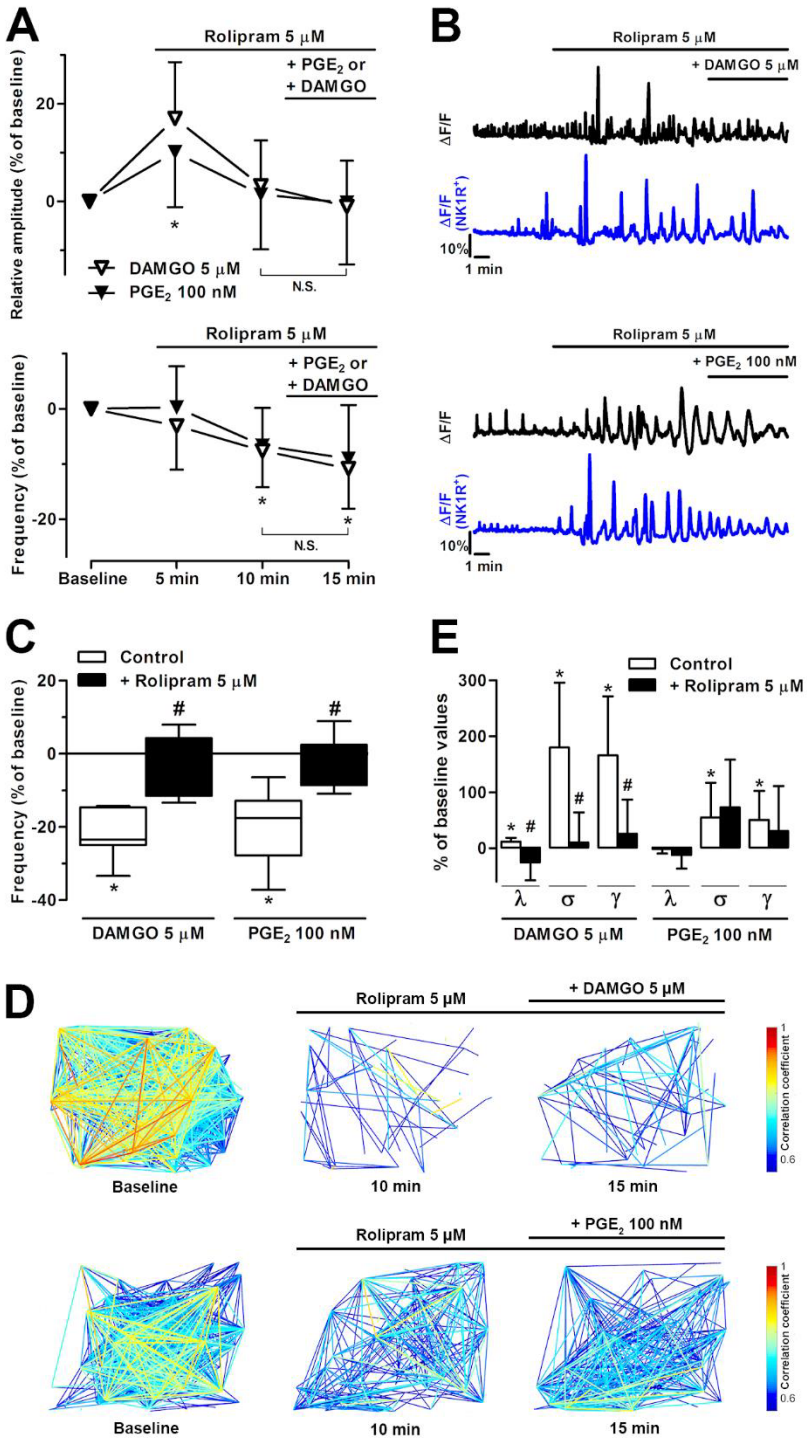

Figure 4.21. Administration of rolipram (5 μM) prevented both DAMGO (5 μM)- and PGE_2 (100 nM)-induced reduction in preBötC network activity and connectivity. **(A)** Effect of rolipram (5 μM) and subsequent administration of DAMGO (5 μM) or PGE_2 (100 nM) on Ca^{2+} transient relative amplitude (top) and frequency (bottom). Note that neither DAMGO nor PGE_2 modified the Ca^{2+} transient relative amplitude or frequency after administration of rolipram. **(B)** Representative Ca^{2+} traces showing the effect of rolipram and subsequent DAMGO or PGE_2 administration as $\Delta F/F_0$ from regular cells (top black) and $NK1R^+$ cells (respiratory neurons, bottom blue). **(C)** Effect of DAMGO (5 μM) or PGE_2 (100 nM) in the presence of rolipram (5 μM) on Ca^{2+} transient frequency compared to their respective control in the absence of rolipram. The effects were normalized to their baseline in

control or baseline in the presence of rolipram). **(D)** Graphical depiction of the network structure. Each line represents the correlation coefficient above the set cut-off for the cell pairs, and warmer colors are a stronger correlation between the cells connected by the line. Administration of rolipram (5 μM) decreased the correlation coefficient in WT mice, and subsequent application of DAMGO (5 μM) (top) or PGE_2 (100 nM) (bottom) did not decrease the mean correlation any further. **(E)** Rolipram (5 μM) prevented the increase in network parameter values induced by DAMGO (5 μM), but not that of PGE_2 (100 nM). The experimental values were normalized to their respective baseline. Data are presented as means ± SD. * $P < 0.05$ compared to baseline (paired Student's t-test) and # $P < 0.05$ when compared among groups (unpaired Student's t-test).

Involvement of GIRK channel activation in the inhibitory effect caused by PGE_2 and DAMGO on the cellular activity of the preBötC in vitro

Opioid-induced respiratory depression *in vivo* is thought to be mediated by GIRK channels[290]. Thus, to verify the involvement of GIRK channels in the inhibitory effect caused by DAMGO or PGE_2 *in vitro*, we incubated the organotypic slices with the GIRK channel blocker SCH-23390 (15 μM) for 30 min during Fluo-8 loading, and then, we tested the effect of DAMGO (5 μM) or PGE_2 (100 nM) by time-lapse Ca^{2+} imaging. Incubation with SCH-23390 (15 μM) did not alter the basal Ca^{2+} transient amplitude (baseline $\Delta F/F_0$ without SCH-23390 = 31.3 ± 3.0 *vs.* with SCH-23390 = 27.5 ± 3.4; $n = 8$, $P > 0.05$) nor frequency (baseline without SCH-23390 = 55.6 ± 3.6 mHz *vs.* with SCH-23390 = 57.3 ± 5.5 mHz; $n = 8$, $P > 0.05$) compared to baseline values before DAMGO (5 μM) administration in controls. However, GIRK channel blockade with SCH-23390 completely prevented the inhibitory effect of DAMGO (5 μM) on Ca^{2+} transient amplitude and frequency in the whole network and $NK1R^+$ cells ($n = 8$, $P < 0.05$ compared to control in the absence of SCH-23390; Table 4.9, Figures 4.22A and B). This result indicates that GIRK channel activation is involved in the opioid-induced inhibition of respiratory network and respiratory neurons *in vitro*.

Next, we determined whether SCH-23390 would hinder as well the PGE_2-induced inhibition in Ca^{2+} oscillatory frequency. Thus, upon SCH-23390 (15 μM) incubation, PGE_2 (100 nM) did not reduce the Ca^{2+} transient frequency in the whole network and respiratory neurons ($P < 0.05$ compared to control in the absence of SCH-23390; Table 4.9, Figures 4.22A and B). This result suggests that GIRK channel activation seemed to participate in both the opioid- and PGE_2-induced inhibition of cellular calcium activity and respiratory neurons in preBötC organotypic cultures.

Regarding the network connectivity, slice incubation with SCH-23390 (15 μM) did not change the baseline values of mean correlation above cut-off (without SCH-23390: 0.74 ± 0.06 *vs*. 0.80 ± 0.09 with SCH-23390; $n = 8$, $P > 0.05$ compared to baseline values before DAMGO 5 μM administration in controls). However, SCH-23390 hampered DAMGO (5 μM)-induced reduction in the mean correlation above cut-off (from 0.80 ± 0.09 to 0.70 ± 0.09; $n = 8$, $P < 0.05$ compared to control in the absence of SCH-23390; Figure 4.22C) and the number of correlations per active cell (from 23 ± 15 to 16 ± 15; $n = 8$, $P < 0.05$ compared to control in the absence of SCH-23390). Therefore, GIRK channel activation seemed to contribute to the asynchronous network activity caused by DAMGO in the preBötC. Further, incubation with SCH-23390 (15 μM) did not change the σ, γ or λ parameters compared to control ($n = 8$, $P < 0.05$ compared to control in the absence of SCH-23390). However, SCH-23390 blocked the DAMGO (5 μM)-induced modification of small-world features, as it prevented the increase in σ and γ parameters caused by DAMGO ($n = 8$, $P < 0.05$ compared to control in the absence of SCH-23390; Figure 4.22D). Therefore, in view of these data, GIRK channel activation was involved in the reduction of cellular calcium activity produced by DAMGO, and also in the modification of the network synchronicity and small-world topology of preBötC cells *in vitro*.

On the other hand, after slice incubation with SCH-23390 (15 μM), PGE_2 (100 nM) did not significantly reduce the mean correlation above cut-off (from 0.79 ± 0.08 to 0.75 ± 0.09; $n = 9$, $P > 0.05$ compared to baseline; Figure 4.22C) but this effect was not different from that observed under control conditions ($n = 9$, $P > 0.05$ compared to control in the absence of SCH-23390). Furthermore, GIRK channel blockade with SCH-23390 did not prevent the reduction in the number of correlations per active cell caused by PGE_2 (100 nM) (from 30 ± 23 to 4 ± 2; $n = 9$, $P < 0.05$ compared to baseline and $P > 0.05$ *vs.* control in the absence of SCH-23390). Thus, GIRK channel activation was not apparently involved in the PGE_2-induced reduction of the network synchronicity. Further, PGE_2 (100 nM) administration after slice incubation with SCH-23390 did not increase the σ and γ parameters (Figure 4.22D), and this effect was not different from control in the absence of SCH-23390 ($n = 9$; $P > 0.05$ compared to control). Thus, blocking the GIRK channel activation did not seem to prevent the asynchronous network activity and small-world topology caused by PGE_2 in preBötC organotypic cultures. Overall, these data indicate that GIRK channel activation seems to mediate the opioid- and PGE_2-induced inspiratory frequency inhibition, but it does not apparently intervene in the network rewiring induced by the latter.

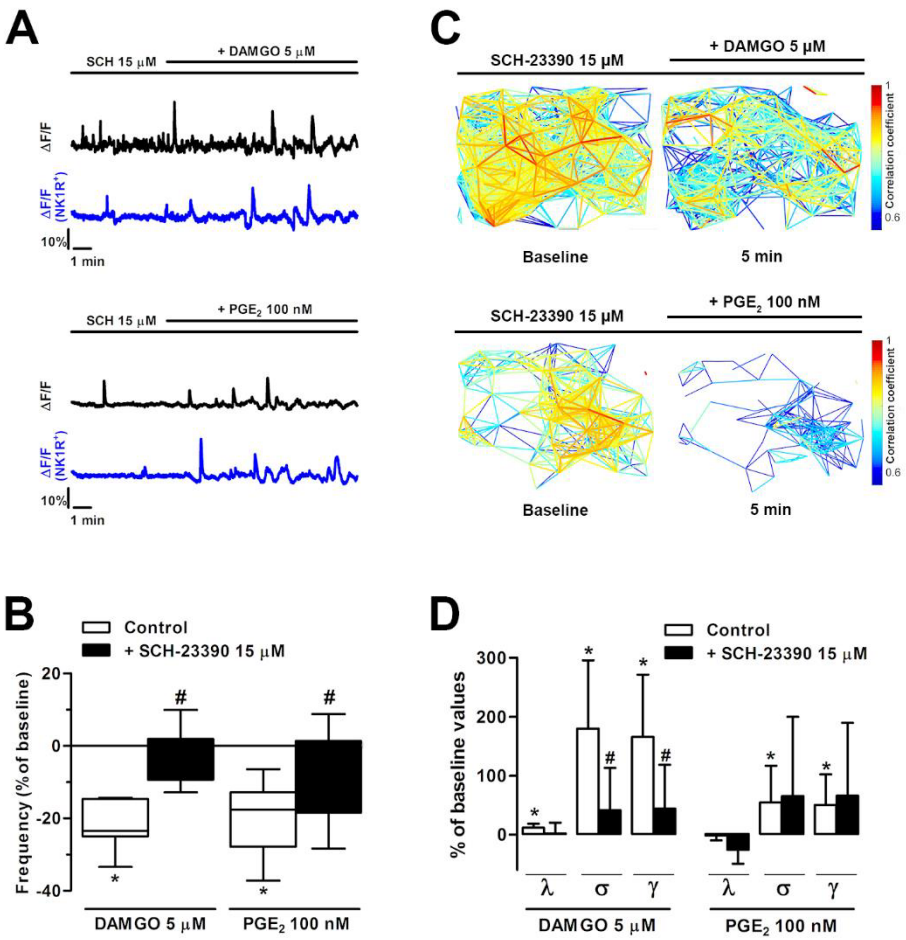

Figure 4.22. Administration of SCH-23390 (15 μM) prevented both DAMGO (5 μM)- and PGE_2 (100 nM)-induced reduction in preBötC network activity. **(A)** Representative Ca^{2+} traces showing the effect of SCH-23390 and subsequent DAMGO or PGE_2 administration as $\Delta F/F_0$ from regular cells (top black) and $NK1R^+$ cells (respiratory neurons, bottom blue). Note that neither DAMGO nor PGE_2 modified the Ca^{2+} transient relative amplitude or frequency after administration of rolipram. **(B)** Effect of DAMGO (5 μM) or PGE_2 (100 nM) after incubation SCH-23390 (15 μM) on Ca^{2+} transient frequency compared to their respective control in the absence of SCH-23390. The effects were normalized to their respective baseline. **(C)** Graphical depiction of the network structure. Each line represents the correlation coefficient above the set cut-off for the cell pairs, and warmer colors are a stronger correlation between the cells connected by the line. Incubation with SCH-23390 (15 μM) prevented the decrease in the number of correlated cells and the correlation coefficient induced by DAMGO (5 μM), but not that induced by PGE_2 (100 nM). **(D)** SCH-23390 (15 μM) prevented the increase in network parameter values induced by DAMGO (5 μM), but not that of PGE_2 (100 nM). The experimental values were normalized to their respective baseline. Data are presented as means ± SD. * $P < 0.05$ compared to baseline (paired Student's t-test) and # $P < 0.05$ when compared among groups (unpaired Student's t-test).

Table 4.9. Effect of SCH-23390 (15 μM) incubation on the Ca^{2+} transient frequency of preBötC cells (network) and respiratory neurons ($NK1R^+$) *in vitro* and effect of subsequent DAMGO (5 μM) or PGE_2 (100 nM) administration in the presence of SCH-23390 (15 μM). N: number of slices, n: number of cells. Data are presented as mean ± SD. N.S.: not significant when the group of DAMGO or PGE_2 was compared to their respective baseline.

			Mean frequency (mHz)		
	Cells	Sample size	Baseline	+ DAMGO or PGE_2	
DAMGO (5 μM)	network	N=8, n=755	57.3 ± 5.5	55.2 ± 7.6	N.S.
	$NK1R^+$	N=5, n=72	54.6 ± 7.4	55.9 ± 4.6	N.S.
PGE_2 (100 nM)	network	N=9, n=1000	59.0 ± 6.8	53.8 ± 5.2	N.S.
	$NK1R^+$	N=4, n=83	59.0 ± 6.2	60.1 ± 5.6	N.S.

5 DISCUSSION

5.1 STUDY I – INHIBITION OF RAT LOCUS COERULEUS NEURONS VIA PROSTAGLANDIN E_2 EP3 RECEPTOR: PHARMACOLOGICAL CHARACTERIZATION *IN VITRO*

The present work was undertaken to characterize the functional role of EP3 receptors in LC neurons in rat brain slices. Our results show that the EP3 receptor agonists sulprostone, PGE_2, and misoprostol inhibits in a concentration-dependent manner the neuronal activity of LC cells *in vitro*. This inhibitory effect was blocked by the selective EP3 receptor antagonist L-798,106, but not by the EP2 or EP4 receptor antagonists, indicating that the observed effect was mediated by EP3 receptor activation. Furthermore, sulprostone-induced inhibition of the firing rate was hindered by pretreatment with the $G_{i/o}$ protein inhibitor PTX and the GIRK blockers $BaCl_2$ and SCH-23390. Thus, our results suggest that the EP3 receptor activation inhibits the firing activity of LC neurons, presumably by its coupling to $G_{i/o}$ proteins and the subsequent opening of GIRK channels.

Dense EP3 receptor immunoreactivity has been found by double immunofluorescence in the neuropil and in a few cell bodies of the LC[65], where there is also strong expression of EP3 receptor mRNA[63]. Furthermore, the LC contains constitutive COX-2, the rate-limiting enzyme for prostaglandin synthesis[21], suggesting the presence of endogenous prostaglandins in this nucleus. In our study, we assessed the functional role of EP3 receptors by using extracellular recordings *in vitro* and application of EP3 receptor agonists. Sulprostone was selected as an EP3 receptor agonist based on its more than 300-fold higher affinity for the EP3 than for the EP1 receptor[357]. Sulprostone was perfused at similar concentrations previously used to study EP3 receptor-mediated effects in rodent brain slices from the cortex[318] and the LC[338]. We also assessed the biological relevance of the endogenous prostanoid system by perfusing PGE_2, which has high affinity for all the EP receptors but especially for the EP3 receptor (EP3 ≥ EP4 > EP2 > EP1)[357]. Moreover, we tested the PGE_1 analog, commercially available misoprostol, which has higher selectivity for the EP3 receptor (affinity: EP3 > EP4 > EP2)[357]. On the other hand, we used as EP3 receptor antagonist L-798,106, which is highly selective for the EP3 receptor compared to the EP4 receptor[361]. Finally, the EP2 receptor antagonist has no affinity for the EP3 receptor at the concentrations herein used[341], while L-161,982 shows much higher affinity for the EP4 than for the EP3 receptor[362].

In the present study, sulprostone, PGE_2, and misoprostol completely inhibited the firing activity of LC neurons. The inhibitory effect was blocked by an EP3 receptor antagonist but not by EP2 or EP4 receptor antagonists, ruling out the involvement of EP2 or EP4 receptors in this inhibition. EP1 receptor-mediated effects may be unlikely in our system because low EP1 receptor mRNA expression has been reported in the brainstem[54]. In our study, the determined EC_{50} values of the concentration-effect curves for sulprostone, misoprostol, and PGE_2 and the rank order of potency found for firing activity inhibition (sulprostone > misoprostol > PGE_2) were consistent with preceding data in rodent brain cortex slices, where the same agonists inhibited the NA release with 0.4-1.0 fold higher pIC_{50} values (8.22, 8.00, and 7.74, respectively[318]). Furthermore, in guinea-pig aorta comparable EC_{50} values were found for the sulprostone-induced vasoconstriction (23 nM)[390]. The pK_B value for the EP3 receptor antagonist L-798,106 herein reported was equivalent when either sulprostone or misoprostol were used as standard agonist (5.8 – 5.9), which supports the evidence for the activation of a common EP3 receptor. However, when PGE_2 was used as an agonist, the pK_B value was 0.4 units higher, suggesting that PGE_2 may also activate interfering non-EP3 receptors. In this regard, in the presence of PF-04418948 and L-161,982, the concentration-effect curve for PGE_2 was shifted to the left, which could suggest that PGE2 may also activate G_s protein-coupled EP2 and EP4 receptors counteracting the EP3 receptor-mediated inhibition. Other authors have estimated a 2 units higher pK_B value for L-798,106 when sulprostone and PGE_2 were used as standard agonists in peripheral tissues, such as guinea-pig smooth muscle[339,391]. This disparity could be due to the high lipophilicity of L-798,106, which determines the equilibration kinetics and the pK_B calculation[339], or to the different tissues (muscle *vs.* brain slices) and species employed (guinea-pig *vs.* rat). In summary, EP3 receptor activation by selective agonists inhibits the firing rate of LC neurons.

In line with our results, c-fos expression, an indicator of neuronal activity, is increased in the LC from morphine-dependent rats and this enhancement is reversed by EP3 receptor agonists administered centrally[120], suggesting that the neuronal activity of LC cells is inhibited by EP3 receptor activation. Furthermore, a single concentration of sulprostone has recently been shown to hyperpolarize LC neurons in slices from mice[338]. Likewise, other electrophysiological studies have demonstrated an EP3 receptor-mediated inhibition of central neurotransmission in other brain regions. Thus, EP3 receptor activation by PGE_2 reduces glutamatergic transmission in the dorsolateral periaqueductal gray[301], GABAergic

transmission in the paraventricular nucleus of the hypothalamus[392], and network activity in the neocortex[305]. In contrast to our results, a neuronal activity increase has been described upon PGE_2 administration in serotonergic neurons of the dorsal raphe nucleus, but the exact mechanism has not been fully elucidated[393].

EP3 receptor activation has been described to be coupled to $G_{i/o}$ proteins [373]. In our research, the sulprostone-induced inhibitory effect was reduced by the $G_{i/o}$ signaling inhibitor PTX[394], indicating that EP3 receptor activation leads to cell inhibition by stimulation of $G_{i/o}$ proteins. $G_{i/o}$-mediated effects have been previously described for the EP3 receptor in other brain regions, such as in the hippocampus, where PTX blocks the EP3 receptor-induced ischemic excitotoxicity[373]. Inhibition of firing activity of LC neurons has been described to occur after opening of GIRK channels by $G_{i/o}$-protein $\beta\gamma$ subunits[166], such as upon activation of $G_{i/o}$ protein-coupled μ-opioid receptors and α_2 adrenoceptors[375,395]. Barium and SCH-23390 are effective GIRK channel blockers[396] that have been reported to stimulate the firing rate of LC cells[397]. Indeed, in our study, administration of barium and SCH-23390 increased the firing rate of LC neurons and prevented the effect of sulprostone, supporting an involvement of GIRK channels in the EP3 receptor-mediated effect in the LC. Similarly, in sympathetic neurons, PGE_2 activates GIRK channels probably through a $G_{i/o}$-dependent mechanism[374].

Our results show that EP3 receptor activation inhibits the activity of LC neurons in rat brain slices, likely through opening of postsynaptic $G_{i/o}$-coupled GIRK channels. This inhibitory effect on the LC may regulate NA release throughout projection areas of the CNS and thus add to the local inhibitory EP3 receptors on nerve terminals regulating NA release[318,320]. The prostanoid system in the LC could play a role in the regulation of pain. Thus, the LC exerts a supraspinal descending control of pain[135] and activation of a neuronal subpopulation of the LC evokes an anti-nociceptive response[135]. One possible consequence would be that EP3 receptor activation in the LC may lead to a hyperalgesic effect. In line with this hypothesis, inflammatory stimuli reduce the analgesic effect induced by opioids in the LC[197]. Likewise, in the PAG, EP3 receptor activation exerts pro-nociceptive actions[115]. Prostaglandin release and EP3 receptor activation in the LC may also modulate the neuroinflammatory response and febrile response. In this regard, c-Fos expression is increased in the LC by inflammatory insults through the prostanoid synthesis[180] and the febrigenic effect of PGE_2, which involves EP3 receptors[91], is mediated by a neuronal network including the LC[204]. Finally, EP3 receptors in the LC may be relevant for some neuropsychiatric diseases. Thus, enhanced

expression of EP3 receptor has been found around amyloid plaques in LC-projecting areas in Alzheimer's disease[398]. Furthermore, lesions of the LC enhance both pro-inflammatory cytokines[232] and amyloid-β deposition in the hippocampus of a mouse model of Alzheimer's disease[198]. Regarding psychiatry, stimulation of prefrontal-projecting neurons in the LC results in anxiety-like behavior[136], thereby reduction of LC-noradrenergic cell activity by the EP3 receptor could attenuate anxiety, as shown by a previous study in which sulprostone infusion into the LC produced anxiolytic effects[338]. In conclusion, the prostaglandin system in the LC would play a relevant role in the regulation of central physiology, and the EP3 receptor in this nucleus might be a suitable pharmacological target for the development of novel treatments for different neuropsychiatric disorders.

5.2 STUDY II – PHARMACOLOGICAL CHARACTERIZATION OF PROSTANOID EP2 RECEPTOR IN RAT LOCUS COERULEUS NEURONS *IN VITRO*

Our study was aimed to pharmacologically characterize the EP2 receptor in LC neurons from rat brain slices by extracellular electrophysiological techniques. We found that the EP2 receptor agonists butaprost and treprostinil increase the firing activity of LC neurons *in vitro*. This excitatory effect was blocked by the EP2 receptor antagonist PF-04418948, but not by the EP3 or EP4 receptor antagonists (L-798,106 and L-161,982, respectively), indicating that it was mediated by EP2 receptor activation. The butaprost-induced increase in the firing rate of LC cells was prevented in the presence of low sodium-containing aCSF and the $G_{\beta\gamma}$-signaling inhibitor gallein. However, blockers of the $G_{\alpha s}$/cAMP/PKA pathway or TRP and Kir6.2 channels failed to change the butaprost-induced stimulatory effect. These results suggest that activation of the EP2 receptor stimulates the neuronal activity of LC cells, presumably by its coupling to $G_{\beta\gamma}$ proteins and an inward sodium current.

In our study, we assessed the functional role of EP2 receptors in LC neurons by using extracellular electrophysiology *in vitro* and application of EP2 receptor agonists. Butaprost was selected as an EP2 receptor agonist since its free acid form shows an 18-fold higher affinity for the EP2 than for the EP3 receptor[357] and has been previously used at similar concentrations to explore EP2 receptors in brain slices[93]. We also assessed the effect of treprostinil, a clinically used PGI_2 analog that has high affinity for several prostanoid receptors, especially high for the EP2 receptor (EP2=DP1>IP>EP1>EP4>EP3)[358]. On the other hand, we used PF-04418948 as EP2 receptor antagonist since it has very low affinity for any other prostanoid receptor[341]. L-161,982 has much higher affinity for the EP4 than for EP3 receptors[362], while L-798,106 shows higher affinity for the EP3 than for the EP4 or other EP receptors[361].

In the current study, butaprost and treprostinil increased the neuronal activity of LC cells and generated similar parameters of the concentration-effect curves (EC_{50} and Emax), suggesting equivalent efficacy and potency in the LC. Furthermore, the EC_{50} of the concentration-effect curve for butaprost was in accordance with that found in other systems (0.64 μM)[399]. In our work, the excitatory effect caused by butaprost and treprostinil was blocked by PF-04418948, and not by L-798,106 or L-161,982. In fact, PF-04418948 displaced to the right the concentration-effect curve for butaprost, whereas it reduced the Emax for treprostinil without any rightward shift. This difference could be explained by additional activation of other receptors or mechanisms by treprostinil, such as the phylogenetically related G_s-coupled DP1

receptor[358,400]. However, the blockade of the treprostinil-induced effect with PF-04418948 supports the involvement of, at least, the EP2 receptor. Alternatively, one could speculate that a slow dissociation rate of PF-04418948 from the EP2 receptor and a higher receptor reserve[369] for butaprost than for treprostinil could account for the differences observed with butaprost and treprostinil in the presence of PF-04418948. In any case, the calculated pK_B of PF-04418948 for the EP2 receptor was equivalent when obtained by butaprost or by treprostinil. Furthermore, similar pK_B values for PF-04418948 are obtained when PGE_2 is used in other tissues[341]. These data indicate that the excitatory effect observed with butaprost and treprostinil in LC neurons was mediated by EP2 receptor activation.

EP2 receptor activation in neurons has been described to elicit a sodium current through the cAMP/PKA pathway[376]. In our work, the butaprost-induced excitatory effect was completely abolished by replacement of 80% of the extracellular sodium by TRIS, indicating the involvement of sodium current. In agreement, PGE_2 elicits a sodium current in cerebellar[376] and spinal neurons[300], leading to neuronal depolarization in the latter case. In the LC, sodium currents could be generated by TRP channels, as previously reported in response to CO_2[213]. In our study, perfusion with the non-selective TRP channel blocker 2-APB at concentrations previously used in other brain regions *in vitro*[401] failed to change the butaprost-induced excitatory effect. On the other hand, inhibition of Kir6.2 channels has been shown to contribute to excitatory responses in LC neurons, which could be hindered by the Kir6.2 channel blocker glibenclamide[344]. However, in our study, glibenclamide did not affect the butaprost-induced excitatory response. Therefore, our data indicate that sodium current is a final downstream effector of EP2 receptor activation, and Kir6.2 or TRP channels do not seem to be involved in this effect.

In LC noradrenergic neurons, inward sodium currents are activated by the cAMP/PKA pathway[327]. In our research, the butaprost-induced excitatory effect was not mediated by the cAMP/PKA/HCN pathway as the PKA activator 8-Br-cAMP, the PKA inhibitor H-89 or the HCN channel blocker ZD7288 failed to modify the stimulatory effect caused by butaprost. Our results contrast with the main signaling mechanism described for excitatory responses mediated by the EP2 receptor in other brain regions. Thus, PGE_2 increases the hypothalamic neuronal activity[3] and hippocampal synaptic transmission[26] via EP2 receptor-mediated activation of the cAMP/PKA pathway. However, other authors have previously suggested that cAMP/PKA/HCN is not involved in EP2 receptor-mediated responses. Thus, in nodose

ganglion neurons, PGE_2 elicits a sodium current by EP2 receptors without the intervention of the cAMP/PKA pathway[402].

The EP2 receptor has been published to be coupled to G_s proteins[58]. However, NF449, a selective inhibitor of the association between $G_{\alpha s}$ and GTP[347], failed to reduce the butaprost-induced excitation, while it blocked the effect of VIP, which increases the firing rate of LC cells by a $G_{\alpha s}$/cAMP/PKA-dependent sodium current[173]. This means that butaprost effect is not mediated by $G_{\alpha s}$ proteins. On the other hand, the excitation caused by butaprost was prevented by the $G_{\beta\gamma}$-signaling inhibitor gallein, which binds to the "hot spot" of the G_β subunit[403]. In our study, gallein did not modify the inhibitory effect of the μ opioid receptor agonist ME on the LC, which is mediated by $G_{i/o}$ protein βγ subunits[404]. Likewise, other authors have described that a gallein analog fails to affect $G_{i/o}$ protein βγ-mediated effects in other systems[405], suggesting diversity and selectivity of the $G_{\beta\gamma}$ subunits for different downstream signaling mechanisms. Furthermore, a direct binding of $G_{\beta\gamma}$ subunits to voltage-gated sodium channels (Na_v) have been reported in cell cultures[406,407]. In LC neurons, tetrodotoxin (TTX)-sensitive Na_v contribute to the pacemaker activity[150], although a TTX-resistant current has also been described[150]. Furthermore, EP2 receptor activation has been associated with the enhancement of TTX-resistant sodium current in ganglion neurons[402]. However, in our study, we cannot conclude that the Na_v channel mediates the effect of EP2 receptors on sodium currents and whether it is directly modulated by EP2 receptor-activated $G_{\beta\gamma}$ subunits.

Finally, in our research, blockade of GABAergic or glutamatergic transmission in the LC did not decrease but rather enhanced the butaprost-induced stimulatory effect. These results are congruent with the presence of EP2 receptors enhancing inhibitory GABAergic regulation of noradrenergic cells or glutamatergic afferents, which blockade would increase the butaprost-induced excitatory effect. However, the neuronal subpopulation expressing the EP2 receptor is yet to be characterized in the brain.

In conclusion, our work supports the existence of functional postsynaptic EP2 receptors in LC neurons, which activation results in a concentration-dependent increase of the spontaneous firing rate *in vitro*. The underlying mechanism may require $G_{\beta\gamma}$ subunits and sodium currents, but it does not involve a $G_{\alpha s}$, TRP or cAMP/PKA-dependent pathway. According to previous data from our laboratory, the endogenous PGE_2 has a preferential inhibitory effect on LC neurons mediated by EP3 receptor activation (see Study I), and herein, we demonstrate the functional role of EP2 receptors in the regulation of the firing rate. Since the LC has been shown to contribute to the affective processing of nociception by promoting anxiogenic-like

behavior during chronic pain[408], EP2 receptor activation in the LC may be of relevance in the integration of pain stimuli by enhancing NA release throughout the CNS. This suggestion is supported by the cognitive impairment observed in mice lacking the EP2 receptor[409]. Furthermore, both β-adrenoreceptor and EP2 receptor activation elicit anti-inflammatory effects in microglial cells[198,351]. Therefore, it may be reasonable to suggest that the EP2 receptor in the LC could further tune the inflammatory response to PGE_2 in the brain. An immunomodulatory effect of EP2 receptors may be relevant for the pathophysiology of Alzheimer's disease, and the prevention of neuronal death upon amyloid β-peptide exposure[410]. Consequently, the EP2 receptor signaling in the LC could become a novel therapeutic target for pain and neuroinflammatory diseases.

5.3 STUDY III – PHARMACOLOGICAL CHARACTERIZATION OF PROSTANOID EP4 RECEPTOR IN RAT LOCUS COERULEUS NEURONS *IN VITRO*

The purpose of this study was to characterize the functional role of EP4 receptors in LC neurons by extracellular electrophysiological techniques. We found that the EP4 receptor agonists rivenprost and TCS 2510 increase the neuronal activity of LC cells *in vitro*. This excitatory effect was blocked by the EP4 receptor antagonist L-161,982, but not by the EP2 or EP3 receptor antagonists PF-04418948 and L-798,106, respectively, indicating an EP4 receptor-mediated effect. The increase in firing rate of LC neurons caused by rivenprost was blocked by extracellular sodium replacement and a $G_{\alpha s}$ signaling inhibitor, but not by blockers of the cAMP/PKA pathway, TRP channels, $G_{\beta\gamma}$ subunits, PI3K or PKC signaling. Thus, these results suggest that EP4 receptor activation stimulates the neuronal activity of LC cells, presumably by its coupling to $G_{\alpha s}$ proteins and an inward sodium current.

In our study, we characterized the functional role of EP4 receptors in LC neurons by using extracellular electrophysiology *in vitro*, EP4 receptor agonists, and EP receptor antagonists. The concentrations of the EP4 receptor agonists rivenprost and TCS 2510 used herein were based on the affinity data demonstrated in radioligand binding experiments, which show that rivenprost has 80-fold higher affinity for the EP4 than for EP3 or EP2 receptors[359] and TCS 2510 fails to have affinity at the tested concentration range for non-EP4 receptors[360]. Furthermore, the involvement of the EP4 receptor was demonstrated with the specific antagonist L-161,982, which shows a more than 200-fold higher affinity for the EP4 than for EP3 receptors[362]. The EP2 receptor antagonist PF-04418948 does not show antagonistic affinity for any other EP receptor[341], while L-798,106 has much higher affinity for the EP3 than for EP4 receptors[361].

In the present study, administration of rivenprost or TCS 2510 increased the firing rate of LC neurons. In the case of rivenprost, the EC_{50} value (1.43 nM) was similar to its K_i value measured in cell membranes (0.7 nM)[359], whereas the EC_{50} value for TCS 2510 (18.0 nM) was higher than that of rivenprost, but at the same range as that described in other tissues (e.g., isolated smooth muscle, pIC_{50}: 7.6)[411]. The excitatory effect of rivenprost or TCS 2510 was mediated by EP4 receptor activation since it was only blocked by L-161,982, but not by perfusion with L-798,106 or PF-04418948. In our work, L-161,982 shifted to the right the concentration-effect curve for rivenprost but reduced the Emax for TCS 2510 without any rightward shift. This disparity of effects was unlikely to be caused by activation of other EP receptors, given the high selectivity of these ligands for the EP4 receptor. Furthermore, the Schild slope for L-

161,982 was less than unity when calculated with rivenprost and furthermore different pK_B values were found for various concentrations of L-161,982. According to different authors, a slow dissociation rate of the antagonist and a higher receptor reserve for one of the agonist[369] (i.e., rivenprost) could explain the different pharmacological profiles observed with rivenprost and TCS 2510 in the presence of L-161,982. Moreover, the calculated pK_B of L-161,982 for the EP4 receptor resulted in 7.69 by double equieffective concentrations of TCS 2510, which was at similar concentration ranges to the pK_B obtained for L-161,982 with rivenprost (7.67). Furthermore, the result obtained in our study for L-161,982 was akin to its K_i value (32 nM) measured by binding assays in cell cultures with PGE_2 as an agonist[362]. Overall, these data indicate that the observed excitatory effect of rivenprost or TCS 2510 was mediated by EP4 receptor activation.

Activation of G_s-coupled EP4 receptors modulates sodium currents in brain neurons (e.g., cerebellar granule cells[376]). In our work, the blockade of the rivenprost-induced stimulation of LC cells by extracellular sodium replacement reveals the involvement of sodium currents. In agreement, PGE_2 has been shown to enhance sodium currents via EP4 receptors in cerebellar[376] and nodose ganglion neurons[402]. Furthermore, EP4 receptor activation increases the firing rate of supraoptic neurons, which has been suggested to be mediated by non-selective cation channels[303]. In the LC, sodium currents can be elicited by non-selective cation TRP channels in response to hypercapnia[213]. However, in our study, the TRP channel blocker 2-APB did not prevent the excitatory effect induced by rivenprost, which indicates that the TRP channel is not involved in the rivenprost-induced excitatory effect.

EP4 receptor activation elicits a sodium current via activation of G_s proteins and cAMP/PKA pathway[376]. In the current study, the rivenprost-induced stimulation was blocked by the $G_{\alpha s}$ signaling inhibitor NF449, but not by the $G_{\beta\gamma}$ signaling inhibitor gallein, which suggests that the EP4 receptor is coupled to $G_{\alpha s}$ proteins in the LC. However, the rivenprost-induced excitatory effect was not mediated by the cAMP/PKA pathway as it was not occluded by the PKA activator 8-Br-cAMP nor blocked by the PKA inhibitor H-89, which were perfused at the same concentrations used in other brain areas *in vitro*[173,345]. Although these results are in contrast with the signaling mechanism described for the EP4 receptor in neurons[412], some other authors have pointed out a cAMP-independent pathway for EP4 receptor-mediated effects. For example, chronic exposure to PGE_2 downregulates the EP4 receptor-mediated cAMP/PKA pathway activation in cultured DRG neurons[413] and TCS 2510 fails to raise cAMP levels in mast cells[368]. Likewise, activation of the EP2 receptor, which also induces excitatory responses

in LC neurons, is not dependent on the cAMP/PKA pathway (see Study II). Since both EP2 and EP4 receptors activate sodium currents in the LC via a non cAMP/PKA pathway, in the present work, we compared the effect of rivenprost with or without administration of the EP2. Thus, the excitatory effect of rivenprost was not occluded by butaprost effect, which suggests an uncommon signaling pathway for both EP2 and EP4 receptors. This divergence could be explained by phylogenetic differences, as they only share a 31% amino acid identity in mice[61]. Overall, these data indicate that EP4 receptor activation in LC neurons is coupled to a $G_{\alpha s}$ protein and a sodium current, but not dependent on cAMP/PKA and $G_{\beta\gamma}$ subunit signaling.

On the other hand, EP4 receptor activation has been linked to the PI3K signaling pathway in cell cultures[81,352] and DRG neurons[82]. In the latter case, activation of the PI3K promotes the externalization of the EP4 receptor, which could enhance the nociceptive transmission[82]. However, according to our data, the PI3K inhibitor wortmannin did not block the excitatory effect of rivenprost in LC cells but rather potentiated it. It has been shown that EP4 receptor activation stimulates the PI3K pathway via $G_{i/o}$ proteins in cultured cells[81]. Furthermore, the EP4 receptor can couple to both G_s and $G_{i/o}$ proteins in cell cultures, with the degree of activation of G_s and $G_{i/o}$ protein depending on the functional selectivity of EP4 receptor agonists[414]. In our system, we cannot exclude a simultaneous coupling of the EP4 receptor to the $G_{i/o}$/PI3K pathway in LC cells, which would counteract the excitatory effect of EP4-$G_{\alpha s}$ and would be unmasked in the presence of wortmannin. In addition to the PI3K, a PKC-dependent pathway has been described for EP4 receptor-mediated effects, such as in DRG neurons[353]. However, in our work, the PKC inhibitor chelerythrine did not block the excitatory effect of rivenprost but further enhanced it, which rules out the implication of this enzyme in the rivenprost-induced stimulation.

In summary, our work supports the existence of functional EP4 receptors in LC neurons, which activation results in a concentration-dependent increase in the spontaneous firing rate. The underlying mechanism may involve the $G_{\alpha s}$ protein and a sodium current, but it does not seem to involve $G_{\beta\gamma}$, TRP, cAMP/PKA, PI3K, or PKC-dependent pathways. Further studies will be carried out to test whether the coupling of EP4-Gαs and sodium currents is a direct mechanism. According to previous data from our laboratory, the endogenous PGE_2 has a preferential inhibitory effect on LC neurons mediated by EP3 receptor activation (see Study I). We have also described a stimulatory effect of LC neurons caused by EP2 receptor activation (see Study II). In this study, we demonstrate the presence of EP4 receptors in the LC, which could further tune the inflammatory response to PGE_2 in the brain. Thus, EP4 receptor signaling in the LC

may gain relevance during inflammatory states, since peripheral inflammation has been reported to upregulate EP4 receptor expression in DRG[107] and brain catecholaminergic neurons[57]. This suggestion is also supported by the rise in c-Fos immunoreactivity in response to an inflammatory insult in brain regions expressing the EP4 receptor[57]. Furthermore, chronic inflammatory pain, which is known to release PGE_2, has been shown to enhance anxiety-like behaviors in rodents[415] and the LC mediates some of the affective events involved in the processing of nociception by promoting anxiogenic-like behavior during chronic pain[408]. It is therefore tempting to speculate that EP4 receptor activation in the LC may be of relevance in the integrative reaction to pain stimuli possibly by enhancing NA release throughout the CNS. Therefore, the prostaglandin system and the EP4 receptor in the LC might be suitable pharmacological targets for the development of novel treatments for inflammatory pain and anxiety-derived disorders.

5.4 STUDY IV – INTERACTION BETWEEN OPIOIDS AND PROSTAGLANDIN E_2 IN THE INSPIRATION-GENERATING PREBÖTZINGER COMPLEX

The purpose of this study was to assess whether the opioid-induced respiratory depression was intensified under inflammatory conditions (i.e., those caused by PGE_2) by time-lapse calcium imaging in brainstem organotypic cultures. In the preBötC cellular network, we found that both MOR agonist DAMGO and EP3 receptor agonist PGE_2 reduced Ca^{2+} oscillatory activity. The effect of DAMGO was blocked by naloxone, whereas deletion of the EP3 receptor abolished the PGE_2-induced effect and delayed that of DAMGO. The reduction in Ca^{2+} oscillatory activity caused by DAMGO was occluded by prior administration of PGE_2, which suggested a common signaling pathway. Indeed, both DAMGO and PGE_2-induced modification in Ca^{2+} activity was prevented by blocking cAMP degradation and GIRK channel activation. Furthermore, both DAMGO and PGE_2 reduced the number of connections among cells and the synchronicity.

Recently, we have developed brainstem organotypic slice cultures containing the preBötC that allow the study of the respiratory brainstem activity *in vitro*[97]. These cultured slice preparations maintain the respiratory-related rhythm[97,252] identical to acute slices[252] while preserving the cytoarchitecture[97]. These features, along with the tissue flattening over time[97,252], create an optimal model for the activity evaluation of a broad population of cells by calcium imaging techniques and their synchronicity by means of cross-correlation analysis[278]. Furthermore, preBötC respiratory neurons *in vitro* preserve rhythmic Ca^{2+} transients in phase with the inspiratory motor output measured on the hypoglossal XII nerve[239], and therefore, the observed calcium oscillatory activity in our study is representative of the respiratory rhythm. The PreBötC was identified in our slices with the fluorescent ligand TMR-SP, which labels the NK1R-positive cells and thereby, the respiratory neurons[119]. In our study, we measured the effect of DAMGO as MOR agonist since it has high affinity and selectivity for the MOR[416]. The effect of DAMGO was antagonized by using naloxone, which shows high affinity for all opioid receptors, but especially for the MOR[416]. The endogenous inflammatory response was mimicked by using PGE_2, a non-selective EP receptor agonist that shows high affinity for the EP3 receptor[357]. Finally, the fluorescent dye employed here was non-ratiometric, so the described amplitude data is relative to its baseline, and no intracellular Ca^{2+} concentration could be inferred.

In the current study, DAMGO and PGE_2 reduced Ca^{2+} transient frequency in what seemed a concentration-dependent fashion, as we tested two different concentrations of each and the

highest concentration produced a greater inhibition in the frequency than the lowest. Furthermore, the DAMGO (5 μM)-induced reduction in Ca^{2+} transient frequency of the whole population (22%) was similar to that observed with PGE_2 (100 nM) (19%), and further, similar to the breathing frequency reduction (18%) *in vivo* caused by microinjection of DAMGO into the preBötC described elsewhere[253]. An improvement in the data analysis allowed us to know how single cells behaved over time and how many of them varied their frequency compared to their baseline. By using this script, 75% of the cells showed a marked frequency reduction of 34% upon DAMGO, and similarly, 72% of the cells displayed a frequency reduction with PGE_2 of 32%. Moreover, $NK1R^+$ data revealed that the reduction in Ca^{2+} transient frequency in respiratory neurons upon DAMGO and PGE_2 is representative of the whole population, which may suggest that the respiratory neurons define the activity of the entire network. This result is in agreement with previous reports in similar brainstem slice culture preparations, which observed Ca^{2+} oscillatory activity only from neurons and not from glial cells[252]. Furthermore, previous data from our laboratory demonstrated that $NK1R^+$ cells respond to PGE_2 in the preBötC[97] and co-express EP3 receptor in medullary sections at the preBötC level[38]. In line, other studies showed a co-expression of MOR and NK1R in the preBötC[119,253], and accordingly, preBötC respiratory neurons have been considered fundamental for the opioid-induced respiratory depression[254].

In our study, the DAMGO-induced reduction in Ca^{2+} transient frequency was prevented by the application of the MOR antagonist naloxone and delayed by deleting the EP3 receptor. Thus, in $Ptger3^{-/-}$ mice, DAMGO (5 μM) needed 15 min instead of 5 min to cause the same magnitude of effect as in WT mice, suggesting a hindered effect of DAMGO in $Ptger3^{-/-}$ mice. Interestingly, this late effect was similar to that observed with the lowest concentration of DAMGO (0.5 μM) in WT mice. Furthermore, the PGE_2-induced frequency decrease was absent in mice lacking the EP3 receptor, in agreement with previous results from our laboratory[97]. These results highlight the functional relevance of the EP3 receptor in the preBötC. Similarly, activation of the EP3 receptor has been shown to have inhibitory actions in other brain regions, for example, it inhibits the network frequency in the neocortex[305] and the neuronal activity of the central chemosensitive LC cells (see Study I). In contrast with our study, PGE_2 has shown to increase the fictive sigh frequency in preBötC acute slices, and even increase the eupnoeic frequency at higher concentrations than those employed in our study[99]. These differences could be due to a loss of selectivity at higher concentrations of PGE_2, given that it has a high affinity for many other prostanoid receptors, and the receptor mediating this effect was not determined in that study.

In the present work, the onset of the PGE_2-induced inhibitory effect occluded any further reduction in Ca^{2+} oscillatory activity caused by DAMGO. Furthermore, this result is congruent with the attenuation of the morphine-induced respiratory depression observed in a neuropathic pain model[417], where the involvement of PGE_2 is widely known[418]. This occlusion could be caused by the reach of a maximum reduction in Ca^{2+} transient frequency, considering the ongoing Ca^{2+} dynamics that are partly regulated by intracellular stores, and thus a basal Ca^{2+} fluctuation. However, a common signaling pathway was elsewhere mentioned[324], so we tested whether it would be plausible. The nature of the proposed common mechanism would be the result of a signaling pathway convergence in either the cAMP or the GIRK channels, based on previous data[290,324]. In our study, administration of the blocker of cAMP degradation rolipram prevented the DAMGO- and PGE_2-induced reduction in Ca^{2+} oscillatory activity. This result agrees with previous studies showing that rolipram restores the inspiratory-related rhythm after DAMGO-induced inhibition in acute slices[288] and that high cAMP levels reverse the DAMGO- and PGE_1-induced respiratory depression in brainstem-spinal cord preparations[324]. On the other hand, incubation with the GIRK channel blocker SCH-23390 prevented the reduction in Ca^{2+} transient frequency caused by both DAMGO and PGE_2 in our study. These data agree with previous reports *in vivo*, describing that the respiratory rate decrease produced by microperfusion of DAMGO into the preBötC is blocked by a GIRK channel inhibitor[290]. Furthermore, immunohistochemical techniques have demonstrated that $NK1R^+$ cells in the preBötC co-express GIRK channels[289], which suggests that these channels are present in respiratory neurons, and thus, that may intervene in the opioid- and PGE_2-induced respiratory depression. Overall, the inhibitory actions of PGE_2 and DAMGO on the cellular Ca^{2+} transient frequency seems to be mutually dependent on cAMP levels and GIRK channels.

The respiratory rhythmogenesis is thought to be driven by preBötC cellular activity coordination into a group pacemaker mediated by glutamatergic transmission and electrical coupling[262,275]. Thus, the study of the network synchronization may be key for understanding the mechanism of opioid- and prostaglandin-induced respiratory depression. Herein, both DAMGO and PGE_2 reduced the mean correlation above cut-off and the number of correlations per active cell, suggesting a reduction in the network circuitry and synchronization. In line with our results, elimination of correlated population activity and desynchronization of Ca^{2+} activity have been observed in the preBötC *in vitro* after blockade of gap junctions[97] and glutamatergic synaptic transmission[262]. It is therefore tempting to speculate that the DAMGO- and PGE_2-induced respiratory depression may be caused by the lack of integrated group pacemaker activity. Intriguingly, in our results, DAMGO restored the baseline values of mean correlation

and number of correlations per active cell after the reduction caused by PGE_2. This means that the effect of DAMGO in the presence of PGE_2 was the opposite than in the absence, suggesting that DAMGO administration might affect a broader number of cells that reconfigure the circuit, possibly through an additional mechanism. Furthermore, synchronized bursting activity depends on the network topology[389], and the preBötC is organized into a small-world architecture[97,276], where the neuronal connections are favored within clusters, in comparison with across clusters[276]. In fact, in our work, both DAMGO and PGE_2 increased the clustering coefficient and small-world parameter, suggesting segregation into local clusters and a shift towards a more regular topology, which is less synchronizable than the small-world composition[277]. Similar alterations of small-world structures have been observed in patients with Alzheimer's disease and neuromyelitis optica[419,420], where the global activity integration may be compromised, leading to a weaker population bursting in a computational model[389]. Overall, the opioid-induced asynchronous network seems to be mediated by MOR activation with the involvement of the cAMP pathway and GIRK channels; while the PGE_2-induced asynchrony seemed to be partly mediated by the EP3 receptor and the cAMP pathway. These results may suggest a different mechanism for PGE_2-induced disruption of network organization, possibly mediated by persistent sodium current and gap junctions as previously suggested for other effects caused by PGE_2 in the preBötC[97,99].

In conclusion, PGE_2 modulates preBötC activity *in vitro* and it seems to interact with the opioid-induced inhibitory effect, so a common signaling pathway was proposed, with the apparent involvement of the cAMP pathway and GIRK channels. Furthermore, both opioids and prostaglandins seem to disrupt the structural integrity of the network, leading to less wiring and synchronicity. Thus, the current study supports that preBötC inspiratory neurons mediate the opioid- and PGE_2-induced respiratory depression by reducing their activity and synchronization. However, it remains unknown the possible implication of other areas of the breathing brainstem[421,422], such as the recently discovered postinspiratory complex (PiCo)[261], that may shape the *in vivo* opioid response into a quantal slowing of the respiratory rhythm[323]. The endogenous release of PGE_2 during inflammation and the concurrent treatment with opioids may condition the ventilatory behavior, which may be of relevance in post-operative states. Moreover, the pediatric population should receive special consideration given the endogenous release of PGE_2 at birth[388] and the implication of PGE_2 in neonatal breathing disorders[98,423], which may ultimately lead to apneas during infections by attenuating the hypercapnic and hypoxic response[98].

6 CONCLUSIONS

1. EP3 receptor activation inhibits LC neuron firing activity in rat brain *in vitro* with a rank order of agonist potencies being: sulprostone > misoprostol > PGE_2. An EP3 receptor antagonist, but not EP2 or EP4 receptor antagonists, causes rightward shifts of the concentration-effect curves for the EP3 receptor agonists. These results indicate that acute administration of sulprostone, PGE_2 or misoprostol induces an inhibitory effect on the LC neuron activity via EP3 receptor activation.

2. The concentration-effect curve for sulprostone is shifted to the right by the blocker of the $G_{i/o}$ protein-dependent pathway pertussis toxin. Furthermore, GIRK channel blockers prevent the sulprostone-induced inhibitory effect. This shows that the EP3 receptor may be coupled to $G_{i/o}$ proteins and its activation may lead to the opening of GIRK channels, causing an inhibition of the firing activity of LC neurons.

3. The EP2 receptor agonists butaprost and treprostinil increase LC neuron firing activity in rat brain *in vitro*. An EP2 receptor antagonist, but not EP3 or EP4 receptor antagonists causes a rightward shift of the concentration-effect curve for butaprost and reduces the maximal excitatory effect caused by treprostinil. These results suggest that butaprost and treprostinil increase LC neuron activity via EP2 receptor activation.

4. The butaprost-induced excitatory effect is blocked by a decrease in the extracellular concentration of sodium, which suggests that the excitation caused by EP2 receptors depends on a sodium current. According to pharmacological assays, this sodium current is not mediated by TRP, HCN or potassium Kir6.2 channels. Furthermore, the butaprost-induced excitatory effect is not prevented by manipulation of the cAMP/PKA pathway, inhibition of synaptic transmission or blockade of $G_{\alpha s}$ subunits. Only $G_{\beta\gamma}$-signaling inhibition reduces the excitatory effect caused by butaprost, thus revealing a role for the $G_{\beta\gamma}$ subunits. These data suggest that EP2 receptor activation postsynaptically may excite LC neuron activity via a sodium current and $G_{\beta\gamma}$-dependent pathway, but not through the $G_{\alpha s}$/cAMP/PKA pathway.

5. The EP4 receptor agonists rivenprost and TCS 2510 increase LC neuron firing activity in rat brain *in vitro*. This excitatory effect is prevented by an EP4 receptor antagonist, as it induces a shift to the right in the concentration-effect curve for rivenprost and

reduces the maximal excitatory effect caused by TCS 2510. These results suggest that rivenprost and TCS 2510 may increase LC neuron activity via EP4 receptor activation.

6. The rivenprost-induced excitatory effect is blocked by a decrease in the extracellular concentration of sodium, which suggests that the excitation caused by EP4 receptors depends on a sodium current. According to pharmacological assays, this sodium current does not seem to be mediated by TRP channels or the cAMP/PKA pathway. Furthermore, the rivenprost-induced excitatory effect is not changed by blockers of the PI3K, PKC, and $G_{\beta\gamma}$ signaling. Previous administration of the EP2 receptor agonist butaprost does not occlude the excitatory effect caused by rivenprost, suggesting a divergent signaling pathway for both receptors. Inhibition of $G_{\alpha s}$ signaling reduces the excitatory effect induced by rivenprost. These data reveal that EP4 receptor activation may excite LC neuron activity via $G_{\alpha s}$-dependent trigger of a sodium current, but not by the cAMP/PKA, PI3K or PKC pathways.

7. The MOR agonist DAMGO and the PGE_2 reduce the Ca^{2+} transient frequency of preBötC cells and respiratory neurons in organotypic slices. The effect of DAMGO is blocked by previous administration of the MOR antagonist naloxone and delayed on time by deleting the Ptger3 gene ($Ptger3^{-/-}$ mice). These results suggest that the inhibitory effect on Ca^{2+} oscillatory activity caused by DAMGO is mediated by MOR activation and that there may be an interaction between MOR and EP3 receptors. On the other hand, the effect of PGE_2 is absent in $Ptger3^{-/-}$ mice, which indicates that the PGE_2-induced effect is mediated by EP3 receptor activation.

8. The inhibitory effect of DAMGO on Ca^{2+} transient frequency is occluded by previous administration of PGE_2, suggesting that PGE_2 interferes with the opioid-induced respiratory depression. Blockers of the cAMP degradation and GIRK channels prevent both DAMGO- and PGE_2-induced reductions in Ca^{2+} oscillatory activity, suggesting a convergence on the cAMP pathway and GIRK channels in preBötC cells.

9. Furthermore, DAMGO and PGE_2 reduce the cellular connectivity and synchronicity of the respiratory network, which alters the small-world features. The effect of DAMGO is abolished by naloxone and blockers of the cAMP degradation and GIRK channels, while the effect of PGE_2 is partially hindered by Ptger3 gene deletion ($Ptger3^{-/-}$ mice)

and blockers of the cAMP degradation. These data suggest that the DAMGO-induced asynchrony may be mediated by MOR activation, GIRK channel opening, and possibly also by inhibition of the cAMP pathway. On the other hand, the PGE_2-induced asynchrony seems to be only partially mediated by EP3 receptor activation and inhibition of the cAMP pathway.

Taken together, these results provide functional data regarding the role of the prostanoid system in modulating the cellular activity of the LC and the preBötC *in vitro*. In addition, our results highlight the signaling mechanism downstream of EP receptors. Our data support an inhibitory and excitatory regulation of the firing activity of LC neurons *in vitro* by EP3, EP2, or EP4 receptors. EP3 receptor-mediated inhibition of LC neurons may occur through $G_{i/o}$ proteins and GIRK channels, whereas EP2 and EP4 receptor-mediated excitation of LC neurons appear to be mediated through $G_{\beta\gamma}$ and $G_{\alpha s}$-dependent activation of sodium currents, respectively. On the other hand, PGE_2 inhibits the preBötC cellular activity and interferes with the opioid-induced respiratory depression. Given the role of the LC and the preBötC in the regulation of nociception and its affective component, as well as in the induction of fever, anxious states, and the inspiratory pattern, the presence of the prostanoid system in these brain areas may constitute a suitable target for the treatment of neuropsychiatric or breathing disorders triggered or mediated by neuroinflammatory mediators.

7 REFERENCES

1. Engblom, D. *et al.* Prostaglandins as inflammatory messengers across the blood-brain barrier. *J. Mol. Med.* **80**, 5–15 (2002).

2. Hétu, P.-O. & Riendeau, D. Cyclo-oxygenase-2 contributes to constitutive prostanoid production in rat kidney and brain. *Biochem. J.* **391**, 561–566 (2005).

3. Clasadonte, J. *et al.* Prostaglandin E2 release from astrocytes triggers gonadotropin-releasing hormone (GnRH) neuron firing via EP2 receptor activation. *Proc. Natl. Acad. Sci.* **108**, 16104–16109 (2011).

4. Forsberg, D., Ringstedt, T. & Herlenius, E. Astrocytes release prostaglandin E2 to modify respiratory network activity. *Elife* **6**, (2017).

5. Ranels, H. J. & Griffin, J. D. The effects of prostaglandin E2 on the firing rate activity of thermosensitive and temperature insensitive neurons in the ventromedial preoptic area of the rat hypothalamus. *Brain Res.* **964**, 42–50 (2003).

6. Poon, D. C.-H., Ho, Y.-S., Chiu, K., Wong, H.-L. & Chang, R. C.-C. Sickness: From the focus on cytokines, prostaglandins, and complement factors to the perspectives of neurons. *Neurosci. Biobehav. Rev.* **57**, 30–45 (2015).

7. Legler, D. F., Bruckner, M., Uetz-von Allmen, E. & Krause, P. Prostaglandin E2 at new glance: Novel insights in functional diversity offer therapeutic chances. *Int. J. Biochem. Cell Biol.* **42**, 198–201 (2010).

8. Spencer, A. G., Woods, J. W., Arakawa, T., Singer, I. I. & Smith, W. L. Subcellular localization of prostaglandin endoperoxide H synthases-1 and -2 by immunoelectron microscopy. *J. Biol. Chem.* **273**, 9886–9893 (1998).

9. Milatovic, D., Montine, T. J. & Aschner, M. Prostanoid signaling: Dual role for prostaglandin E2 in neurotoxicity. *Neurotoxicology* **32**, 312–319 (2011).

10. Yamagata, K., Andreasson, K. I., Kaufmann, W. E., Barnes, C. A. & Worley, P. F. Expression of a mitogen-inducible cyclooxygenase in brain neurons: Regulation by synaptic activity and glucocorticoids. *Neuron* **11**, 371–386 (1993).

11. Burian, M. & Geisslinger, G. COX-dependent mechanisms involved in the antinociceptive action of NSAIDs at central and peripheral sites. *Pharmacol. Ther.* **107**,

139–154 (2005).

12. Tachikawa, M. *et al.* Role of the blood-cerebrospinal fluid barrier transporter as a cerebral clearance system for prostaglandin E2 produced in the brain. *J. Neurochem.* **123**, 750–760 (2012).

13. Park, J. Y., Pillinger, M. H. & Abramson, S. B. Prostaglandin E2 synthesis and secretion: the role of PGE2 synthases. *Clin. Immunol.* **119**, 229–240 (2006).

14. Clasadonte, J., Sharif, A., Baroncini, M. & Prevot, V. Gliotransmission by prostaglandin E2: A prerequisite for GnRH neuronal function? *Front. Endocrinol. (Lausanne)*. **2**, 1–12 (2011).

15. Chandrasekharan, N. V *et al.* COX-3, a cyclooxygenase-1 variant inhibited by acetaminophen and other analgesic/antipyretic drugs: cloning, structure, and expression. *Proc. Natl. Acad. Sci. U. S. A.* **99**, 13926–31 (2002).

16. Yasojima, K., Schwab, C., McGeer, E. G. & McGeer, P. L. Distribution of cyclooxygenase-1 and cyclooxygenase-2 mRNAs and proteins in human brain and peripheral organs. *Brain Res.* **830**, 226–236 (1999).

17. Kis, B., Snipes, A., Bari, F. & Busija, D. W. Regional distribution of cyclooxygenase-3 mRNA in the rat central nervous system. *Mol. Brain Res.* **126**, 78–80 (2004).

18. Beiche, F., Scheuerer, S., Brune, K., Geisslinger, G. & Goppelt-Struebe, M. Up-regulation of cyclooxygenase-2 mRNA in the rat spinal cord following peripheral inflammation. *FEBS Lett* **390**, 165–169 (1996).

19. Beiche, F., Klein, T., Nüsing, R., Neuhuber, W. & Goppelt-Struebe, M. Localization of cyclooxygenase-2 and prostaglandin E2 receptor EP3 in the rat lumbar spinal cord. *J. Neuroimmunol.* **89**, 26–34 (1998).

20. Yaksh, T. L. *et al.* The acute antihyperalgesic action of nonsteroidal, anti-inflammatory drugs and release of spinal prostaglandin E2 is mediated by the inhibition of constitutive spinal cyclooxygenase-2 (COX-2) but not COX-1. *J. Neurosci.* **21**, 5847–5853 (2001).

21. Yamaguchi, N. & Okada, S. Cyclooxygenase-1 and -2 in spinally projecting neurons are involved in CRF-induced sympathetic activation. *Auton. Neurosci. Basic Clin.* **151**, 82–89 (2009).

22. Engblom, D. *et al.* Induction of microsomal prostaglandin E synthase in the rat brain endothelium and parenchyma in adjuvant-induced arthritis. *J. Comp. Neurol.* **452**, 205–214 (2002).

23. Lacroix, A. *et al.* COX-2-Derived Prostaglandin E2 Produced by Pyramidal Neurons Contributes to Neurovascular Coupling in the Rodent Cerebral Cortex. *J. Neurosci.* **35**, 11791–810 (2015).

24. Aïd, S. & Bosetti, F. Targeting Cyclooxygenases-1 and -2 in neuroinflammation: therapeutic implications. *Biochimie* **93**, 46–51 (2011).

25. Brock, T. G., McNish, R. W. & Peters-Golden, M. Arachidonic acid is preferentially metabolized by cyclooxygenase-2 to prostacyclin and prostaglandin E2. *J. Biol. Chem.* **274**, 11660–11666 (1999).

26. Sang, N., Zhang, J., Marcheselli, V., Bazan, N. G. & Chen, C. Postsynaptically synthesized prostaglandin E2 (PGE2) modulates hippocampal synaptic transmission via a presynaptic PGE2 EP2 receptor. *J. Neurosci.* **25**, 9858–70 (2005).

27. Bosetti, F., Langenbach, R. & Weerasinghe, G. R. Prostaglandin E2 and microsomal prostaglandin E synthase-2 expression are decreased in the cyclooxygenase-2-deficient mouse brain despite compensatory induction of cyclooxygenase-1 and Ca2+-dependent phospholipase A2. *J. Neurochem.* **91**, 1389–1397 (2004).

28. Choi, S. H., Langenbach, R. & Bosetti, F. Cyclooxygenase-1 and -2 enzymes differentially regulate the brain upstream NF-kB pathway and downstream enzymes involved in prostaglandin biosynthesis. *J. Neurochem.* **98**, 801–811 (2006).

29. Kishimoto, K., Matsumura, K., Kataoka, Y., Morii, H. & Watanabe, Y. Localization of cytosolic phospholipase A2 messenger RNA mainly in neurons in the rat brain. *Neuroscience* **92**, 1061–1077 (1999).

30. Yang, H., Siddiqi, N. J., Alhomida, A. S. & Ong, W. Y. Expression and localization of sPLA2-III in the rat CNS. *Neurochem. Res.* **38**, 753–760 (2013).

31. Murakami, M., Kambe, T., Shimbara, S. & Kudo, I. Functional coupling between various phospholipase A2s and cyclooxygenases in immediate and delayed prostanoid biosynthetic pathways. *J. Biol. Chem.* **274**, 3103–3115 (1999).

32. Eskilsson, A., Tachikawa, M., Hosoya, K. I. & Blomqvist, A. Distribution of

microsomal prostaglandin E synthase-1 in the mouse brain. *J. Comp. Neurol.* **522**, 3229–3244 (2014).

33. Inoue, W. *et al.* Brain-specific endothelial induction of prostaglandin E2 synthesis enzymes and its temporal relation to fever. *Neurosci. Res.* **44**, 51–61 (2002).

34. Xu, J. *et al.* Prostaglandin E2 production in astrocytes: Regulation by cytokines, extracellular ATP, and oxidative agents. *Prostaglandins Leukot. Essent. Fat. Acids* **69**, 437–448 (2003).

35. Yucel-Lindberg, T., Olsson, T. & Kawakami, T. Signal pathways involved in the regulation of prostaglandin E synthase-1 in human gingival fibroblasts. *Cell. Signal.* **18**, 2131–2142 (2006).

36. Molina-Holgado, E., Ortiz, S., Molina-Holgado, F. & Guaza, C. Induction of COX-2 and PGE(2) biosynthesis by IL-1beta is mediated by PKC and mitogen-activated protein kinases in murine astrocytes. *Br. J. Pharmacol.* **131**, 152–159 (2000).

37. Samad, T. a *et al.* Interleukin-1beta-mediated induction of Cox-2 in the CNS contributes to inflammatory pain hypersensitivity. *Nature* **410**, 471–475 (2001).

38. Hofstetter, A. O., Saha, S., Siljehav, V., Jakobsson, P.-J. & Herlenius, E. The induced prostaglandin E2 pathway is a key regulator of the respiratory response to infection and hypoxia in neonates. *Proc. Natl. Acad. Sci. U. S. A.* **104**, 9894–9899 (2007).

39. Kojima, F. *et al.* Membrane-associated prostaglandin E synthase-1 is upregulated by proinflammatory cytokines in chondrocytes from patients with osteoarthritis. *Arthritis Res. Ther.* **6**, R355–R365 (2004).

40. Qu, Y. *et al.* Imaging of brain serotonergic neurotransmission involving phospholipase A2 activation and arachidonic acid release in unanesthetized rats. *Brain Res. Protoc.* **12**, 16–25 (2003).

41. Chen, R. *et al.* D 9 -THC-Caused Synaptic and Memory Impairments Are Mediated through COX-2 Signaling. *Cell* **155**, 1154–1165 (2013).

42. Kanai, N. *et al.* Identification and characterization of a prostaglandin transporter. *Science* **268**, 866–869 (1995).

43. Chan, B. S., Endo, S., Kanai, N. & Schuster, V. L. Identification of lactate as a driving

force for prostanoid transport by prostaglandin transporter PGT. *Am. J. Physiol. Renal Physiol.* **282**, F1097–F1102 (2002).

44. Tachikawa, M. *et al.* A clearance system for prostaglandin D2, a sleep-promoting factor, in cerebrospinal fluid: role of the blood-cerebrospinal barrier transporters. *J Pharmacol Exp Ther* **343**, 608–616 (2012).

45. Akanuma, S. *et al.* Involvement of multidrug resistance-associated protein 4 in efflux transport of prostaglandin E(2) across mouse blood-brain barrier and its inhibition by intravenous administration of cephalosporins. *J. Pharmacol. Exp. Ther.* **333**, 912–919 (2010).

46. Nomura, T., Lu, R., Pucci, M. L. & Schuster, V. L. The two-step model of prostaglandin signal termination: in vitro reconstitution with the prostaglandin transporter and prostaglandin 15 dehydrogenase. *Mol. Pharmacol.* **65**, 973–978 (2004).

47. Alix, E., Schmitt, C., Strazielle, N. & Ghersi-Egea, J.-F. Prostaglandin E2 metabolism in rat brain: Role of the blood-brain interfaces. *Cerebrospinal Fluid Res.* **5**, 5 (2008).

48. Markovič, T., Jakopin, Ž., Dolenc, M. S. & Mlinarič-Raščan, I. Structural features of subtype-selective EP receptor modulators. *Drug Discov. Today* **22**, 57–71 (2017).

49. Bhattacharya, M. *et al.* Nuclear localization of prostaglandin E2 receptors. *Proc. Natl. Acad. Sci. U. S. A.* **95**, 15792–15797 (1998).

50. Bhattacharya, M. *et al.* Localization of Functional Prostaglandin E 2 Receptors EP 3 and EP 4 in the Nuclear Envelope. *J. Biol. Chem.* **274**, 15719–15724 (1999).

51. Gobeil, F. *et al.* Regulation of eNOS expression in brain endothelial cells by perinuclear EP3 receptors. *Circ. Res.* **90**, 682–689 (2002).

52. Fernández-Martínez, A. B. & Lucio-Cazaña, F. J. Transactivation of EGFR by prostaglandin E2 receptors: A nuclear story? *Cell. Mol. Life Sci.* **72**, 2187–2198 (2015).

53. Levitzki, A. & Klein, S. G-protein subunit dissociation is not an integral part of G-protein action. *ChemBioChem* **3**, 815–818 (2002).

54. Candelario-Jalil, E. *et al.* Regional distribution of the prostaglandin E2 receptor EP1 in the rat brain. *J. Mol. Neurosci.* **27**, 303–310 (2005).

55. Tabata, H. *et al.* Possible coupling of prostaglandin E receptor EP1 to TRP5 expressed

in Xenopus laevis oocytes. *Biochem. Biophys. Res. Commun.* **298**, 398–402 (2002).

56. Ji, R. *et al.* EP1 Prostanoid Receptor Coupling to G i / o Up-Regulates the Expression of Hypoxia-Inducible Factor-1 through Activation of a Phosphoinositide-3 Kinase Signaling Pathway. *Mol. Pharmacol.* **77**, 1025–1036 (2010).

57. Zhang, J. & Rivest, S. Distribution, regulation and colocalization of the genes encoding the EP 2 - and EP 4 -PGE 2 receptors in the rat brain and neuronal responses to systemic inflammation. *Eur. J. Neurosci.* **11**, 2651–2668 (1999).

58. Yano, A. *et al.* An aromatic amino acid within intracellular loop 2 of the prostaglandin EP2 receptor is a prerequisite for selective association and activation of Gαs. *Biochim. Biophys. Acta - Mol. Cell Biol. Lipids* **1862**, 615–622 (2017).

59. Emery, E. C., Young, G. T. & McNaughton, P. a. HCN2 ion channels: An emerging role as the pacemakers of pain. *Trends Pharmacol. Sci.* **33**, 456–463 (2012).

60. Kawahara, K., Hohjoh, H., Inazumi, T., Tsuchiya, S. & Sugimoto, Y. Prostaglandin E2-induced inflammation: Relevance of prostaglandin E receptors. *Biochim. Biophys. Acta - Mol. Cell Biol. Lipids* **1851**, 414–421 (2015).

61. Sugimoto, Y. & Narumiya, S. Prostaglandin E receptors. *J. Biol. Chem.* **282**, 11613–11617 (2007).

62. Sugimoto, Y. *et al.* Distribution of the messenger RNA for the prostaglandin E receptor subtype EP3 in the mouse nervous system. *Neuroscience* **62**, 919–928 (1994).

63. Ek, M., Arias, C., Sawchenko, P. & Ericsson-Dahlstrand, A. Distribution of the EP3 prostaglandin E2 receptor subtype in the rat brain: Relationship to sites of interleukin-1 - Induced cellular responsiveness. *J. Comp. Neurol.* **428**, 5–20 (2000).

64. Nakamura, K. *et al.* Immunohistochemical localization of prostaglandin EP3 receptor in the rat nervous system. *J. Comp. Neurol.* **421**, 543–569 (2000).

65. Nakamura, K., Li, Y. Q., Kaneko, T., Katoh, H. & Negishi, M. Prostaglandin EP3 receptor protein in serotonin and catecholamine cell groups: a double immunofluorescence study in the rat brain. *Neuroscience* **103**, 763–75 (2001).

66. Zhu, P. *et al.* Heterogeneous expression and regulation of hippocampal prostaglandin E2 receptors. *J. Neurosci. Res.* **81**, 817–826 (2005).

67. Kitanaka, J. *et al.* Expression pattern of messenger RNAs for prostanoid receptors in glial cell cultures. *Brain Res.* **707**, 282–287 (1996).

68. Slawik, H., Volk, B., Fiebich, B. & Hüll, M. Microglial expression of prostaglandin EP3 receptor in excitotoxic lesions in the rat striatum. *Neurochem. Int.* **45**, 653–660 (2004).

69. Irie, a *et al.* Third isoform of the prostaglandin E receptor EP 3 subtype with different C-terminal tail coupling to both stimulation and inhibition of adenylate cyclase. *Eur. J. Biochem* **217**, 313–318 (1993).

70. Namba, T. *et al.* Alternative splicing of C-terminal tail of prostaglandin E receptor subtype EP3 determines G-protein specificity. *Nature* **365**, 166–170 (1993).

71. Negishi, M., Sugimoto, Y., Irie, A., Narumiya, S. & Ichikawa, A. Two isoforms of prostaglandin E receptor EP3 subtype: Different COOH-terminal domains determine sensitivity to agonist-induced desensitization. *J. Biol. Chem.* **268**, 9517–9521 (1993).

72. Irie, a. *et al.* The C-terminus of the prostaglandin-E-receptor EP3 subtype is essential for activation of GTP-binding protein. *Eur. J. Biochem.* **224**, 161–166 (1994).

73. Bilson, H. a., Mitchell, D. L. & Ashby, B. Human prostaglandin EP3 receptor isoforms show different agonist-induced internalization patterns. *FEBS Lett.* **572**, 271–275 (2004).

74. Neuschäfer-Rube, F. *et al.* A Ser/Thr cluster within the C-terminal domain of the rat prostaglandin receptor EP3alpha is essential for agonist-induced phosphorylation, desensitization and internalization. *Br. J. Pharmacol.* **145**, 1132–1142 (2005).

75. Vasilache, A. M., Andersson, J. & Nilsberth, C. Expression of PGE2 EP3 receptor subtypes in the mouse preoptic region. *Neurosci. Lett.* **423**, 179–183 (2007).

76. Hasegawa, H., Negishi, M. & Ichikawa, A. Two isoforms of the prostaglandin E receptor EP3 subtype different in agonist-independent constitutive activity. *J. Biol. Chem.* **271**, 1857–1860 (1996).

77. Natarajan, C., Hata, A. N., Hamm, H. E., Zent, R. & Breyer, R. M. Extracellular loop II modulates GTP sensitivity of the prostaglandin EP3 receptor. *Mol. Pharmacol.* **83**, 206–16 (2013).

78. Negishi, M., Hasegawa, H. & Ichikawa, A. Prostaglandin E receptor EP3γ isoform, with

mostly full constitutive Gi activity and agonist-dependent Gs activity. *FEBS Lett.* **386**, 165–168 (1996).

79. Nishigaki, N., Negishi, M. & Ichikawa, a. Two Gs-coupled prostaglandin E receptor subtypes, EP2 and EP4, differ in desensitization and sensitivity to the metabolic inactivation of the agonist. *Mol. Pharmacol.* **50**, 1031–1037 (1996).

80. St-Jacques, B. & Ma, W. Preferred recycling pathway by internalized PGE2 EP4 receptor following agonist stimulation in cultured dorsal root ganglion neurons contributes to enhanced EP4 receptor sensitivity. *Neuroscience* **326**, 56–68 (2016).

81. Fujino, H. & Regan, J. W. EP 4 Prostanoid Receptor Coupling to a Pertussis Toxin-Sensitive Inhibitory G Protein. *Mol. Pharmacol.* **69**, 5–10 (2006).

82. Ma, W. & St-Jacques, B. Signalling transduction events involved in agonist-induced PGE2/EP4 receptor externalization in cultured rat dorsal root ganglion neurons. *Eur. J. Pain* **22**, 845–861 (2018).

83. Alboni, S. *et al.* Fluoxetine treatment affects the inflammatory response and microglial function according to the quality of the living environment. *Brain. Behav. Immun.* **58**, 261–271 (2016).

84. Silva, A. P., Martins, T., Baptista, S., Gonçalves, J. & Agasse, F. Brain Injury Associated With Widely Abused Amphetamines: Neuroinflammation, Neurogenesis And Blood-Brain Barrier. *Curr. Drug Abuse Rev.* **3**, 239–254 (2010).

85. Venkataraman, A., Kalk, N., Sewell, G., Ritchie, C. W. & Lingford-Hughes, A. Alcohol and Alzheimer's disease-does alcohol dependence contribute to beta-amyloid deposition, neuroinflammation and neurodegeneration in Alzheimer's disease? *Alcohol Alcohol.* **52**, 151–158 (2017).

86. Saper, C. B., Romanovsky, A. a & Scammell, T. E. Neural circuitry engaged by prostaglandins during the sickness syndrome. *Nat. Neurosci.* **15**, 1088–1095 (2012).

87. Davidson, J., Abul, H. T., Milton, A. S. & Rotondo, D. Cytokines and cytokine inducers stimulate prostaglandin E2 entry into the brain. *Pflugers Arch. Eur. J. Physiol.* **442**, 526–533 (2001).

88. Komaki, G., Arimura, A. & Koves, K. Effect of intravenous injection of IL-1 beta on PGE2 levels in several brain areas as determined by microdialysis. *Am J Physiol* **262**,

E246-51 (1992).

89. Wilhelms, D. B. *et al.* Deletion of Prostaglandin E2 Synthesizing Enzymes in Brain Endothelial Cells Attenuates Inflammatory Fever. *J. Neurosci.* **34**, 11684–11690 (2014).

90. Eskilsson, A. *et al.* Immune-Induced Fever Is Dependent on Local But Not Generalized Prostaglandin E 2 Synthesis in the Brain. *J. Neurosci.* **37**, 5035–5044 (2017).

91. Ushikubi, F. *et al.* Impaired febrile response in mice lacking the prostaglandin E receptor subtype EP3. *Nature* **395**, 281–284 (1998).

92. Blomqvist, A. & Engblom, D. Neural Mechanisms of Inflammation-Induced Fever. *Neuroscientist* 1–19 (2018). doi:10.1177/1073858418760481

93. Liu, D., Wu, L., Breyer, R., Mattson, M. P. & Andreasson, K. Neuroprotection by the PGE2 EP2 receptor in permanent focal cerebral ischemia. *Ann. Neurol.* **57**, 758–761 (2005).

94. Ahmad, M. *et al.* Stimulation of prostaglandin E2-EP3 receptors exacerbates stroke and excitotoxic injury. *J Neruoimmunol* **184**, 172–179 (2007).

95. Rezq, S. & Abdel-Rahman, A. A. Rostral Ventrolateral Medulla EP3 Receptor Mediates the Sympathoexcitatory and Pressor Effects of Prostaglandin E2 in Conscious Rats. *J. Pharmacol. Exp. Ther. J Pharmacol Exp Ther* **359**, 290–299 (2016).

96. Zhang, Z.-H. *et al.* EP3 receptors mediate PGE2-induced hypothalamic paraventricular nucleus excitation and sympathetic activation. *Am. J. Physiol. Heart Circ. Physiol.* **301**, H1559-69 (2011).

97. Forsberg, D. *et al.* CO2-evoked release of PGE2 modulates sighs and inspiration as demonstrated in brainstem organotypic culture. *Elife* **5**, 1–41 (2016).

98. Siljehav, V., Shvarev, Y. & Herlenius, E. Il-1β and prostaglandin E2 attenuate the hypercapnic as well as the hypoxic respiratory response via prostaglandin E receptor type 3 in neonatal mice. *J. Appl. Physiol.* **117**, 1027–36 (2014).

99. Koch, H. *et al.* Prostaglandin E2 differentially modulates the central control of eupnoea, sighs and gasping in mice. *J. Physiol.* **593**, 305–319 (2015).

100. de Paiva, V. N. *et al.* Prostaglandins mediate depressive-like behaviour induced by

endotoxin in mice. *Behav. Brain Res.* **215**, 146–151 (2010).

101. Cimino, P. J., Keene, C. D., Breyer, R. M., Montine, K. S. & Montine, T. J. Therapeutic targets in prostaglandin E2 signaling for neurologic disease. *Curr. Med. Chem.* **15**, 1863–1869 (2008).

102. Maingret, V. *et al.* PGE2-EP3 signaling pathway impairs hippocampal presynaptic long-term plasticity in a mouse model of Alzheimer's disease. *Neurobiol. Aging* **50**, 13–24 (2017).

103. Sagy-Bross, C. *et al.* The role of cytosolic phospholipase A2alpha in amyloid precursor protein induction by amyloid beta1-42: Implication for neurodegeneration. *J. Neurochem.* **132**, 559–571 (2015).

104. Björk, L., Leifsdottir, K., Saha, S. & Herlenius, E. PGE2 - Metabolite levels in CSF correlate to HIE score and outcome after perinatal asphyxia. *Acta Paediatr. Int. J. Paediatr.* **102**, 1041–1047 (2013).

105. Aley, K. O. & Levine, J. D. Role of protein kinase A in the maintenance of inflammatory pain. *J. Neurosci.* **19**, 2181–6 (1999).

106. St-Jacques, B. & Ma, W. Peripheral prostaglandin E2 prolongs the sensitization of nociceptive dorsal root ganglion neurons possibly by facilitating the synthesis and anterograde axonal trafficking of EP4 receptors. *Exp. Neurol.* **261**, 354–66 (2014).

107. Lin, C. R. *et al.* Prostaglandin E2 Receptor EP4 Contributes to Inflammatory Pain Hypersensitivity. *J. Pharmacol. Exp. Ther.* **319**, 1096–1103 (2006).

108. Natura, G. *et al.* Neuronal prostaglandin E2 receptor subtype EP3 mediates antinociception during inflammation. *PNAS* **110**, 13648–14653 (2013).

109. Taiwo, Y. O. & Levine, J. D. Prostaglandins inhibit endogenous pain control mechanisms by blocking transmission at spinal noradrenergic synapses. *J. Neurosci.* **8**, 1346–1349 (1988).

110. Reinold, H. *et al.* Spinal inflammatory hyperalgesia is mediated by prostaglandin E receptors of the EP2 subtype. *J. Clin. Invest.* **115**, 673–679 (2005).

111. Minami, T. *et al.* Functional evidence for interaction between prostaglandin EP3 and κ-opioid receptor pathways in tactile pain induced by human immunodeficiency virus

type-1 (HIV-1) glycoprotein gp120. *Neuropharmacology* **45**, 96–105 (2003).

112. Ahmadi, S., Lippross, S., Neuhuber, W. L. & Zeilhofer, H. U. PGE(2) selectively blocks inhibitory glycinergic neurotransmission onto rat superficial dorsal horn neurons. *Nat. Neurosci.* **5**, 34–40 (2002).

113. Oliva, P. *et al.* Role of periaqueductal grey prostaglandin receptors in formalin-induced hyperalgesia. *Eur. J. Pharmacol.* **530**, 40–47 (2006).

114. Palazzo, E. *et al.* EP1 receptor within the ventrolateral periaqueductal grey controls thermonociception and rostral ventromedial medulla cell activity in healthy and neuropathic rat. *Mol. Pain* **7**, 82 (2011).

115. Drake, R. A. R. *et al.* Periaqueductal Grey EP3 Receptors Facilitate Spinal Nociception in Arthritic Secondary Hypersensitivity. *J. Neurosci.* **36**, 9026–40 (2016).

116. Bucci, D. *et al.* Systematic Morphometry of Catecholamine Nuclei in the Brainstem. *Front. Neuroanat.* **11**, 1–13 (2017).

117. Le Gallois, M. *Expérience sur le principe de la vie*. (1812).

118. Ramirez, J. M. *The integrative role of the sigh in psychology, physiology, pathology, and neurobiology*. *Progress in Brain Research* **209**, (Elsevier B.V., 2014).

119. Gray, P. A., Rekling, J. C., Bocchiaro, C. M. & Feldman, J. L. Modulation of respiratory frequency by peptidergic input to rhythmogenic neurons in the preBötzinger complex. *Science (80-.).* **286**, 1566–1568 (1999).

120. Nakagawa, T., Masuda, T., Watanabe, T., Minami, M. & Satoh, M. Possible involvement of the locus coeruleus in inhibition by prostanoid EP(3) receptor-selective agonists of morphine withdrawal syndrome in rats. *Eur. J. Pharmacol.* **390**, 257–66 (2000).

121. Wang, H., Stornetta, R. L., Rosin, D. L. & Guyenet, P. G. Neurokinin-1 receptor-immunoreactive neurons of the ventral respiratory group in the rat. *J. Comp. Neurol.* **434**, 128–146 (2001).

122. Lopes, L. T. *et al.* Anatomical and functional connections between the locus coeruleus and the nucleus tractus solitarius in neonatal rats. *Neuroscience* **324**, 446–468 (2016).

123. Yackle, K. *et al.* Breathing control center neurons that promote arousal in mice. *Science*

(80-.). **355**, 1411–1415 (2017).

124. Hakuno, H., Oyamada, Y., Murai, M., Ito, Y. & Yamaguchi, K. Effects of inactivation and stimulation of locus coeruleus on respiratory activity of neonatal rat. *Respir. Physiol. Neurobiol.* **140**, 9–18 (2004).

125. Hilaire, G., Viemari, J. C., Coulon, P., Simonneau, M. & Bévengut, M. Modulation of the respiratory rhythm generator by the pontine noradrenergic A5 and A6 groups in rodents. *Respir. Physiol. Neurobiol.* **143**, 187–197 (2004).

126. Viemari, J.-C. & Ramirez, J.-M. Norepinephrine differentially modulates different types of respiratory pacemaker and nonpacemaker neurons. *J. Neurophysiol.* **95**, 2070–82 (2006).

127. de Carvalho, D. *et al.* Neurochemical and electrical modulation of the Locus coeruleus: Contribution to CO2 drive to breathe. *Front. Physiol.* **5**, 1–13 (2014).

128. Foote, S. L., Bloom, F. E. & Aston-Jones, G. Nucleus locus ceruleus: new evidence of anatomical and physiological specificity. *Physiol. Rev.* **63**, 844–914 (1983).

129. Swanson, L. W. The locus coeruleus: A cytoarchitectonic, golgi and immunohistochemical study in the albino rat. *Brain Res.* **110**, 39–56 (1976).

130. Jedema, H. P. & Grace, a a. Chronic exposure to cold stress alters electrophysiological properties of locus coeruleus neurons recorded in vitro. *Neuropsychopharmacology* **28**, 63–72 (2003).

131. Paxinos, G. & Watson, C. *The rat brain in stereotaxic coordinates*. (2005).

132. Plummer, N. W., Scappini, E. L., Smith, K. G., Tucker, C. J. & Jensen, P. Two Subpopulations of Noradrenergic Neurons in the Locus Coeruleus Complex Distinguished by Expression of the Dorsal Neural Tube Marker Pax7. *Front. Neuroanat.* **11**, 1–11 (2017).

133. Schwarz, L. A. & Luo, L. Organization of the locus coeruleus-norepinephrine system. *Curr. Biol.* **25**, R1051–R1056 (2015).

134. Chandler, D. J., Gao, W.-J. & Waterhouse, B. D. Heterogeneous organization of the locus coeruleus projections to prefrontal and motor cortices. *Proc. Natl. Acad. Sci. U. S. A.* **111**, 6816–21 (2014).

135. Hickey, L. *et al.* Optoactivation of Locus Ceruleus Neurons Evokes Bidirectional Changes in Thermal Nociception in Rats. *J. Neurosci.* **34**, 4148–4160 (2014).

136. Hirschberg, S., Li, Y., Randall, A., Kremer, E. J. & Pickering, A. E. Functional dichotomy in spinal-vs prefrontal-projecting locus coeruleus modules splits descending noradrenergic analgesia from ascending aversion and anxiety in rats. *Elife* **6**, 1–26 (2017).

137. Alvarez-Maubecin, V., Garcia-Hernandez, F., Williams, J. T. & Van Bockstaele, E. J. Functional coupling between neurons and glia. *J. Neurosci.* **20**, 4091–8 (2000).

138. Tang, F. *et al.* Lactate-mediated glia-neuronal signalling in the mammalian brain. *Nat. Commun.* **5**, 1–13 (2014).

139. Aston-Jones, G., Ennis, M., Pieribone, V. A., Nickell, W. T. & Shipley, M. T. The brain nucleus locus coeruleus: restricted afferent control of a broad efferent network. *Science* **234**, 734–7 (1986).

140. Jin, X. *et al.* Identification of a group of GABAergic neurons in the dorsomedial area of the locus coeruleus. *PLoS One* **11**, 1–13 (2016).

141. Samuels, E. R. & Szabadi, E. Functional neuroanatomy of the noradrenergic locus coeruleus: its roles in the regulation of arousal and autonomic function part I: principles of functional organisation. *Curr. Neuropharmacol.* **6**, 235–253 (2008).

142. Valentino, R. J. & Van Bockstaele, E. Convergent regulation of locus coeruleus activity as an adaptive response to stress. *Eur. J. Pharmacol.* **583**, 194–203 (2008).

143. Sara, S. J. The locus coeruleus and noradrenergic modulation of cognition. *Nat. Rev. Neurosci.* **10**, 211–223 (2009).

144. Berridge, C. W. & Waterhouse, B. D. The locus coeruleus-noradrenergic system: Modulation of behavioral state and state-dependent cognitive processes. *Brain Res. Rev.* **42**, 33–84 (2003).

145. Samuels, E. R. & Szabadi, E. Functional neuroanatomy of the noradrenergic locus coeruleus: its roles in the regulation of arousal and autonomic function part II: physiological and pharmacological manipulations and pathological alterations of locus coeruleus activity in humans. *Curr. Neuropharmacol.* **6**, 254–285 (2008).

146. Carter, M. E. *et al.* Tuning arousal with optogenetic modulation of locus coeruleus neurons. *Nat. Neurosci.* **13**, 1526–1533 (2010).

147. Williams, J. T., North, R. A., Shefner, S. A., Nishi, S. & Egan, T. M. Membrane properties of rat locus coeruleus neurones. *Neuroscience* **13**, 137–156 (1984).

148. Sugiyama, D. *et al.* In vivo patch-clamp recording from locus coeruleus neurones in the rat brainstem. *J. Physiol.* **10**, 2225–2231 (2012).

149. Alreja, M. & Aghajanian, G. K. Pacemaker activity of locus coeruleus neurons: whole-cell recordings in brain slices show dependence on cAMP and protein kinase A. *Brain Res.* **556**, 339–343 (1991).

150. de Oliveira, R. *et al.* Pacemaker Currents in Mouse Locus Coeruleus Neurons. *Neuroscience* **170**, 166–177 (2010).

151. De Oliveira, R. B. *et al.* Developmental changes in pacemaker currents in mouse locus coeruleus neurons. *Brain Res.* **1425**, 27–36 (2011).

152. Andrade, R., Vandermaelen, C.P., Aghajanian, G. K. Morphine tolerance and dependence in the locus coeruleus: single cell studies in brain slices. *Eur. J. Pharmacol.* **91**, 161–169 (1983).

153. Andrade, R. & Aghajanian, G. K. Locus coeruleus activity in vitro: intrinsic regulation by a calcium-dependent potassium conductance but not alpha 2-adrenoceptors. *J. Neurosci.* **4**, 161–170 (1984).

154. Rancic, V., Rawal, B., Panaitescu, B., Ruangkittisakul, A. & Ballanyi, K. Suction electrode recording in locus coeruleus of newborn rat brain slices reveals network bursting comprising summated non-synchronous spiking. *Neurosci. Lett.* **671**, 103–107 (2018).

155. Ishimatsu, M. & Williams, J. T. Synchronous activity in locus coeruleus results from dendritic interactions in pericoerulear regions. *J. Neurosci.* **16**, 5196–204 (1996).

156. Nestler, E. J., Alreja, M. & Aghajanian, G. K. Molecular control of locus coeruleus neurotransmission. *Biol. Psychiatry* **46**, 1131–1139 (1999).

157. Alvarez, V. A., Chow, C. C., Van Bockstaele, E. J. & Williams, J. T. Frequency-dependent synchrony in locus ceruleus: role of electrotonic coupling. *Proc Natl Acad*

Sci U S A **99**, 4032–4036 (2002).

158. Aghajanian, G. K. & Wang, Y. Y. Common alpha 2- and opiate effector mechanisms in the locus coeruleus: intracellular studies in brain slices. *Neuropharmacology* **26**, 793–799 (1987).

159. Berridge, C. W. & Abercrombie, E. D. Relationship between locus coeruleus discharge rates and rates of norepinephrine release within neocortex as assessed by in vivo microdialysis. *Neuroscience* **93**, 1263–1270 (1999).

160. Safaai, H., Neves, R., Eschenko, O., Logothetis, N. K. & Panzeri, S. Modeling the effect of locus coeruleus firing on cortical state dynamics and single-trial sensory processing. *Proc. Natl. Acad. Sci.* **112**, 12834–12839 (2015).

161. Egan, B. Y. T. M., Henderson, G., North, R. A. & Williams, J. T. Noradrenaline-mediated synaptic inhibition in rat locus coeruleus neurons. *J Physiol* **345**, 477–488 (1983).

162. Andrade, R. & Aghajanian, K. Opiate- and alpha2-Adrenoceptor-induced Hyperpolarizations of Locus Ceruleus Neurons in Brain Slices: Reversal by Cyclic Adenosine 3':5'-Monophosphate Analogues. *J. Neurosci.* **5**, 2359–2364 (1985).

163. Arima, J., Kubo, C., Ishibashi, H. & Akaike, N. α2- Adrenoceptor- mediated potassium currents in acutely dissociated rat locus coeruleus neurones. *J. Physiol.* **508**, 57–66 (1998).

164. Huang, H.-P. *et al.* Physiology of quantal norepinephrine release from somatodendritic sites of neurons in locus coeruleus. *Front. Mol. Neurosci.* **5**, 1–5 (2012).

165. Lei, Q. *et al.* Activation and inhibition of G protein-coupled inwardly rectifying potassium (Kir3) channels by G protein beta gamma subunits. *Proc. Natl. Acad. Sci. U. S. A.* **97**, 9771–9776 (2000).

166. Albsoul-Younes, A. M. *et al.* Interaction Sites of the G Protein beta Subunit with Brain G Protein- coupled Inward Rectifier K+ Channel. *J. Biol. Chem.* **276**, 12712–12717 (2001).

167. Whorton, M. R. & MacKinnon, R. X-ray structure of the mammalian GIRK2–βγ G-protein complex. *Nature* **498**, 190–197 (2013).

168. Jin, X., Cui, N., Zhong, W., Jin, X.-T. & Jiang, C. GABAergic synaptic inputs of locus coeruleus neurons in wild-type and Mecp2-null mice. *Am. J. Physiol. Cell Physiol.* **304**, C844-57 (2013).

169. Ortega, J. E., Mendiguren, A., Pineda, J. & Meana, J. J. Regulation of central noradrenergic activity by 5-HT 3 receptors located in the locus coeruleus of the rat. *Neuropharmacology* **62**, 2472–2479 (2012).

170. Zitnik, G. A. Control of arousal through neuropeptide afferents of the locus coeruleus. *Brain Res.* **1641**, 338–350 (2016).

171. Zamalloa, T., Bailey, C. P. & Pineda, J. Glutamate-induced post-activation inhibition of locus coeruleus neurons is mediated by AMPA/kainate receptors and sodium-dependent potassium currents. *Br. J. Pharmacol.* **156**, 649–661 (2009).

172. Wang, Y. Y. & Aghajanian, G. K. Excitation of locus coeruleus neurons by vasoactive intestinal peptide: evidence for a G-protein-mediated inward current. *Brain Res.* **500**, 107–118 (1989).

173. Wang, Y. Y. & Aghajanian, G. K. Excitation of locus coeruleus neurons by vasoactive intestinal peptide: role of a cAMP and protein kinase A. *J. Neurosci.* **10**, 3335–3343 (1990).

174. Mendiguren, A. & Pineda, J. Systemic effect of cannabinoids on the spontaneous firing rate of locus coeruleus neurons in rats. *Eur. J. Pharmacol.* **534**, 83–88 (2006).

175. Pineda, J., Ugedo, L. & García-Sevilla, J. A. Stimulatory effects of clonidine, cirazoline and rilmenidine on locus coeruleus noradrenergic neurones: possible involvement of imidazoline-preferring receptors. *Naunyn. Schmiedebergs. Arch. Pharmacol.* **348**, 134–140 (1993).

176. Murai, Y. & Akaike, T. Orexins cause depolarization via nonselective cationic and K + channels in isolated locus coeruleus neurons. *Neurosci. Res.* **51**, 55–65 (2005).

177. Ishibashi, H., Nakahata, Y., Eto, K. & Nabekura, J. Excitation of locus coeruleus noradrenergic neurons by thyrotropin-releasing hormone. *J. Physiol.* **587**, 5709–5722 (2009).

178. Fröhlich, R., Boehm, S. & Illes, P. Pharmacological characterization of P2 purinoceptor types in rat locus coeruleus neurons. *Eur. J. Pharmacol.* **315**, 255–261 (1996).

179. Feng, C.-Y., Wiggins, L. M. & von Bartheld, C. S. The Locus Ceruleus Responds to Signaling Molecules Obtained from the CSF by Transfer through Tanycytes. *J. Neurosci.* **31**, 9147–9158 (2011).

180. Xu, S. *et al.* Effect of indomethacin on the c-fos expression in AVP and TH neurons in rat brain induced by lipopolysaccharide. *Brain Res.* **966**, 13–8 (2003).

181. Borsody, M. & Weiss, J. Peripheral endotoxin causes long-lasting changes in locus coeruleus activity via IL-1 in the brain. *Acta Neuropsychiatr.* **14**, 303–321 (2002).

182. Dallaporta, M. *et al.* c-Fos immunoreactivity induced by intraperitoneal LPS administration is reduced in the brain of mice lacking the microsomal prostaglandin E synthase-1 (mPGES-1). *Brain. Behav. Immun.* **21**, 1109–1121 (2007).

183. Kaneko, Y. S. *et al.* Peripheral injection of lipopolysaccharide enhances expression of inflammatory cytokines in murine locus coeruleus: Possible role of increased norepinephrine turnover. *J. Neurochem.* **94**, 393–404 (2005).

184. Schlachetzki, J. C. M. *et al.* Norepinephrine enhances the LPS-induced expression of COX-2 and secretion of PGE2 in primary rat microglia. *J. Neuroinflammation* **7**, 2 (2010).

185. Borsody, M. & Weiss, J. Alteration of locus coeruleus neuronal activity by interleukin-1 and the involvement of endogenous corticotropin-releasing hormone. *Neuroimmunomodulation* **10**, 101–121 (2002).

186. Gervasoni, D. *et al.* Electrophysiological evidence that noradrenergic neurons of the rat locus coeruleus are tonically inhibited by GABA during sleep. *Eur. J. Neurosci.* **10**, 964–970 (1998).

187. Koh, K. *et al.* Possible involvement of activated locus coeruleus-noradrenergic neurons in pain-related sleep disorders. *Neurosci. Lett.* **589**, 200–206 (2015).

188. Aston-Jones, G. & Cohen, J. D. Adaptive gain and the role of the locus coeruleus-norepinephrine system in optimal performance. *J. Comp. Neurol.* **493**, 99–110 (2005).

189. Janitzky, K. *et al.* Optogenetic silencing of locus coeruleus activity in mice impairs cognitive flexibility in an attentional set-shifting task. *Front. Behav. Neurosci.* **9**, 1–8 (2015).

190. D'Andrea, I. *et al.* Lack of kinase-independent activity of PI3Kγ in locus coeruleus induces ADHD symptoms through increased CREB signaling. *EMBO Mol. Med.* **7**, 904–17 (2015).

191. McCall, J. G. *et al.* Locus coeruleus to basolateral amygdala noradrenergic projections promote anxiety-like behavior. *Elife* **6**, 1–23 (2017).

192. Benarroch, E. E. Locus coeruleus. *Cell Tissue Res.* **373**, 212–232 (2018).

193. Maeda, M., Tsuruoka, M., Hayashi, B., Nagasawa, I. & Inoue, T. Descending pathways from activated locus coeruleus/subcoeruleus following unilateral hindpaw inflammation in the rat. *Brain Res. Bull.* **78**, 170–174 (2009).

194. Tsuruoka, M., Tamkai, J., Maeda, M., Hayashi, B. & Inoue, T. Coeruleospinal inhibition of visceral nociceptive processing in the rat spinal cord. *Front. Integr. Neurosci.* **6**, 87 (2012).

195. Li, Y. *et al.* Retrograde optogenetic characterization of the pontospinal module of the locus coeruleus with a canine adenoviral vector. *Brain Res.* **1641**, 274–290 (2016).

196. Jones, S. L. Descending noradrenergic influences on pain. *Prog. Brain Res.* **88**, 381–94 (1991).

197. Jongeling, A. C., Jouns, E. M., Murphy, A. Z. & Hammond, D. L. Persistent inflammatory pain decreases the antinociceptive effects of the mu opioid receptor agonist DAMGO in the locus coeruleus of male rats. *Neuropharmacology* **56**, 1017–1026 (2009).

198. Heneka, M. T. *et al.* Locus ceruleus controls Alzheimer's disease pathology by modulating microglial functions through norepinephrine. *Proc. Natl. Acad. Sci.* **107**, 6058–6063 (2010).

199. Takeuchi, T. *et al.* Locus coeruleus and dopaminergic consolidation of everyday memory. *Nature* **537**, 357–362 (2016).

200. Uematsu, A. *et al.* Modular organization of the brainstem noradrenaline system coordinates opposing learning states. *Nat. Neurosci.* **20**, 1602–1611 (2017).

201. Kelly, S. C. *et al.* Locus coeruleus cellular and molecular pathology during the progression of Alzheimer's disease. *Acta Neuropathol. Commun.* **5**, 8 (2017).

202. Theofilas, P. *et al.* Locus coeruleus volume and cell population changes during Alzheimer's disease progression: A stereological study in human postmortem brains with potential implication for early-stage biomarker discovery. *Alzheimer's Dement.* **13**, 236–246 (2017).

203. Wang, X., Piñol, R. a, Byrne, P. & Mendelowitz, D. Optogenetic Stimulation of Locus Ceruleus Neurons Augments Inhibitory Transmission to Parasympathetic Cardiac Vagal Neurons via Activation of Brainstem α1 and β1 Receptors. *J. Neurosci.* **34**, 6182–9 (2014).

204. Almeida, M. C., Steiner, A. a, Coimbra, N. C. & Branco, L. G. S. Thermoeffector neuronal pathways in fever: a study in rats showing a new role of the locus coeruleus. *J. Physiol.* **558**, 283–94 (2004).

205. Hajós, M., Engberg, G. & Elam, M. Reduced responsiveness of locus coeruleus neurons to cutaneous thermal stimuli in capsaicin-treated rats. *Neurosci. Lett.* **70**, 382–387 (1986).

206. Da Silva, A. O. F., Gargaglioni, L. H. & Branco, L. G. S. 5-HT2A serotoninergic receptor in the locus coeruleus participates in the first phase of lipopolysaccharide-induced fever. *Can. J. Physiol. Pharmacol.* **85**, 497–501 (2007).

207. Soriano, R. N., Kwiatkoski, M., Batalhao, M. E., Branco, L. G. & Carnio, E. C. Interaction between the carbon monoxide and nitric oxide pathways in the locus coeruleus during fever. *Neuroscience* **206**, 69–80 (2012).

208. Fabris, G., Steiner, A. A., Anselmo-Franci, J. A. & Branco, L. G. Role of nitric oxide in rat locus coeruleus in hypoxia-induced hyperventilation and hypothermia. *Brazilian J. Med. Biol. Res.* **32**, 1389–1398 (1999).

209. Putnam, R. W. Cellular mechanisms involved in CO2 and acid signaling in chemosensitive neurons. *AJP Cell Physiol.* **287**, C1493–C1526 (2004).

210. Guyenet, P. G., Koshiya, N., Huangfu, D., Verberne, A. J. & Riley, T. A. Central respiratory control of A5 and A6 pontine noradrenergic neurons. *Am J Physiol* **264**, R1035–R1044 (1993).

211. Pineda, J. & Aghajanian, G. K. Carbon dioxide regulates the tonic activity of locus coeruleus neurons by modulating a proton- and polyamine-sensitive inward rectifier

potassium current. *Neuroscience* **77**, 723–43 (1997).

212. Imber, A. N. & Putnam, R. W. Postnatal development and activation of L-type Ca 2+ currents in locus ceruleus neurons: implications for a role for Ca 2+ in central chemosensitivity. *J. Appl. Physiol.* **112**, 1715–1726 (2012).

213. Cui, N. *et al.* Involvement of TRP channels in the CO 2 chemosensitivity of locus coeruleus neurons. *J Neurophysiol* **105**, 2791–2801 (2011).

214. Nichols, N. L., Hartzler, L. K., Conrad, S. C., Dean, J. B. & Putnam, R. W. Intrinsic chemosensitivity of individual nucleus tractus solitarius (NTS) and locus coeruleus (LC) neurons from neonatal rats. *Adv. Exp. Med. Biol.* **605**, 348–352 (2008).

215. de Carvalho, D. *et al.* Participation of locus coeruleus in breathing control in female rats. *Respir. Physiol. Neurobiol.* **245**, 29–36 (2017).

216. Oyamada, Y., Ballantyne, D., Mückenhoff, K. & Scheid, P. Respiration-modulated membrane potential and chemosensitivity of locus coeruleus neurones in the in vitro brainstem — spinal cord of the neonatal rat. *J. Physiol.* **513**, 381–398 (1998).

217. Viemari, J. C. *et al.* Phox2a Gene , A6 Neurons , and Noradrenaline Are Essential for Development of Normal Respiratory Rhythm in Mice. *J. Neurosci.* **24**, 928–937 (2004).

218. Kuo, F.-S. *et al.* In vitro characterization of noradrenergic modulation of chemosensitive neurons in the retrotrapezoid nucleus. *J. Neurophysiol.* **116**, 1024–1035 (2016).

219. Doi, A. & Ramirez, J.-M. State-dependent interactions between excitatory neuromodulators in the neuronal control of breathing. *J. Neurosci.* **30**, 8251–8262 (2010).

220. Wang, G. *et al.* Modulation of inspiratory inhibition of the Botzinger complex by raphe pallidus and locus coeruleus in rabbits. *Adv Exp Med Biol* **551**, 127–133 (2004).

221. Viemari, J. C. *et al.* Ret deficiency in mice impairs the development of A5 and A6 neurons and the functional maturation of the respiratory rhythm. *Eur. J. Neurosci.* **22**, 2403–2412 (2005).

222. Gargaglioni, L. H., Hartzler, L. K. & Putnam, R. W. The locus coeruleus and central chemosensitivity. *Respir. Physiol. Neurobiol.* **173**, 264–273 (2010).

223. Taneja, P. *et al.* Pathophysiology of Locus Ceruleus neurons in a mouse model of Rett

Syndrome. *J. Neurocience* **29**, 12187–12195 (2009).

224. Oliveira, L. M., Tuppy, M., Moreira, T. S. & Takakura, A. C. Role of the locus coeruleus catecholaminergic neurons in the chemosensory control of breathing in a Parkinson's disease model. *Exp. Neurol.* **293**, 172–180 (2017).

225. Molina-Holgado, F. & Guaza, C. Endotoxin administration induced differential neurochemical activation of the rat brain stem nuclei. *Brain Res. Bull.* **40**, 151–156 (1996).

226. Lacroix, S. & Rivest, S. Functional circuitry in the brain of immune-challenged rats: partial involvement of prostaglandins. *J Comp Neurol* **387**, 307–324 (1997).

227. Hopp, S. C. *et al.* Differential Neuroprotective and Anti-Inflammatory Effects of L-Type Voltage Dependent Calcium Channel and Ryanodine Receptor Antagonists in the Substantia Nigra and Locus Coeruleus. *J. Neuroimmune Pharmacol.* **10**, 35–44 (2015).

228. Bardou, I. *et al.* Age and duration of inflammatory environment differentially affect the neuroimmune response and catecholaminergic neurons in the midbrain and brainstem. *Neurobiol. Aging* **35**, 1065–1073 (2014).

229. O'Donnell, J., Zeppenfeld, D., McConnell, E., Pena, S. & Nedergaard, M. Norepinephrine: A neuromodulator that boosts the function of multiple cell types to optimize CNS performance. *Neurochem. Res.* **37**, 2496–2512 (2012).

230. Heneka, M. T. *et al.* Noradrenergic depletion increases inflammatory responses in brain: effects on IkappaB and HSP70 expression. *J. Neurochem.* **85**, 387–398 (2003).

231. Iravani, M. M., Sadeghian, M., Rose, S. & Jenner, P. Loss of locus coeruleus noradrenergic neurons alters the inflammatory response to LPS in substantia nigra but does not affect nigral cell loss. *J. Neural Transm.* **121**, 1493–1505 (2014).

232. Bharani, K. L., Derex, R., Granholm, A. C. & Ledreux, A. A noradrenergic lesion aggravates the effects of systemic inflammation on the hippocampus of aged rats. *PLoS One* **12**, 1–20 (2017).

233. Kogan, J. H., Nestler, E. J. & Aghajanian, G. K. Elevated basal firing rates and enhanced responses to 8-Br-cAMP in locus coeruleus neurons in brain slices from opiate-dependent rats. *Eur. J. Pharmacol.* **211**, 47–53 (1992).

234. Dang, V. C. & Christie, M. J. Mechanisms of rapid opioid receptor desensitization, resensitization and tolerance in brain neurons. *Br. J. Pharmacol.* **165**, 1704–1716 (2012).

235. Smith, J. C., Ellenberger, H. H., Ballanyi, K. & Feldman, J. L. Pre-Bötzinger Complex: A brainstem region that may generate respiratory rhythm in mammals. *Science (80-.).* **254**, 726–729 (1991).

236. Alsahafi, Z., Dickson, C. T. & Pagliardini, S. Optogenetic excitation of preBotzinger complex neurons potently drives inspiratory activity in vivo. *J. Physiol.* **593**, 3673–3692 (2015).

237. Gray, P. A., Janczewski, W. A., Mellen, N., McCrimmon, D. R. & Feldman, J. L. Normal breathing requires preBötzinger complex neurokinin-1 receptor-expressing neurons. *Nat. Neurosci.* **4**, 927–30 (2001).

238. Lieske, S. P., Thoby-Brisson, M., Telgkamp, P. & Ramirez, J. M. Reconfiguration of the neural network controlling multiple breathing patterns: eupnea, sighs and gasps. *Nat. Neurosci.* **3**, 600–607 (2000).

239. Koizumi, H. *et al.* Structural-Functional Properties of Identified Excitatory and Inhibitory Interneurons within Pre-Botzinger Complex Respiratory Microcircuits. *J. Neurosci.* **33**, 2994–3009 (2013).

240. Wang, X. *et al.* Laser ablation of Dbx1 neurons in the pre-Bötzinger complex stops inspiratory rhythm and impairs output in neonatal mice. *Elife* **3**, e03427 (2014).

241. Ramirez, J.-M. M., Dashevskiy, T., Marlin, I. A. & Baertsch, N. Microcircuits in respiratory rhythm generation: commonalities with other rhythm generating networks and evolutionary perspectives. *Curr. Opin. Neurobiol.* **41**, 53–61 (2016).

242. Kang, J.-J. *et al.* Catecholaminergic neurons in synaptic connections with pre-Bötzinger complex neurons in the rostral ventrolateral medulla in normoxic and daily acute intermittent hypoxic rats. *Exp. Neurol.* **287**, 165–175 (2017).

243. Ruangkittisakul, A., Kottick, A., Picardo, M. C. D., Ballanyi, K. & Del Negro, C. A. Identification of the pre-Bötzinger complex inspiratory center in calibrated 'sandwich' slices from newborn mice with fluorescent Dbx1 interneurons. *Physiol. Rep.* **2**, 1–16 (2014).

244. Stornetta, R. L. Identification of neurotransmitters and co-localization of transmitters in brainstem respiratory neurons. *Respir. Physiol. Neurobiol.* **164**, 18–27 (2008).

245. Smith, J. C., Abdala, A. P. L., Borgmann, A., Rybak, I. A. & Paton, J. F. R. Brainstem respiratory networks: Building blocks and microcircuits. *Trends Neurosci.* **36**, 152–162 (2013).

246. Ikeda, K. *et al.* The respiratory control mechanisms in the brainstem and spinal cord: integrative views of the neuroanatomy and neurophysiology. *J. Physiol. Sci.* **67**, 45–62 (2017).

247. Gray, P. A. *et al.* Developmental Origin of PreBotzinger Complex Respiratory Neurons. *J. Neurosci.* **30**, 14883–14895 (2010).

248. Hayes, J. A. *et al.* Transcriptome of neonatal preBötzinger complex neurones in Dbx1 reporter mice. *Sci. Rep.* **7**, 8669 (2017).

249. Guyenet, P. G., Sevigny, C. P., Weston, M. C. & Stornetta, R. L. Neurokinin-1 receptor-expressing cells of the ventral respiratory group are functionally heterogeneous and predominantly glutamatergic. *J. Neurosci.* **22**, 3806–3816 (2002).

250. Cui, Y. *et al.* Defining preBötzinger Complex Rhythm- and Pattern-Generating Neural Microcircuits In Vivo. *Neuron* **91**, 602–614 (2016).

251. Liu, Y. *et al.* Substance P and enkephalinergic synapses onto neurokinin-1 receptor-immunoreactive neurons in the pre-Bötzinger complex of rats. *Eur. J. Neurosci.* **19**, 65–75 (2004).

252. Phillips, W. S., Herly, M., Del Negro, C. A. & Rekling, J. C. Organotypic slice cultures containing the preBötzinger complex generate respiratory-like rhythms. *J. Neurophysiol.* **115**, 1063–1070 (2016).

253. Qi, J. *et al.* Inhibitory Effect of Endomorphin-2 Binding to the μ-Opioid Receptor in the Rat Pre-Bötzinger Complex on the Breathing Activity. *Mol. Neurobiol.* **54**, 461–469 (2017).

254. Montandon, G. *et al.* PreBotzinger Complex Neurokinin-1 Receptor-Expressing Neurons Mediate Opioid-Induced Respiratory Depression. *J. Neurosci.* **31**, 1292–1301 (2011).

255. Montandon, G. & Horner, R. CrossTalk proposal: The preBotzinger complex is essential for the respiratory depression following systemic administration of opioid analgesics. *J. Physiol.* **592**, 1159–62 (2014).

256. Liu, Y.-Y. *et al.* Relationship between two types of vesicular glutamate transporters and neurokinin-1 receptor-immunoreactive neurons in the pre-Bötzinger complex of rats: light and electron microscopic studies. *Eur. J. Neurosci.* **17**, 41–8 (2003).

257. Liu, Y. Y. *et al.* GABAergic and glycinergic synapses onto neurokinin-1 receptor-immunoreactive neurons in the pre-Bötzinger complex of rats: Light and electron microscopic studies. *Eur. J. Neurosci.* **16**, 1058–1066 (2002).

258. Bochorishvili, G., Stornetta, R. L., Coates, M. B. & Guyenet, P. G. Pre-Bötzinger complex receives glutamatergic innervation from galaninergic and other retrotrapezoid nucleus neurons. *J Comp Neurol* **520**, 1047–1061 (2012).

259. Tan, W., Pagliardini, S., Yang, P., Janczewski, W. A. & Feldman, J. L. Projections of PreBötzinger Complex Neurons in Adult Rats. *J Comp Neurol* **518**, 1862–1878 (2010).

260. Yang, C. F. & Feldman, J. L. Efferent projections of excitatory and inhibitory preBotzinger complex neurons. *J.Comp Neurol.* 1389–1402 (2018). doi:10.1002/cne.24415

261. Anderson, T. M. *et al.* A novel excitatory network for the control of breathing. *Nature* **536**, 76–80 (2016).

262. Koshiya, N. & Smith, J. C. Neuronal pacemaker for breathing visualized in vitro. *Nature* **400**, 360–363 (1999).

263. Koshiya, N. *et al.* Anatomical and functional pathways of rhythmogenic inspiratory premotor information flow originating in the pre-Bötzinger complex in the rat medulla. *Neuroscience* **268**, 194–211 (2014).

264. McKay, L. C., Janczewski, W. A. & Feldman, J. L. Sleep-disordered breathing after targeted ablation of preBötzinger complex neurons. *Nat. Neurosci.* **8**, 1142–4 (2005).

265. Huckstepp, R. T. R., Henderson, L. E., Cardoza, K. P. & Feldman, J. L. Interactions between respiratory oscillators in adult rats. *Elife* **5**, 1–22 (2016).

266. Sherman, D., Worrell, J. W., Cui, Y. & Feldman, J. L. Optogenetic perturbation of

preBötzinger complex inhibitory neurons modulates respiratory pattern. *Nat. Neurosci.* **18**, 408–414 (2015).

267. Okada, Y. *et al.* Preinspiratory calcium rise in putative pre-Bötzinger complex astrocytes. *J. Physiol.* **590**, 4933–4944 (2012).

268. Oku, Y., Fresemann, J., Miwakeichi, F. & Hülsmann, S. Respiratory calcium fluctuations in low-frequency oscillating astrocytes in the pre-Bötzinger complex. *Respir. Physiol. Neurobiol.* **226**, 11–17 (2016).

269. Carroll, M. S., Viemari, J. C. & Ramirez, J.-M. Patterns of inspiratory phase-dependent activity in the in vitro respiratory network. *J. Neurophysiol.* 285–295 (2012). doi:10.1152/jn.00619.2012

270. Zavala-Tecuapetla, C., Tapia, D., Rivera-Angulo, A. J., Galarraga, E. & Peña-Ortega, F. Morphological characterization of respiratory neurons in the pre-bötzinger complex. *Prog. Brain Res.* **209**, 39–56 (2014).

271. Peña, F., Parkis, M. A., Tryba, A. K. & Ramirez, J. M. Differential contribution of pacemaker properties to the generation of respiratory rhythms during normoxia and hypoxia. *Neuron* **43**, 105–117 (2004).

272. Anderson, T. M. & Ramirez, J.-M. Respiratory rhythm generation: triple oscillator hypothesis. *F1000Research* **6**, 139 (2017).

273. Koizumi, H. & Smith, J. C. Persistent Na+ and K+-Dominated Leak Currents Contribute to Respiratory Rhythm Generation in the Pre-Botzinger Complex In Vitro. *J. Neurosci.* **28**, 1773–1785 (2008).

274. Rekling, J. C. & Feldman, J. L. PREBÖTZINGER COMPLEX AND PACEMAKER NEURONS: Hypothesized Site and Kernel for Respiratory Rhythm Generation. *Annu. Rev. Physiol.* **60**, 385–405 (1998).

275. Rekling, J. C., Shao, X. M. & Feldman, J. L. Electrical Coupling and Excitatory Synaptic Transmission between Rhythmogenic Respiratory Neurons in the PreBötzinger Complex. *J Neurosci.* **20**, RC113 (2000).

276. Hartelt, N. *et al.* Imaging of respiratory network topology in living brainstem slices. *Mol. Cell. Neurosci.* **37**, 425–431 (2008).

277. Watts, D. J. & Strogatz, S. H. Collective dynamics of ‘small-world’ networks. *Nature* **393**, 440–442 (1998).

278. Smedler, E., Malmersjö, S. & Uhlén, P. Network analysis of time-lapse microscopy recordings. *Front. Neural Circuits* **8**, 1–10 (2014).

279. Kam, K., Worrell, J. W., Ventalon, C., Emiliani, V. & Feldman, J. L. Emergence of Population Bursts from Simultaneous Activation of Small Subsets of preBotzinger Complex Inspiratory Neurons. *J. Neurosci.* **33**, 3332–3338 (2013).

280. Muldoon, S. F., Bridgeford, E. W. & Bassett, D. S. Small-world propensity and weighted brain networks. *Sci. Rep.* **6**, 1–13 (2016).

281. Janczewski, W. A. & Feldman, J. L. Distinct rhythm generators for inspiration and expiration in the juvenile rat. *J. Physiol.* **570**, 407–420 (2006).

282. Feldman, J. L. & Del Negro, C. A. Looking for inspiration: new perspectives on respiratory rhythm. *Nat. Rev. Neurosci.* **7**, 232–242 (2006).

283. Barnes, B. J., Tuong, C.-M. & Mellen, N. M. Functional imaging reveals respiratory network activity during hypoxic and opioid challenge in the neonate rat tilted sagittal slab preparation. *J. Neurophysiol.* **97**, 2283–92 (2007).

284. Lavezzi, A. M. & Matturri, L. Functional neuroanatomy of the human pre-Bötzinger complex with particular reference to sudden unexplained perinatal and infant death. *Neuropathology* **28**, 10–16 (2008).

285. Dahan, a *et al.* Anesthetic potency and influence of morphine and sevoflurane on respiration in mu-opioid receptor knockout mice. *Anesthesiology* **94**, 824–832 (2001).

286. Johnson, S. M. *et al.* Modulation of respiratory rhythm in vitro : role of Gi / o protein-mediated mechanisms. *J Appl Physiol* **80**, 2120–2133 (1996).

287. Ruangkittisakul, A. & Ballanyi, K. Reversal by phosphodiesterase-4 blockers of in vitro apnea in the isolated brainstem-spinal cord preparation from newborn rats. *Neurosci. Lett.* **401**, 194–198 (2006).

288. Ruangkittisakul, A. & Ballanyi, K. Methylxanthine reversal of opioid-evoked inspiratory depression via phosphodiesterase-4 blockade. *Respir. Physiol. Neurobiol.* **172**, 94–105 (2010).

289. Montandon, G., Liu, H. & Horner, R. L. Contribution of the respiratory network to rhythm and motor output revealed by modulation of GIRK channels, somatostatin and neurokinin-1 receptors. *Sci. Rep.* **6**, 32707 (2016).

290. Montandon, G. *et al.* G-protein-gated Inwardly Rectifying Potassium Channels Modulate Respiratory Depression by Opioids. *Anesthesiology* **124**, 641–50 (2016).

291. Niesters, M., Overdyk, F., Smith, T., Aarts, L. & Dahan, A. Opioid-induced respiratory depression in paediatrics: A review of case reports. *Br. J. Anaesth.* **110**, 175–182 (2013).

292. Xia, Y. & Haddad, G. G. Ontogeny and distribution of opioid receptors in the rat brainstem. *Brain Res.* **549**, 181–93 (1991).

293. Stuth, E. a E., Stucke, A. G. & Zuperku, E. J. Effects of anesthetics, sedatives, and opioids on ventilatory control. *Compr. Physiol.* **2**, 2281–2367 (2012).

294. Phillips, R. S. *et al.* Pain-facilitating medullary neurons contribute to opioid-induced respiratory depression. *J. Neurophysiol.* **108**, 2393–2404 (2012).

295. Hill, R. *et al.* Ethanol Reversal of Tolerance to the Respiratory Depressant Effects of Morphine. *Neuropsychopharmacology* **41**, 762–773 (2016).

296. Emery, M. J., Groves, C. C., Kruse, T. N., Shi, C. & Terman, G. W. Ventilation and the response to hypercapnia after morphine in opioid-naive and opioid-tolerant rats. *Anesthesiology* **124**, 945–957 (2016).

297. Gold, M. S., Reichling, D. B., Shuster, M. J. & Levine, J. D. Hyperalgesic agents increase a tetrodotoxin-resistant Na+ current in nociceptors. *Proc. Natl. Acad. Sci. U. S. A.* **93**, 1108–12 (1996).

298. Vanegas, H. & Schaible, H. G. Prostaglandins and cyclooxygenases in the spinal cord. *Prog Neurobiol* **64**, 327–363 (2001).

299. Momin, A., Cadiou, H., Mason, A. & McNaughton, P. a. Role of the hyperpolarization-activated current I h in somatosensory neurons. *J. Physiol.* **586**, 5911–5929 (2008).

300. Baba, H. *et al.* Direct activation of rat spinal dorsal horn neurons by prostaglandin E2. *J. Neurosci.* **21**, 1750–6 (2001).

301. Lu, J., Xing, J. & Li, J. Prostaglandin E2 (PGE2) inhibits glutamatergic synaptic transmission in dorsolateral periaqueductal gray (dl-PAG). *Brain Res.* **1162**, 38–47

(2007).

302. Matsumura, K. *et al.* Prostaglandin E2 excites neurons of the nucleus tractus solitarius by activating cation channels. *Brain Res.* **626**, 343–346 (1993).

303. Shibuya, I. *et al.* Involvement of postsynaptic EP4 and presynaptic EP3 receptors in actions of prostaglandin E2 in rat supraoptic neurones. *J. Neuroendocrinol.* **14**, 64–72 (2002).

304. Yang, H., Zhang, J., Breyer, R. M. & Chen, C. Altered hippocampal long-term synaptic plasticity in mice deficient in the PGE2 EP2 receptor. *J Neurochem* **108**, 295–304 (2009).

305. Koch, H. *et al.* Prostaglandin E2-Induced Synaptic Plasticity in Neocortical Networks of Organotypic Slice Cultures. *J. Neurosci.* **30**, 11678–11687 (2010).

306. Hoffer, B. J., Siggins, G. R. & Bloom, F. E. Prostaglandins E1 and E2 Antagonize Norepinephrine Effects on Cerebellar Purkinje Cells : Microelectrophoretic Study. *Science (80-.).* **166**, 1418–1420 (1969).

307. Chen, C. & Bazan, N. G. Endogenous PGE2 regulates membrane excitability and synaptic transmission in hippocampal CA1 pyramidal neurons. *J. Neurophysiol.* **93**, 929–941 (2005).

308. Kurosawa, N., Shimizu, K. & Seki, K. The development of depression-like behavior is consolidated by IL-6-induced activation of locus coeruleus neurons and IL-1B-induced elevated leptin levels in mice. *Psychopharmacology (Berl).* **233**, 1725–1737 (2016).

309. Feinstein, D. L., Kalinin, S. & Braun, D. Causes, consequences, and cures for neuroinflammation mediated via the locus coeruleus: noradrenergic signaling system. *J. Neurochem.* **139**, 154–178 (2016).

310. Lee, H. J., Park, H. J., Starkweather, A., An, K. & Shim, I. Decreased Interleukin-4 Release from the Neurons of the Locus Coeruleus in Response to Immobilization Stress. *Mediators Inflamm.* **2016**, 1–8 (2016).

311. Johnson, J. D. *et al.* Catecholamines mediate stress-induced increases in peripheral and central inflammatory cytokines. *Neuroscience* **135**, 1295–1307 (2005).

312. Ross, J. a., McGonigle, P. & Van Bockstaele, E. J. Locus coeruleus, norepinephrine and

AB peptides in Alzheimer's disease. *Neurobiol. Stress* **2**, 73–84 (2015).

313. Hall, S., Milne, B. & Loomis, C. Spinal action of ketorolac, S(+) and R(-)-ibuprofen on non-noxious activation of the catechol oxidation in the rat locus coeruleus. *Anesthesiology* **90**, 165–73 (1999).

314. Tassorelli, C., Greco, R., Sandrini, G. & Nappi, G. Central components of the analgesic/antihyperalgesic effect of nimesulide: studies in animal models of pain and hyperalgesia. *Drugs* **63**, 9–22 (2003).

315. Nakagawa, T., Minami, M., Katsumata, S., Ienaga, Y. & Satoh, M. Suppression of naloxone-precipitated withdrawal jumps in morphine-dependent mice by stimulation of prostaglandin EP3 receptor. *Br. J. Pharmacol.* **116**, 2661–6 (1995).

316. Dray, F. & Heaulme, M. Prostaglandins of the E series inhibit release of noradrenaline in rat hypothalamus by a mechanism unrelated to classical alpha 2 adrenergic presynaptic inhibition. *Neuropharmacology* **23**, 457–462 (1984).

317. Allgaier, C., Jäger, T. & Hertting, G. Endogenous noradrenaline impairs the prostaglandin-induced inhibition of noradrenaline release. *Naunyn. Schmiedebergs. Arch. Pharmacol.* **340**, 472–474 (1989).

318. Exner, H. J. & Schlicker, E. Prostanoid receptors of the EP3 subtype mediate the inhibitory effect of prostaglandin E2 on noradrenaline release in the mouse brain cortex. *Naunyn. Schmiedebergs. Arch. Pharmacol.* **351**, 46–52 (1995).

319. Schlicker, E. & Marr, I. Mutual interactions of the presynaptic histamine H3 and the prostaglandin EP3 receptors on the noradrenergic terminals in the mouse brain. *Neuroscience* **79**, 247–254 (1997).

320. Günther, J., Schulte, K., Wenzel, D., Malinowska, B. & Schlicker, E. Prostaglandins of the e series inhibit monoamine release via EP3 receptors: Proof with the competitive EP3 receptor antagonist L-826,266. *Naunyn. Schmiedebergs. Arch. Pharmacol.* **381**, 21–31 (2010).

321. Stein, C., Machelska, H., Binder, W., Schäfer, M. Peripheral opioid analgesia: from experimental to clinical studies. *Curr. Opin. Pharmacol.* **1**, 62–65 (2001).

322. Williams, J. T., Christie, M. J. & Manzoni, O. Cellular and synaptic adaptations mediating opioid dependence. *Physiol Rev* **81**, 299–343 (2001).

323. Mellen, N. M., Janczewski, W. A., Bocchiaro, C. M. & Feld, J. L. Opioid-induced quantal slowing reveals dual networks for respiratory rhythm generation. *Neuron* **37**, 821–826 (2003).

324. Ballanyi, K., Lalley, P. M., Hoch, B. & Richter, D. W. cAMP-dependent reversal of opioid- and prostaglandin-mediated depression of the isolated respiratory network in newborn rats. *J. Physiol.* **504**, 127–134 (1997).

325. Siljehav, V., Olsson Hofstetter, A., Jakobsson, P.-J. & Herlenius, E. mPGES-1 and prostaglandin E2: vital role in inflammation, hypoxic response, and survival. *Pediatr. Res.* **72**, 460–7 (2012).

326. Sanchez-Alavez, M. *et al.* Night eating and obesity in the EP3R-deficient mouse. *Proc. Natl. Acad. Sci. USA* **104**, 3009–14 (2007).

327. Wang, Y. Y. & Aghajanian, G. K. Excitation of Locus Coeruleus Neurons by an Adenosine 3′,5′-Cyclic Monophosphate-Activated Inward Current: Extracellular and Intracellular Studies in Rat Brain Slices. *Synapse* **1**, 481–487 (1987).

328. Alreja, M. & Aghajanian, G. K. Opiates suppress a resting sodium-dependent inward current and activate an outward potassium current in locus coeruleus neurons. *J. Neurosci.* **13**, 3525–3532 (1993).

329. Pineda, J., Kogan, J. H. & Aghajanian, G. K. Nitric oxide and carbon monoxide activate locus coeruleus neurons through a cGMP-dependent protein kinase: involvement of a nonselective cationic channel. *J. Neurosci.* **16**, 1389–99 (1996).

330. Aghajanian, G. K. & Rasmussen, K. Intracellular studies in the facial nucleus illustrating a simple new method for obtaining viable motoneurons in adult rat brain slices. *Synapse* **3**, 331–338 (1989).

331. Mendiguren, A. & Pineda, J. Cannabinoids enhance N-methyl-D-aspartate-induced excitation of locus coeruleus neurons by CB1 receptors in rat brain slices. *Neurosci. Lett.* **363**, 1–5 (2004).

332. Jun, S. B., Cuzon Carlson, V., Ikeda, S. & Lovinger, D. Vibrodissociation of Neurons from Rodent Brain Slices to Study Synaptic Transmission and Image Presynaptic Terminals. *J. Vis. Exp.* 2–9 (2011). doi:10.3791/2752

333. Ruangkittisakul, A. *et al.* High Sensitivity to Neuromodulator-Activated Signaling

Pathways at Physiological [K+] of Confocally Imaged Respiratory Center Neurons in On-Line-Calibrated Newborn Rat Brainstem Slices. *J. Neurosci.* **26**, 11870–11880 (2006).

334. Frantseva, M. V., Carlen, P. L. & El-Beheiry, H. A submersion method to induce hypoxic damage in organotypic hippocampal cultures. *J. Neurosci. Methods* **89**, 25–31 (1999).

335. Stoppini, L., Buchs, P.-A. & Muller, D. A simple method for organotypic cultures of nervous tissue. *J. Neurosci. Methods* **37**, 173–182 (1991).

336. Chee, M. J., Price, C. J., Statnick, M. a & Colmers, W. F. Nociceptin/orphanin FQ suppresses the excitability of neurons in the ventromedial nucleus of the hypothalamus. *J. Physiol.* **589**, 3103–3114 (2011).

337. Zwicker, J. D. *et al.* Glial TLR4 signaling does not contribute to opioid-induced depression of respiration. *J. Appl. Physiol.* **117**, 857–68 (2014).

338. Mulvey, B. *et al.* Molecular and Functional Sex Differences of Noradrenergic Neurons in the Mouse Locus Coeruleus. *Cell Rep.* **23**, 2225–2235 (2018).

339. Jones, R. L., Woodward, D. F., Wang, J. W. & Clark, R. L. Roles of affinity and lipophilicity in the slow kinetics of prostanoid receptor antagonists on isolated smooth muscle preparations. *Br. J. Pharmacol.* **162**, 863–879 (2011).

340. Chessell, I. P., Black, M. D., Feniuk, W. & Humphrey, P. P. A. Operational characteristics of somatostatin receptors mediating inhibitory actions on rat locus coeruleus neurones. *Br. J. Pharmacol.* **117**, 1673–1678 (1996).

341. Forselles, K. J. *et al.* In vitro and in vivo characterization of PF-04418948, a novel, potent and selective prostaglandin EP2 receptor antagonist. *Br. J. Pharmacol.* **164**, 1847–56 (2011).

342. Birrell, M. A. *et al.* Selectivity profiling of the novel EP2 receptor antagonist, PF-04418948, in functional bioassay systems: Atypical affinity at the guinea pig EP2 receptor. *Br. J. Pharmacol.* **168**, 129–138 (2013).

343. Martinez-Cutillas, M., Mañé, N., Gallego, D., Jimenez, M. & Martin, M. T. EP2 and EP4 receptors mediate PGE2 induced relaxation in murine colonic circular muscle: Pharmacological characterization. *Pharmacol. Res.* **90**, 76–86 (2014).

344. Ugedo, L., Pineda, J., Ruiz-Ortega, J. A. & Martin-Ruiz, R. Stimulation of locus coeruleus neurons by non-I1/I2-type imidazoline receptors: an in vivo and in vitro electrophysiological study. *Br J Pharmacol* **125**, 1685–1694 (1998).

345. Jolas, T., Nestler, E. J. & Aghajanian, G. K. Chronic morphine increases GABA tone on serotonergic neurons of the dorsal raphe nucleus: Association with an up-regulation of the cyclic AMP pathway. *Neuroscience* **95**, 433–443 (2000).

346. Zolles, G. *et al.* Pacemaking by HCN Channels Requires Interaction with Phosphoinositides. *Neuron* **52**, 1027–1036 (2006).

347. Hohenegger, M. *et al.* G salpha-selective G protein antagonists. *Pharmacology* **95**, 346–351 (1998).

348. Kurowski, P., Gawlak, M. & Szulczyk, P. Muscarinic receptor control of pyramidal neuron membrane potential in the medial prefrontal cortex (mPFC) in rats. *Neuroscience* **303**, 474–488 (2015).

349. Mendiguren, A. & Pineda, J. CB1 cannabinoid receptors inhibit the glutamatergic component of KCl-evoked excitation of locus coeruleus neurons in rat brain slices. *Neuropharmacology* **52**, 617–625 (2007).

350. Medrano, M. C., Gerrikagoitia, I., Martínez-Millán, L., Mendiguren, A. & Pineda, J. Functional and morphological characterization of glutamate transporters in the rat locus coeruleus. *Br. J. Pharmacol.* **169**, 1781–1794 (2013).

351. Bonfill-Teixidor, E., Otxoa-de-Amezaga, A., Font-Nieves, M., Sans-Fons, M. G. & Planas, A. M. Differential expression of E-type prostanoid receptors 2 and 4 in microglia stimulated with lipopolysaccharide. *J. Neuroinflammation* **14**, 3 (2017).

352. Fujino, H., Salvi, S. & Regan, J. W. Differential Regulation of Phosphorylation of the cAMP Response Element-Binding Protein after Activation of EP 2 and EP 4 Prostanoid Receptors by Prostaglandin E 2. *Mol. Pharmacol.* **68**, 251–259 (2005).

353. Eijkelkamp, N. *et al.* Low nociceptor GRK2 prolongs prostaglandin E2 hyperalgesia via biased cAMP signaling to Epac/Rap1, protein kinase Cepsilon, and MEK/ERK. *J. Neurosci.* **30**, 12806–12815 (2010).

354. Bailey, C. P., Kelly, E. & Henderson, G. Protein Kinase C Activation Enhances Morphine-Induced Rapid Desensitization of -Opioid Receptors in Mature Rat Locus

Ceruleus Neurons. *Mol. Pharmacol.* **66**, 1592–1598 (2004).

355. Hill, J. W. *et al.* Acute effects of leptin require PI3K signaling in hypothalamic proopiomelanocortin neurons in mice. *J. Clin. Invest.* **118**, 1796–1805 (2008).

356. Boie, Y. *et al.* Molecular cloning and characterization of the four rat prostaglandin E2 prostanoid receptor subtypes. *Eur. J. Pharmacol.* **340**, 227–241 (1997).

357. Abramovitz, M. *et al.* The utilization of recombinant prostanoid receptors to determine the affinities and selectivities of prostaglandins and related analogs. *Biochim. Biophys. Acta - Mol. Cell Biol. Lipids* **1483**, 285–293 (2000).

358. Whittle, B. J., Silverstein, A. M., Mottola, D. M. & Clapp, L. H. Binding and activity of the prostacyclin receptor (IP) agonists, treprostinil and iloprost, at human prostanoid receptors: Treprostinil is a potent DP 1 and EP 2 agonist. *Biochem. Pharmacol.* **84**, 68–75 (2012).

359. Yoshida, K. *et al.* Stimulation of bone formation and prevention of bone loss by prostaglandin E EP4 receptor activation. *Proc. Natl. Acad. Sci.* **99**, 4580–4585 (2002).

360. Young, R. N. *et al.* Discovery and synthesis of a potent, selective and orally bioavailable EP4 receptor agonist. *Heterocycles* **64**, 437–446 (2004).

361. Su, X. *et al.* Modulation of bladder function by prostaglandin EP3 receptors in the central nervous system. *Am. J. Physiol. Renal Physiol.* **295**, F984-94 (2008).

362. Machwate, M. *et al.* Prostaglandin receptor EP(4) mediates the bone anabolic effects of PGE(2). *Mol. Pharmacol.* **60**, 36–41 (2001).

363. Weimer, M. *et al.* The impact of data transformations on concentration-response modeling. *Toxicol. Lett.* **213**, 292–298 (2012).

364. Lazareno, S. & Birdsall, N. J. M. Estimation of competitive antagonist affinity from functional inhibition curves using the Gaddum Schild and Cheng-Prusoff equations. *Br. J. Pharmacol.* **109**, 1110–1119 (1993).

365. Negus, S. S., Burke, T. F., Medzihradsky, F. & Woods, J. H. Effects of opioid agonists selective for mu, kappa and delta opioid receptors on schedule-controlled responding in rhesus monkeys: antagonism by quadazocine. *J. Pharmacol. Exp. Ther.* **267**, 896–903 (1993).

366. Schild, H. O. pAx and competitive drug antagonism. *Br. J. Pharmacol. Chemother.* **4**, 277–280 (1949).

367. Kenakin, T. P. Chapter 6 – Orthosteric Drug Antagonism. in *A Pharmacology Primer* 119–154 (2014). doi:10.1016/B978-0-12-407663-1.00006-5

368. Kay, L. J. *et al.* Characterization of the EP receptor subtype that mediates the inhibitory effects of prostaglandin E2 on IgE-dependent secretion from human lung mast cells. *Clin. Exp. Allergy* **43**, 741–751 (2013).

369. Kenakin, T., Jenkinson, S. & Watson, C. Determining the potency and molecular mechanism of action of insurmountable antagonists. *J. Pharmacol. Exp. Ther.* **319**, 710–723 (2006).

370. Malmersjo, S. *et al.* Neural progenitors organize in small-world networks to promote cell proliferation. *Proc. Natl. Acad. Sci.* **110**, E1524–E1532 (2013).

371. Achard, S. & Bullmore, E. Efficiency and cost of economical brain functional networks. *PLoS Comput. Biol.* **3**, 0174–0183 (2007).

372. Uhlén, P. Spectral Analysis of Calcium Oscillations. *Sci STKE* **258**, 1–13 (2004).

373. Ikeda-Matsuo, Y. *et al.* Microsomal prostaglandin e synthase-1 contributes to ischaemic excitotoxicity through prostaglandin E 2 EP 3 receptors. *Br. J. Pharmacol.* **160**, 847–859 (2010).

374. Ruiz-Velasco, V. & Ikeda, S. R. Heterologous expression and coupling of G protein-gated inwardly rectifying K+ channels in adult rat sympathetic neurons. *J. Physiol.* **513**, 761–773 (1998).

375. Torrecilla, M. *et al.* G-protein-gated potassium channels containing Kir3.2 and Kir3.3 subunits mediate the acute inhibitory effects of opioids on locus ceruleus neurons. *J. Neurosci.* **22**, 4328–4334 (2002).

376. Fang, Y.-J., Zhou, M.-H., Gao, X.-F., Gu, H. & Mei, Y.-A. Arachidonic acid modulates Na + currents by non-metabolic and metabolic pathways in rat cerebellar granule cells. *Biochem. J.* **438**, 203–215 (2011).

377. Poppe, H. *et al.* Cyclic nucleotide analogs as probes of signaling pathways. *Nat. Methods* **5**, 277–278 (2008).

378. Santin, J. M. & Hartzler, L. K. Activation state of the hyperpolarization-activated current modulates temperature-sensitivity of firing in locus coeruleus neurons from bullfrogs. *Am. J. Physiol. - Regul. Integr. Comp. Physiol.* **308**, R1045–R1061 (2015).

379. Grzelka, K., Kurowski, P., Gawlak, M. & Szulczyk, P. Noradrenaline Modulates the Membrane Potential and Holding Current of Medial Prefrontal Cortex Pyramidal Neurons via β1-Adrenergic Receptors and HCN Channels. *Front. Cell. Neurosci.* **11**, 1–22 (2017).

380. Emery, E. C., Young, G. T., Berrocoso, E. M., Chen, L. & McNaughton, P. A. HCN2 ion channels play a central role in inflammatory and neuropathic pain. *Science (80-.).* **333**, 1462–6 (2011).

381. Kenakin, T. P. The Schild regression in the process of receptor classification. *Can. J. Physiol. Pharmacol.* **60**, 249–265 (1982).

382. Alreja, M. & Aghajanian, G. K. Use of the whole-cell patch-clamp method in studies on the role of cAMP in regulating the spontaneous firing of locus coeruleus neurons. *J. Neurosci. Methods* **59**, 67–75 (1995).

383. Moriyama, T. *et al.* Sensitization of TRPV1 by EP1 and IP reveals peripheral nociceptive mechanism of prostaglandins. *Mol. Pain* **1**, 1–13 (2005).

384. Shi, J. *et al.* The prostaglandin E2 E-prostanoid 4 receptor exerts anti-inflammatory effects in brain innate immunity. *J. Immunol.* **184**, 7207–7218 (2010).

385. Gold, M. S., Levine, J. D. & Correa, A. M. Modulation of TTX-R INa by PKC and PKA and their role in PGE2-induced sensitization of rat sensory neurons in vitro. *J. Neurosci.* **18**, 10345–10355 (1998).

386. Sachs, D., Villarreal, C., Cunha, F., Parada, C. & Ferreira, S. The role of PKA and PKCε pathways in prostaglandin E2-mediated hypernociception. *Br. J. Pharmacol.* **156**, 826–834 (2009).

387. Lowe, J. D., Kelly, E. & Henderson, G. Desensitization of Mu opioid receptors in the preBötzinger complex. *Proc. Br. Pharmacol. Soc.* **11**, (2013).

388. Mitchell, M. D. *et al.* Prostaglandins in the Human Umbilical Circulation At Birth. *BJOG An Int. J. Obstet. Gynaecol.* **85**, 114–118 (1978).

389. Gaiteri, C. & Rubin, J. E. The Interaction of Intrinsic Dynamics and Network Topology in Determining Network Burst Synchrony. *Front. Comput. Neurosci.* **5**, 10 (2011).

390. Jones, R. L., Qian, Y. M., Chan, K. M. & Yim, a P. Characterization of a prostanoid EP3-receptor in guinea-pig aorta: partial agonist action of the non-prostanoid ONO-AP-324. *Br. J. Pharmacol.* **125**, 1288–1296 (1998).

391. Clarke, D. L., Giembycz, M. A., Patel, H. J. & Belvisi, M. G. E-ring 8-isoprostanes inhibit ACh release from parasympathetic nerves innervating guinea-pig trachea through agonism of prostanoid receptors of the EP3-subtype. *Br. J. Pharmacol.* **141**, 600–9 (2004).

392. Khazaeipool, Z., Wiederman, M. & Inoue, W. Prostaglandin E2 depresses GABA release onto parvocellular neuroendocrine neurones in the paraventricular nucleus of the hypothalamus via presynaptic receptors. *J. Neuroendocrinol.* **30**, 1–10 (2018).

393. Momiyama, T., Todo, N., Sugimoto, Y., Ichikawa, A. & Narumiya, S. Membrane depolarization by activation of prostaglandin E receptor EP 3 subtype of putative serotonergic neurons in the dorsal raphe nucleus of the rat. *Naunyn. Schmiedebergs. Arch. Pharmacol.* **353**, 377–381 (1996).

394. Mangmool, S. & Kurose, H. Gi/o protein-dependent and -independent actions of pertussis toxin (ptx). *Toxins (Basel).* **3**, 884–899 (2011).

395. Torrecilla, M., Fernández-Aedo, I., Arrue, A., Zumarraga, M. & Ugedo, L. Role of GIRK channels on the noradrenergic transmission in vivo: an electrophysiological and neurochemical study on GIRK2 mutant mice. *Int. J. Neuropsychopharmacol.* **16**, 1093–1104 (2013).

396. Kuzhikandathil, E. V & Oxford, G. S. Classic D1 Dopamine Receptor AntagonistR-(+)-7-Chloro-8-hydroxy-3-methyl-1-phenyl-2,3,4,5-tetrahydro-1H-3-benzazepine hydrochloride (SCH23390) Directly Inhibits G Protein-Coupled Inwardly Rectifying Potassium Channels. *Mol. Pharmacol.* **62**, 119–126 (2002).

397. Li, K.-Y. & Putnam, R. W. Transient outwardly rectifying A currents are involved in the firing rate response to altered CO2 in chemosensitive locus coeruleus neurons from neonatal rats. *Am J Physiol Regul Integr Comp Physiol* **305**, R780–R792 (2013).

398. Shi, J. *et al.* Inflammatory prostaglandin E2 signalning in a mouse model of Alzheimer's

disease. *Ann Neurol.* **72**, 788–798 (2012).

399. Fu, Y. *et al.* EP2 receptor signaling regulates microglia death. *Mol. Pharmacol.* **88**, 161–170 (2015).

400. Daiyasu, H., Hirokawa, T., Kamiya, N. & Toh, H. Computational analysis of ligand recognition mechanisms by prostaglandin E2 (subtype 2) and D2 receptors. *Theor. Chem. Acc.* **130**, 1131–1143 (2011).

401. Song, K. *et al.* The TRPM2 channel is a hypothalamic heat sensor that limits fever and can drive hypothermia. *Science (80-.).* **353**, 1393–1398 (2016).

402. Matsumoto, S. *et al.* Prostaglandin E2-induced modification of tetrodotoxin-resistant Na+ currents involves activation of both EP2 and EP4 receptors in neonatal rat nodose ganglion neurones. *Br. J. Pharmacol.* **145**, 503–13 (2005).

403. Lehmann, D., Seneviratne, A. & Smrcka, A. Small molecule disruption of G protein βγ subunit signaling inhibits neutrophil chemotaxis and inflammation. *Mol. Pharmacol.* **73**, 410–418 (2008).

404. Connor, M. & Christie, M. J. Opioid Receptor Signalling Mechanisms. *Clin Exp Pharmacol Physiol.* **26**, 493–499 (1999).

405. Casey, L. M. *et al.* Small molecule disruption of Gβγ signaling inhibits the progression of heart failure. *Circ. Res.* **107**, 532–539 (2010).

406. Ma, J. Y., Catterall, W. A. & Scheuer, T. Persistent sodium currents through brain sodium channels induced by G protein βγ subunits. *Neuron* **19**, 443–452 (1997).

407. Mantegazza, M. *et al.* Molecular Determinants for Modulation of Persistent Sodium Current by G-Protein βγ Subunits. *J. Neurosci.* **25**, 3341–3349 (2005).

408. Alba-Delgado, C. *et al.* Chronic pain leads to concomitant noradrenergic impairment and mood disorders. *Biol. Psychiatry* **73**, 54–62 (2013).

409. Savonenko, A. *et al.* Impaired cognition, sensorimotor gating, and hippocampal long-term depression in mice lacking the prostaglandin E2 EP2 receptor. *Exp. Neurol.* **217**, 63–73 (2009).

410. Echeverria, V., Clerman, A. & Doré, S. Stimulation of PGE2 receptors EP2 and EP4 protects cultured neurons against oxidative stress and cell death following β-amyloid

exposure. *Eur. J. Neurosci.* **22**, 2199–2206 (2005).

411. Jones, R. L., Wan Ahmad, W. A. N., Woodward, D. F. & Wang, J. Nature of the slow relaxation of smooth muscle induced by a EP2 receptor agonist with a non-prostanoid structure. *Prostaglandins Leukot. Essent. Fat. Acids* **88**, 321–330 (2013).

412. Wise, H. Lack of interaction between prostaglandin E2 receptor subtypes in regulating adenylyl cyclase activity in cultured rat dorsal root ganglion cells. *Eur. J. Pharmacol.* **535**, 69–77 (2006).

413. Malty, R. H., Hudmon, A., Fehrenbacher, J. C. & Vasko, M. R. Long-term exposure to PGE2 causes homologous desensitization of receptor-mediated activation of protein kinase A. *J. Neuroinflammation* **13**, 181 (2016).

414. Leduc, M. *et al.* Functional Selectivity of Natural and Synthetic Prostaglandin EP 4 Receptor Ligands. *Pharmacology* **331**, 297–307 (2009).

415. Parent, A. J. *et al.* Increased anxiety-like behaviors in rats experiencing chronic inflammatory pain. *Behav. Brain Res.* **229**, 160–167 (2012).

416. Raynor, K. *et al.* Pharmacological Characterization of the Cloned kappa-, delta-, and mu-Opioid Receptors. *Mol. Pharmacol.* **45**, 330–334 (1993).

417. Kamei, J., Ohsawa, M., Hayashi, S. S. & Nakanishi, Y. Effect of chronic pain on morphine-induced respiratory depression in mice. *Neuroscience* **174**, 224–233 (2011).

418. Ma, W. & Quirion, R. Does COX2-dependent PGE2 play a role in neuropathic pain? *Neurosci. Lett.* **437**, 165–169 (2008).

419. He, Y., Chen, Z. & Evans, A. Structural Insights into Aberrant Topological Patterns of Large-Scale Cortical Networks in Alzheimer's Disease. *J. Neurosci.* **28**, 4756–4766 (2008).

420. Liu, Y. *et al.* Altered Topological Organization of White Matter Structural Networks in Patients with Neuromyelitis Optica. *PLoS One* **7**, (2012).

421. Lalley, P. M., Pilowsky, P. M., Forster, H. V. & Zuperku, E. J. CrossTalk opposing view: The pre-Bötzinger complex is not essential for respiratory depression following systemic administration of opioid analgesics. *J. Physiol.* **592**, 1163–1166 (2014).

422. Levitt, E. S., Abdala, A. P., Paton, J. F., Bissonnette, J. M. & Williams, J. T. Mu opioid

receptor activation hyperpolarizes respiratory-controlling Kölliker-Fuse neurons and suppresses post-inspiratory drive. *J. Physiol.* **19**, 4453–4469 (2015).

423. Siljehav, V., Hofstetter, A. M., Leifsdottir, K. & Herlenius, E. Prostaglandin E2 Mediates Cardiorespiratory Disturbances during Infection in Neonates. *J. Pediatr.* **167**, 1207–1213 (2015).

8 ACCOMPANYING MANUSCRIPTS

Submitted to the *British Journal of Pharmacology*

TITLE:

Inhibition of rat locus coeruleus neurons via prostaglandin E_2 EP3 receptor: pharmacological characterization *in vitro*

RUNNING TITLE:

EP3 receptor in rat LC neurons

AUTHORS:

Amaia Nazabal, Aitziber Mendiguren and Joseba Pineda*

[1] Department of Pharmacology, Faculty of Medicine and Nursing, University of the Basque Country (UPV/EHU), Leioa Bizkaia, Spain

***Corresponding author:**

Joseba Pineda. M.D., Ph.D.

Department of Pharmacology,

Faculty of Medicine and Nursing

University of the Basque Country (UPV/EHU)

Leioa Bizkaia, E-48940, Spain

E-mail address: joseba.pineda@ehu.eus (Dr. J. Pineda).

Tel: +34-946015577.

Orcid ID: 0000-0002-9421-1081

Word count:

Abstract: 250	References: 60
Introduction: 530	Tables: 3
Results: 1212	Figures: 5
Discussion: 1500	

Acknowledgements

This work was supported by the University of the Basque Country (UPV/EHU) [Grant GIU14/29] and Ministerio de Sanidad, Consumo y Bienestar Social. Delegación del Gobierno para el Plan Nacional Sobre Drogas (PND18/04). A. Nazabal was supported by predoctoral fellowships from the Basque Government. The experiments comply with the current laws of Spain.

Conflict of interest

The authors declare that they have no conflict of interest.

Non-approved abbreviations

- aCSF: artificial cerebrospinal fluid
- FR: firing rate
- GIRK: inwardly rectifying potassium channel
- LC: locus coeruleus
- ME: [Met]enkephalin
- NA: noradrenaline
- NSAID: Nonsteroidal anti-inflammatory drugs
- PAG: periaqueductal gray
- PTX: pertussis toxin
- PGE_2: prostaglandin E_2
- PGE_1: prostaglandin E_1

Bullet point summary

What is already known:

- PGE_2, inflammatory mediator involved in pain and fever, modulates the activity of brain neurons
- EP3 receptor agonist sulprostone activation hyperpolarizes mice LC neurons

What this study adds:

- Endogenous PGE_2 reduces the neuronal activity of rat LC cells through EP3 receptors
- EP3 receptor activation inhibits LC neurons via $G_{i/o}$ proteins and GIRK channels

Clinical significance:

- The LC, the main noradrenergic nucleus, is susceptible to inflammatory mediators
- Prostanoid system in the LC might be a pharmacological target against inflammation-mediated neuropsychiatric processes

Abstract

BACKGROUND AND PURPOSE: Prostaglandin E_2 (PGE_2) is an inflammatory mediator synthesized by the brain constitutive cyclooxygenase (COX) enzyme. PGE_2 binds to G protein-coupled EP1-4 receptors (EP1 to G_q, EP2 and EP4 to G_s, and EP3 to $G_{i/o}$). The EP2, EP3, and EP4 receptors are expressed in the locus coeruleus (LC), the main noradrenergic nucleus in the brain. EP3 receptors have been extensively studied in the CNS, although its role regulating the LC neuronal activity is unclear. Our aim was to pharmacologically characterize the EP3 receptor in the LC.

EXPERIMENTAL APPROACH: We studied the effect of EP3 receptor agonists on the firing activity of LC cells in rat brain slices by single-unit extracellular electrophysiology.

KEY RESULTS: The EP3 receptor agonist sulprostone (0.15 nM – 1.28 μM), the endogenous PGE_2 (0.31 nM – 10.2 μM), and the PGE_1 analogue misoprostol (0.31 nM – 2.56 μM) inhibited

the firing rate of LC neurons in a concentration-dependent manner (EC_{50}=15 nM, 51 nM, and 110 nM, respectively). The EP3 receptor antagonist L-798,106 (10 μM), but not the EP2 (PF-04418948 10 μM) or EP4 (L-161,982 10 μM) receptor antagonists, caused a more than 8-fold rightward shift in the concentration-effect curves for the EP3 receptor agonists. Sulprostone-induced effect was attenuated by the $G_{i/o}$-protein blocker pertussis toxin (PTX, 500 ng ml^{-1}) and the inhibitors of inwardly rectifying potassium channels (GIRK) $BaCl_2$ (300 μM) and SCH-23390 (15 μM).

CONCLUSIONS AND IMPLICATIONS: LC neuronal firing activity is regulated in an inhibitory manner by EP3 receptors, presumably by a $G_{i/o}$ protein and GIRK-mediated mechanism.

Keywords: locus coeruleus; PGE_2; EP3 receptor; firing; slice; prostanoid

Introduction

Prostaglandins, as pain and inflammatory mediators, are synthesized from membrane phospholipids on demand, which are transformed into arachidonic acid, and then into a common precursor by the rate-limiting enzyme cyclooxygenase (COX). Nonsteroidal anti-inflammatory drugs (NSAIDs), widely used as analgesic, antipyretic, and anti-inflammatory drugs, act by blocking COX and thereby suppressing the synthesis of prostaglandins. In human and animal brain, both COX-1 and COX-2 isoforms are constitutively expressed under non-inflammatory conditions (Hétu and Riendeau, 2005; Kirkby et al., 2016). Moreover, the COX-2 is found in specific brain areas such as the cortical dendritic spines (Kaufmann et al., 1996), supporting the idea that prostaglandins play an essential role in regulating the function of the central nervous system (CNS). Indeed, prostaglandin E_2 (PGE_2), the main final product of this pathway, modulates synaptic transmission in the hippocampus (Sang et al., 2005), the periaqueductal grey (Lu et al., 2007), and the paraventricular nucleus of the hypothalamus (Khazaeipool et al., 2018). The variety of PGE_2 actions are believed to be the result of four PGE_2 receptor subtypes (EP1-4) which are coupled to different G-protein pathways, primarily EP1 to G_q, EP2 and EP4 to G_s, and EP3 to $G_{i/o}$. The EP2, EP3, and EP4 receptors are widely expressed in the CNS, including the

hypothalamus and the locus coeruleus (LC) (Zhang and Rivest, 1999; Ek et al., 2000). Among all EP receptors, the functional role of the EP3 receptor has been one of the most extensively studied in the brain. Thus, EP3 receptor activation mediates the response to hypercapnia in the chemosensitive parafacial respiratory group (Forsberg et al., 2016), weakens the long-term potentiation in the hippocampus (Maingret et al., 2017), depolarizes serotonergic neurons in the dorsal raphe nucleus (Momiyama et al., 1996), and leads to hyperalgesia in the periaqueductal gray (Drake et al., 2016).

The LC, the main source of noradrenaline (NA) in the brain, is involved in the regulation of numerous functions, such as sleep-wake cycle, arousal, cognition, pain, and reward behavior. Several pieces of evidence have associated the LC with the EP3 receptor. First, *in situ* hybridization and immunohistochemistry techniques have shown the presence of a high density of the EP3 receptor or its mRNA in the LC (Ek et al., 2000; Nakamura et al., 2001). Second, LC neurons also possess the enzymatic machinery to synthesize prostaglandins such as the constitutive COX-2 (Yamaguchi and Okada, 2009). Third, a very recent electrophysiological study has shown that administration of a single EP3 receptor agonist hyperpolarizes LC neurons in mice (Mulvey et al., 2018). In addition, behavioral studies have demonstrated that administration of an EP3 receptor agonist reverses naloxone-induced c-fos expression in the LC from morphine-dependent rats (Nakagawa et al., 2000). Finally, presynaptic EP3 receptors mediate the inhibition of NA release in the main projection areas of the LC, including the cortex and the hippocampus (Exner and Schlicker, 1995; Günther et al., 2010).

Despite evidence suggesting a functional role for the EP3 receptor in the LC, it remains to be pharmacologically examined in this nucleus. Therefore, the aim of our research was to characterize pharmacologically the EP3 receptor and to study the signaling mechanism coupled to EP3 receptor by single-unit extracellular recordings in LC neurons from rat brain slices.

Methods

Animals and ethics statement

87 male adult Sprague-Dawley rats (200-300 g) were used in this study. Experiments were performed in compliance with the ARRIVE guidelines (Kilkenny et al., 2010; McGrath and Lilley, 2015) and with the recommendations made by the *British Journal of Pharmacology*.

Rats were obtained from the animal unit of the University of the Basque Country (Leioa, Spain) and housed under standard environmental conditions (22 ºC, 12:12 h light/dark cycles) with free access to food and water. One slice was taken from each animal and, unless stated otherwise, only one experiment was performed in each slice. The number of experiments in each group was typically five to nine, depending on the level of variability. Treatments and controls were performed in parallel in a randomized manner. As electrophysiological outcomes were collected *in situ*, data recording could not be blinded to the operator. However, the data analysis performed by the experimenter was confirmed separately by an additional researcher. All the experiments were carried out according to EU Directive 2010/63 on the protection of animals used for scientific purposes and approved by the local Ethical Committee for Research and Teaching of the University of the Basque Country (UPV/EHU, Spain) and the Department of Sustainability and Natural Environment of Provincial Council from Bizkaia (ref. CEEA M20-2015-152; CEEA M20-2018-026). All the efforts were made to minimize the animal suffering and to reduce the number of animals used.

Brain slice preparation

Animals were anesthetized with chloral hydrate (400 mg kg^{-1}, i.p.) and decapitated (Mendiguren and Pineda, 2007). The brain was rapidly extracted and a block of tissue including the brainstem was immersed in an ice-cold modified artificial cerebrospinal fluid (aCSF) where NaCl was equiosmolarly substituted for sucrose to improve neuronal viability. Coronal slices of 500-600 μm thickness containing the LC were cut using a vibratome (Leica VT1200 S, Leica Biosystems, Nussloch, Germany). The tissue was allowed to recover from the slicing for 90 min, placed on a nylon mesh, and incubated at 33 ± 1ºC on a modified Haas-type interface chamber which provided excellent perfusion to the slice. The tissue was continuously perfused with aCSF saturated with 95% O_2/ 5% CO_2 (final pH = 7.34) at a flow rate of 1.5 ml min^{-1} and left for equilibration before recordings were made. The aCSF contained (in mM): NaCl 130, KCl 3, NaH_2PO_4 1.25, D-glucose 10, $NaHCO_3$ 21, $CaCl_2$ 2 and $MgSO_4$ 2. The LC was recognized visually in the rostral pons as a dark oval area on the lateral borders of the central gray and the fourth ventricle, at or just anterior to the *genu* of the facial nerve.

Electrophysiological recordings

Single-unit extracellular recordings of LC noradrenergic cells were made as previously described (Mendiguren and Pineda, 2004; 2007). The recording electrode consisted of an Omegadot glass micropipette pulled (Sutter Instruments, Novato, CA, USA) and filled with 50 mM NaCl. The tip of the electrode was broken back to a size of 2 – 5 μm (3 – 5 MΩ) and positioned in the LC. The extracellular signal from the electrode was passed through a high-input impedance amplifier (Axoclamp 2B, Molecular devices, Union City, CA, USA) and monitored with an audio-amplifier and also on an oscilloscope (Aumon 14, Cibertec S.A., Madrid, Spain). Individual neuronal spikes were isolated from the background noise with a window discriminator (PDV 225, Cibertec S.A.). The firing rate (FR) was continuously recorded and analyzed before, during, and after experimental manipulations by a PC-based custom-made program which generated consecutive 10 s bin histogram bars of the cumulative number of spikes (HFCP®, Cibertec S.A., Madrid, Spain). Noradrenergic cells in the LC were identified by their spontaneous and regular discharge activities, the slow FR and the long-lasting biphasic positive-negative waveforms (Andrade and Aghajanian, 1984). We only recorded cells that showed stable FRs between 0.5 and 1.5 Hz for at least 3-5 min and inhibitory responses to [Met]enkephalin (ME 0.8 μM, 1 min) higher than 80% (Pablos et al., 2015), which was used as control for the perfusion system.

Pharmacological procedures

The firing rate of LC neurons was recorded for several minutes before drug applications to obtain the baseline activity and then, during and after drug perfusion. To study the effect of EP3 receptor agonists on the firing rate of LC neurons, we perfused increasing concentrations of the EP3 receptor agonist sulprostone (0.15 nM – 1.28 μM, 2x), PGE_2 (0.31 nM – 10.2 μM, 2x) or the PGE_1 analogue misoprostol (0.31 nM – 2.56 μM, 2x). Concentrations were based on previous studies in brain slices (Exner and Schlicker, 1995; Mulvey et al., 2018). Each concentration of the EP receptor agonists was perfused for enough time to reach its plateau effect and each agonist was used up to concentrations that achieved the maximal effect of the drug. To identify the subtype of EP receptor involved in the effect of sulprostone, PGE_2, and misoprostol, concentration-effect curves for these agonists were performed in the presence of different EP receptor subtype selective antagonists. First, for sulprostone, the EP2 receptor antagonist PF-04418948 (3 and 10 μM), the EP3 receptor antagonist L-798,106 (3 and 10 μM), and the EP4 receptor antagonist L-161,982 (3 and 10 μM) were used at the concentrations previously reported (Jones et al., 2011). Next, for PGE_2 and misoprostol, the

EP3 receptor antagonist L-798,106 at 10 μM and a combination of the aforementioned EP2 and EP4 receptor antagonists at 10 μM were used. All the antagonists were perfused for 30 min before performing the concentration-effect curves for the EP receptor agonists.

Based on its pharmacological profile sulprostone was selected to further characterize the molecular mechanism underlying EP3 receptor activation. In order to study the involvement of $G_{i/o}$ proteins, concentration-effect curves for sulprostone were made after overnight incubation of the slices with the irreversible $G_{i/o}$ protein inhibitor pertussis toxin (PTX, 500 ng ml^{-1}, 18 h) in an oxygenated glass beaker at room temperature (modified from Chessell et al., 1996). In order to verify that PTX had effectively blocked the $G_{i/o}$ protein, the effect of the $G_{i/o}$-coupled MOR agonist ME was tested. Thus, only cells with a reduced inhibitory effect of ME (inhibiton <80% of basal FR) were considered to perform the concentration-effect curve for sulprostone. In those cells, proper drug perfusion was assessed with GABA (1 mM, 1 min). To confirm the involvement of inwardly rectifying potassium channels (GIRK), concentration-effect curves for sulprostone were performed in the presence of the GIRK blocker $BaCl_2$ (300 μM, 15 min) or the selective GIRK2 gating inhibitor SCH-23390 (15 μM, 30 min) at the concentrations previously used (Pineda and Aghajanian, 1997; Chee et al., 2011).

Analysis and statistics of electrophysiological data

The data and statistical analysis were carried out with the computer programs GraphPad Prism (version 5.0 for Windows, GraphPad Software, Inc., San Diego, CA, USA) and SPSS (version 22.0 for Windows, SPSS Inc, Chicago, IL, USA) and comply with the recommendations on experimental design and analysis in pharmacology (Curtis et al., 2018). The inhibitory effect of GABA (1 mM, 1 min) and ME (0.8 μM, 1 min) was normalized to the initial FR in each cell as follows: $E\ (\%) = (FR_{basal} - FR_{post}) \cdot 100/FR_{initial}$, where $FR_{initial}$ is the average basal FR of each neuron calculated for 60 s at the beginning of the recording and FR_{basal} is the average FR of each pre-agonist condition calculated for 60 s immediately before drug application. FR_{post} is the average FR after the drug application calculated for 60-90 s. Whereas in the case of the EP3 receptor agonists, the effect of each concentration of the drug was normalized to the FR_{basal}. The intervals were chosen to integrate the whole period of maximal effect of each drug administration (Medrano et al., 2017). Normalization to $FR_{initial}$ or FR_{basal} was made to obtain comparable measures across groups.

To construct concentration-effect curves for the EP3 receptor agonists, fitting analysis was performed to obtain the best simple nonlinear fit to the following three-parameter logistic

equation: $E = E_{max}[A]^n / (EC_{50}^n + [A]^n)$, where E and [A] are the observed effect and the concentration of the agonist, respectively; E_{max} is the maximal effect of the EP3 receptor agonist with the E_{max} being constrained to 100% in all those neurons in which the observed effect reached a full cessation of the FR. EC_{50} is the concentration of the agonist required to promote the 50% of E_{max}, and *n* represents the slope factor of the function. These parameters were determined in individual assays by the nonlinear analysis and then averaged to obtain the theoretical parameters in each group. For comparison purposes, the EC_{50} values were converted and expressed as negative logarithm (pEC_{50}) which adjusted the variable into a Gaussian distribution (Pineda et al., 1997).

The antagonist affinity value was calculated as the negative logarithm of the equilibrium dissociation constant of the antagonist-receptor complex (pK_B). The pK_B value was estimated using the Gaddum/Schild equation modified for global fitting of the curves using GraphPad Prism 5.0 (Lazareno and Birdsall, 1993; Säfholm et al., 2013), where the minimum and maximum effects were constrained to 0 and 100%, respectively, and the Schild slope was constrained to 1.0 in accordance with previous reports (Lazareno and Birdsall, 1993; Säfholm et al., 2013).

Data are expressed as the mean ± SEM of *n* number of slices. Statistical analyses were performed by a two-tailed paired Student's *t*-test when the response values were compared before and after drug applications within the same cell, and by a two-tailed two-sample Student's *t*-test when the FRs, responses or parameters were two independent experimental conditions. Statistical comparison of the results among more than two experimental conditions (including a control group) were done by one-way analysis of variance (ANOVA) followed by a *post hoc* pairwise comparisons with a Dunnett's test or a Bonferroni's Multiple Comparison test and only if *F* achieved the necessary level of statistical significance (i.e. $P < 0.05$) and there was no significant variance inhomogeneity. Dunnett's procedure was used for comparisons with a control group and Bonferroni's test, for comparisons among all the groups. The threshold of significance was set at $P = 0.05$ and only one level of probability ($P < 0.05$) is reported.

Materials and drugs

For electrophysiological recordings, the following drugs were used (drug source): $BaCl_2$ (Sigma-Aldrich Química S.A., Madrid, Spain), γ-aminobutyric acid (GABA, Sigma-Aldrich), L-161,982 (Tocris Bioscience, Bristol, UK), L-798,106 (Tocris Bioscience), ME acetate salt (Bachem, Weil am Rhein, Germany), misoprostol free acid (Cayman Chemical,

Ann Arbor, MI, USA), pertussis toxin (Tocris Bioscience), PF-04418948 (Tocris Bioscience), prostaglandin E_2 (PGE_2) (Tocris Bioscience), SCH-23390 (Tocris Bioscience), and sulprostone (Cayman Chemical). Stock solutions of L-161,982, L-798,106, PF-04418948, and PGE_2 were first prepared in pure DMSO and then diluted in aCSF to obtain a final concentration of DMSO lower than 0.1%, which does not affect the firing activity of LC neurons *in vitro* (Pineda et al., 1996). Misoprostol and sulprostone were purchased already dissolved in methyl acetate and the final concentrations were obtained by diluting it in the aCSF at the moment of the experiment. Control assays were performed with equivalent volumes of the vehicles in which the drugs were dissolved. The final concentration of methyl acetate in the aCSF was < 0.01%. Stock solutions of the rest of the drugs were first prepared in Milli-Q water and then diluted 1000- to 10000-fold in aCSF for the desired concentration. Final solutions were freshly prepared just before each experiment and stock solutions were kept at -20 ºC.

Nomenclature of targets and ligands

Key protein targets and ligands in this article are hyperlinked to corresponding entries in http://www.guidetopharmacology.org, the common portal for data from the IUPHAR/BPS Guide to PHARMACOLOGY (Harding et al., 2018), and are permanently archived in the Concise Guide to PHARMACOLOGY 2017/18 (Alexander et al., 2017).

Results

Effect of the EP3 receptor agonist sulprostone on the firing rate of LC neurons

EP3 receptors are expressed in catecholaminergic neurons of the brain, including the LC (Nakamura et al., 2001). To investigate the effect of EP3 receptor activation on the firing rate of LC neurons, we performed concentration-effect curves for sulprostone, an EP3 receptor agonist that shows more than 300-fold higher affinity for the EP3 receptor than for the EP1 receptor (Abramovitz et al., 2000). Increasing concentrations of sulprostone (1.25 – 320 nM, 2x, 1 min each) inhibited the neuronal activity of LC cells in a concentration-dependent manner with an EC_{50} value in the nanomolar range (Figures 1A and C; Table 1). Complete inhibition of the firing rate of noradrenergic cells was achieved at the highest concentration of sulprostone used (20 – 320 nM) and persisted for 265 ± 53 s on average (n = 9).

In order to study the EP receptor involved in the sulprostone-induced inhibitory effect, concentration-effect curves for sulprostone (0.15 nM – 1.28 μM) were performed in the presence of the EP3 receptor antagonist (L-798,106), the EP2 receptor antagonist (PF-04418948) or the EP4 receptor antagonist (L-161,982) at 3 and 10 μM. Perfusion with L-798,106 (3 μM) for 30 min did not significantly change the firing rate of LC neurons, but reduced the steepness of the concentration-effect curve for sulprostone (Figure 1C; Table 1). Moreover, a higher concentration of L-798,106 (10 μM, 10 min) reduced by 17.7 ± 3.8 % within the same cell the firing rate of LC neurons (n = 6, P < 0.05 compared to baseline) (data not shown) and shifted by 8 fold to the right the concentration-effect curve for sulprostone (Figures 1B and C; Table 1). The apparent affinity of L-798,106 for the EP3 receptor (pK_B) was calculated to be 5.77 ± 0.10 (n = 12). On the other hand, the EP2 receptor antagonist PF-04418948 (3 μM) failed to cause significant changes in the firing rate or any rightward shift in the concentration-effect curve for sulprostone (Figure 2B; Table 1). Indeed, unexpectedly, the highest concentration of PF-04418938 (10 μM) caused a 4-fold leftward shift in the concentration-effect curve for sulprostone (Figures 2A and B; Table 1). Similar to the EP2 receptor antagonist, perfusion with the EP4 receptor antagonist L-161,982 (3 and 10 μM) failed to change the firing rate or to shift to the right the concentration-effect curve for sulprostone (Figures 2C and D; Table 1).

Altogether, these results suggest that the inhibitory effect of sulprostone on the firing rate of LC neurons is mainly mediated by the EP3 receptor.

Effect of PGE_2 and the PGE_1 analog misoprostol on the firing rate of LC neurons

To study whether the endogenous PGE_2 and the PGE_1 synthetic analog misoprostol mimic the inhibitory effect observed with sulprostone on the firing rate of LC cells, we performed concentration-effect curves for PGE_2 and misoprostol. PGE_2 (0.31 nM – 1.28 μM, 2x, 1 min each) concentration-dependently inhibited the firing rate of LC neurons with an EC_{50} value in the nanomolar range (Figures 3A and C; Table 2). Likewise, misoprostol (0.31 – 320 nM, 2x, 1 min each) inhibited the neuronal activity of LC cells with similar potency (Figures 4A and C; Table 2).

Perfusion with the EP3 receptor antagonist L-798,106 (10 μM) shifted by 19 and 9 fold, respectively, to the right the concentration-effect curves for PGE_2 (0.31 nM – 10.2 μM) and misoprostol (0.31 nM – 2.56 μM) (Figures 3B and C, 4B and C; Table 2). When PGE_2 was used as the standard agonist, the pK_B value for L-798,106 was higher ($pK_B = 6.26 \pm 0.05$; $n = 5$, $P < 0.05$, one-way ANOVA followed by Bonferroni's Multiple Comparison test) than that with sulprostone (see above). However, the pK_B value estimated for L-798,106 with misoprostol ($pK_B = 5.91 \pm 0.14$; $n = 5$, $P > 0.05$) was not different from that obtained with sulprostone. On the other hand, administration of a combination of the EP2 receptor antagonist PF-04418948 (10 μM) and the EP4 receptor antagonist L-161,982 (10 μM) caused a more than 6-fold leftward shift in the concentration-effect curve for PGE_2 (Figure 3C; Table 2). However, both antagonists in combination did not cause any shift in the concentration-effect curve for misoprostol (Figures 4C; Table 2). Finally, none of these antagonists changed the slope of the concentration-effect curves.

As a whole, these results suggest that the endogenous ligand PGE_2 and the PGE_1 analog misoprostol inhibit the activity of LC neurons, preferentially through the EP3 receptor. In addition, administration of the EP2 and EP4 receptor antagonists apparently potentiate the inhibitory effect of PGE_2.

Molecular mechanisms involved in the effect of EP3 receptor agonists on the firing rate of LC neurons

The EP3 receptor has been shown to be coupled to $G_{i/o}$ proteins (Ikeda-Matsuo et al., 2010) and GIRK channels (Ruiz-Velasco and Ikeda, 1998). Thus, to identify the molecular mechanisms involved in the EP3 receptor-mediated inhibition of firing activity of LC cells, we performed concentration-effect curves for sulprostone (0.31 nM – 1.28 μM, 2x) in slices incubated for 18 h with the irreversible $G_{i/o}$ protein blocker PTX, 500 ng ml^{-1}. In order to confirm that PTX had effectively blocked the $G_{i/o}$ protein, only cells with a reduced inhibitory response (inhibition <80% of basal firing rate) to the $G_{i/o}$-coupled MOR agonist ME (0.8 μM, 1 min) were selected to perform the concentration-effect curves for sulprostone (Figure 5A). Moreover, proper drug perfusion was tested with GABA (1 mM, 1 min) (Figure 5A), which has been shown to fully inhibit the firing rate through $GABA_A$ ionotropic receptors (Mendiguren and Pineda, 2007). Thus, overnight treatment of the slices with PTX shifted by 6 fold to the right the concentration-effect curve for sulprostone, without affecting significantly the maximal response or the basal firing rate (Figures 5A, D; Table 3).

To study the involvement of GIRK channels, we performed concentration-effect curves for sulprostone (0.31 nM – 2.56 μM, 2x) in the presence of the non-selective GIRK channel blocker $BaCl_2$ or the selective GIRK2 gating inhibitor SCH-23390. Since ME-induced inhibitory effect depends on the opening of GIRK channels, ME (0.8 μM, 1 min) was previously applied in the presence of the GIRK channel blockers to confirm the blockade action. Thus, GIRK channel blockade with Ba^{2+} (300 μM, 15 min) and SCH-23390 (15 μM, 30 min) reduced the inhibitory effect of ME by 29.6 ± 6.3% (n = 5, P < 0.05; Figure 5B) and 25.2 ± 8.6% (n = 5, P < 0.05; Figure 5C), respectively, as previously described (Torrecilla et al., 2002). Bath perfusion with $BaCl_2$ (300 μM, 15 min) increased the firing rate of LC neurons by 42.6 ± 13.1% (n = 5, P < 0.05 compared to baseline) and shifted by 3 fold to the right the concentration-effect curve for sulprostone (Figures 5B and D; Table 3). Likewise, bath administration of SCH-23390 (15 μM, 30 min) increased the firing activity of LC neurons by 144 ± 57% (n = 5, P < 0.05 compared to baseline) and shifted by 2 fold to the right the concentration-effect curve for sulprostone (Figures 5C and D; Table 3). $BaCl_2$ and SCH-23390 slightly reduced the maximal effect of sulprostone, but these changes did not reach statistical significances (Table 3).

These results suggest that EP3 receptor activation inhibits the LC neuronal activity through activation of $G_{i/o}$ proteins and GIRK channels.

Discussion

The present work was undertaken to characterize the functional role of EP3 receptors in LC neurons in rat brain slices. Our results show that the EP3 receptor agonists sulprostone, PGE_2, and misoprostol inhibits in a concentration-dependent manner the neuronal activity of LC cells *in vitro*. This inhibitory effect was blocked by the selective EP3 receptor antagonist L-798,106, but not by the EP2 or EP4 receptor antagonists, indicating that the observed effect was mediated by EP3 receptor activation. Furthermore, sulprostone-induced inhibition of the firing rate was hindered by pretreatment with the $G_{i/o}$ protein inhibitor PTX and the GIRK blockers $BaCl_2$ and SCH-23390. Thus, our results suggest that EP3 receptor activation inhibits the firing activity of LC neurons, presumably by its coupling to $G_{i/o}$ proteins and the subsequent opening of GIRK channels.

Dense EP3 receptor immunoreactivity has been found by double immunofluorescence in the neuropil and in a few cell bodies of the LC (Nakamura et al., 2001), where there is also strong expression of EP3 receptor mRNA (Ek et al., 2000). Furthermore, the LC contains constitutive COX-2, the rate-limiting enzyme for prostanoid synthesis (Yamaguchi and Okada, 2009), suggesting the presence of endogenous prostaglandins in this nucleus. In our study, we assessed the functional role of EP3 receptors by using extracellular recordings *in vitro* and application of EP3 receptor agonists. Sulprostone was selected as an EP3 receptor agonist based on its more than 300-fold higher affinity for the EP3 than for the EP1 receptor (Abramovitz et al., 2000). Sulprostone was perfused at similar concentrations previously used to study EP3 receptor-mediated effects in rodent brain slices from the cortex (Exner and Schlicker, 1995) and the LC (Mulvey et al., 2018). We also assessed the biological relevance of the endogenous prostanoid system by perfusing PGE_2, which has high affinity for all the EP receptors but especially for the EP3 receptor (EP3≥EP4>EP2>EP1) (Abramovitz et al., 2000). Moreover, we tested the PGE_1 analog, commercially available misoprostol, which has higher selectivity for the EP3 receptor (affinity: EP3>EP4>EP2) (Abramovitz et al., 2000). On the other hand, we used as EP3 receptor antagonist L-798,106, which is highly selective for the EP3 receptor compared to the EP4 receptor (Su et al., 2008). Finally, the EP2 receptor antagonist PF-04418948 has no affinity for the EP3 receptor at the concentrations herein used

(Forselles et al., 2011), while L-161,982 shows much higher affinity for the EP4 than for the EP3 receptor (Machwate et al., 2001)

In the present study, sulprostone, PGE_2, and misoprostol completely inhibited the firing activity of LC neurons. This inhibitory effect was blocked by an EP3 receptor antagonist but not by EP2 or EP4 receptor antagonists, ruling out the involvement of EP2 or EP4 receptors in this inhibition. EP1 receptor-mediated effects may be unlikely in our system because low EP1 receptor mRNA expression has been reported in the brainstem (Candelario-Jalil et al., 2005). In our study, the determined EC_{50} values of the concentration-effect curves for sulprostone, misoprostol, and PGE_2 and the rank order of potency found for firing activity inhibition (sulprostone > misoprostol > PGE_2) were consistent with preceding data in rodent brain cortex slices, where the same agonists inhibited the NA release with 0.4-1.0 fold higher pIC_{50} values (8.22, 8.00, and 7.74, respectively; Exner and Schlicker, 1995). Furthermore, in guinea-pig aorta, comparable EC_{50} values were found for the sulprostone-induced vasoconstriction (23 nM) (Jones et al., 1998). The pK_B value for the EP3 receptor antagonist L-798,106 herein reported was equivalent when either sulprostone or misoprostol were used as standard agonist (5.8 – 5.9), which supports the evidence for the activation of a common EP3 receptor. However, when PGE_2 was used as an agonist, the estimated pK_B value was 0.4 units higher, suggesting that PGE_2 may also activate interfering non-EP3 receptors. In this regard, in the presence of PF-04418948 and L-161,982, the concentration-effect curve for PGE_2 was shifted to the left, which could suggest that PGE_2 may also activate G_s protein-coupled EP2 and EP4 receptors counteracting the EP3 receptor-mediated inhibition. Other authors have estimated a 2 units higher pK_B value for L-798,106 when sulprostone and PGE_2 were used as standard agonists in peripheral tissues, such as guinea-pig smooth muscle (Jones et al., 2011). This disparity could be due to the high lipophilicity of L-798,106, which determines the equilibration kinetics and the pK_B calculation (Jones et al., 2011), or to the different tissues (muscle *vs.* brain slices) and species employed (guinea-pig *vs.* rat). In summary, EP3 receptor activation by selective agonists inhibits the firing rate of LC neurons.

In line with our results, c-fos expression, an indicator of neuronal activity, is increased in the LC from morphine-dependent rats and this enhancement is reversed by EP3 receptor agonists administered centrally (Nakagawa et al., 2000), suggesting that the neuronal activity of LC cells is inhibited by EP3 receptor activation. Furthermore, a single concentration of sulprostone has recently been shown to hyperpolarize LC neurons in slices from mice

(Mulvey et al., 2018). Likewise, other electrophysiological studies have demonstrated an EP3 receptor-mediated inhibition of central neurotransmission in other brain regions. Thus, EP3 receptor activation by PGE_2 reduces glutamatergic transmission in the dorsolateral periaqueductal gray (PAG) (Lu et al., 2007), GABAergic transmission in the paraventricular nucleus of the hypothalamus (Khazaeipool et al., 2018), and network activity in the neocortex (Koch et al., 2010). In contrast to our results, a neuronal activity increase has been described upon PGE_2 administration in serotonergic neurons of the dorsal raphe nucleus, but the exact mechanism has not been fully elucidated (Momiyama et al., 1996).

EP3 receptor activation has been described to be coupled to $G_{i/o}$ proteins (Ikeda-Matsuo et al., 2010). In our research, the sulprostone-induced inhibitory effect was reduced by the $G_{i/o}$ signaling inhibitor PTX (Mangmool and Kurose, 2011), indicating that EP3 receptor activation leads to cell inhibition by stimulation of $G_{i/o}$ proteins. $G_{i/o}$-mediated effects have been previously described for the EP3 receptor in other brain regions, such as the hippocampus, where PTX blocks the EP3 receptor-induced ischemic excitotoxicity (Ikeda-Matsuo et al., 2010). Inhibition of firing activity of LC neurons has been described to occur after opening of GIRK channels by $G_{i/o}$-protein βγ subunits (Albsoul-Younes et al., 2001), such as upon activation of $G_{i/o}$ protein-coupled μ-opioid receptors or α_2 adrenoceptors (Torrecilla et al., 2002; 2013). Barium and SCH-23390 are effective GIRK channel blockers (Kuzhikandathil and Oxford, 2002) that have been reported to increase the firing rate of LC cells (Li and Putnam, 2013). Indeed, in our study, administration of barium and SCH-23390 increased the firing rate of LC neurons and prevented the effect of sulprostone, supporting an involvement of GIRK channels in the EP3 receptor-mediated effect in the LC. Similarly, in sympathetic neurons, PGE_2 activates GIRK channels probably through a $G_{i/o}$-dependent mechanism (Ruiz-Velasco and Ikeda, 1998).

Our results show that EP3 receptor activation inhibits the activity of LC neurons in rat brain slices, likely through opening of postsynaptic $G_{i/o}$ protein-coupled GIRK channels. This inhibitory effect on the LC may regulate NA release throughout projection areas of the CNS and thus add to the local inhibitory EP3 receptors on nerve terminals regulating NA release (Exner and Schlicker, 1995; Günther et al., 2010). The prostanoid system in the LC could play a role in the regulation of pain. Thus, the LC exerts a supraspinal descending control of pain (Hickey et al., 2014) and activation of a neuronal subpopulation of the LC evokes an anti-

nociceptive response (Hickey et al., 2014). One possible consequence would be that EP3 receptor activation in the LC may lead to a hyperalgesic effect. In line with this hypothesis, inflammatory stimuli reduce the analgesic effect induced by opioids in the LC (Jongeling et al., 2009). Likewise, in the PAG, EP3 receptor activation exerts pro-nociceptive actions (Drake et al., 2016). Prostaglandin release and EP3 receptor activation in the LC may also modulate the neuroinflammatory and febrile response. In this regard, c-Fos expression is increased in the LC by inflammatory insults through prostanoid synthesis (Xu et al., 2003) and the febrigenic effect of PGE_2, which involves EP3 receptors (Ushikubi et al., 1998), is mediated by a neuronal network including the LC (Almeida et al., 2004). Finally, EP3 receptors in the LC may be relevant for some neuropsychiatric diseases. Thus, an enhanced expression of the EP3 receptor has been found around amyloid plaques in LC-projecting areas in Alzheimer's disease (Shi et al., 2012). Furthermore, lesions of the LC enhance both pro-inflammatory cytokines (Bharani et al., 2017) and amyloid-β deposition in the hippocampus of a mouse model of Alzheimer's disease (Heneka et al., 2010). Regarding psychiatry, stimulation of prefrontal-projecting neurons in the LC results in anxiety-like behavior (Hirschberg et al., 2017), thereby reduction of LC-noradrenergic cell activity by the EP3 receptor could attenuate anxiety, as shown by a previous study in which sulprostone infusion into the LC produced anxiolytic effects (Mulvey et al., 2018). In conclusion, the prostaglandin system in the LC would play a relevant role in the regulation of central physiology and the EP3 receptor in this nucleus might be a suitable pharmacological target for the development of novel treatments for different neuropsychiatric disorders.

Author contributions

A. N. performed the electrophysiological assays and wrote the first draft of the manuscript. A. M. and J.P. conceived and designed the study and wrote the manuscript.

References

Abramovitz, M., Adam, M., Boie, Y., Carrière, M.C., Denis, D., Godbout, C., et al. (2000). The utilization of recombinant prostanoid receptors to determine the affinities and selectivities of prostaglandins and related analogs. Biochim. Biophys. Acta - Mol. Cell Biol. Lipids *1483*: 285–293.

Albsoul-Younes, A.M., Sternweis, P.M., Zhao, P., Nakata, H., Nakajima, Y., and Kozasa, T.

(2001). Interaction Sites of the G Protein beta Subunit with Brain G Protein- coupled Inward Rectifier K+ Channel. J. Biol. Chem. *276*: 12712–12717.

Alexander, S.P.H., Christopoulos, A., Davenport, A.P., Kelly, E., Marrion, N. V., Peters, J.A., et al. (2017). THE CONCISE GUIDE TO PHARMACOLOGY 2017/18: G protein-coupled receptors. Br. J. Pharmacol. *174*: S17–S129.

Almeida, M.C., Steiner, A. a, Coimbra, N.C., and Branco, L.G.S. (2004). Thermoeffector neuronal pathways in fever: a study in rats showing a new role of the locus coeruleus. J. Physiol. *558*: 283–94.

Andrade, R., and Aghajanian, G.K. (1984). Locus coeruleus activity in vitro: intrinsic regulation by a calcium-dependent potassium conductance but not alpha 2-adrenoceptors. J. Neurosci. *4*: 161–170.

Bharani, K.L., Derex, R., Granholm, A.C., and Ledreux, A. (2017). A noradrenergic lesion aggravates the effects of systemic inflammation on the hippocampus of aged rats. PLoS One *12*: 1–20.

Candelario-Jalil, E., Slawik, H., Ridelis, I., Waschbisch, A., Akundi, R.S., Hüll, M., et al. (2005). Regional distribution of the prostaglandin E2 receptor EP1 in the rat brain. J. Mol. Neurosci. *27*: 303–310.

Chee, M.J., Price, C.J., Statnick, M. a, and Colmers, W.F. (2011). Nociceptin/orphanin FQ suppresses the excitability of neurons in the ventromedial nucleus of the hypothalamus. J. Physiol. *589*: 3103–3114.

Chessell, I.P., Black, M.D., Feniuk, W., and Humphrey, P.P.A. (1996). Operational characteristics of somatostatin receptors mediating inhibitory actions on rat locus coeruleus neurones. Br. J. Pharmacol. *117*: 1673–1678.

Curtis, M.J., Alexander, S., Cirino, G., Docherty, J.R., George, C.H., Giembycz, M.A., et al. (2018). Experimental design and analysis and their reporting II: updated and simplified guidance for authors and peer reviewers. Br. J. Pharmacol. *175*: 987–993.

Drake, R.A.R., Leith, J.L., Almahasneh, F., Martindale, J., Wilson, A.W., Lumb, B., et al. (2016). Periaqueductal Grey EP3 Receptors Facilitate Spinal Nociception in Arthritic Secondary Hypersensitivity. J. Neurosci. *36*: 9026–40.

Ek, M., Arias, C., Sawchenko, P., and Ericsson-Dahlstrand, A. (2000). Distribution of the EP3 prostaglandin E2 receptor subtype in the rat brain: Relationship to sites of interleukin-1 - Induced cellular responsiveness. J. Comp. Neurol. *428*: 5–20.

Exner, H.J., and Schlicker, E. (1995). Prostanoid receptors of the EP3 subtype mediate the inhibitory effect of prostaglandin E2 on noradrenaline release in the mouse brain cortex. Naunyn. Schmiedebergs. Arch. Pharmacol. *351*: 46–52.

Forsberg, D., Horn, Z., Tserga, E., Smedler, E., Silberberg, G., Shvarev, Y., et al. (2016). CO2-evoked release of PGE2 modulates sighs and inspiration as demonstrated in brainstem organotypic culture. Elife *5*: 1–41.

Forselles, K.J., Root, J., Clarke, T., Davey, D., Aughton, K., Dack, K., et al. (2011). In vitro and in vivo characterization of PF-04418948, a novel, potent and selective prostaglandin EP2 receptor antagonist. Br. J. Pharmacol. *164*: 1847–56.

Günther, J., Schulte, K., Wenzel, D., Malinowska, B., and Schlicker, E. (2010). Prostaglandins of the e series inhibit monoamine release via EP3 receptors: Proof with the competitive EP3 receptor antagonist L-826,266. Naunyn. Schmiedebergs. Arch. Pharmacol. *381*: 21–31.

Harding, S., Sharman, J., Faccenda, E., Southan, C., Pawson, A., Ireland, S., et al. (2018). The IUPHAR/BPS Guide to PHARMACOLOGY in 2018: updates and expansion to encompass the new guide to IMMUNOPHARMACOLOGY. Nucleic Acids Res. *46*: D1091–D1106.

Heneka, M.T., Nadrigny, F., Regen, T., Martinez-Hernandez, A., Dumitrescu-Ozimek, L., Terwel, D., et al. (2010). Locus ceruleus controls Alzheimer's disease pathology by modulating microglial functions through norepinephrine. Proc. Natl. Acad. Sci. *107*: 6058–6063.

Hétu, P.-O., and Riendeau, D. (2005). Cyclo-oxygenase-2 contributes to constitutive prostanoid production in rat kidney and brain. Biochem. J. *391*: 561–566.

Hickey, L., Li, Y., Fyson, S.J., Watson, T.C., Perrins, R., Hewinson, J., et al. (2014). Optoactivation of Locus Ceruleus Neurons Evokes Bidirectional Changes in Thermal Nociception in Rats. J. Neurosci. *34*: 4148–4160.

Hirschberg, S., Li, Y., Randall, A., Kremer, E.J., and Pickering, A.E. (2017). Functional dichotomy in spinal-vs prefrontal-projecting locus coeruleus modules splits descending noradrenergic analgesia from ascending aversion and anxiety in rats. Elife *6*: 1–26.

Ikeda-Matsuo, Y., Tanji, H., Ota, a., Hirayama, Y., Uematsu, S., Akira, S., et al. (2010). Microsomal prostaglandin e synthase-1 contributes to ischaemic excitotoxicity through prostaglandin E 2 EP 3 receptors. Br. J. Pharmacol. *160*: 847–859.

Jones, R.L., Qian, Y.M., Chan, K.M., and Yim, a P. (1998). Characterization of a prostanoid EP3-receptor in guinea-pig aorta: partial agonist action of the non-prostanoid ONO-AP-324. Br. J. Pharmacol. *125*: 1288–1296.

Jones, R.L., Woodward, D.F., Wang, J.W., and Clark, R.L. (2011). Roles of affinity and lipophilicity in the slow kinetics of prostanoid receptor antagonists on isolated smooth muscle preparations. Br. J. Pharmacol. *162*: 863–879.

Jongeling, A.C., Jouns, E.M., Murphy, A.Z., and Hammond, D.L. (2009). Persistent inflammatory pain decreases the antinociceptive effects of the mu opioid receptor agonist DAMGO in the locus coeruleus of male rats. Neuropharmacology *56*: 1017–1026.

Kaufmann, W.E., Worley, P.F., Pegg, J., Bremer, M., and Isakson, P. (1996). COX-2, a synaptically induced enzyme, is expressed by excitatory neurons at postsynaptic sites in rat cerebral cortex. Proc. Natl. Acad. Sci. U. S. A. *93*: 2317–2321.

Khazaeipool, Z., Wiederman, M., and Inoue, W. (2018). Prostaglandin E2 depresses GABA release onto parvocellular neuroendocrine neurones in the paraventricular nucleus of the hypothalamus via presynaptic receptors. J. Neuroendocrinol. *30*: 1–10.

Kilkenny, C., Browne, W., Cuthill, I.C., Emerson, M., and Altman, D.G. (2010). Animal research: Reporting in vivo experiments: The ARRIVE guidelines. Br. J. Pharmacol. *160*: 1577–1579.

Kirkby, N.S., Chan, M. V., Zaiss, A.K., Garcia-Vaz, E., Jiao, J., Berglund, L.M., et al. (2016). Systematic study of constitutive cyclooxygenase-2 expression: Role of NF-κB and NFAT transcriptional pathways. Proc. Natl. Acad. Sci. *113*: 434–439.

Koch, H., Huh, S.-E., Elsen, F.P., Carroll, M.S., Hodge, R.D., Bedogni, F., et al. (2010). Prostaglandin E2-Induced Synaptic Plasticity in Neocortical Networks of Organotypic Slice Cultures. J. Neurosci. *30*: 11678–11687.

Kuzhikandathil, E. V, and Oxford, G.S. (2002). Classic D1 Dopamine Receptor AntagonistR-(+)-7-Chloro-8-hydroxy-3-methyl-1-phenyl-2,3,4,5-tetrahydro-1H-3-benzazepine

hydrochloride (SCH23390) Directly Inhibits G Protein-Coupled Inwardly Rectifying Potassium Channels. Mol. Pharmacol. *62*: 119–126.

Lazareno, S., and Birdsall, N.J.M. (1993). Estimation of competitive antagonist affinity from functional inhibition curves using the Gaddum Schild and Cheng-Prusoff equations. Br. J. Pharmacol. *109*: 1110–1119.

Li, K.-Y., and Putnam, R.W. (2013). Transient outwardly rectifying A currents are involved in the firing rate response to altered CO2 in chemosensitive locus coeruleus neurons from neonatal rats. Am J Physiol Regul Integr Comp Physiol *305*: R780–R792.

Lu, J., Xing, J., and Li, J. (2007). Prostaglandin E2 (PGE2) inhibits glutamatergic synaptic transmission in dorsolateral periaqueductal gray (dl-PAG). Brain Res. *1162*: 38–47.

Machwate, M., Harada, S., Leu, C.T., Seedor, G., Labelle, M., Gallant, M., et al. (2001). Prostaglandin receptor EP(4) mediates the bone anabolic effects of PGE(2). Mol. Pharmacol. *60*: 36–41.

Maingret, V., Barthet, G., Deforges, S., Jiang, N., Mulle, C., and Amédée, T. (2017). PGE2-EP3 signaling pathway impairs hippocampal presynaptic long-term plasticity in a mouse model of Alzheimer's disease. Neurobiol. Aging *50*: 13–24.

Mangmool, S., and Kurose, H. (2011). Gi/o protein-dependent and -independent actions of pertussis toxin (ptx). Toxins (Basel). *3*: 884–899.

McGrath, J.C., and Lilley, E. (2015). Implementing guidelines on reporting research using animals (ARRIVE etc.): New requirements for publication in BJP. Br. J. Pharmacol. *172*: 3189–3193.

Medrano, M.C., Santamarta, M.T., Pablos, P., Aira, Z., Buesa, I., Azkue, J.J., et al. (2017). Characterization of functional μ opioid receptor turnover in rat locus coeruleus: an electrophysiological and immunocytochemical study. Br. J. Pharmacol. *174*: 2758–2772.

Mendiguren, A., and Pineda, J. (2004). Cannabinoids enhance N-methyl-D-aspartate-induced excitation of locus coeruleus neurons by CB1 receptors in rat brain slices. Neurosci. Lett. *363*: 1–5.

Mendiguren, A., and Pineda, J. (2007). CB1 cannabinoid receptors inhibit the glutamatergic component of KCl-evoked excitation of locus coeruleus neurons in rat brain slices.

Neuropharmacology *52*: 617–625.

Momiyama, T., Todo, N., Sugimoto, Y., Ichikawa, A., and Narumiya, S. (1996). Membrane depolarization by activation of prostaglandin E receptor EP 3 subtype of putative serotonergic neurons in the dorsal raphe nucleus of the rat. Naunyn. Schmiedebergs. Arch. Pharmacol. *353*: 377–381.

Mulvey, B., Bhatti, D.L., Gyawali, S., Lake, A.M., Kriaucionis, S., Ford, C.P., et al. (2018). Molecular and Functional Sex Differences of Noradrenergic Neurons in the Mouse Locus Coeruleus. Cell Rep. *23*: 2225–2235.

Nakagawa, T., Masuda, T., Watanabe, T., Minami, M., and Satoh, M. (2000). Possible involvement of the locus coeruleus in inhibition by prostanoid EP(3) receptor-selective agonists of morphine withdrawal syndrome in rats. Eur. J. Pharmacol. *390*: 257–66.

Nakamura, K., Li, Y.Q., Kaneko, T., Katoh, H., and Negishi, M. (2001). Prostaglandin EP3 receptor protein in serotonin and catecholamine cell groups: a double immunofluorescence study in the rat brain. Neuroscience *103*: 763–75.

Pablos, P., Mendiguren, A., and Pineda, J. (2015). Contribution of nitric oxide-dependent guanylate cyclase and reactive oxygen species signaling pathways to desensitization of μ-opioid receptors in the rat locus coeruleus. Neuropharmacology *99*: 422–431.

Pineda, J., and Aghajanian, G.K. (1997). Carbon dioxide regulates the tonic activity of locus coeruleus neurons by modulating a proton- and polyamine-sensitive inward rectifier potassium current. Neuroscience *77*: 723–43.

Pineda, J., Kogan, J.H., and Aghajanian, G.K. (1996). Nitric oxide and carbon monoxide activate locus coeruleus neurons through a cGMP-dependent protein kinase: involvement of a nonselective cationic channel. J. Neurosci. *16*: 1389–99.

Pineda, J., Ugedo, L., and García-Sevilla, J. a (1997). Enhanced alpha2A-autoreceptor reserve for clonidine induced by reserpine and cholinomimetic agents in the rat vas deferens. Br. J. Pharmacol. *122*: 833–840.

Ruiz-Velasco, V., and Ikeda, S.R. (1998). Heterologous expression and coupling of G protein-gated inwardly rectifying K+ channels in adult rat sympathetic neurons. J. Physiol. *513*: 761–773.

Säfholm, J., Dahlén, S.-E., Delin, I., Maxey, K., Stark, K., Cardell, L.-O., et al. (2013). PGE 2 maintains the tone of the guinea pig trachea through a balance between activation of contractile EP 1 receptors and relaxant EP 2 receptors. Br. J. Pharmacol. *168*: 794–806.

Sang, N., Zhang, J., Marcheselli, V., Bazan, N.G., and Chen, C. (2005). Postsynaptically synthesized prostaglandin E2 (PGE2) modulates hippocampal synaptic transmission via a presynaptic PGE2 EP2 receptor. J. Neurosci. *25*: 9858–70.

Shi, J., Wang, Q., Johansson, J.U., Liang, X., Breyer, R.M., Montine, T.J., et al. (2012). Inflammatory prostaglandin E2 signalning in a mouse model of Alzheimer's disease. Ann Neurol. *72*: 788–798.

Su, X., Leon, L. a, Wu, C.W., Morrow, D.M., Jaworski, J.-P., Hieble, J.P., et al. (2008). Modulation of bladder function by prostaglandin EP3 receptors in the central nervous system. Am. J. Physiol. Renal Physiol. *295*: F984-94.

Torrecilla, M., Fernández-Aedo, I., Arrue, A., Zumarraga, M., and Ugedo, L. (2013). Role of GIRK channels on the noradrenergic transmission in vivo: an electrophysiological and neurochemical study on GIRK2 mutant mice. Int. J. Neuropsychopharmacol. *16*: 1093–1104.

Torrecilla, M., Marker, C.L., Cintora, S.C., Stoffel, M., Williams, J.T., and Wickman, K. (2002). G-protein-gated potassium channels containing Kir3.2 and Kir3.3 subunits mediate the acute inhibitory effects of opioids on locus ceruleus neurons. J. Neurosci. *22*: 4328–4334.

Ushikubi, F., Segi, E., Sugimoto, Y., Murata, T., Matsuoka, T., Kobayashi, T., et al. (1998). Impaired febrile response in mice lacking the prostaglandin E receptor subtype EP3. Nature *395*: 281–284.

Xu, S., Guo, S., Jiang, X., Yin, Q., Umezawa, T., and Hisamitsu, T. (2003). Effect of indomethacin on the c-fos expression in AVP and TH neurons in rat brain induced by lipopolysaccharide. Brain Res. *966*: 13–8.

Yamaguchi, N., and Okada, S. (2009). Cyclooxygenase-1 and -2 in spinally projecting neurons are involved in CRF-induced sympathetic activation. Auton. Neurosci. Basic Clin. *151*: 82–89.

Zhang, J., and Rivest, S. (1999). Distribution , regulation and colocalization of the genes encoding the EP 2 - and EP 4 -PGE 2 receptors in the rat brain and neuronal responses to systemic inflammation. Eur. J. Neurosci. *11*: 2651–2668.

Tables

Table 1.

Basal firing rate and concentration-effect curve parameters for the inhibitory action of the EP3 receptor agonist sulprostone on LC neurons in the absence (control) or in the presence of the EP3 (L-798,106), EP2 (PF-04418948), and EP4 (L-161,982) receptor antagonists.

			Concentration-effect curves[1]			
Drugs	Concentration	Basal firing rate (Hz)	pEC_{50} (M)	(EC_{50}, nM)	Slope factor	*n*
Sulprostone						
Control		0.84 ± 0.07	7.83 ± 0.08	(14.8)	2.39 ± 0.37	9
+ L-798,106	3 μM	0.64 ± 0.11	7.49 ± 0.09	(32.4)	1.39 ± 0.16*	6
	10 μM	0.87 ± 0.22	6.89 ± 0.11*	(128)	1.07 ± 0.12*	6
+ PF-04418948	3 μM	0.66 ± 0.11	7.63 ± 0.15	(23.5)	1.89 ± 0.14	6
	10 μM	0.58 ± 0.08	8.49 ± 0.10*	(3.25)	1.61 ± 0.21	5
+ L-161,982	3 μM	0.64 ± 0.11	8.05 ± 0.11	(8.93)	1.92 ± 0.36	5
	10 μM	0.71 ± 0.12	8.08 ± 0.11	(8.34)	1.49 ± 0.11	5

[1]Values are expressed as mean ± SEM obtained by nonlinear regression of *n* cells. Maximal effect values were 100% in all cases. pEC_{50} is the negative logarithm of the concentration needed to elicit a 50% of the maximal effect. *$P < 0.05$ when compared to the control group (one-way ANOVA followed by a Dunnett's *post hoc* test).

Table 2.

Basal firing rate and concentration-effect curve parameters for the inhibitory action of the EP3 receptor agonists PGE_2 and misoprostol on LC neurons in the absence (control) or in the presence of the EP3 (L-798,106) or a combination of the EP2 (PF-04418948) and EP4 (L-161,982) receptor antagonists.

			Concentration-effect curves[1]			
Drugs	Concentration	Basal firing rate (Hz)	pEC_{50} (M)	(EC_{50}, nM)	Slope factor	*n*
PGE_2						
Control		0.76 ± 0.10	6.96 ± 0.20	(110)	1.92 ± 0.36	5
+ L-798,106	10 μM	0.87 ± 0.14	5.68 ± 0.05*	(2098)	2.55 ± 0.47	5
+ PF-04418948	10 μM					
L-161,982	10 μM	0.83 ± 0.24	7.78 ± 0.19*	(16.6)	1.07 ± 0.06	5
Misoprostol						
Control		0.80 ± 0.12	7.30 ± 0.13	(50.7)	1.85 ± 0.30	5
+ L-798,106	10 μM	0.67 ± 0.11	6.34 ± 0.12*	(455)	1.36 ± 0.28	5
+ PF-04418948	10 μM					
L-161,982	10 μM	0.72 ± 0.11	7.31 ± 0.12	(49.5)	1.76 ± 0.33	5

[1]Values are expressed as mean ± SEM obtained by nonlinear regression of *n* cells. Maximal effect values were 100% in all cases. pEC_{50} is the negative logarithm of the concentration needed to elicit a 50% of the maximal effect. *$P < 0.05$ when compared to their respective control group (one-way ANOVA followed by a Dunnett's *post hoc* test).

Table 3.

Basal firing rate and concentration-effect curve parameters for the inhibitory action of sulprostone on LC neurons in the absence (control) or in the presence of PTX, $BaCl_2$, and SCH-23390.

			Concentration-effect curves[1]				
Drugs	Concentration	Basal firing rate (Hz)	Emax (%)	pEC_{50} (M)	(EC_{50}, nM)	Slope factor	*n*
Sulprostone							
Control		0.84 ± 0.07	100	7.83 ± 0.08	(14.8)	2.39 ± 0.37	9
+ PTX	500 ng ml^{-1}	1.12 ± 0.18	94.9	7.04 ± 0.15*	(90.9)	1.65 ± 0.28	5
+ $BaCl_2$	300 µM	1.03 ± 0.13	94.6	7.27 ± 0.09*	(53.7)	1.37 ± 0.18	5
+ SCH-23390	15 µM	1.37 ± 0.28	87.5	7.46 ± 0.05*	(34.6)	1.56 ± 0.17	5

[1]Values are expressed as mean ± SEM obtained by nonlinear regression of *n* cells. Emax is the maximal inhibitory effect and pEC_{50} is negative logarithm of the concentration needed to elicit a 50% of the Emax. *$P < 0.05$ when compared to the control group (one-way ANOVA followed by a Dunnett's *post hoc* test).

Figure legends

Figure 1. Effect of the EP3 receptor agonist sulprostone on the firing rate of LC neurons in the absence or presence of the EP3 receptor antagonist L-798,106. **(A, B)** Representative examples of firing rate recordings of two LC neurons showing the effect of increasing concentrations of sulprostone in the absence **(A)** and presence of L-798,106 (10 μM) **(B)**. The vertical lines represent the number of spikes recorded every 10 s and the horizontal bars the period of drug application. **(C)** Concentration-effect curves for sulprostone in control (filled squares) and in the presence of L-798,106 (3 μM, open circles or 10 μM, filled circles). The horizontal axis shows the sulprostone concentration on a semi-logarithmic scale. The vertical axis expresses the reduction in firing rate of LC neurons as the percentage of the baseline. Data points are the mean ± SEM at each sulprostone concentration obtained from *n* number of experiments. The lines through the data are the theoretical curves in each group constructed from the mean of the individual concentration-effect curve parameters, as estimated by nonlinear regressions. Note that the concentration-effect curve for sulprostone is shifted to the right by the EP3 receptor antagonist.

Figure 2. Effect of the EP3 receptor agonist sulprostone on the firing rate of LC neurons in the presence of the EP2 receptor antagonist PF-04418948 or the EP4 receptor antagonist L-161,982. **(A, B)** Representative examples of firing rate recordings of two LC neurons showing the effect of increasing concentrations of sulprostone in the presence of PF-04418948 (10 μM) **(A)** or L-161,982 (10 μM) **(B)**. **(C, D)** Concentration-effect curves for sulprostone in control (filled squares) and in the presence of PF-04418948 (3 μM, open triangles or 10 μM, filled triangles) **(C)** or L-161,982 (3 μM, open diamonds or 10 μM, filled diamonds) **(D)**. The horizontal axis shows the sulprostone concentration on a semi-logarithmic scale. The vertical axis expresses the reduction in firing rate of LC neurons as the percentage of the baseline. Data points are the mean ± SEM at each sulprostone concentration obtained from *n* number of experiments. The lines through the data are the theoretical curves in each group constructed from the mean of the individual concentration-effect curve parameters, as estimated by nonlinear regressions.

Figure 3. Effect of PGE_2 on the firing rate of LC neurons in the absence or presence of the EP3 receptor antagonist L-798,106 or a combination of the EP2 receptor antagonist PF-04418948 and the EP4 receptor antagonist L-161,982. **(A, B)** Representative examples of firing rate recordings of two LC neurons showing the effect of increasing concentrations of

PGE_2 in the absence **(A)** and presence of L-798,106 (10 μM) **(B)**. The vertical lines represent the number of spikes recorded every 10 s and the horizontal bars the period of drug application. **(C)** Concentration-effect curves for PGE_2 in control (filled squares) and in the presence of L-798,106 (10 μM, filled circles) or PF-04418948 and L-161,982 (10 μM each, half-filled diamonds). The horizontal axis shows the PGE_2 concentration on a semi-logarithmic scale. The vertical axis expresses the reduction in firing rate of LC neurons as the percentage of the baseline. Data points are the mean ± SEM at each PGE_2 concentration obtained from *n* number of experiments. The lines through the data are the theoretical curves in each group constructed from the mean of the individual concentration-effect curve parameters, as estimated by nonlinear regressions. Note that the concentration-effect curve for PGE_2 is shifted to the right by the EP3 receptor antagonist and to the left by the EP2 and EP4 receptor antagonists.

Figure 4. Effect of misoprostol on the firing rate of LC neurons in the absence or presence of the EP3 receptor antagonist L-798,106 or a combination of the EP2 receptor antagonist PF-04418948 and the EP4 receptor antagonist L-161,982. **(A, B)** Representative examples of firing rate recordings of two LC neurons showing the effect of increasing concentrations of misoprostol in the absence **(A)** and presence of L-798,106 (10 μM) **(B)**. The vertical lines represent the number of spikes recorded every 10 s and the horizontal bars the period of drug application. **(C)** Concentration-effect curves for misoprostol in control (filled squares) and in the presence of L-798,106 (10 μM, filled circles) or PF-04418948 and L-161,982 (10 μM each, half-filled diamonds). The horizontal axis shows the misoprostol concentration on a semi-logarithmic scale. The vertical axis expresses the reduction in firing rate of LC neurons as the percentage of the baseline. Data points are the mean ± SEM at each misoprostol concentration obtained from *n* number of experiments. The lines through the data are the theoretical curves in each group constructed from the mean of the individual concentration-effect curve parameters, as estimated by nonlinear regressions. Note that the concentration-effect curve for misoprostol is shifted to the right by the EP3 receptor antagonist.

Figure 5. Effect of sulprostone on the firing rate of LC neurons after overnight treatment of the slices with the $G_{i/o}$ inhibitor pertussis toxin (PTX) or in the presence of the GIRK blockers Ba^{2+} or SCH-23390. Representative examples of firing rate recordings of three LC neurons showing the effect of increasing concentrations of sulprostone after overnight treatment with PTX (500 ng ml^{-1}) **(A)** or in the presence of $BaCl_2$ (300 μM) **(B)** or SCH-23390 (15 μM) **(C)**.

The vertical lines represent the number of spikes recorded every 10 s and the horizontal bars the period of drug application. Note that the effect of ME (0.8 μM) is reduced compared to control (see Figure 4.1) while the inhibitory effect of GABA (1 mM) is maintained (A). **(D)** Concentration-effect curves for sulprostone in control (filled squares) or after overnight treatment with PTX (500 ng ml^{-1}, open triangles) or in the presence of Ba^{2+} (300 μM, filled circles) or SCH-23390 (15 μM, open squares). The vertical axis expresses the reduction in firing rate of LC as the percentage of the baseline. Data points are the mean ± SEM at each sulprostone concentration obtained from *n* number of experiments. The lines through the data are the theoretical curves in each group constructed from the mean of the individual concentration-effect curve parameters, as estimated by nonlinear regressions. Note that the concentration-effect curve for sulprostone is shifted to the right by PTX, Ba^{2+}, and SCH-23390.

Figure 1

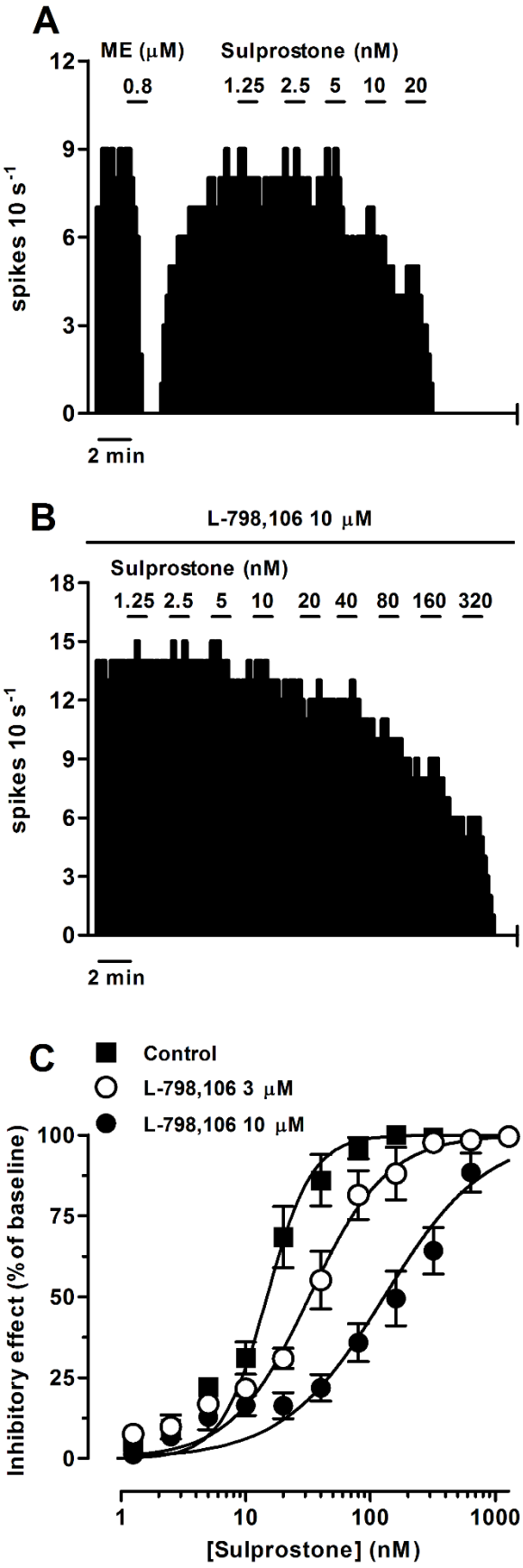
A
ME (μM)
Sulprostone (nM)
0.8
1.25 2.5 5 10 20
spikes 10 s-1
12
9
6
3
0
2 min
B
L-798,106 10 μM
Sulprostone (nM)
1.25 2.5 5 10 20 40 80 160 320
spikes 10 s-1
18
15
12
9
6
3
0
2 min
C
Control
L-798,106 3 μM
L-798,106 10 μM
Inhibitory effect (% of baseline)
100
75
50
25
0
1
10
100
1000
[Sulprostone] (nM)

Figure 2

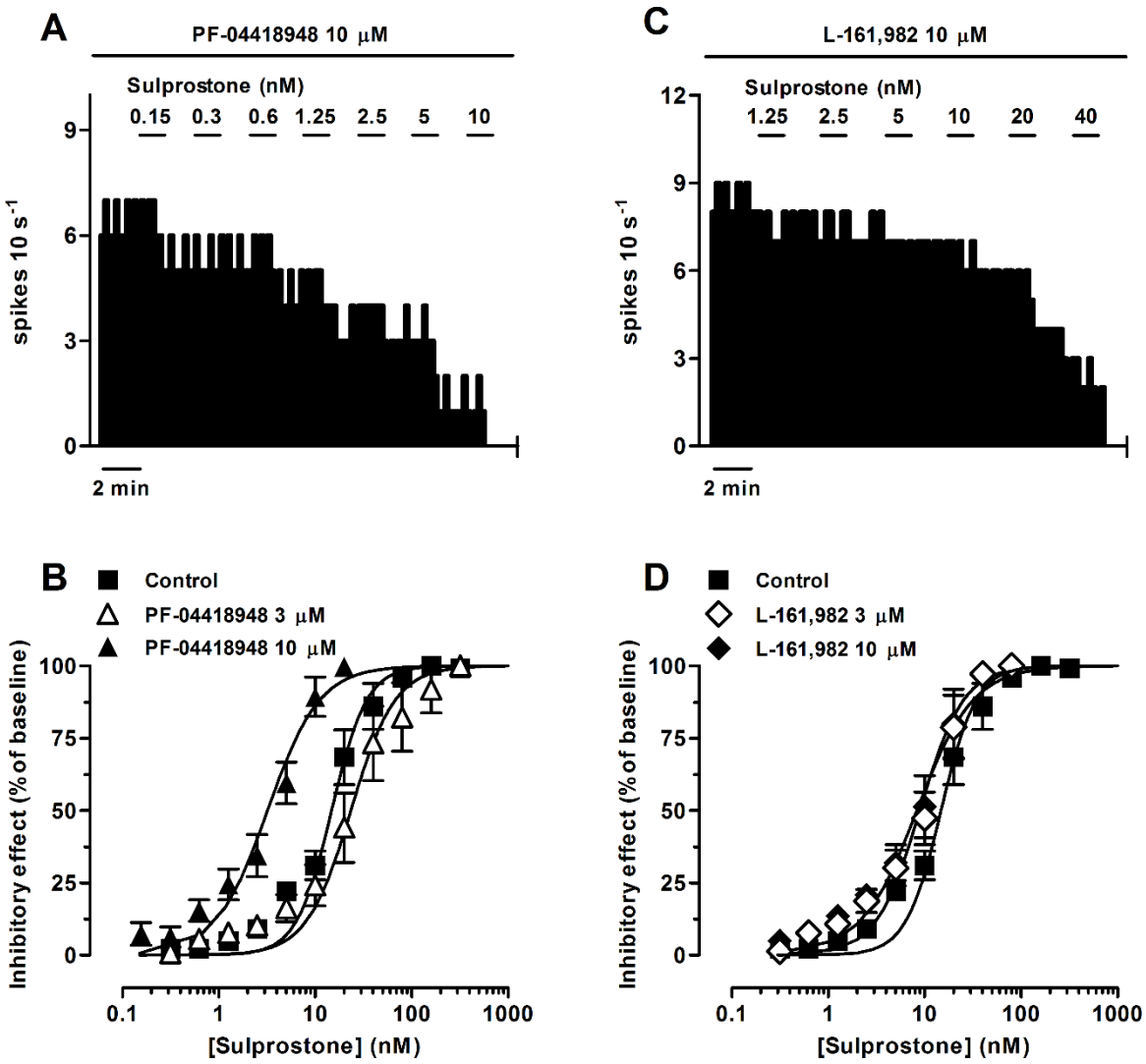
A
PF-04418948 10 μM
Sulprostone (nM)
0.15 0.3 0.6 1.25 2.5 5 10
spikes 10 s-1
2 min
C
L-161,982 10 μM
Sulprostone (nM)
1.25 2.5 5 10 20 40
spikes 10 s-1
2 min
B
Control
PF-04418948 3 μM
PF-04418948 10 μM
Inhibitory effect (% of baseline)
[Sulprostone] (nM)
D
Control
L-161,982 3 μM
L-161,982 10 μM
Inhibitory effect (% of baseline)
[Sulprostone] (nM)

Figure 3

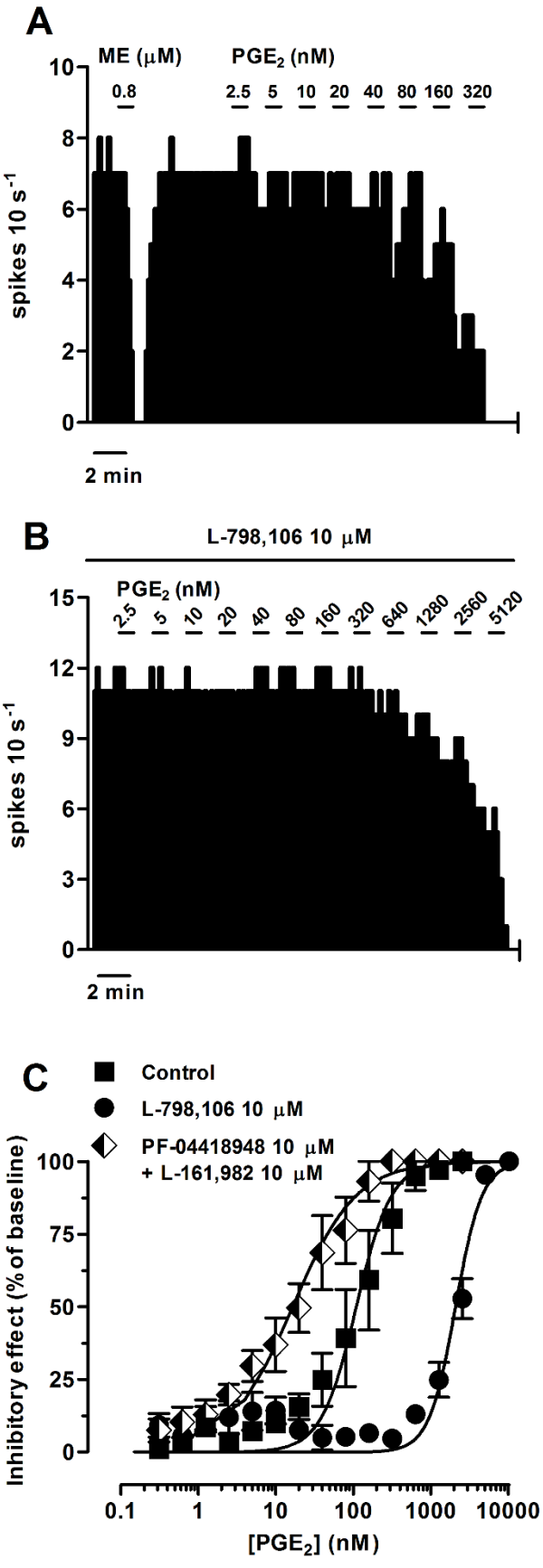
A
ME (μM)
PGE2 (nM)
0.8
2.5 5 10 20 40 80 160 320
spikes 10 s-1
2 min
B
L-798,106 10 μM
PGE2 (nM)
2.5 5 10 20 40 80 160 320 640 1280 2560 5120
spikes 10 s-1
2 min
C
Control
L-798,106 10 μM
PF-04418948 10 μM
+ L-161,982 10 μM
Inhibitory effect (% of baseline)
[PGE2] (nM)

Figure 4

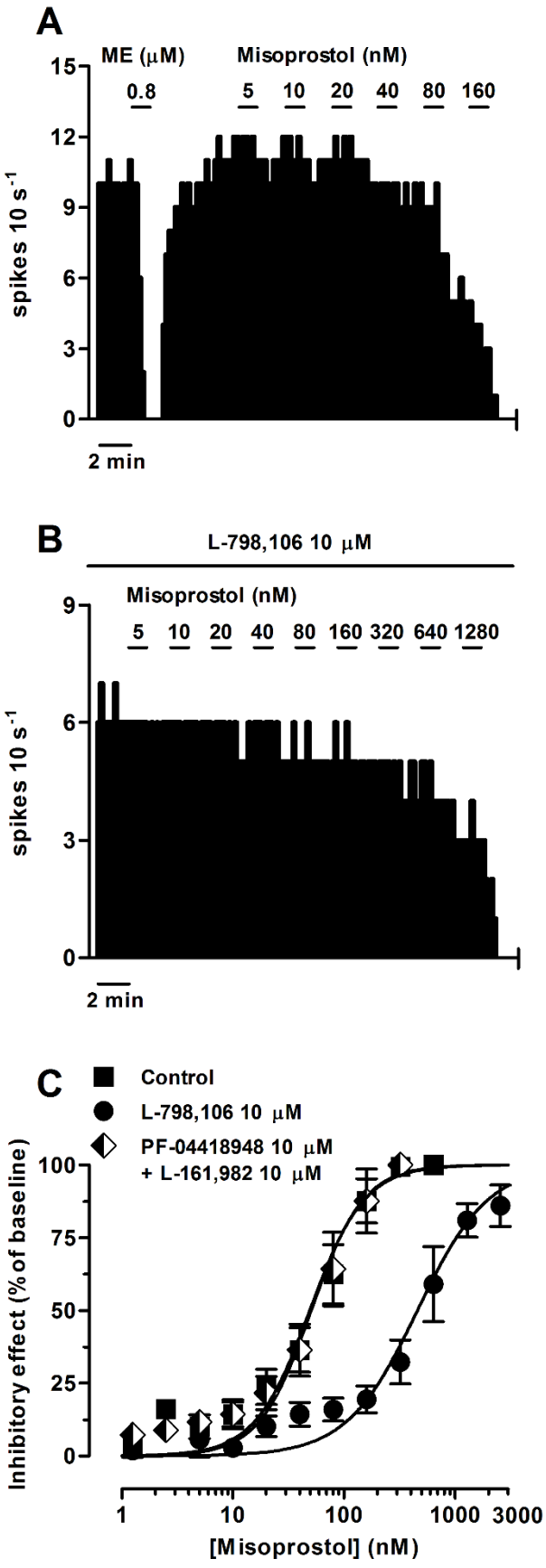
A
ME (μM)
Misoprostol (nM)
0.8
5
10
20
40
80
160
spikes 10 s-1
2 min
B
L-798,106 10 μM
Misoprostol (nM)
5
10
20
40
80
160
320
640
1280
spikes 10 s-1
2 min
C
Control
L-798,106 10 μM
PF-04418948 10 μM
+ L-161,982 10 μM
Inhibitory effect (% of baseline)
[Misoprostol] (nM)

Figure 5

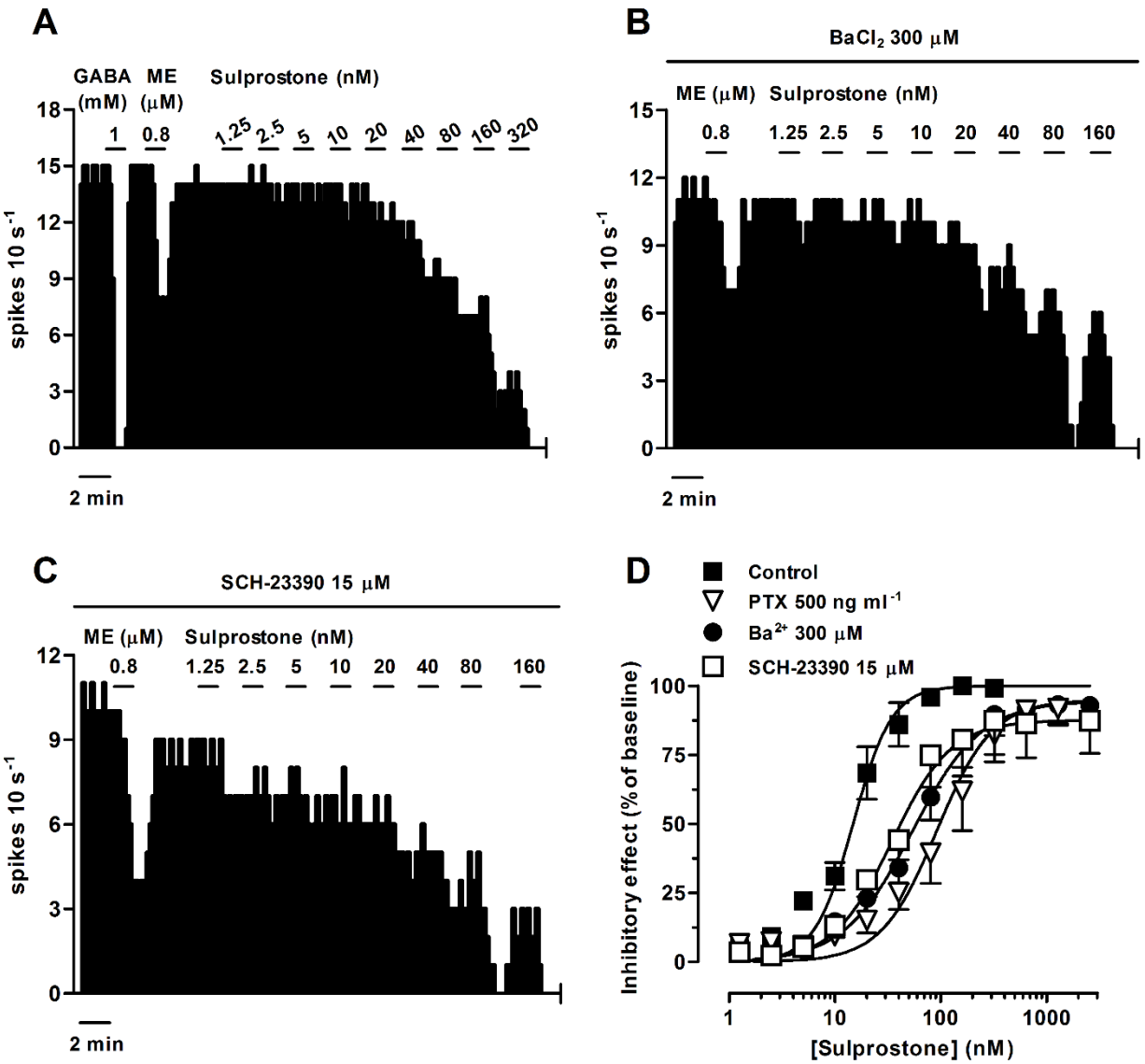
A
GABA (mM)
ME (μM)
Sulprostone (nM)
1
0.8
1.25
2.5
5
10
20
40
80
160
320
spikes 10 s-1
2 min
B
BaCl2 300 μM
ME (μM)
Sulprostone (nM)
0.8
1.25
2.5
5
10
20
40
80
160
spikes 10 s-1
2 min
C
SCH-23390 15 μM
ME (μM)
Sulprostone (nM)
0.8
1.25
2.5
5
10
20
40
80
160
spikes 10 s-1
2 min
D
Control
PTX 500 ng ml-1
Ba2+ 300 μM
SCH-23390 15 μM
Inhibitory effect (% of baseline)
[Sulprostone] (nM)

To be submitted to the *British Journal of Pharmacology*

TITLE:

Pharmacological characterization of prostanoid EP2 receptor in rat locus coeruleus neurons *in vitro*

RUNNING TITLE:

EP2 receptor in rat LC neurons

AUTHORS:

Amaia Nazabal, Aitziber Mendiguren and Joseba Pineda*

[1] Department of Pharmacology, Faculty of Medicine and Nursing, University of the Basque Country (UPV/ EHU), E-48940 Leioa, Bizkaia, Spain

***Corresponding author:**

Joseba Pineda. M.D., Ph.D.

Department of Pharmacology,

Faculty of Medicine and Nursing

University of the Basque Country (UPV/EHU)

Leioa Bizkaia, E-48940, Spain

E-mail address: joseba.pineda@ehu.eus (Dr. J. Pineda)

Tel: +34-946015577

Orcid ID: 0000-0002-9421-1081

Word count:

Abstract: 250	References: 58
Introduction: 449	Tables: 1
Results: 2059	Figures: 5
Discussion: 1510	

Acknowledgements

This work was supported by the Ministerio de Ciencia e Innovación [Grant SAF2008-03612] and the University of the Basque Country (UPV/EHU) [Grant GIU14/29]. Pineda´s research group takes part in a network unit supported by the University of the Basque Country [UFI 11/35]. A. Nazabal was supported by predoctoral fellowships from the Basque Government. The experiments comply with the current laws of Spain.

Conflict of interest

The authors declare that they have no conflict of interest.

Non-approved abbreviations

- aCSF: artificial cerebrospinal fluid
- FR: firing rate
- LC: locus coeruleus
- ME: [Met]enkephalin
- NA: noradrenaline
- Na_v: voltage-gated sodium channels
- PGE_2: prostaglandin E_2
- PGI_2: prostacyclin
- TTX: tetrodotoxin
- VIP: vasoactive intestinal peptide

Bullet point summary (each bullet max. 15 words, max. 2 bullets per heading)

What is already known:

- PGE_2, an inflammatory mediator involved in pain and fever, modulates the activity of brain neurons
- EP3 receptor activation inhibits locus coeruleus (LC) neurons, which also express EP2 receptors

What does this study add:

- EP2 receptor agonists stimulates the neuronal activity of LC noradrenergic cells *in vitro*
- Postsynaptic EP2 receptor activation in LC neurons involves $G_{\beta\gamma}$ subunits and a sodium current

Clinical significance:

- The LC, the main noradrenergic nucleus, is susceptible to inflammatory mediators
- Prostanoid system in the LC might be a pharmacological target against inflammatory pain anxiety

Abstract

BACKGROUND AND PURPOSE: We have shown that the inflammatory mediator prostaglandin E_2 (PGE_2) inhibits locus coeruleus (LC) neurons *in vitro* via $G_{i/o}$-coupled EP3 receptors. PGE_2 also binds to G_q-coupled EP1 and G_s-coupled EP2 and EP4 receptors. In the brainstem, the EP2 receptor is expressed almost exclusively in the LC, the main noradrenergic nucleus of the brain, but its functional role remains unknown. Thus, we aimed to characterize pharmacologically EP2 receptors in LC neurons.

EXPERIMENTAL APPROACH: We studied the effect of EP2 receptor agonists on the LC firing activity in rat brain slices by single-unit extracellular electrophysiology.

KEY RESULTS: EP2 receptor agonist butaprost (0.01-10 μM) and treprostinil (0.03-10 μM) increased the firing rate of LC neurons in a concentration-dependent manner (EC_{50}=0.45 μM and 0.54 μM; Emax=74.3% and 81.3%, respectively). The EP2 receptor antagonist PF-04418948 (10 nM), but not the EP3 (L-798,106, 10 nM) or EP4 receptor antagonists (L-161,982, 10 nM), hindered the excitatory effect of butaprost and treprostinil. Furthermore, extracellular sodium replacement and $G_{\beta\gamma}$ blockade (gallein, 20 μM) prevented the butaprost-induced stimulation of neuronal activity. However, the excitatory effect caused by butaprost was not reduced by a PKA activator (8-Br-cAMP, 1 mM) or PKA inhibitor (H-89, 10 μM), nor was it modified by synaptic blockade or by inhibitors of the $G_{\alpha s}$ subunits (NF449, 10 μM), HCN channels (ZD7288, 30 μM), TRP channels (2-APB, 30 μM), and Kir6.2 channels (glibenclamide, 3 μM).

CONCLUSIONS AND IMPLICATIONS: activation of postsynaptic EP2 receptor excites LC noradrenergic neurons, seemingly through a $G_{\beta\gamma}$-dependent activation of sodium current.

Keywords*:* locus coeruleus; PGE_2; EP2 receptor; prostanoid; slice; firing

Introduction

Prostaglandins are inflammatory mediators synthetized on demand from membrane phospholipids, which are transformed into arachidonic acid, and then into a common precursor by the rate-limiting enzyme cyclooxygenase (COX). Nonsteroidal anti-inflammatory drugs (NSAID) are commonly used as analgesic, antipyretic, and anti-inflammatory drugs as they prevent the synthesis of prostanoids by blocking the enzymatic activity of the COX. In mammal brain, the COX enzyme is constitutively expressed under non-inflammatory circumstances (Yasojima et al., 1999; Hétu and Riendeau, 2005) suggesting a role of prostaglandins on basal conditions. On this premise, COX is found in neuronal cell bodies and dendrites (Yasojima et al., 1999), which further highlights the implication of the prostanoid system in neuronal physiology. The main final product of COX synthesis is the prostaglandin E_2 (PGE_2), which binds to G protein-coupled receptors: EP1-EP4. Thus, the EP1 receptor is coupled to G_q, EP3 to $G_{i/o}$, and EP2 and EP4 to G_s proteins. The EP2, EP3, and EP4 receptors are extensively expressed in the CNS, including the hypothalamus and the locus coeruleus (LC) (Zhang and Rivest, 1999; Ek et al., 2000).

Activation of these receptors can modulate the neuronal activity, which has been broadly studied in the case of the EP2 receptor. For instance, EP2 receptor activation regulates synaptic transmission in the hippocampus (Sang et al., 2005) and elicits membrane depolarization in neurons from the hypothalamus (Clasadonte et al., 2011) and dorsal horn (Baba et al., 2001). Furthermore, PGE_2 elicits a sodium current in ganglion (Matsumoto et al., 2005) and cerebellar neurons (Fang et al., 2011) via EP2 receptor activation.

The LC, the main source of noradrenaline (NA) in the brain, controls many physiological functions, including sleep-wake cycle, arousal, cognition, and pain by sending noradrenergic projections to virtually all brain regions. Additionally, the LC receives inputs mainly from glutamatergic and GABAergic afferences (Aston-Jones et al., 1986). Some findings have suggested a connection between prostaglandins and the LC. First, LC cells possess the enzymatic equipment to synthesize prostaglandins, as spinally-projecting LC neurons constitutively express COX enzyme (Yamaguchi and Okada, 2009). Thus, NSAID administration attenuates the activation of LC cells in response to nociception and inflammation (Xu et al., 2003). Second, previous results from our laboratory have shown that EP3 receptor activation by the endogenous PGE_2 inhibits the neuronal activity of LC cells *in vitro* (Nazabal et al., unpublished results). Finally, in the brainstem, the EP2 receptor is almost exclusively expressed in the LC, as demonstrated by *in situ* hybridization (Zhang and Rivest, 1999). However, little is known about the function of the EP2 receptor in LC neurons. Thus, we aimed to characterize the EP2 receptor pharmacologically and to study its signaling mechanism by single-unit extracellular recordings in LC noradrenergic neurons from rat brain slices.

Methods

Animals and ethics statement

97 male adult Sprague-Dawley rats (200-300 g) were used to perform the experiments and are reported in compliance with the ARRIVE guidelines (Kilkenny et al., 2010; McGrath and Lilley, 2015) and with the recommendations made by the *British Journal of Pharmacology*. Rats were obtained from the animal house of the University of the Basque Country (Leioa, Spain) and housed under standard environmental conditions (22 ºC, 12:12 h light/dark cycles) with free access to food and water. One slice was taken from each animal, and unless stated otherwise, only one experiment was performed in each slice. The number of experiments in each group was typically five to eight, depending on the level of variability. Treatments and

controls were performed in parallel in a randomized manner. As electrophysiological outcomes were collected *in situ*, data recording could not be blinded to the operator. However, the data analysis performed by the experimenter was confirmed separately by an additional researcher in all cases. All the experiments were carried out according to EU Directive 2010/63 on the protection of animals used for scientific purposes and approved by the local Ethical Committee for Research and Teaching of the University of the Basque Country (UPV/EHU, Spain) and the Department of Sustainability and Natural Environment of Provincial Council from Bizkaia (ref. CEEA M20-2015-152; CEEA M20-2018-026). All the efforts were made to minimize the animal suffering and to reduce the number of animals used.

Brain slice preparation

Animals were anesthetized with chloral hydrate (400 mg kg^{-1}, i.p.) and decapitated (Mendiguren and Pineda, 2007). The brain was rapidly extracted, and a block of tissue containing the brainstem was immersed in ice-cold modified artificial cerebrospinal fluid (aCSF) where NaCl was equiosmolarly substituted for sucrose to improve neuronal viability. Coronal slices of 500-600 μm thickness containing the LC were cut using a vibratome (Leica VT1200 S, Leica Biosystems, Nussloch, Germany). The tissue was allowed to recover from the slicing for 90 min, placed on a nylon mesh, and incubated at 33 ± 1 ºC on a modified Haas-type interface chamber. The tissue was continuously perfused with aCSF saturated with 95% O_2/ 5% CO_2 (final pH = 7.34) at a flow rate of 1.5 ml min^{-1}. The aCSF contained (in mM): NaCl 130, KCl 3, NaH_2PO_4 1.25, D-glucose 10, $NaHCO_3$ 21, $CaCl_2$ 2 and $MgSO_4$ 2. The LC was recognized visually in the rostral pons as a dark oval area on the lateral borders of the central gray and the 4th ventricle, at or just anterior to the genu of the facial nerve.

Electrophysiological recordings

Single-unit extracellular recordings of LC cells were made as previously described (Mendiguren and Pineda, 2007). The recording electrode consisted of an Omegadot glass micropipette puller (Sutter Instruments, Novato, CA, USA) and filled with 50 mM NaCl. The tip was broken back to a size of 2 – 5 μm (3 – 5 MΩ) and positioned in the LC. The extracellular signal from the electrode was passed through a high-input impedance amplifier (Axoclamp 2B, Molecular Devices, Union City, CA, USA) and monitored on an audio-amplifier and an oscilloscope (Aumon 14, Cibertec S.A., Madrid, Spain). Individual neuronal spikes were isolated from the background noise with a window discriminator (PDV 225,

Cibertec S.A.). The firing rate (FR) was continuously recorded and analyzed before, during, and after experimental manipulations by a PC-based custom-made program which generated consecutive 10 s bin histograms bars of the cumulative number of spikes (HFCP®, Cibertec S.A., Madrid, Spain). Noradrenergic cells in the LC were identified by their spontaneous and regular discharge activities, the slow FR and the long-lasting biphasic positive-negative waveforms (Andrade and Aghajanian, 1984). We only recorded cells that showed stable FRs between 0.5 and 1.5 Hz for at least 3-5 min and the inhibitory responses to [Met]enkephalin (ME 0.8 μM, 1 min) higher than 80% (Medrano et al., 2017), which was used as a control for the perfusion system.

Pharmacological procedures

The firing rate of LC neurons was recorded for several minutes before drug applications to obtain the baseline activity, and then, during and after drug perfusion. To characterize the effect of EP2 receptor agonists in LC neurons, we perfused increasing concentrations of the EP2 receptor agonist butaprost free acid (10 nM – 10 μM, 3x) and the synthetic prostacyclin (PGI_2) analog treprostinil, which has a high affinity for the EP2 receptor (30 nM – 10 μM, 3x). Concentrations were based on other studies made in brain slices (Liu et al., 2005). Each concentration of the EP2 receptor agonists was perfused for at least 10 min to reach its plateau effect and each agonist was used up to concentrations that achieved the maximal effect of the drug. To verify that the EP2 receptor was mediating the effect caused by butaprost and treprostinil, concentration-effect curves for these agonists were made in the presence of the EP2 receptor antagonist PF-04418948 (3 and 10 nM) or a combination of the EP3 receptor antagonist L-798,106 (10 nM) and the EP4 receptor antagonist L-161,982 (10 nM). Concentrations of the antagonists were selected according to preceding reports (Forselles et al., 2011). All the antagonists employed were perfused for 30 min before performing the concentration-effect curves for the EP2 receptor agonists.

Butaprost was used for subsequent characterization of the molecular mechanism involved in EP2 receptor activation. Activation of EP2 receptors increases a sodium current in neurons from different CNS areas such as the cerebellum (Fang et al., 2011) or the spinal dorsal horn (Baba et al., 2001). Then, to investigate the involvement of a sodium current in the butaprost-mediated effect, a low sodium-containing aCSF was prepared by replacing 80% of the NaCl equiosmolarly with Trizma hydrochloride/base (TRIS) (Pineda et al., 1996) and then the effect of butaprost was tested. To further describe the involvement of sodium currents, we checked

whether the transient receptor potential (TRP) ion channels (Cui et al., 2011) might contribute to the effect of butaprost by using the nonselective TRP blocker 2-APB (30 μM, 10 min). Finally, to discard the activation of other channels that may mediate excitatory effects in the LC neurons (Ugedo et al., 1998), we examined the effect of butaprost in the presence of the ATP-sensitive potassium channel (Kir6.2) specific blocker glibenclamide (3 μM, 15 min).

In the LC, noradrenergic cells are stimulated by a cAMP/PKA-induced inward sodium current (Wang and Aghajanian, 1987). To test whether the sodium current was induced by a rise in the cAMP levels and the resultant activation of the PKA, we performed an occlusion experiment with the non-hydrolyzable cell-permeable cAMP analog 8-Br-cAMP (1 mM, 8 min) (Wang and Aghajanian, 1990). Thus, in case EP2 receptor activation depends on the cAMP/PKA pathway, administration of a saturating concentration of 8-Br-cAMP would occlude the subsequent effect of butaprost. In addition, the cAMP/PKA-dependency was further determined by testing butaprost in the presence of the PKA inhibitor H-89 (10 μM, 20 min) (Jolas et al., 2000) or the HCN channel blocker ZD7288 (30 μM, 20 min) (Zolles et al., 2006).

Then, we tested whether the $G_{\alpha s}$ protein would intermediate in the effect of butaprost by application of the blocker of the $G_{\alpha s}$-dependent signaling NF449 (10 μM, 30 min) (Hohenegger et al., 1998). In these assays, vasoactive intestinal peptide (VIP) (0.5 μM, 5 min) administration was used as a positive control to confirm that NF449 was effectively blocking the $G_{\alpha s}$ protein, as previously reported in LC neurons (Wang and Aghajanian, 1990). Finally, to assess the involvement of the $G_{\beta\gamma}$ subunits, the effect of butaprost was tested in slices previously incubated with gallein (20 μM) in an aluminum foil-covered glass beaker for 120 min (Kurowski et al., 2015).

In order to study the involvement of presynaptic mechanisms in the effect caused by EP2 receptor activation, butaprost was applied in the presence of the $GABA_A$ channel blocker picrotoxin (100 μM), the non-NMDA ionotropic glutamate receptor antagonist CNQX (30 μM), the NMDA receptor antagonist d-AP5 (100 μM), and the non-selective metabotropic glutamate receptor antagonist RS-MCPG (500 μM) (Mendiguren and Pineda, 2007). All mentioned drugs were bath perfused for at least 10 min before and during testing the effect of butaprost.

Analysis and statistics of electrophysiological data

The data and statistical analysis were carried out with the computer program GraphPad Prism (version 5.0 for Windows, GraphPad Software, Inc., San Diego, CA, USA) and comply with

the recommendations on experimental design and analysis in pharmacology (Curtis et al., 2018). The effect (E) was normalized to baseline (FR_{basal}) in each cell according to the following equation $E = (FR_{basal} - FR_{post}) \cdot 100/FR_{basal}$, where FR_{basal} is the average FR of each pre-agonist condition calculated for 60 s immediately before drug application, and FR_{post} is the average FR of the last 60 s for each concentration of agonist, once it had reached a plateau. In the case of the perfusion test with ME (0.8 μM, 1 min), the inhibitory effect was calculated similarly but normalized to the initial FR ($FR_{initial}$), being the average FR of each neuron calculated for 60 s immediately before drug application and FR_{post} the average FR after drug application for 60-90 s. The intervals were chosen to integrate the whole period of maximal effect of each drug administration (Medrano et al., 2017). Normalization to FR_{basal} or $FR_{initial}$ was used for comparison purposes across groups.

To construct concentration-effect curves for the EP2 receptor agonists, fitting analysis was performed to obtain the best simple nonlinear fit to the following three-parameter logistic equation: $E = E_{max}[A]^n / (EC_{50}^n + [A]^n)$, where E and [A] are the observed effect and the concentration of the agonist, respectively; E_{max} is the maximal excitatory effect of the EP2 receptor agonist, EC_{50} is the concentration of the agonist required to promote the 50% of E_{max}, and n represents the slope factor of the function. These parameters were determined in individual assays by the nonlinear analysis and then averaged to obtain the theoretical parameters in each group. For comparison purposes, the EC_{50} values were converted and expressed as the negative logarithm (pEC_{50}), which adjusted the variable into a Gaussian distribution.

The antagonist affinity value was calculated as the negative logarithm of the equilibrium dissociation constant of the antagonist-receptor complex (pK_B). The pK_B value was estimated for parallel shifts by using the modified Gaddum/Schild equation for global fitting of the curves using GraphPad Prism 5.0 (Lazareno and Birdsall, 1993), where the minimum and maximum effects were constrained to 0 and 100% respectively, and the Schild slope was constrained to 1.0 in accordance with previous reports (Lazareno and Birdsall, 1993). In the case of treprostinil, the affinity measurement was obtained from the Gaddum method (Kenakin et al., 2006) by plotting double equieffective concentrations of treprostinil in the absence (ordinates) and presence (abscissae) of the antagonist.

Data are expressed as the mean ± SEM of n number of rats. Statistical significances were obtained by a two-tailed paired Student's t-test when the response values were compared before and after drug applications within the same cell, and by a two-tailed two-sample Student's t-test when the FRs, responses or parameters were two independent experimental

conditions. Comparisons among more than two experimental conditions by one-way analysis of variance (ANOVA) followed by a Dunnett's *post hoc* for comparison with a control group and only if F achieved the necessary level of statistical significance (i.e. $P < 0.05$) and there was no significant variance inhomogeneity. The threshold of significance was set at $P = 0.05$, and only one level of probability ($P < 0.05$) is reported.

Materials and drugs

For electrophysiological recordings, the following drugs were purchased from Tocris Bioscience (Bristol, UK): CNQX, d-AP5, gallein, glibenclamide, H-89, L-161,982, L-798,106, RS-MCPG, NF449, PF-04418948, and ZD7288. The following drugs were acquired from Sigma-Aldrich Química S.A. (Madrid, Spain): picrotoxin and Trizma hydrochloride. From Bachem (Weil am Rhein, Germany) were purchased: [Met]enkephalin acetate salt (ME) and vasoactive intestinal peptide (VIP). Finally, 8-Bromo-cAMP was from Enzo Life Sciences Inc. (New York, USA) and butaprost free acid from Cayman Chemical (Ann Arbor, MI, USA). Stock solutions of gallein, glibenclamide, L-161,982, L-798,106, PF-04418948, and treprostinil were first prepared in pure DMSO and then diluted in aCSF to obtain a final concentration of DMSO lower than 0.1%, which does not affect the LC cell firing responses (Pineda et al., 1996). Butaprost free acid was purchased already dissolved in methyl acetate, and the final concentrations were obtained by diluting it in the aCSF at the moment of the experiment. The final concentration of methyl acetate in aCSF was < 0.03%. Control assays were performed with equivalent volumes of the vehicles in which the drugs were dissolved. RS-MCPG and picrotoxin were directly dissolved in aCSF the day of the experiment. Stock solutions of the rest of the drugs were first prepared in Milli-Q water and then diluted 1000- to 10000-fold in aCSF for the desired concentration. Final solutions were prepared freshly just before each experiment, and stock solutions were kept at -20 ºC.

Nomenclature of targets and ligands

Key protein targets and ligands in this article are hyperlinked to corresponding entries in http://www.guidetopharmacology.org, the common portal for data from the IUPHAR/BPS Guide to PHARMACOLOGY (Harding et al., 2018), and are permanently archived in the Concise Guide to PHARMACOLOGY 2017/18 (Alexander et al., 2017).

Results

Effect of the EP2 receptor agonist butaprost on the firing rate of LC neurons

In the brainstem, the EP2 receptor is expressed almost exclusively in the LC (Zhang and Rivest, 1999), but its functional role remains unknown. To investigate the effect of EP2 receptor activation on the firing rate of LC neurons, we performed concentration-effect curves for the EP2 receptor agonist butaprost (10 nM – 10 μM). Administration of increasing concentrations of butaprost (10 nM – 10 μM, 3x, 15 min each) increased the firing rate of LC neurons (from 0.85 ± 0.09 Hz to 1.38 ± 0.11 Hz; $n = 8$, $P < 0.05$) in a concentration-dependent manner with an EC_{50} value in the nanomolar range (Figures 1A and D; Table 1).

To elucidate which EP receptor was mediating the excitatory effect observed with butaprost, we constructed concentration-effect curves for this EP2 receptor agonist in the presence of the EP2 receptor antagonist PF-04418948 (3 and 10 nM) or a combination of the EP3 receptor antagonist L-798,106 (10 nM) and the EP4 receptor antagonist L-161,982 (10 nM). Bath application of PF-04418948 (3 and 10 nM) for 30 min did not change the firing rate, but the highest concentration (10 nM) shifted by 6 fold ($n = 6$, $P < 0.05$) to the right the concentration-effect curve for butaprost without affecting the maximal effect significantly (Figures 1B and D; Table 1). The calculated affinity for the EP2 receptor antagonist (pK_B) was 8.39 ± 0.16 ($n = 11$). On the other hand, perfusion with a combination of L-798,106 and L-161,982 (10 nM each) for 30 min did not change the firing activity or shift to the right the concentration-effect curve for butaprost (Figures 1C and D; Table 1). There was a trend for the Emax to be higher after the combination of L-798,106 and L-161,982, but this increase was not significant (Figure 1D; Table 1). Altogether, these results suggest that butaprost increased the LC neuronal activity via activation of the EP2 receptor.

Effect of the PGI_2 analog treprostinil on the firing rate of LC neurons

To further study the effect of EP2 receptor activation in the LC, we used the PGI_2 analog treprostinil, a clinically relevant drug that shows high affinity for the EP2 receptor in binding studies (Whittle et al., 2012). Thus, administration of increasing concentrations of treprostinil (30 nM – 10 μM, 3x, 15 min each concentration) induced an excitatory effect on the firing

rate of LC neurons in a concentration-dependent manner (from 0.68 ± 0.07 Hz to 1.22 ± 0.17 Hz; $n = 6$, $P < 0.05$), with an EC_{50} value in the nanomolar range (Figures 2A and D; Table 1).

Considering that treprostinil has high affinity for other prostanoid receptors, we assessed whether the observed excitatory response was produced by the activation of the EP2 receptor by using the specific EP2 (PF-04418948), EP3 (L-798,106), or EP4 (L-161,982) receptor antagonists at 10 nM. Perfusion with PF-04418948 (10 nM) for 30 min did not modify the firing rate or the EC_{50} of the concentration-effect curve for treprostinil. However, the EP2 receptor antagonist decreased by 47.4% the Emax value of the concentration-effect curve for treprostinil ($n = 6$, $P < 0.05$; Figures 2B and D; Table 1). Given the apparent non-competitive binding, the affinity value of PF-04418948 for the EP2 receptor was calculated from the double reciprocal plot of equieffective agonist concentrations in the presence and absence of the antagonist (Kenakin et al., 2006). Thus, the estimated pK_B for PF-04418948 using treprostinil as an agonist was 8.34 (95% CI: 8.29 – 8.38). In addition, bath application of a combination of L-798,106 and L-161,982 did not produce any rightward shift but increased the Emax value of the concentration-effect curve for treprostinil by 77.7% ($n = 5$, $P < 0.05$; Figures 2C and D; Table 1). Thus, these results suggest that the treprostinil-induced stimulation of the LC neuronal firing rate is caused, at least in part, by activation of the EP2 receptor.

Study of cationic currents and cAMP/PKA signaling pathway involvement in EP2 receptor activation in LC neurons

It is known that PGE_2 increases a sodium current via activation of the EP2 receptor in neurons from different CNS areas such as the cerebellum (Fang et al., 2011) or the spinal dorsal horn (Baba et al., 2001). In the LC, noradrenergic cells are stimulated by a cAMP/PKA-induced inward sodium current (Wang and Aghajanian, 1987). Therefore, to test the putative involvement of sodium current in the butaprost-induced stimulation of LC cells, we used a low sodium-containing aCSF, in which 80% of the sodium had been replaced by TRIS (Alreja and Aghajanian, 1993; Pineda et al., 1996). Switching from the regular aCSF to a low-sodium aCSF (TRIS 80%) reduced the spontaneous activity of LC neurons by 66.5 ± 2.3% (from 1.11 ± 0.34 to 0.35 ± 0.11; $n = 7$, $P < 0.05$; Figure 3A) and completely blocked the excitation caused by butaprost (1 μM) ($n = 7$, $P < 0.05$ *vs.* control; Figures 3A and B).

This suggests that the excitatory effect of the EP2 receptor agonist butaprost is dependent on a sodium current. Next, to further describe the ion channel responsible for this sodium current, we tested whether the cation-permeable transient receptor potential (TRP) channel could be involved in the butaprost-induced effect. This family of channels has been reported to participate in the hypercapnic response of the LC (Cui et al., 2011). Perfusion with the non-selective TRP channel blocker 2-APB (30 μM) reduced the LC cell firing rate by 40.2 ± 4.9% (from 0.76 ± 0.09 to 0.46 ± 0.07, $n = 5$, $P < 0.05$), but did not block the excitatory effect caused by butaprost (1 μM) (Figure 3C). Thus, the TRP channels do not appear to mediate the sodium current induced by the EP2 receptor agonist butaprost. Excitatory effects on the LC cell firing activity have also been reported to be elicited by the inhibitory ATP-sensitive K^+ channels (the Kir6.2) (Ugedo et al., 1998). Therefore, we tested the Kir6.2 channel blocker glibenclamide (3 μM), which administration for 15 min failed to affect the excitatory response induced by butaprost (1 μM) ($n = 5$, $P > 0.05$ *vs*. control; Figure 3C). This suggests that the ATP-dependent K^+ channels are not involved in the excitatory effect of EP2 receptor activation on LC neurons.

Then, to test whether the butaprost-induced activation of a sodium current is mediated by the cAMP/PKA pathway, we used 8-Br-cAMP (1 mM), a non-hydrolyzable cell-permeable cAMP analog that activates the PKA and sodium currents (Wang and Aghajanian, 1987). In the case that activation of the EP2 receptor by butaprost depended on the cAMP/PKA pathway, prior administration of a saturating concentration of 8-Br-cAMP would occlude the excitatory effect of butaprost. As expected from previous reports (Wang and Aghajanian, 1987), perfusion with 8-Br-cAMP (1 mM) for 8 min produced a 2-fold increase in the firing activity of LC neurons (from 0.71 ± 0.06 Hz to 1.40 ± 0.14 Hz; $n = 5$, $P < 0.05$) (Figures 4A and B). However, administration of butaprost (1 μM, 15 min) in the presence of 8-Br-cAMP further increased the firing activity of LC cells (from 1.40 ± 0.14 Hz to 1.97 ± 0.18 Hz; $n = 5$, $P < 0.05$) (Figures 4A and B), which suggests that the effect of butaprost was not occluded by 8-Br-cAMP. Therefore, the excitatory effect of the EP2 receptor agonist does not seem to depend on the cAMP/PKA pathway. To confirm it, we studied the effect of butaprost in the presence of the PKA inhibitor H-89. Bath application of H-89 (10 μM) for 20 min increased the LC firing rate by 18.0 ± 5.5% (from 0.87 ± 0.11 Hz to 1.02 ± 0.14 Hz; $n = 5$, $P < 0.05$). However, H-89 did not change the parameters of the concentration-effect curve for butaprost (0.3 – 3 μM, 3x). Thus, the Emax value in the presence of H-89 was 86.3 ± 7.1% and the pEC_{50} was 6.19 ± 0.07 (EC_{50}=0.64 μM; Figure 4C), not different from those obtained in

control (n = 5, P > 0.05; see Table 1). Hence, these data rule out the implication of the PKA in the excitatory effect of butaprost. On the other hand, a cationic current has been reported to be activated directly by increased levels of cAMP (Momin et al., 2008; Santin and Hartzler, 2015) or the $G_{\beta\gamma}$ subunits (Grzelka et al., 2017) via activation of HCN channels without the involvement of PKA. In fact, HCN channels play a functional role in some responses of LC cells (Santin and Hartzler, 2015) and to PGE_2 in other CNS (Chen and Bazan, 2005) and peripherical neurons (Emery et al., 2011). Then, to analyze whether the HCN channels may be involved in the stimulatory effect of butaprost, we perfused the EP2 receptor agonist in the presence of the HCN blocker ZD7288. Perfusion of ZD7288 (30 μM) for 20 min increased the spontaneous firing rate of LC neurons by 77.0 ± 14.1% (from 0.70 ± 0.09 Hz to 1.20 ± 0.09 Hz; n = 5, P < 0.05). However, the HCN blocker did not change the concentration-effect curve for butaprost (0.3 – 3 μM, 3x) (Emax = 64.4 ± 17.1%, pEC_{50} = 6.40 ± 0.06, and EC_{50} = 0.40 μM; n = 5, P > 0.05 *vs.* control; see Table 1) (Figure 4C). Thus, the EP2 receptor activation does not seem to regulate LC neurons through the cAMP/PKA signaling pathway or the HCN channels.

Study of the involvement of $G_{\alpha s}$ and $G_{\beta\gamma}$ subunits and presynaptic mechanisms on EP2 receptor activation in LC neurons

The EP2 receptor has been described to couple to G_s protein (Yano et al., 2017). Therefore, we addressed whether the $G_{\alpha s}$ and $G_{\beta\gamma}$ subunits would be involved in the stimulatory effect of butaprost. For this purpose, we used the $G_{\alpha s}$-dependent signaling inhibitor NF449 (Hohenegger et al., 1998) and the $G_{\beta\gamma}$-dependent signaling inhibitor gallein. Administration of NF449 (10 μM) for 30 min did not modify the spontaneous firing activity of LC neurons. To verify that NF449 was effectively blocking the $G_{\alpha s}$ subunit, we used VIP (0.5 μM) as a positive control, given that VIP excites LC neurons via G_s-dependent activation of sodium current (Wang and Aghajanian, 1990). Perfusion of VIP (0.5 μM, 5 min) increased the firing rate by 82.5 ± 16.6% (from 0.69 ± 0.09 Hz to 1.24 ± 0.16 Hz; n = 5, P < 0.05) (Figure 5A). In the presence of NF449, the VIP-induced excitatory effect was reduced by 53% (n = 5, P < 0.05 *vs*. control) (Figure 5A), which indicates that NF449 was readily blocking the $G_{\alpha s}$-dependent signaling. However, unlike VIP, the excitatory effect of butaprost (1 μM) was not modified in the presence of NF449 (n = 6, P > 0.05 *vs*. control; Figure 5A). This result indicates that the effect of butaprost on LC neurons does not appear to require the $G_{\alpha s}$ signaling proteins. On the other hand, slice incubation with the $G_{\beta\gamma}$-signaling inhibitor gallein

(20 μM, 120 min) reduced the basal firing rate of LC neurons compared to baseline in controls before the administration of butaprost (0.85 ± 0.09 Hz in controls *vs*. 0.47 ± 0.10 Hz after gallein incubation; $n = 7$, $P < 0.05$) and reduced to nearly the half the excitatory effect of butaprost (1 μM) ($n = 7$, $P < 0.05$ *vs*. control; Figure 5B). In light of these results, the $G_{\beta\gamma}$ subunits may be involved in the excitatory effect induced by the EP2 receptor agonist butaprost on LC neurons.

Finally, to investigate whether a presynaptic mechanism could be involved in the excitatory effect of butaprost on the LC, we blocked the main inhibitory and excitatory receptors regulating the firing rate of LC cells: GABA and glutamate receptors. Perfusion with a combination of the $GABA_A$ channel blocker picrotoxin (100 μM), the non-NMDA receptor antagonist CNQX (30 μM), the NMDA receptor antagonist d-AP5 (100 μM), and the metabotropic receptor antagonist RS-MCPG (500 μM) increased the activity of noradrenergic cells by 110 ± 14.3% (from 0.69 ± 0.10 Hz to 1.41 ± 0.14 Hz; $n = 6$, $P < 0.05$), as previously described (Mendiguren and Pineda, 2007). However, blockade of presynaptic mechanisms did not reduce the excitation caused by butaprost (1 μM) but further potentiated it ($n = 6$, $P < 0.05$; Figure 5C). Thus, these results suggest that the butaprost-induced excitatory effect on LC neurons is not caused by presynaptic EP2 receptors.

Discussion

Our study was aimed to pharmacologically characterize the EP2 receptor in LC neurons from rat brain slices by extracellular electrophysiological techniques. We found that the EP2 receptor agonists butaprost and treprostinil increase the firing activity of LC neurons *in vitro*. This excitatory effect was blocked by the EP2 receptor antagonist PF-04418948, but not by the EP3 or EP4 receptor antagonists (L-798,106 and L-161,982, respectively), indicating that it was mediated by EP2 receptor activation. The butaprost-induced increase in the firing rate of LC cells was prevented in the presence of low sodium-containing aCSF and the $G_{\beta\gamma}$-signaling inhibitor gallein. However, blockers of the $G_{\alpha s}$/cAMP/PKA pathway or TRP and Kir6.2 channels failed to change the butaprost-induced stimulatory effect. These results suggest that activation of the EP2 receptor stimulates the neuronal activity of LC cells, presumably by its coupling to $G_{\beta\gamma}$ proteins and an inward sodium current.

In our study, we assessed the functional role of EP2 receptors in LC neurons by using extracellular electrophysiology *in vitro* and application of EP2 receptor agonists. Butaprost was selected as an EP2 receptor agonist since its free acid form shows an 18-fold higher affinity for the EP2 than for the EP3 receptor (Abramovitz et al., 2000) and has been previously used at similar concentrations to explore EP2 receptors in brain slices (Liu et al., 2005). We also assessed the effect of treprostinil, a clinically used PGI_2 analog that has high affinity for several prostanoid receptors, especially high for the EP2 receptor (EP2=DP1>IP>EP1>EP4>EP3) (Whittle et al., 2012). On the other hand, we used PF-04418948 as EP2 receptor antagonist since it has very low affinity for any other prostanoid receptor (Forselles et al., 2011). L-161,982 has much higher affinity for the EP4 than for EP3 receptors (Machwate et al., 2001), while L-798,106 shows higher affinity for the EP3 than for the EP4 or other EP receptors (Su et al., 2008).

In the current study, butaprost and treprostinil increased the neuronal activity of LC cells and generated similar parameters of the concentration-effect curves (EC_{50} and Emax), suggesting equivalent efficacy and potency in the LC. Furthermore, the EC_{50} of the concentration-effect curve for butaprost was in accordance with that found in other systems (0.64 μM) (Fu et al., 2015). In our work, the excitatory effect caused by butaprost and treprostinil was blocked by PF-04418948, and not by L-798,106 or L-161,982. In fact, PF-04418948 displaced to the right the concentration-effect curve for butaprost, whereas it reduced the Emax for treprostinil without any rightward shift. This difference could be explained by additional activation of other receptors or mechanisms by treprostinil, such as the phylogenetically related G_s-coupled DP1 receptor (Daiyasu et al., 2011; Whittle et al., 2012). However, the blockade of the treprostinil-induced effect with PF-04418948 supports the involvement of, at least, the EP2 receptor. Alternatively, one could speculate that a slow dissociation rate of PF-04418948 from the EP2 receptor and a higher receptor reserve (Kenakin et al., 2006) for butaprost than for treprostinil could account for the differences observed with butaprost and treprostinil in the presence of PF-04418948. In any case, the calculated pK_B of PF-04418948 for the EP2 receptor was equivalent when obtained by butaprost or by treprostinil. Furthermore, similar pK_B values for PF-04418948 are obtained when PGE_2 is used in other tissues (Forselles et al., 2011). These data indicate that the excitatory effect observed with butaprost and treprostinil in LC neurons was mediated by EP2 receptor activation.

EP2 receptor activation in neurons has been described to elicit a sodium current through the cAMP/PKA pathway (Fang et al., 2011). In our work, the butaprost-induced excitatory effect was completely abolished by replacement of 80% of the extracellular sodium by TRIS, indicating the involvement of sodium current. In agreement, PGE_2 elicits a sodium current in cerebellar (Fang et al., 2011) and spinal neurons (Baba et al., 2001), leading to neuronal depolarization in the latter case. In the LC, sodium currents could be generated by TRP channels, as previously reported in response to CO_2 (Cui et al., 2011). In our study, perfusion with the non-selective TRP channel blocker 2-APB at concentrations previously used in other brain regions *in vitro* (Song et al., 2016) failed to change the butaprost-induced excitatory effect. On the other hand, inhibition of Kir6.2 channels has been shown to contribute to excitatory responses in LC neurons, which could be hindered by the Kir6.2 channel blocker glibenclamide (Ugedo et al., 1998). However, in our study, glibenclamide did not affect the butaprost-induced excitatory response. Therefore, our data indicate that sodium current is a final downstream effector of EP2 receptor activation, and Kir6.2 or TRP channels do not seem to be involved in this effect.

In LC noradrenergic neurons, inward sodium currents are activated by the cAMP/PKA pathway (Wang and Aghajanian, 1987). In our research, the butaprost-induced excitatory effect was not mediated by the cAMP/PKA/HCN pathway as the PKA activator 8-Br-cAMP, the PKA inhibitor H-89 or the HCN channel blocker ZD7288 failed to modify the stimulatory effect caused by butaprost. Our results contrast with the main signaling mechanism described for excitatory responses mediated by EP2 receptors in other brain regions. Thus, PGE_2 increases the hypothalamic neuronal activity (Clasadonte et al., 2011) and hippocampal synaptic transmission (Sang et al., 2005) via EP2 receptor-mediated activation of the cAMP/PKA pathway. However, other authors have previously suggested that cAMP/PKA/HCN is not involved in EP2 receptor-mediated responses. Thus, in nodose ganglion neurons, PGE_2 elicits a sodium current by EP2 receptors without the intervention of the cAMP/PKA pathway (Matsumoto et al., 2005).

The EP2 receptor has been published to be coupled to G_s proteins (Yano et al., 2017). However, NF449, a selective inhibitor of the association between $G_{\alpha s}$ and GTP (Hohenegger et al., 1998), failed to reduce the butaprost-induced excitation, while it blocked the effect of VIP, which increases the firing rate of LC cells by a $G_{\alpha s}$/cAMP/PKA-dependent sodium current (Wang and Aghajanian, 1990). This means that butaprost effect is not mediated by $G_{\alpha s}$ proteins. On the

other hand, the excitation caused by butaprost was prevented by the $G_{\beta\gamma}$-signaling inhibitor gallein, which binds to the "hot spot" of the G_{β} subunit (Lehmann et al., 2008). In our study, gallein did not modify the inhibitory effect of the μ opioid receptor agonist ME on the LC, which is mediated by $G_{i/o}$ protein βγ subunits (Connor and Christie, 1999). Likewise, other authors have described that a gallein analog fails to affect $G_{i/o}$ protein βγ-mediated effects in other systems (Casey et al., 2010), suggesting diversity and selectivity of the $G_{\beta\gamma}$ subunits for different downstream signaling mechanisms. Furthermore, direct binding of $G_{\beta\gamma}$ subunits to voltage-gated sodium channels (Na_v) have been reported in cell cultures (Ma et al., 1997; Mantegazza et al., 2005). In LC neurons, tetrodotoxin (TTX)-sensitive Na_v contribute to the pacemaker activity (de Oliveira et al., 2010), although a TTX-resistant current has also been described (de Oliveira et al., 2010). Furthermore, EP2 receptor activation has been associated with the enhancement of TTX-resistant sodium current in ganglion neurons (Matsumoto et al., 2005). However, in our study, we cannot conclude that the Na_v channel mediates the effect of EP2 receptors on sodium currents and whether it is directly modulated by EP2 receptor-activated $G_{\beta\gamma}$ subunits.

Finally, in our research, blockade of GABAergic or glutamatergic transmission in the LC did not decrease but rather enhanced the butaprost-induced stimulatory effect. These results are congruent with the presence of EP2 receptors enhancing inhibitory GABAergic regulation of noradrenergic cells or glutamatergic afferents, which blockade would increase the butaprost-induced excitatory effect. However, the neuronal subpopulation expressing EP2 receptors is yet to be characterized in the brain.

In conclusion, our work supports the existence of functional postsynaptic EP2 receptors in LC neurons, which activation results in a concentration-dependent increase of the spontaneous firing rate *in vitro*. The underlying mechanism may require $G_{\beta\gamma}$ subunits and sodium currents, but it does not involve a $G_{\alpha s}$, TRP, or cAMP/PKA-dependent pathway. According to previous data from our laboratory, the endogenous PGE_2 has a preferential inhibitory effect on LC neurons mediated by EP3 receptor activation (Nazabal et al., unpublished results), and herein, we demonstrate the functional role of EP2 receptors in the regulation of the firing rate. Since the LC has been shown to contribute to the affective processing of nociception by promoting anxiogenic-like behavior during chronic pain (Alba-Delgado et al., 2013), EP2 receptor activation in the LC may be of relevance in the integration of pain stimuli by enhancing NA release throughout the CNS. This suggestion is supported by the cognitive impairment

observed in mice lacking the EP2 receptor (Savonenko et al., 2009). Furthermore, both β-adrenoreceptor and EP2 receptor activation elicit anti-inflammatory effects in microglial cells (Heneka et al., 2010; Bonfill-Teixidor et al., 2017). Therefore, it may be reasonable to suggest that the EP2 receptor in the LC could further tune the inflammatory response to PGE_2 in the brain. An immunomodulatory effect of EP2 receptors may be relevant for the pathophysiology of Alzheimer's disease, and the prevention of neuronal death upon amyloid β-peptide exposure (Echeverria et al., 2005). Consequently, the EP2 receptor signaling in the LC could become a novel therapeutic target for pain and neuroinflammatory diseases.

Author contributions

A. N. performed the electrophysiological assays and wrote the first draft of the manuscript. A. M. and J.P. conceived and designed the study and wrote the manuscript.

References

Abramovitz, M., Adam, M., Boie, Y., Carrière, M.C., Denis, D., Godbout, C., et al. (2000). The utilization of recombinant prostanoid receptors to determine the affinities and selectivities of prostaglandins and related analogs. Biochim. Biophys. Acta - Mol. Cell Biol. Lipids *1483*: 285–293.

Alba-Delgado, C., Llorca-Torralba, M., Horrillo, I., Ortega, J.E., Mico, J.A., Sánchez-Blázquez, P., et al. (2013). Chronic pain leads to concomitant noradrenergic impairment and mood disorders. Biol. Psychiatry *73*: 54–62.

Alexander, S.P.H., Christopoulos, A., Davenport, A.P., Kelly, E., Marrion, N. V., Peters, J.A., et al. (2017). THE CONCISE GUIDE TO PHARMACOLOGY 2017/18: G protein-coupled receptors. Br. J. Pharmacol. *174*: S17–S129.

Alreja, M., and Aghajanian, G.K. (1993). Opiates suppress a resting sodium-dependent inward current and activate an outward potassium current in locus coeruleus neurons. J. Neurosci. *13*: 3525–3532.

Andrade, R., and Aghajanian, G.K. (1984). Locus coeruleus activity in vitro: intrinsic regulation by a calcium-dependent potassium conductance but not alpha 2-adrenoceptors. J. Neurosci. *4*: 161–170.

Aston-Jones, G., Ennis, M., Pieribone, V.A., Nickell, W.T., and Shipley, M.T. (1986). The brain nucleus locus coeruleus: restricted afferent control of a broad efferent network. Science *234*: 734–7.

Baba, H., Baba, H., Kohno, T., Kohno, T., Moore, K. a, Moore, K. a, et al. (2001). Direct activation of rat spinal dorsal horn neurons by prostaglandin E2. J. Neurosci. *21*: 1750–6.

Bonfill-Teixidor, E., Otxoa-de-Amezaga, A., Font-Nieves, M., Sans-Fons, M.G., and Planas, A.M. (2017). Differential expression of E-type prostanoid receptors 2 and 4 in microglia stimulated with lipopolysaccharide. J. Neuroinflammation *14*: 3.

Casey, L.M., Pistner, A.R., Belmonte, S.L., Migdalovich, D., Stolpnik, O., Nwakanma, F.E., et al. (2010). Small molecule disruption of Gβγ signaling inhibits the progression of heart failure. Circ. Res. *107*: 532–539.

Chen, C., and Bazan, N.G. (2005). Endogenous PGE2 regulates membrane excitability and

synaptic transmission in hippocampal CA1 pyramidal neurons. J. Neurophysiol. *93*: 929–941.

Clasadonte, J., Poulain, P., Hanchate, N.K., Corfas, G., Ojeda, S.R., and Prevot, V. (2011). Prostaglandin E2 release from astrocytes triggers gonadotropin-releasing hormone (GnRH) neuron firing via EP2 receptor activation. Proc. Natl. Acad. Sci. *108*: 16104–16109.

Connor, M., and Christie, M.J. (1999). Opioid Receptor Signalling Mechanisms. Clin Exp Pharmacol Physiol. *26*: 493–499.

Cui, N., Zhang, X., Tadepalli, J.S., Yu, L., Gai, H., Petit, J., et al. (2011). Involvement of TRP channels in the CO 2 chemosensitivity of locus coeruleus neurons. J Neurophysiol *105*: 2791–2801.

Curtis, M.J., Alexander, S., Cirino, G., Docherty, J.R., George, C.H., Giembycz, M.A., et al. (2018). Experimental design and analysis and their reporting II: updated and simplified guidance for authors and peer reviewers. Br. J. Pharmacol. *175*: 987–993.

Daiyasu, H., Hirokawa, T., Kamiya, N., and Toh, H. (2011). Computational analysis of ligand recognition mechanisms by prostaglandin E2 (subtype 2) and D2 receptors. Theor. Chem. Acc. *130*: 1131–1143.

Echeverria, V., Clerman, A., and Doré, S. (2005). Stimulation of PGE2 receptors EP2 and EP4 protects cultured neurons against oxidative stress and cell death following β-amyloid exposure. Eur. J. Neurosci. *22*: 2199–2206.

Ek, M., Arias, C., Sawchenko, P., and Ericsson-Dahlstrand, A. (2000). Distribution of the EP3 prostaglandin E2 receptor subtype in the rat brain: Relationship to sites of interleukin-1 - Induced cellular responsiveness. J. Comp. Neurol. *428*: 5–20.

Emery, E.C., Young, G.T., Berrocoso, E.M., Chen, L., and McNaughton, P.A. (2011). HCN2 ion channels play a central role in inflammatory and neuropathic pain. Science (80-.). *333*: 1462–6.

Fang, Y.-J., Zhou, M.-H., Gao, X.-F., Gu, H., and Mei, Y.-A. (2011). Arachidonic acid modulates Na + currents by non-metabolic and metabolic pathways in rat cerebellar granule cells. Biochem. J. *438*: 203–215.

Forselles, K.J., Root, J., Clarke, T., Davey, D., Aughton, K., Dack, K., et al. (2011). In vitro and in vivo characterization of PF-04418948, a novel, potent and selective prostaglandin EP2

receptor antagonist. Br. J. Pharmacol. *164*: 1847–56.

Fu, Y., Yang, M.-S., Jiang, J., Ganesh, T., Joe, E., and Dingledine, R. (2015). EP2 receptor signaling regulates microglia death. Mol. Pharmacol. *88*: 161–170.

Grzelka, K., Kurowski, P., Gawlak, M., and Szulczyk, P. (2017). Noradrenaline Modulates the Membrane Potential and Holding Current of Medial Prefrontal Cortex Pyramidal Neurons via β1-Adrenergic Receptors and HCN Channels. Front. Cell. Neurosci. *11*: 1–22.

Harding, S., Sharman, J., Faccenda, E., Southan, C., Pawson, A., Ireland, S., et al. (2018). The IUPHAR/BPS Guide to PHARMACOLOGY in 2018: updates and expansion to encompass the new guide to IMMUNOPHARMACOLOGY. Nucleic Acids Res. *46*: D1091–D1106.

Heneka, M.T., Nadrigny, F., Regen, T., Martinez-Hernandez, A., Dumitrescu-Ozimek, L., Terwel, D., et al. (2010). Locus ceruleus controls Alzheimer's disease pathology by modulating microglial functions through norepinephrine. Proc. Natl. Acad. Sci. *107*: 6058–6063.

Hétu, P.-O., and Riendeau, D. (2005). Cyclo-oxygenase-2 contributes to constitutive prostanoid production in rat kidney and brain. Biochem. J. *391*: 561–566.

Hohenegger, M., Waldhoer, M., Beindl, W., Bing, B., Kreimeyer, A., Nickel, P., et al. (1998). G salpha-selective G protein antagonists. Pharmacology *95*: 346–351.

Jolas, T., Nestler, E.J., and Aghajanian, G.K. (2000). Chronic morphine increases GABA tone on serotonergic neurons of the dorsal raphe nucleus: Association with an up-regulation of the cyclic AMP pathway. Neuroscience *95*: 433–443.

Kenakin, T., Jenkinson, S., and Watson, C. (2006). Determining the potency and molecular mechanism of action of insurmountable antagonists. J. Pharmacol. Exp. Ther. *319*: 710–723.

Kilkenny, C., Browne, W., Cuthill, I.C., Emerson, M., and Altman, D.G. (2010). Animal research: Reporting in vivo experiments: The ARRIVE guidelines. Br. J. Pharmacol. *160*: 1577–1579.

Kurowski, P., Gawlak, M., and Szulczyk, P. (2015). Muscarinic receptor control of pyramidal neuron membrane potential in the medial prefrontal cortex (mPFC) in rats. Neuroscience *303*: 474–488.

Lazareno, S., and Birdsall, N.J.M. (1993). Estimation of competitive antagonist affinity from

functional inhibition curves using the Gaddum Schild and Cheng-Prusoff equations. Br. J. Pharmacol. *109*: 1110–1119.

Lehmann, D., Seneviratne, A., and Smrcka, A. (2008). Small molecule disruption of G protein βγ subunit signaling inhibits neutrophil chemotaxis and inflammation. Mol. Pharmacol. *73*: 410–418.

Liu, D., Wu, L., Breyer, R., Mattson, M.P., and Andreasson, K. (2005). Neuroprotection by the PGE2 EP2 receptor in permanent focal cerebral ischemia. Ann. Neurol. *57*: 758–761.

Ma, J.Y., Catterall, W.A., and Scheuer, T. (1997). Persistent sodium currents through brain sodium channels induced by G protein βγ subunits. Neuron *19*: 443–452.

Machwate, M., Harada, S., Leu, C.T., Seedor, G., Labelle, M., Gallant, M., et al. (2001). Prostaglandin receptor EP(4) mediates the bone anabolic effects of PGE(2). Mol. Pharmacol. *60*: 36–41.

Mantegazza, M., Yu, F.H., Powell, A.J., Clare, J.J., Catterall, W.A., and Scheuer, T. (2005). Molecular Determinants for Modulation of Persistent Sodium Current by G-Protein βγ Subunits. J. Neurosci. *25*: 3341–3349.

Matsumoto, S., Ikeda, M., Yoshida, S., Tanimoto, T., Takeda, M., and Nasu, M. (2005). Prostaglandin E2-induced modification of tetrodotoxin-resistant Na+ currents involves activation of both EP2 and EP4 receptors in neonatal rat nodose ganglion neurones. Br. J. Pharmacol. *145*: 503–13.

McGrath, J.C., and Lilley, E. (2015). Implementing guidelines on reporting research using animals (ARRIVE etc.): New requirements for publication in BJP. Br. J. Pharmacol. *172*: 3189–3193.

Medrano, M.C., Santamarta, M.T., Pablos, P., Aira, Z., Buesa, I., Azkue, J.J., et al. (2017). Characterization of functional μ opioid receptor turnover in rat locus coeruleus: an electrophysiological and immunocytochemical study. Br. J. Pharmacol. *174*: 2758–2772.

Mendiguren, A., and Pineda, J. (2007). CB1 cannabinoid receptors inhibit the glutamatergic component of KCl-evoked excitation of locus coeruleus neurons in rat brain slices. Neuropharmacology *52*: 617–625.

Momin, A., Cadiou, H., Mason, A., and McNaughton, P. a. (2008). Role of the

hyperpolarization-activated current I h in somatosensory neurons. J. Physiol. *586*: 5911–5929.

Oliveira, R. de, Howlett, M., Gravina, F., Imtiaz, M., Callister, R., Brichta, A., et al. (2010). Pacemaker Currents in Mouse Locus Coeruleus Neurons. Neuroscience *170*: 166–177.

Pineda, J., Kogan, J.H., and Aghajanian, G.K. (1996). Nitric oxide and carbon monoxide activate locus coeruleus neurons through a cGMP-dependent protein kinase: involvement of a nonselective cationic channel. J. Neurosci. *16*: 1389–99.

Sang, N., Zhang, J., Marcheselli, V., Bazan, N.G., and Chen, C. (2005). Postsynaptically synthesized prostaglandin E2 (PGE2) modulates hippocampal synaptic transmission via a presynaptic PGE2 EP2 receptor. J. Neurosci. *25*: 9858–70.

Santin, J.M., and Hartzler, L.K. (2015). Activation state of the hyperpolarization-activated current modulates temperature-sensitivity of firing in locus coeruleus neurons from bullfrogs. Am. J. Physiol. - Regul. Integr. Comp. Physiol. *308*: R1045–R1061.

Savonenko, A., Munoz, P., Melnikova, T., Wang, Q., Liang, X., Breyer, R.M., et al. (2009). Impaired cognition, sensorimotor gating, and hippocampal long-term depression in mice lacking the prostaglandin E2 EP2 receptor. Exp. Neurol. *217*: 63–73.

Song, K., Wang, H., Kamm, G.B., Pohle, J., Castro Reis, F. De, Heppenstall, P., et al. (2016). The TRPM2 channel is a hypothalamic heat sensor that limits fever and can drive hypothermia. Science (80-.). *353*: 1393–1398.

Su, X., Leon, L. a, Wu, C.W., Morrow, D.M., Jaworski, J.-P., Hieble, J.P., et al. (2008). Modulation of bladder function by prostaglandin EP3 receptors in the central nervous system. Am. J. Physiol. Renal Physiol. *295*: F984-94.

Ugedo, L., Pineda, J., Ruiz-Ortega, J.A., and Martin-Ruiz, R. (1998). Stimulation of locus coeruleus neurons by non-I1/I2-type imidazoline receptors: an in vivo and in vitro electrophysiological study. Br J Pharmacol *125*: 1685–1694.

Wang, Y.Y., and Aghajanian, G.K. (1987). Excitation of Locus Coeruleus Neurons by an Adenosine 3′,5′-Cyclic Monophosphate-Activated Inward Current: Extracellular and Intracellular Studies in Rat Brain Slices. Synapse *1*: 481–487.

Wang, Y.Y., and Aghajanian, G.K. (1990). Excitation of locus coeruleus neurons by vasoactive intestinal peptide: role of a cAMP and protein kinase A. J. Neurosci. *10*: 3335–3343.

Whittle, B.J., Silverstein, A.M., Mottola, D.M., and Clapp, L.H. (2012). Binding and activity of the prostacyclin receptor (IP) agonists, treprostinil and iloprost, at human prostanoid receptors: Treprostinil is a potent DP 1 and EP 2 agonist. Biochem. Pharmacol. *84*: 68–75.

Xu, S., Guo, S., Jiang, X., Yin, Q., Umezawa, T., and Hisamitsu, T. (2003). Effect of indomethacin on the c-fos expression in AVP and TH neurons in rat brain induced by lipopolysaccharide. Brain Res. *966*: 13–8.

Yamaguchi, N., and Okada, S. (2009). Cyclooxygenase-1 and -2 in spinally projecting neurons are involved in CRF-induced sympathetic activation. Auton. Neurosci. Basic Clin. *151*: 82–89.

Yano, A., Takahashi, Y., Moriguchi, H., Inazumi, T., Koga, T., Otaka, A., et al. (2017). An aromatic amino acid within intracellular loop 2 of the prostaglandin EP2 receptor is a prerequisite for selective association and activation of Gαs. Biochim. Biophys. Acta - Mol. Cell Biol. Lipids *1862*: 615–622.

Yasojima, K., Schwab, C., McGeer, E.G., and McGeer, P.L. (1999). Distribution of cyclooxygenase-1 and cyclooxygenase-2 mRNAs and proteins in human brain and peripheral organs. Brain Res. *830*: 226–236.

Zhang, J., and Rivest, S. (1999). Distribution, regulation and colocalization of the genes encoding the EP 2 - and EP 4 -PGE 2 receptors in the rat brain and neuronal responses to systemic inflammation. Eur. J. Neurosci. *11*: 2651–2668.

Zolles, G., Klöcker, N., Wenzel, D., Weisser-Thomas, J., Fleischmann, B.K., Roeper, J., et al. (2006). Pacemaking by HCN Channels Requires Interaction with Phosphoinositides. Neuron *52*: 1027–1036.

Tables

Table 1. Basal firing rate and concentration-effect curve parameters for the excitatory action of the EP2 receptor agonists butaprost and treprostinil on LC neurons in the absence (control) or in the presence of the EP2 (PF-04418948) or a combination of the EP3 (L-798,106) and EP4 (L-161,982) receptor antagonists.

			Concentration-effect curves[1]				
Drugs	Concentration	Basal firing rate (Hz)	Emax (%)	pEC_{50} (M)	(EC_{50}, μM)	Slope factor	*n*
Butaprost							
Control		0.85 ± 0.09	74.3 ± 11.6	6.35 ± 0.10	(0.45)	1.65 ± 0.41	8
+PF-04418948	3 nM	0.87 ± 0.12	82.1 ± 18.4	5.98 ± 0.15	(1.05)	1.55 ± 0.30	5
	10 nM	0.73 ± 0.08	105 ± 15	5.57 ± 0.08*	(2.67)	1.55 ± 0.41	6
+L-798,106	10 nM						
L-161,982	10 nM	0.67 ± 0.11	135 ± 29	6.25 ± 0.07	(0.56)	1.27 ± 0.14	5
Treprostinil							
Control		0.68 ± 0.07	81.3 ± 6.5	6.27 ± 0.15	(0.54)	0.95 ± 0.12	6
+PF-04418948	10 nM	0.78 ± 0.13	42.8 ± 8.1*	6.55 ± 0.19	(0.28)	1.29 ± 0.34	6
+L-798,106	10 nM						
L-161,982	10 nM	0.80 ± 0.12	144 ± 8*	6.34 ± 0.12	(0.46)	1.20 ± 0.09	5

[1]Values are expressed as mean ± SEM obtained by nonlinear regression of *n* cells. Emax is the maximal excitatory effect, and pEC_{50} is the negative logarithm of the concentration needed to elicit a 50% of the Emax. *$P < 0.05$ when compared to their respective control group (one-way ANOVA followed by a Dunnett's *post hoc* test).

Figure legends

Figure 1. Effect of the EP2 receptor agonist butaprost on the firing rate of LC neurons in the absence or presence of the EP2 receptor antagonist PF-04418948 or a combination of the EP3 receptor antagonist L-798,106 and EP4 receptor antagonist L-161,982. **(A, B, C)** Representative examples of firing rate recordings of LC neurons showing the effect of increasing concentrations of butaprost in the absence **(A)** and presence of PF-04418948 (10 nM) **(B)** or presence of L-798,106 and L-161,982 (10 nM each) **(C)**. The vertical lines represent the number of spikes recorded every 10 s and the horizontal bars the period of drug application. **(D)** Concentration-effect curves for butaprost in control (filled circles) and in the presence of PF-04418948 (3 nM, open squares or 10 nM, filled squares) (left) or in the presence of L-798,106 and L-161,982 (10 nM each, open diamonds) (right). The horizontal axis shows the butaprost concentration on a semi-logarithmic scale. The vertical axis expresses the increase in firing rate of LC neurons as the percentage of the baseline. Data points are the mean ± SEM at each butaprost concentration obtained from *n* number of experiments (see Table 1). The lines through the data are the theoretical curves in each group constructed from the mean of the individual concentration-effect curve parameters, as estimated by nonlinear regressions. Note that the concentration-effect curve for butaprost is shifted to the right by the EP2 receptor antagonist.

Figure 2. Effect of the EP2 receptor agonist treprostinil on the firing rate of LC neurons in the absence or presence of the EP2 receptor antagonist PF-04418948 or a combination of the EP3 receptor antagonist L-798,106 and the EP4 receptor antagonist L-161,982. **(A, B, C)** Representative examples of firing rate recordings of LC neurons showing the effect of increasing concentrations of treprostinil in the absence **(A)** and presence of PF-04418948 (10 nM) **(B)** or presence of L-798,106 and L-161,982 (10 nM each) **(C)**. The vertical lines represent the number of spikes recorded every 10 s and the horizontal bars the period of drug application. **(D)** Concentration-effect curves for treprostinil in control (filled circles) and in the presence of PF-04418948 (10 nM, filled squares) (left) or in the presence of L-798,106 and L-161,982 (10 nM each, open diamonds) (right). The horizontal axis shows the treprostinil concentration on a semi-logarithmic scale. The vertical axis expresses the increase in firing rate of LC neurons as the percentage of the baseline. Data points are the mean ± SEM at each treprostinil concentration obtained from *n* number of experiments (see Table 1). The lines through the data are the theoretical curves in each group constructed from the mean of the individual concentration-effect curve parameters, as estimated by nonlinear

regressions. Note that the Emax of treprostinil decreases in the presence of the EP2 receptor antagonist.

Figure 3. Effect of cationic current blockers on the butaprost-induced excitatory effect on LC neurons. **(A)** Representative example of the firing rate recording of an LC neuron showing the effect of butaprost (1 μM, 15 min) in the presence of low-sodium aCSF (TRIS 80%, 5 min). The vertical lines represent the number of spikes recorded every 10 s and the horizontal bars the period of drug application. Note that TRIS 80% abolishes the stimulatory effect of butaprost. **(B, C)** Bar graphs showing the excitatory effect of butaprost (1 μM, 15 min) as the increase in the number of spikes per 10 s in the absence (control) and in the presence of TRIS 80% (n = 7) **(B)** or 2-APB (30 μM, black bar) or glibenclamide (3 μM, hatched bar) (both n = 5) **(C)**. Bars are the mean ± SEM of n experiments. *$P < 0.05$ when compared to the control group (unpaired Student's t-test).

Figure 4. Effect of blocking the cAMP/PKA pathway and HCN channels on the butaprost-induced excitatory effect on LC neurons. **(A)** Representative example of the firing rate recording of an LC neuron showing the effect of butaprost (1 μM, 15 min) in the presence of 8-Br-cAMP (1 mM, 8 min). The vertical lines represent the number of spikes recorded every 10 s and the horizontal bars the period of drug application. Note that 8-Br-cAMP increases the spontaneous discharge of the LC neuron and that butaprost produce an additional stimulatory effect. **(B)** Bar graph showing the increase in the number of spikes per 10 s caused by butaprost (1 μM, white bar), 8-Br-cAMP (1 mM, black bar), butaprost in the presence of 8-Br-cAMP (hatched bar), and the arithmetic sum of the effects of butaprost and 8-Br-cAMP (black and white bar). Application of butaprost in the presence of 8-Br-cAMP further increased the excitatory effect caused by 8-Br-cAMP (paired Student's t-test). Note that application of 8-Br-cAMP does not occlude the excitatory response to butaprost since no difference was found between the effect of butaprost in the presence of 8-Br-cAMP and the sum of effects (unpaired Student's t-test). Bars are the mean ± SEM of n experiments. **(C)** Concentration-effect curves for butaprost in control (filled circles, n = 8) and in the presence of the PKA inhibitor H-89 (10 μM, open circles) or the HCN channel blocker ZD7288 (30 μM, open triangles). The horizontal axis shows the butaprost concentration on a semi-logarithmic scale. The vertical axis expresses the increase in firing rate of LC neurons as the percentage of the baseline. Data points are the mean ± SEM at each butaprost concentration

obtained from *n* number of experiments (*n* = 5 in all experimental groups). The lines through the data are the theoretical curves in each group constructed from the mean of the individual concentration-effect curve parameters, as estimated by nonlinear regressions.

Figure 5. Effect of blocking the $G_{\alpha s}$ and $G_{\beta\gamma}$-dependent signaling and the presynaptic afferences on the butaprost-induced excitatory effect on LC neurons. **(A, B)** Bar graphs showing the excitatory effect of butaprost (1 μM, 15 min) as the increase in the number of spikes per 10 s in the absence (control, *n* = 8) and in the presence of NF449 (10 μM, 30 min, *n* = 6) **(A)** or gallein (20 μM, 120 min, *n* = 7) **(B)**. VIP (0.5 μM, 5 min) was used as a positive control to demonstrate that NF449 was effectively blocking the $G_{\alpha s}$ subunits (both *n* = 5). **(C)** Bar graph showing the excitatory effect of butaprost in control (white bar) and after the administration of the synaptic blockers: Picrotoxin (100 μM), CNQX (30 μM), d-AP5 (100 μM), and RS-MCPG (500 μM) for 10 min (*n* = 6). Bars are the mean ± SEM of *n* experiments. **P* < 0.05 when compared to their respective control group (unpaired Student's t-test).

Figure 1

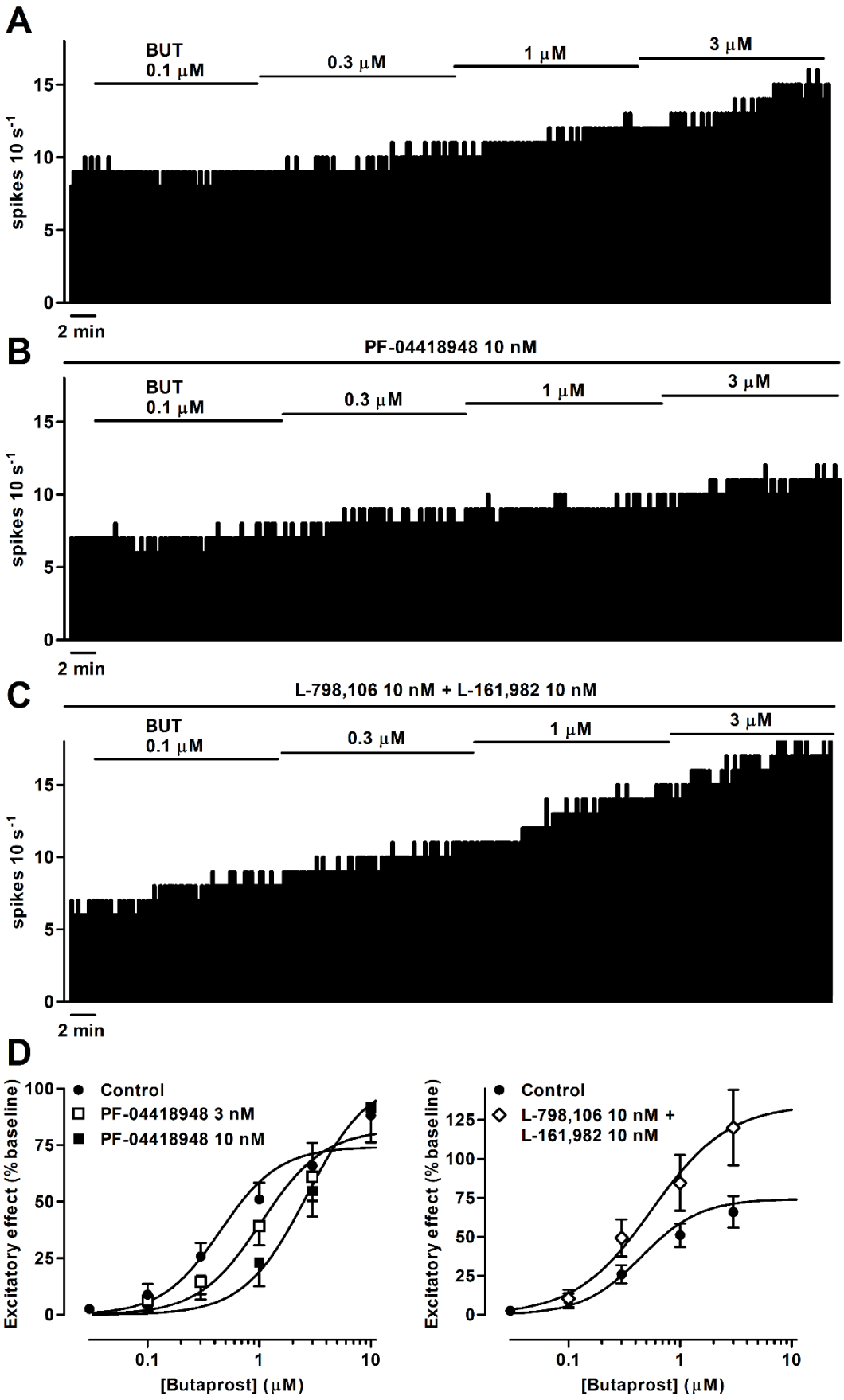
A
BUT
0.1 μM
0.3 μM
1 μM
3 μM
spikes 10 s-1
2 min
B
PF-04418948 10 nM
C
L-798,106 10 nM + L-161,982 10 nM
D
Control
PF-04418948 3 nM
PF-04418948 10 nM
Excitatory effect (% baseline)
[Butaprost] (μM)
L-798,106 10 nM +
L-161,982 10 nM

Figure 2

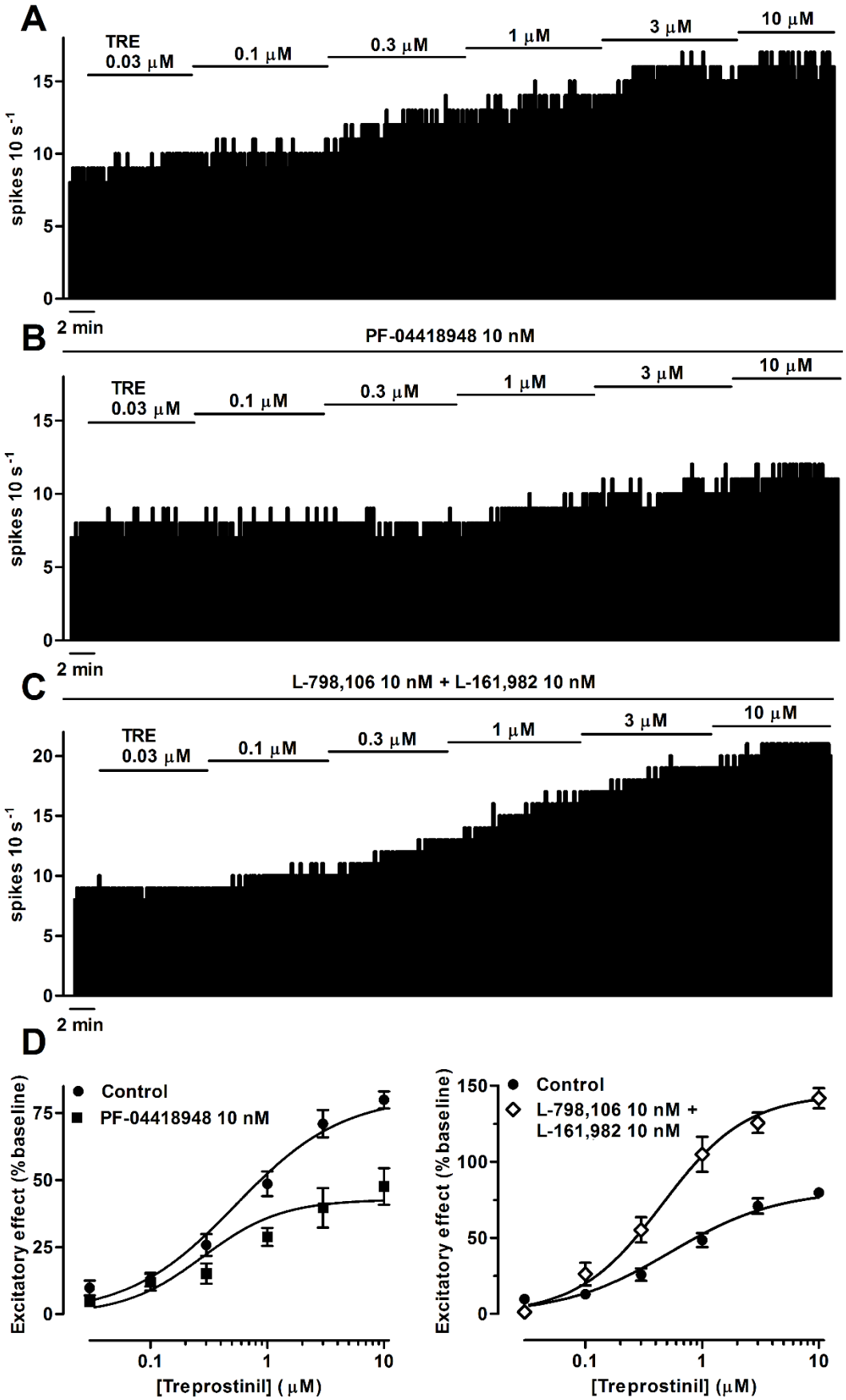
A
TRE
0.03 μM
0.1 μM
0.3 μM
1 μM
3 μM
10 μM
spikes 10 s-1
2 min
B
PF-04418948 10 nM
C
L-798,106 10 nM + L-161,982 10 nM
D
Control
PF-04418948 10 nM
Excitatory effect (% baseline)
[Treprostinil] (μM)
L-798,106 10 nM +
L-161,982 10 nM

Figure 3

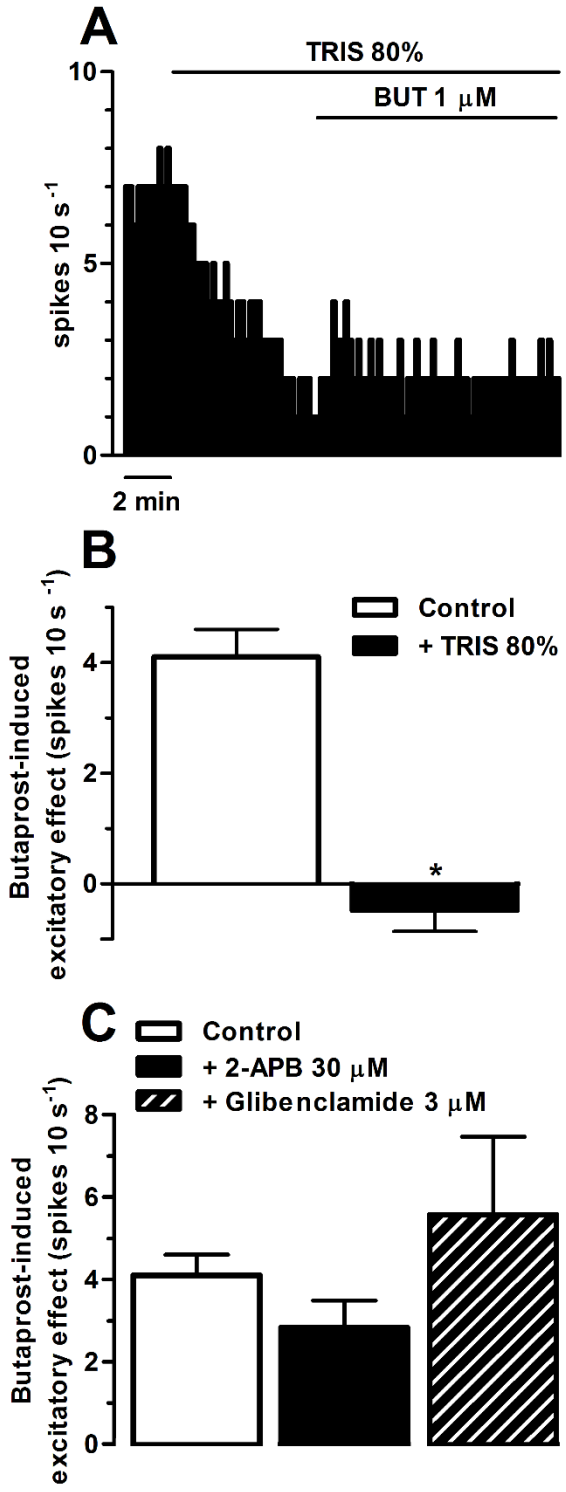
A
TRIS 80%
BUT 1 μM
spikes 10 s-1
10
5
0
2 min
B
Control
+ TRIS 80%
Butaprost-induced excitatory effect (spikes 10 s-1)
4
2
0
*
C
Control
+ 2-APB 30 μM
+ Glibenclamide 3 μM
Butaprost-induced excitatory effect (spikes 10 s-1)
8
6
4
2
0

Figure 4

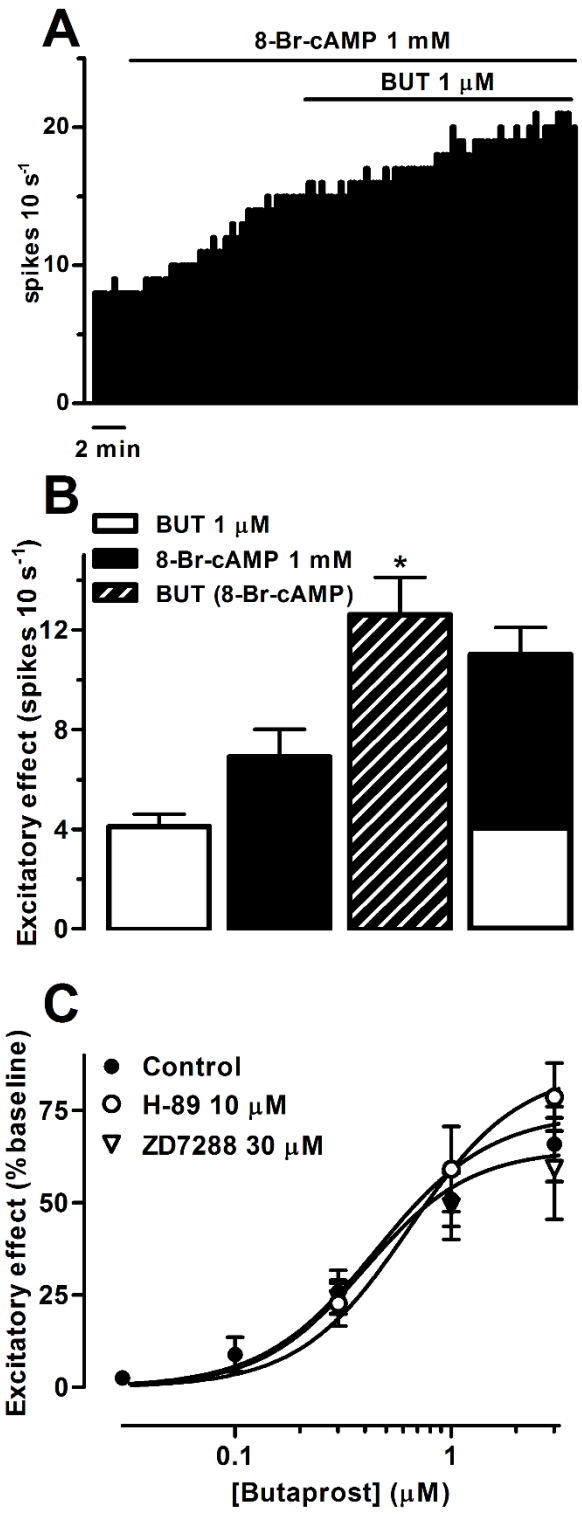
A
8-Br-cAMP 1 mM
BUT 1 μM
spikes 10 s-1
20
10
0
2 min
B
BUT 1 μM
8-Br-cAMP 1 mM
BUT (8-Br-cAMP)
*
Excitatory effect (spikes 10 s-1)
12
8
4
0
C
Control
H-89 10 μM
ZD7288 30 μM
Excitatory effect (% baseline)
75
50
25
0
0.1
1
[Butaprost] (μM)

Figure 5

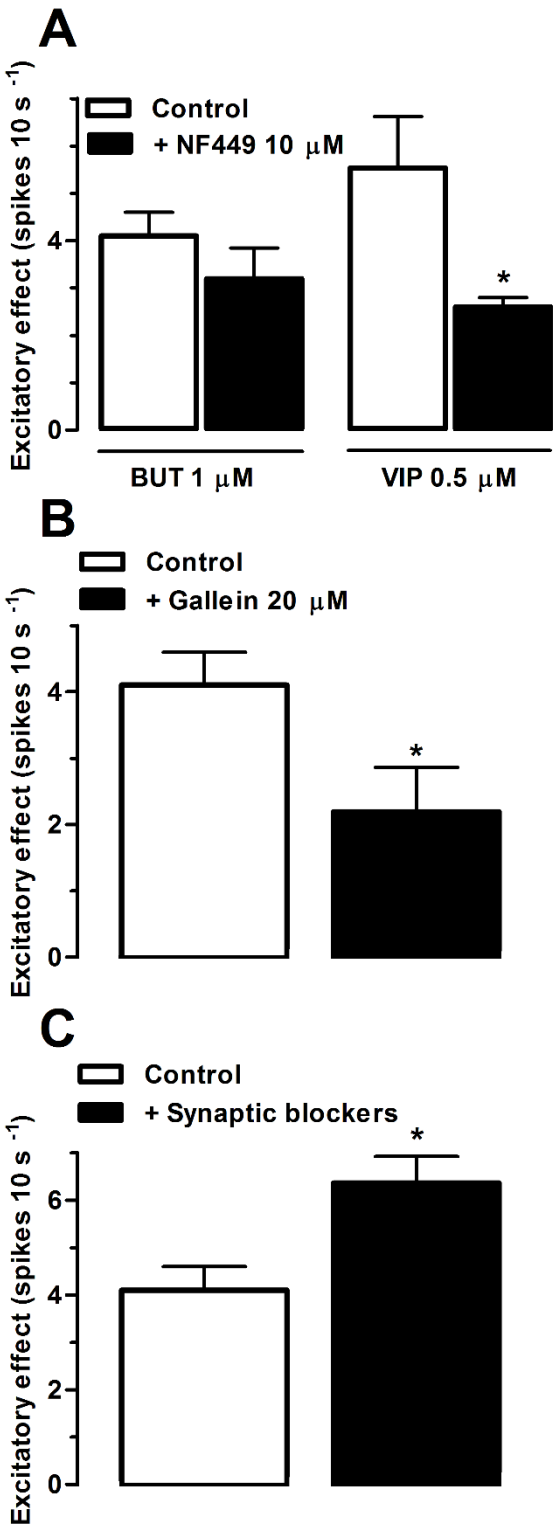
A
Control
+ NF449 10 μM
Excitatory effect (spikes 10 s -1)
0
4
*
BUT 1 μM
VIP 0.5 μM
B
Control
+ Gallein 20 μM
Excitatory effect (spikes 10 s -1)
0
2
4
*
C
Control
+ Synaptic blockers
Excitatory effect (spikes 10 s -1)
0
2
4
6
*

To be submitted to the *British Journal of Pharmacology*

TITLE:

Pharmacological characterization of prostanoid EP4 receptor in rat locus coeruleus neurons *in vitro*

RUNNING TITLE:

EP4 receptor in rat LC neurons

AUTHORS:

Amaia Nazabal, Aitziber Mendiguren and Joseba Pineda*

[1] Department of Pharmacology, Faculty of Medicine and Nursing, University of the Basque Country (UPV/ EHU), E-48940 Leioa, Bizkaia, Spain

***Corresponding author:**

Joseba Pineda. M.D., Ph.D.

Department of Pharmacology,

Faculty of Medicine and Nursing

University of the Basque Country (UPV/EHU)

Leioa Bizkaia, E-48940, Spain

E-mail address: joseba.pineda@ehu.eus (Dr. J. Pineda).

Tel: +34-946015577

Orcid ID: 0000-0002-9421-1081

Word count:

Abstract: 250	References: 59
Introduction: 479	Tables: 1
Results: 1868	Figures: 4
Discussion: 1620	

Acknowledgements

This work was supported by the Ministerio de Ciencia e Innovación [Grant SAF2008-03612] and the University of the Basque Country (UPV/EHU) [Grant GIU14/29]. Pineda´s research group takes part in a network unit supported by the University of the Basque Country [UFI 11/35]. A. Nazabal was supported by predoctoral fellowships from the Basque Government. The experiments comply with the current laws of Spain.

Conflict of interest

The authors declare that they have no conflict of interest.

Non-approved abbreviations

- aCSF: artificial cerebrospinal fluid
- DRG: dorsal root ganglion
- FR: firing rate
- LC: locus coeruleus
- ME: [Met]enkephalin
- NA: noradrenaline
- PGE_2: prostaglandin E_2

Bullet point summary (each bullet max. 15 words, max. 2 bullets per heading)

What is already known:

- PGE_2, an inflammatory mediator involved in pain and fever, modulates the activity of brain neurons
- EP2 and EP3 receptor activation regulates LC neuronal activity, which also expresses the EP4 receptor

What does this study add:

- EP4 receptor agonists stimulate the neuronal activity of LC noradrenergic cells *in vitro*
- EP4 receptor activation in LC neurons involves $G_{\alpha s}$ subunits and a sodium current

Clinical significance:

- The LC, the main noradrenergic nucleus, is susceptible to inflammatory mediators
- Prostanoid system in the LC might be a pharmacological target against inflammation-mediated neuropsychiatric processes

Abstract

BACKGROUND AND PURPOSE: The inflammatory mediator prostaglandin E_2 (PGE_2) inhibits locus coeruleus (LC) neurons *in vitro* via $G_{i/o}$-coupled EP3 receptors, and EP2 receptor activation excites LC neurons via $G_{\beta\gamma}$-signaling. The LC, the main noradrenergic nucleus in the brain, also expresses G_s-coupled EP4 receptors, which functional role is unknown. Thus, we aimed to characterize pharmacologically EP4 receptors in LC neurons.

EXPERIMENTAL APPROACH: We studied the effect of EP4 receptor agonists on the LC firing activity in rat brain slices by single-unit extracellular electrophysiology.

KEY RESULTS: EP4 receptor agonists rivenprost (0.01 nM–1 μM) and TCS 2510 (0.20 nM–2 μM) increased the firing rate of LC cells in a concentration-dependent manner (EC_{50}=1.43 nM and 18.0 nM; Emax=83.7% and 98.4%, respectively). EP4 receptor antagonist L-161,982 (30 and 300 nM), but not EP2 (PF-04418948, 300 nM) or EP3 receptor antagonists (L-798,106, 300 nM), hindered the excitatory effect caused by rivenprost and TCS 2510. Furthermore, extracellular sodium replacement and $G_{\alpha s}$ blockade (NF449, 10 μM) prevented the rivenprost-induced stimulation of neuronal activity. However, it was not attenuated by a PKA activator (8-Br-cAMP, 1 mM) or inhibitor (H-89, 10 μM), nor was it reduced by blockers of the PI3K (wortmannin, 100 nM), PKC (chelerythrine, 10 μM), and $G_{\beta\gamma}$ signaling (gallein, 20 μM). Furthermore, the rivenprost-induced stimulation was not occluded by the previous administration of butaprost (EP2 receptor agonist, 1 μM), suggesting different signaling pathways for EP2 and EP4 receptors.

CONCLUSIONS AND IMPLICATIONS: EP4 receptors activation excites LC noradrenergic neurons, seemingly through $G_{\alpha s}$-dependent activation of sodium current.

Keywords: locus coeruleus; PGE_2; EP4 receptor; prostanoid; firing; slice

Introduction

Prostaglandins, as inflammatory mediators are synthesized on demand from membrane phospholipids, which are transformed into arachidonic acid, and then into a common precursor by the rate-limiting enzyme cyclooxygenase (COX). Nonsteroidal anti-inflammatory drugs (NSAID) are commonly used as analgesic, antipyretic, and anti-inflammatory drugs act by preventing the synthesis of prostanoids by blocking the enzymatic activity of the COX. Despite the involvement of prostaglandins in inflammation, COX enzyme is found constitutively in the human and animal brain under non-inflammatory circumstances (Yasojima et al., 1999; Hétu and Riendeau, 2005), suggesting that the prostanoids may be playing a role under normal conditions. In line with this hypothesis, COX is detected in the soma and dendrites of neurons, indicating that the main final enzymatic product, the prostaglandin E_2 (PGE_2) may contribute to neuronal physiology. The PGE_2 exerts its actions by binding to G protein-coupled EP1-EP4 receptors (EP1 to G_q, EP2 and

EP4 to G_s, and EP3 to $G_{i/o}$). The EP2, EP3, and EP4 receptors are widely expressed in the CNS (Zhang and Rivest, 1999; Ek et al., 2000). In particular, high EP4 receptor expression levels have been found in the supraoptic nucleus of the hypothalamus, the cerebellum, and the locus coeruleus (LC), among other brain areas (Zhang and Rivest, 1999). However, in response to peripheral inflammation, its expression is upregulated in neurons from the dorsal root ganglion (DRG) (Lin et al., 2006) and brain catecholaminergic regions (Zhang and Rivest, 1999), where it may stimulate the neuronal activity (Zhang and Rivest, 1999). In fact, EP4 receptor activation excites supraoptic neurons (Shibuya et al., 2002) and results in membrane depolarization of preganglionic neurons (Miura et al., 2002). Furthermore, PGE_2 elicits a sodium current in ganglion (Matsumoto et al., 2005) and cerebellar neurons (Fang et al., 2011) via EP4 receptor activation.

The LC is the main source of noradrenaline (NA) in the brain and controls many physiological functions, including sleep-wake cycle, arousal, cognition, and pain. Some findings have associated the LC with the prostaglandin system. First, LC cells possess the enzymatic equipment to synthesize prostaglandins, as spinally-projecting LC neurons constitutively express COX enzyme (Yamaguchi and Okada, 2009). Thus, NSAID administration hinders the activation of LC cells in response to nociception and inflammation (Xu et al., 2003). Second, previous results from our laboratory have shown that activation of the EP3 receptor by the endogenous PGE_2 inhibits the neuronal activity of LC cells *in vitro* (Nazabal et al., unpublished results), whereas it was stimulated by activation of the EP2 receptor (Nazabal et al., unpublished results). Finally, the expression of EP4 receptor mRNA in the LC has been demonstrated by *in situ* hybridization techniques (Zhang and Rivest, 1999). However, little is known about the functional role of the EP4 receptor in LC neurons. Thus, we aimed to characterize pharmacologically the EP4 receptor and to study its signaling mechanism by single-unit extracellular recordings in LC noradrenergic neurons from rat brain slices.

Methods

Animals and ethics statement

84 male adult Sprague-Dawley rats (200-300 g) were used to perform the experiments and are reported in compliance with the ARRIVE (Kilkenny et al., 2010; McGrath and Lilley, 2015) and with the recommendations made by the *British Journal of Pharmacology*. Rats were obtained from the animal facility of the University of the Basque Country (Leioa, Spain)

and housed under standard environmental conditions (22 ºC, 12:12 h light/dark cycles) with free access to food and water. One slice was taken from each animal, and unless stated otherwise, only one experiment was performed in each slice. The number of experiments in each group was typically five to six, depending on the level of variability. Treatments and controls were performed in parallel in a randomized manner. As electrophysiological outcomes were collected *in situ*, data recording could not be blinded to the operator. However, the data analysis performed by the experimenter was confirmed separately by an additional researcher in all cases. All the experiments were carried out according to EU Directive 2010/63 on the protection of animals used for scientific purposes and approved by the local Ethical Committee for Research and Teaching (CEID) of the University of the Basque Country (UPV/EHU, Spain) and the Department of Sustainability and Natural Environment of Provincial Council from Bizkaia (ref. CEEA M20-2015-152; CEEA M20-2018-026). All the efforts were made to minimize the animal suffering and to reduce the number of animals used.

Brain slice preparation

Animals were anesthetized with chloral hydrate (400 mg kg^{-1}, i.p.) and decapitated (Mendiguren and Pineda, 2007). The brain was rapidly extracted, and a block of tissue containing the brainstem was immersed in ice-cold modified artificial cerebrospinal fluid (aCSF) where NaCl was equiosmolarly substituted for sucrose to improve neuronal viability. Coronal slices of 500-600 μm thickness containing the LC were cut using a vibratome (FHC Inc., Brunswick, USA). The tissue was allowed to recover from the slicing for 90 min, placed on a nylon mesh, and incubated at 33 ± 1 ºC on a modified Haas-type interface chamber. The tissue was continuously perfused with aCSF saturated with 95% O_2/ 5% CO_2 (final pH = 7.34) at a flow rate of 1.5 ml min^{-1}. The aCSF contained (in mM): NaCl 130, KCl 3, NaH_2PO_4 1.25, D-glucose 10, $NaHCO_3$ 21, $CaCl_2$ 2 and $MgSO_4$ 2. The LC was identified visually in the rostral pons as a dark oval area on the lateral borders of the central gray and the 4th ventricle, at or just anterior to the genu of the facial nerve.

Electrophysiological recordings

Single-unit extracellular recordings of LC cells were made as previously described (Mendiguren and Pineda, 2004, 2007). The recording electrode consisted of an Omegadot glass micropipette puller (Sutter Instruments, Novato, CA, USA) and filled with 50 mM NaCl. The tip was broken back to a size of 2 – 5 μm (3 – 5 MΩ) and positioned in the LC.

The extracellular signal from the electrode was passed through a high-input impedance amplifier (Axoclamp 2B, Molecular Devices, Union City, CA, USA) and monitored on an audio-amplifier and an oscilloscope (Aumon 14, Cibertec S.A., Madrid, Spain). Individual neuronal spikes were isolated from the background noise with a window discriminator (PDV 225, Cibertec S.A.). The firing rate (FR) was continuously recorded and analyzed before, during, and after experimental manipulations by a PC-based custom-made program which generated consecutive 10 s bin histogram bars of the cumulative number of spikes (HFCP®, Cibertec S.A., Madrid, Spain). Noradrenergic cells in the LC were identified by their spontaneous and regular discharge activities, the slow FR and the long-lasting biphasic positive-negative waveforms (Andrade and Aghajanian, 1984). We only recorded cells that showed stable FRs between 0.5 and 1.5 Hz for at least 3-5 min and the inhibitory effect induced by [Met]enkephalin (ME 0.8 μM, 1 min) was higher than 80% (Medrano et al., 2017) as a control for the perfusion system.

Pharmacological procedures

The firing rate of LC neurons was recorded for several minutes before drug applications to obtain the baseline activity, and then, during and after drug perfusion. To characterize the effect of EP4 receptor agonists in LC neurons, we perfused increasing concentrations of the EP4 receptor agonist rivenprost (0.01 – 100 nM, 3x) and TCS 2510 (0.20 nM – 2 μM, 3x) for at least 8 min each concentration, until a plateau effect was reached and based on previous studies (Bonfill-Teixidor et al., 2017). To pinpoint the EP receptor involved in the observed effect, concentration-effect curves for rivenprost were made in the presence of the EP4 receptor antagonist L-161,982 (3, 30, and 300 nM), the EP2 receptor antagonist PF-04418948 (300 nM), and the EP3 receptor antagonist L-798,106 (300 nM). In the case of TCS 2510, concentration-effect curves were made in the presence of a single concentration of L-161,982 (300 nM). All the antagonists were perfused for 30 min at the concentrations based on other studies (Machwate et al., 2001) before performing the concentration-effect curves for the EP4 agonists.

Rivenprost was used for subsequent characterization of the molecular mechanism involved in EP4 receptor activation. Excitatory responses of LC neurons are described to consist of a cAMP/PKA-induced opening of a non-selective cation current (Wang and Aghajanian, 1987). Then, to investigate the involvement of a sodium current in the rivenprost-mediated effect, low sodium-containing aCSF (TRIS 80%) was prepared by replacing 80% of the NaCl equiosmolarly with Trizma hydrochloride/base (TRIS) (Pineda et al., 1996) and then the

effect of rivenprost was tested. To further describe the involvement of sodium currents, we checked whether the transient receptor potential (TRP) ion channels (Cui et al., 2011) might contribute to the effect of rivenprost by using the nonselective TRP blocker 2-APB (30 μM, 10 min). Next, to test whether the cation current was induced by a rise in the cAMP levels, we used the cAMP analog 8-Br-cAMP (1 mM, 8 min) (Wang and Aghajanian, 1990). Thus, in case EP4 receptor activation depends on the cAMP/PKA pathway, administration of a saturating concentration of 8-Br-cAMP would occlude the subsequent effect of rivenprost. In addition, the cAMP/PKA-dependency was further determined by testing butaprost in the presence of the PKA inhibitor H-89 (10 μM, 20 min) (Jolas et al., 2000). Considering the similarities between the effects of EP2 and EP4 receptor activation (Nazabal et al., unpublished results), we performed an occlusion experiment in the presence of a submaximal concentration of butaprost (1 μM, 15 min) to examine the possible convergence of both signaling pathways. In addition, the effect of rivenprost was tested in the presence of the $G_{\alpha s}$-dependent signaling blocker NF449 (10 μM, 30 min) (Hohenegger et al., 1998) or the $G_{\beta\gamma}$-dependent signaling blocker gallein (20 μM, 120 min incubation in an aluminum foil-covered glass) (Kurowski et al., 2015) to further characterize the G-protein subunits involved. Finally, since the EP4 receptor has been described to couple to the PI3K and PKC signaling pathways (Fujino et al., 2005; Fujino and Regan, 2006; Eijkelkamp et al., 2010), the PI3K inhibitor wortmannin (100 nM, 20 min) and the cell-permeable PKC inhibitor chelerythrine (10 μM, 30 min) were used at previously tested concentrations (Bailey et al., 2004; Hill et al., 2008). Except otherwise stated, all mentioned drugs were bath perfused for at least 10 min before testing the effect of rivenprost.

Analysis and statistics of electrophysiological data

The data and statistical analysis were carried out with the computer program GraphPad Prism (version 5.0 for Windows, GraphPad Software, Inc., San Diego, CA, USA) and comply with the recommendations on experimental design and analysis in pharmacology (Curtis et al., 2018). The effect (E) was normalized to baseline (FR_{basal}) in each cell according to the following equation $E = (FR_{basal} - FR_{post}) \cdot 100/FR_{basal}$, where FR_{basal} is the average FR for 60 s immediately before the prostanoid agonist administration, and FR_{post} is the average FR of the last 60 s for each concentration of agonist, once it had reached a plateau. In the case of the perfusion test with ME (0.8 μM, 1 min), the inhibitory effect was calculated similarly but normalized to the initial FR ($FR_{initial}$), being the average FR of each neuron calculated for 60

s immediately before drug application and FR_{post} the average FR after drug application for 60-90 s. Normalization to FR_{basal} or $FR_{initial}$ was used for comparison purposes across groups. To construct the concentration-effect curves for the EP4 receptor agonists, fitting analysis was performed to obtain the best simple nonlinear fit to the following three-parameter logistic equation: $E = E_{max}[A]^n / (EC_{50}^n + [A]^n)$, where E and [A] are the observed effect and the concentration of the agonist, respectively; E_{max} is the maximal excitatory effect of the EP4 agonist. EC_{50} is the concentration of the agonist required to promote the 50% of E_{max}, and n represents the slope factor of the function. These parameters were determined in individual assays by the nonlinear analysis and then averaged to obtain the theoretical parameters in each group. For comparison purposes, the EC_{50} values were converted and expressed as the negative logarithm (pEC_{50}), which adjusted the variable into a Gaussian distribution (Pineda et al., 1997).

The antagonist affinity value was calculated as the negative logarithm of the equilibrium dissociation constant of the antagonist-receptor complex (pK_B). The pK_B value was estimated for parallel shifts by using the modified Gaddum/Schild equation for global fitting of the curves using GraphPad Prism 5.0 (Lazareno and Birdsall, 1993), where the minimum and maximum effects were constrained to 0 and 100% respectively, and the Schild slope was constrained to 1.0. In the case of TCS 2510, the affinity measurement was obtained from the Gaddum method (Kenakin et al., 2006) by plotting double equieffective concentrations of TCS 2510 in the absence (ordinates) and presence (abscissae) of the antagonist.

Data are expressed as the mean ± SEM of n number of rats. Statistical significances were obtained by a two-tailed paired Student's t-test when the response values were compared before and after drug applications within the same cell, and by a two-tailed two-sample Student's t-test when the FRs, responses or parameters were two independent experimental conditions. Statistical comparison of the results among more than two experimental conditions (including a control group) were done by one-way analysis of variance (ANOVA) followed by a post hoc pairwise comparisons with a Dunnett's *post hoc* test or Bonferroni's Multiple Comparison test only if F achieved the necessary level of statistical significance (i.e. $P < 0.05$) and there was no significant variance inhomogeneity. Dunnett's method is used for comparison with a control group and Bonferroni's test for comparison among all the groups. The threshold of significance was set at $P = 0.05$ and only one level of probability ($P < 0.05$) is reported.

Materials and drugs

For electrophysiological recordings, the following drugs were purchased from Tocris Bioscience (Bristol, UK): gallein, H-89, L-161,982, L-798,106, NF449, PF-04418948, and TCS 2510. The following drug was acquired from Sigma-Aldrich Química S.A. (Madrid, Spain): Trizma hydrochloride. From Bachem (Weil am Rhein, Germany) was purchased: [Met]enkephalin acetate salt (ME). Finally, 8-Bromo-cAMP was from Enzo Life Sciences Inc. (New York, USA) and rivenprost from Cayman Chemical (Ann Arbor, MI, USA). Rivenprost and TCS 2510 were purchased already dissolved in methyl acetate and anhydrous ethanol, respectively, so the required volume was directly extracted from the vial and incorporated to aCSF at the moment of the experiment. The final concentration of methyl acetate in aCSF was < 0.0005% and < 0.015% for anhydrous ethanol. Stock solutions of gallein, L-161,982, L-798,106, PF-04418948 were first prepared in pure DMSO and then diluted in aCSF to obtain a final concentration of DMSO lower than 0.1%, which does not affect the LC cell firing responses (Pineda et al., 1996). Control assays were performed with equivalent volumes of the vehicles in which the drugs were dissolved. Stock solutions of the rest of the drugs were first prepared in Milli-Q water and then diluted 1000- to 10000-fold in aCSF for the desired concentration. Final solutions were prepared freshly just before each experiment and stock solutions were kept at -20 ºC.

Nomenclature of targets and ligands

Key protein targets and ligands in this article are hyperlinked to corresponding entries in http://www.guidetopharmacology.org, the common portal for data from the IUPHAR/BPS Guide to PHARMACOLOGY (Harding et al., 2018), and are permanently archived in the Concise Guide to PHARMACOLOGY 2017/18 (Alexander et al., 2017).

Results

Effect of the EP4 receptor agonists rivenprost and TCS 2510 on the firing rate of LC neurons

In situ hybridization studies have shown mRNA expression for the EP4 receptor in the LC (Zhang and Rivest, 1999). Moreover, c-fos immunoreactivity is increased in response to a systemic pro-inflammatory cytokine in brain areas expressing the EP4 receptor, including the LC (Zhang and Rivest, 1999). To study the role of the EP4 receptor in the regulation of the firing rate of LC neurons, we performed concentration-effect curves for the EP4 receptor agonists rivenprost and TCS 2510. Increasing concentrations of rivenprost (0.01 – 100 nM, 3x, 10 min each) increased the firing rate of LC cells (from 0.70 ± 0.09 Hz to 1.14 ± 0.13 Hz; n = 6, $P < 0.05$) with an EC_{50} value in the nanomolar range (Figures 1A and D; Table 1).

To determine the EP receptor involved in the rivenprost-induced excitatory effect, the specific EP4 receptor antagonist L-161,982 (3, 30 and 300 nM), the EP2 receptor antagonist PF-04418948 (300 nM), and the EP3 receptor antagonist L-798,106 (300 nM) were used. Bath application of L-161,982 (3, 30, and 300 nM, 30 min) did not change the firing rate of LC cells but 30 nM and 300 nM produced a 4-fold and 8-fold shift in the concentration-effect curve for rivenprost, respectively (n = 5, $P < 0.05$ for both 30 and 300 nM; Figures 1B and D; Table 1). On the other hand, perfusion with PF-04418948 (300 nM) and L-798,106 (300 nM) did not change the firing rate and failed to shift the concentration-effect curve for rivenprost (Figures 1C and D; Table 1). These results suggest that the excitatory effect of rivenprost was mediated by EP4 receptor activation.

The antagonist affinity of L-161,982 for the EP4 receptor (pK_B) was estimated to be 8.06 ± 0.18 (mean ± SEM, n = 14) when calculated with the Gaddum/Schild equation and assumed a Schild slope of unity (Kenakin, 1982). However, the calculated pK_B values were variable depending on the concentration of L-161,982 employed, resulting in a higher pK_B value with 3 nM in comparison with 30 or 300 nM (8.84 ± 0.13 for 3 nM different from 7.94 ± 0.24 for 30 nM or 7.40 ± 0.08 for 300 nM; n = 5, $P < 0.05$, one-way ANOVA followed by Bonferroni's Multiple Comparison Test). Therefore, we performed the Schild plot analysis and the resultant pA_2 was 8.69 (95% CI: 15.96-7.92) with a Schild slope of 0.39 (95% CI: 0.05-0.72) different from unity (n = 5, $P < 0.05$). This means that, despite the rightward shift of the concentration-effect curve for rivenprost by L-161,982 (Figure 1D), the Schild slope was found different from 1, which suggest a non-competitive condition for L-161,982 (see discussion).

On the other hand, administration of the structurally different EP4 receptor agonist TCS 2510 (0.20 nM – 2 μM, 3x, 10 min each) increased the firing rate of LC cells (from 0.71 ± 0.08 to 1.55 ± 0.12 Hz; $n = 6$, $P < 0.05$), with an EC_{50} value in the nanomolar range (Figures 2A and C; Table 1). Administration of the EP4 receptor antagonist L-161,982 (300 nM) for 30 min decreased the maximal effect by 38% ($n = 5$, $P < 0.05$) and increased the slope steepness by 2 fold ($n = 5$, $P < 0.05$) (Figures 2B and C; Table 1), suggesting that the excitatory effect caused by TCS 2510 is mediated by EP4 receptor activation. Considering that the Emax reduction for TCS 2510 by L-161,982 may support the non-competitive behavior of the antagonist, we plotted double equieffective concentrations of TCS 2510 in the absence and presence of L-161,982 (300 nM) by the Gaddum method (Kenakin et al., 2006), which yielded a pK_B yielded of 7.69 (95% CI: 7.61 – 7.76). Overall, these results indicate that the activation of EP4 receptors by the selective agonists rivenprost and TCS 2510 stimulated LC neuronal activity *in vitro*.

Study of cationic currents and cAMP/PKA signaling pathway involvement in EP4 receptor activation in LC neurons

In cerebellar neurons, PGE_2 has been described to elicit a sodium current via activation of G_s-coupled EP4 receptors and in a cAMP/PKA-mediated pathway (Fang et al., 2011). In the LC, activation of the cAMP/PKA pathway is known to drive the spontaneous pacemaker activity (Alreja and Aghajanian, 1991, 1995) through the opening of an inward sodium current (Wang and Aghajanian, 1987). Therefore, to test the involvement of sodium current in the excitatory effect of rivenprost, we used a low sodium-containing aCSF, in which the 80% of the sodium had been replaced by TRIS (TRIS 80%) (Alreja and Aghajanian, 1993; Pineda et al., 1996). Perfusion with TRIS 80% reduced the spontaneous activity of LC neurons by 63.6 ± 2.6% (from 0.92 ± 0.31 to 0.34 ± 0.08; $n = 6$, $P < 0.05$) and completely blocked the excitatory effect caused by rivenprost (30 nM) ($n = 6$, $P < 0.05$; Figures 3A and B). This result implies that the excitatory effect of the EP4 receptor agonist rivenprost is dependent on a sodium current. Next, to characterize the molecular substrate for this sodium current, we checked whether the cation-permeable transient receptor potential (TRP) channel was involved. PGE_2 has been reported to increase the activity of these channels in EP4 receptor-expressing cells (Moriyama et al., 2005). Administration of the non-selective TRP channel blocker 2-APB (30 μM) reduced the LC cell firing activity by 41.7 ± 6.1% (from

0.74 ± 0.09 Hz to 0.45 ± 0.11 Hz; $n = 5$, $P < 0.05$) but it failed to alter the excitatory effect induced by rivenprost (30 nM) (Figure 3B). Therefore, the TRP channels do not appear to mediate the sodium current induced by the EP4 receptor agonist rivenprost.

Next, to test whether the cAMP/PKA pathway is involved in the EP4 receptor agonist effect, we perfused rivenprost in the presence of 8-Br-cAMP, a non-hydrolyzable cell-permeable cAMP analog that activates the PKA enzyme (Poppe et al., 2008). Thus, if rivenprost exerted its effect through the cAMP cascade, prior administration of a saturating concentration of 8-Br-cAMP would occlude the excitatory effect induced by rivenprost. As expected from previous reports (Wang and Aghajanian, 1987; Nazabal et al., unpublished results), PKA activation with 8-Br-cAMP (1 mM, 8 min) increased by 2 fold the firing rate of LC neurons (from 0.73 ± 0.06 Hz to 1.42 ± 0.12 Hz; $n = 5$, $P < 0.05$) (Figure 3C). However, administration of rivenprost (30 nM, 10 min) in the presence of 8-Br-cAMP further increased the firing activity of LC cells (from 1.42 ± 0.12 Hz to 2.02 ± 0.13 Hz; $n = 5$, $P < 0.05$) (Figure 3C), which suggests that the effect of rivenprost was not occluded by 8-Br-cAMP. Therefore, the excitatory effect of the EP4 receptor agonist does not apparently depend on the cAMP/PKA pathway. To further test this hypothesis, we studied the effect of rivenprost (30 nM) in the presence of the PKA inhibitor H-89 (10 μM). Bath application of H-89 (10 μM) for 20 min increased the LC firing rate by 8.99 ± 3.36% (from 0.62 ± 0.06 Hz to 0.68 ± 0.08 Hz; $n = 5$, $P < 0.05$). However, H-89 did not change the magnitude of rivenprost-induced excitation (Figure 3D). Hence, these data indicate that the effect of the EP4 receptor agonist rivenprost on the LC is dependent on a sodium current but independent of the cAMP/PKA pathway.

Study of the involvement of $G_{\alpha s}$ and $G_{\beta\gamma}$ subunits, and PI3K and PKC signaling mechanisms in EP4 receptor activation in LC neurons

We have previously shown that the effect of the EP2 receptor agonist butaprost is also dependent on a sodium current but independent of the cAMP/PKA pathway (Nazabal et al., unpublished results). Therefore, we studied whether the administration of butaprost at a submaximal concentration would occlude the following stimulatory effect of rivenprost. As previously described, administration of butaprost (1 μM, 15 min) increased the firing rate of LC neurons by 61.4 ± 9.7% (from 0.74 ± 0.10 Hz to 1.19 ± 0.17 Hz; $n = 5$, $P < 0.05$) (Figures 4A and B). However, in the presence of butaprost, rivenprost (30 nM) further increased the LC cell firing activity (from 1.19 ± 0.17 Hz to 1.51 ± 0.22 Hz; $n = 5$, $P < 0.05$) (Figures 4A and

B), indicating that the excitatory effect of rivenprost was not occluded by butaprost. These data suggest that the EP2 and EP4 receptors do not share the same signaling pathway to excite the activity of LC neurons.

The EP4 receptor is described to be coupled to G_s protein in cerebellar neurons (Fang et al., 2011). In order to study whether the $G_{\alpha s}$ protein mediated the effect of rivenprost on the LC, we used the specific $G_{\alpha s}$-dependent signaling inhibitor NF449. Administration of NF449 (10 μM) for 20 min did not change the firing activity of LC neurons, but blunted by 42.1% the excitatory effect induced by rivenprost (30 nM) (n = 6, $P < 0.05$ *vs*. control; Figure 4C), suggesting that the effect of rivenprost was mediated by the $G_{\alpha s}$ protein. In addition, we studied the involvement of the $G_{\beta\gamma}$ subunits by testing the effect of rivenprost in the presence of the selective inhibitor gallein. Bath incubation with gallein (20 μM) for 120 min did not change the rivenprost-induced excitation ($n = 5$, $P > 0.05$ *vs*. control; Figure 4C). These results indicate that the $G_{\beta\gamma}$ subunits are not involved in the excitatory effect of rivenprost on LC cells.

In addition to $G_{\alpha s}$ protein, the EP4 receptor has been described to be coupled to the PI3K signaling pathway in cultured cells (Fujino et al., 2005; Fujino and Regan, 2006) and microglia (Shi et al., 2010). Furthermore, PI3K signaling is needed for the leptin-induced excitatory effect in hypothalamic neurons (Hill et al., 2008). Therefore, we tested the effect of rivenprost in the presence of the PI3K inhibitor wortmannin. Administration of wortmannin (100 nM) for 20 min did not change the spontaneous activity of LC cells and failed to block the excitatory effect of rivenprost (30 nM). In fact, in the presence of wortmannin, the effect of rivenprost was increased by 58.3% (n = 5, $P < 0.05$ *vs*. control; Figure 4D), suggesting that the stimulatory effect of rivenprost was not mediated by the PI3K. On the other hand, PKC activity is required for the PGE_2-induced modulation of sodium currents in sensory neurons (Gold et al., 1998) and the PGE_2-induced hypernociception *in vivo* (Sachs et al., 2009). Therefore, we examined the involvement of PKC by testing the effect of rivenprost in the presence of the PKC inhibitor chelerythrine. Bath perfusion of chelerythrine (10 μM) for 30 min did not change the firing activity of LC neurons and failed to prevent the increase in excitability of LC neurons caused by rivenprost (30 nM). Furthermore, the rivenprost-induced excitatory effect was increased by 2 fold in the presence of chelerythrine (n = 5, $P < 0.05$ *vs*. control; Figure 4D). In light of this result, the PKC does not seem to mediate the rivenprost-induced excitation. In summary, the

excitatory effect observed upon EP4 receptor activation seems to be mediated by the $G_{\alpha s}$ subunits, whereas the $G_{\beta\gamma}$ subunits and the PK3K and PKC signaling pathways are not apparently involved.

Discussion

The purpose of this study was to characterize the functional role of EP4 receptors in LC neurons by extracellular electrophysiological techniques. We found that the EP4 receptor agonists rivenprost and TCS 2510 increase the neuronal activity of LC cells *in vitro*. This excitatory effect was blocked by the EP4 receptor antagonist L-161,982, but not by the EP2 or EP3 receptor antagonists PF-04418948 and L-798,106, respectively, indicating an EP4 receptor-mediated effect. The increase in firing rate of LC neurons caused by rivenprost was blocked by extracellular sodium replacement and a $G_{\alpha s}$ signaling inhibitor, but not by blockers of the cAMP/PKA pathway, TRP channels, $G_{\beta\gamma}$ subunits, PI3K or PKC signaling. Thus, these results suggest that EP4 receptor activation stimulates the neuronal activity of LC cells, presumably by its coupling to $G_{\alpha s}$ proteins and an inward sodium current.

In our study, we characterized the functional role of EP4 receptors in LC neurons by using extracellular electrophysiology *in vitro*, EP4 receptor agonists, and EP receptor antagonists. The concentrations of the EP4 receptor agonists rivenprost and TCS 2510 used herein were based on the affinity data demonstrated in radioligand binding experiments, which show that rivenprost has 80-fold higher affinity for the EP4 than for EP3 or EP2 receptors (Yoshida et al., 2002) and TCS 2510 fails to have affinity at the tested concentration range for non-EP4 receptors (Young et al., 2004). Furthermore, the involvement of the EP4 receptor was demonstrated with the specific antagonist L-161,982, which shows a more than 200-fold higher affinity for the EP4 than for EP3 receptors (Machwate et al., 2001). The EP2 receptor antagonist PF-04418948 does not show antagonistic affinity for any other EP receptor (Forselles et al., 2011), while L-798,106 has much higher affinity for the EP3 than for EP4 receptors (Su et al., 2008).

In the present study, administration of rivenprost or TCS 2510 increased the firing rate of LC neurons. In the case of rivenprost, the EC_{50} value (1.43 nM) was similar to its K_i value measured in cell membranes (0.7 nM) (Yoshida et al., 2002), whereas the EC_{50} value for TCS 2510 (18.0 nM) was higher than that of rivenprost, but at the same range as that described in other tissues

(e.g., isolated smooth muscle, pIC_{50}: 7.6) (Jones et al., 2013). The excitatory effect of rivenprost or TCS 2510 was mediated by EP4 receptor activation since it was only blocked by L-161,982, but not by perfusion with L-798,106 or PF-04418948. In our work, L-161,982 shifted to the right the concentration-effect curve for rivenprost but reduced the Emax for TCS 2510 without any rightward shift. This disparity of effects was unlikely to be caused by activation of other EP receptors, given the high selectivity of these ligands for the EP4 receptor. Furthermore, the Schild slope for L-161,982 was less than unity when calculated with rivenprost and furthermore different pK_B values were found for various concentrations of L-161,982. According to different authors, a slow dissociation rate of the antagonist and a higher receptor reserve for one of the agonist (Kenakin et al., 2006) (i.e., rivenprost) could explain the different pharmacological profiles observed with rivenprost and TCS 2510 in the presence of L-161,982. Moreover, the calculated pK_B of L-161,982 for the EP4 receptor resulted in 7.69 by double equieffective concentrations of TCS 2510, which was at similar concentration ranges to the pK_B obtained for L-161,982 with rivenprost (7.67). Furthermore, the result obtained in our study for L-161,982 was akin to its K_i value (32 nM) measured by binding assays in cell cultures with PGE_2 as an agonist (Machwate et al., 2001). Overall, these data indicate that the observed excitatory effect of rivenprost or TCS 2510 was mediated by EP4 receptor activation.

Activation of G_s-coupled EP4 receptors modulates sodium currents in brain neurons (e.g., cerebellar granule cells (Fang et al., 2011)). In our work, the blockade of the rivenprost-induced stimulation of LC cells by extracellular sodium replacement reveals the involvement of sodium currents. In agreement, PGE_2 has been shown to enhance sodium currents via EP4 receptors in cerebellar (Fang et al., 2011) and nodose ganglion neurons (Matsumoto et al., 2005). Furthermore, EP4 receptor activation increases the firing rate of supraoptic neurons, which has been suggested to be mediated by non-selective cation channels (Shibuya et al., 2002). In the LC, sodium currents can be elicited by non-selective cation TRP channels in response to hypercapnia (Cui et al., 2011). However, in our study, the TRP channel blocker 2-APB did not prevent the excitatory effect induced by rivenprost, which indicates that the TRP channel is not involved in the rivenprost-induced excitatory effect.

EP4 receptor activation elicits a sodium current via activation of G_s proteins and cAMP/PKA pathway (Fang et al., 2011). In the current study, the rivenprost-induced stimulation was blocked by the $G_{\alpha s}$ signaling inhibitor NF449, but not by the $G_{\beta\gamma}$ signaling inhibitor gallein, which suggests that the EP4 receptor is coupled to $G_{\alpha s}$ proteins in the LC. However, the rivenprost-induced excitatory effect was not mediated by the cAMP/PKA pathway as it was

not occluded by the PKA activator 8-Br-cAMP nor blocked by the PKA inhibitor H-89, which were perfused at the same concentrations used in other brain areas *in vitro* (Wang and Aghajanian, 1990; Jolas et al., 2000). Although these results are in contrast with the signaling mechanism described for EP4 receptors in neurons (Wise, 2006), some other authors have pointed out a cAMP-independent pathway for EP4 receptor-mediated effects. For example, chronic exposure to PGE_2 downregulates the EP4 receptor-mediated cAMP/PKA pathway activation in cultured DRG neurons (Malty et al., 2016) and TCS 2510 fails to raise cAMP levels in mast cells (Kay et al., 2013). Likewise, activation of the EP2 receptor, which also induces excitatory responses in LC neurons, is not dependent on the cAMP/PKA pathway (Nazabal et al., unpublished results). Since both EP2 and EP4 receptors activate sodium currents in the LC via a non cAMP/PKA pathway, in the present work, we compared the effect of rivenprost with or without administration of the EP2. Thus, the excitatory effect of rivenprost was not occluded by butaprost effect, which suggests an uncommon signaling pathway for EP2 and EP4 receptors. This divergence could be explained by phylogenetic differences, as they only share a 31% amino acid identity in mice (Sugimoto and Narumiya, 2007). Overall, these data indicate that EP4 receptor activation in LC neurons is coupled to a $G_{\alpha s}$ protein and a sodium current, but not dependent on cAMP/PKA and $G_{\beta\gamma}$ subunit signaling.

On the other hand, EP4 receptor activation has been linked to the PI3K signaling pathway in cell cultures (Fujino et al., 2005; Fujino and Regan, 2006) and DRG neurons (Ma and St-Jacques, 2018). In the latter case, activation of the PI3K promotes the externalization of EP4 receptors, which could enhance the nociceptive transmission (Ma and St-Jacques, 2018). However, according to our data, the PI3K inhibitor wortmannin did not block the excitatory effect of rivenprost in LC cells but rather potentiated it. It has been shown that EP4 receptor activation stimulates the PI3K pathway via $G_{i/o}$ proteins in cultured cells (Fujino and Regan, 2006). Furthermore, the EP4 receptor can couple to both G_s and $G_{i/o}$ proteins in cell cultures, with the degree of activation of G_s and $G_{i/o}$ protein depending on the functional selectivity of EP4 receptor agonists (Leduc et al., 2009). In our system, we cannot exclude a simultaneous coupling of EP4 receptors to the $G_{i/o}$/PI3K pathway in LC cells, which would counteract the excitatory effect of EP4-$G_{\alpha s}$ and would be unmasked in the presence of wortmannin. In addition to the PI3K, a PKC-dependent pathway has been described for EP4 receptor-mediated effects, such as in DRG neurons (Eijkelkamp et al., 2010). However, in our work, the PKC inhibitor chelerythrine did not block the excitatory effect of rivenprost but further enhanced it, which rules out the implication of this enzyme in the rivenprost-induced stimulation.

In summary, our work supports the existence of functional EP4 receptors in LC neurons, which activation results in a concentration-dependent increase in the spontaneous firing rate. The underlying mechanism may involve the $G_{\alpha s}$ protein and a sodium current, but it does not seem to involve $G_{\beta\gamma}$, TRP, cAMP/PKA, PI3K, or PKC-dependent pathways. Further studies will be carried out to test whether the coupling of EP4-Gαs and sodium currents is a direct mechanism. According to previous data from our laboratory, the endogenous PGE_2 has a preferential inhibitory effect on LC neurons mediated by EP3 receptor activation (Nazabal et al., unpublished results). We have also described a stimulatory effect of LC neurons caused by EP2 receptor activation (Nazabal et al., unpublished results). In this study, we demonstrate the presence of EP4 receptors in the LC, which could further tune the inflammatory response to PGE_2 in the brain. Thus, EP4 receptor signaling in the LC may gain relevance during inflammatory states, since peripheral inflammation has been reported to upregulate EP4 receptor expression in DRG (Lin et al., 2006) and brain catecholaminergic neurons (Zhang and Rivest, 1999). This suggestion is also supported by the rise in c-Fos immunoreactivity in response to an inflammatory insult in brain regions expressing the EP4 receptor (Zhang and Rivest, 1999). Furthermore, chronic inflammatory pain, which is known to release PGE_2, has been shown to enhance anxiety-like behaviors in rodents (Parent et al., 2012) and the LC mediates some of the affective events involved in processing of nociception by promoting anxiogenic-like behavior during chronic pain (Alba-Delgado et al., 2013). It is therefore tempting to speculate that EP4 receptor activation in the LC may be of relevance in the integrative reaction to pain stimuli possibly by enhancing NA release throughout the CNS. Therefore, the prostaglandin system and the EP4 receptor in the LC might be suitable pharmacological targets for the development of novel treatments for inflammatory pain and anxiety-derived disorders.

Author contributions

A. N. performed the electrophysiological assays and wrote the first draft of the manuscript. A. M. and J.P. conceived and designed the study and wrote the manuscript.

References

Alba-Delgado, C., Llorca-Torralba, M., Horrillo, I., Ortega, J.E., Mico, J.A., Sánchez-Blázquez, P., et al. (2013). Chronic pain leads to concomitant noradrenergic impairment and mood disorders. Biol. Psychiatry *73*: 54–62.

Alexander, S.P.H., Christopoulos, A., Davenport, A.P., Kelly, E., Marrion, N. V., Peters, J.A., et al. (2017). THE CONCISE GUIDE TO PHARMACOLOGY 2017/18: G protein-coupled receptors. Br. J. Pharmacol. *174*: S17–S129.

Alreja, M., and Aghajanian, G.K. (1991). Pacemaker activity of locus coeruleus neurons: whole-cell recordings in brain slices show dependence on cAMP and protein kinase A. Brain Res. *556*: 339–343.

Alreja, M., and Aghajanian, G.K. (1993). Opiates suppress a resting sodium-dependent inward current and activate an outward potassium current in locus coeruleus neurons. J. Neurosci. *13*: 3525–3532.

Alreja, M., and Aghajanian, G.K. (1995). Use of the whole-cell patch-clamp method in studies on the role of cAMP in regulating the spontaneous firing of locus coeruleus neurons. J. Neurosci. Methods *59*: 67–75.

Andrade, R., and Aghajanian, G.K. (1984). Locus coeruleus activity in vitro: intrinsic regulation by a calcium-dependent potassium conductance but not alpha 2-adrenoceptors. J. Neurosci. *4*: 161–170.

Bailey, C.P., Kelly, E., and Henderson, G. (2004). Protein Kinase C Activation Enhances Morphine-Induced Rapid Desensitization of -Opioid Receptors in Mature Rat Locus Ceruleus Neurons. Mol. Pharmacol. *66*: 1592–1598.

Bonfill-Teixidor, E., Otxoa-de-Amezaga, A., Font-Nieves, M., Sans-Fons, M.G., and Planas, A.M. (2017). Differential expression of E-type prostanoid receptors 2 and 4 in microglia stimulated with lipopolysaccharide. J. Neuroinflammation *14*: 3.

Cui, N., Zhang, X., Tadepalli, J.S., Yu, L., Gai, H., Petit, J., et al. (2011). Involvement of TRP channels in the CO 2 chemosensitivity of locus coeruleus neurons. J Neurophysiol *105*: 2791–2801.

Curtis, M.J., Alexander, S., Cirino, G., Docherty, J.R., George, C.H., Giembycz, M.A., et al.

(2018). Experimental design and analysis and their reporting II: updated and simplified guidance for authors and peer reviewers. Br. J. Pharmacol. *175*: 987–993.

Eijkelkamp, N., Wang, H., Garza-Carbajal, A., Willemen, H.L.D.M., Zwartkruis, F.J., Wood, J.N., et al. (2010). Low nociceptor GRK2 prolongs prostaglandin E2 hyperalgesia via biased cAMP signaling to Epac/Rap1, protein kinase Cepsilon, and MEK/ERK. J. Neurosci. *30*: 12806–12815.

Ek, M., Arias, C., Sawchenko, P., and Ericsson-Dahlstrand, A. (2000). Distribution of the EP3 prostaglandin E2 receptor subtype in the rat brain: Relationship to sites of interleukin-1 - Induced cellular responsiveness. J. Comp. Neurol. *428*: 5–20.

Fang, Y.-J., Zhou, M.-H., Gao, X.-F., Gu, H., and Mei, Y.-A. (2011). Arachidonic acid modulates Na + currents by non-metabolic and metabolic pathways in rat cerebellar granule cells. Biochem. J. *438*: 203–215.

Forselles, K.J., Root, J., Clarke, T., Davey, D., Aughton, K., Dack, K., et al. (2011). In vitro and in vivo characterization of PF-04418948, a novel, potent and selective prostaglandin EP2 receptor antagonist. Br. J. Pharmacol. *164*: 1847–56.

Fujino, H., and Regan, J.W. (2006). EP 4 Prostanoid Receptor Coupling to a Pertussis Toxin-Sensitive Inhibitory G Protein. Mol. Pharmacol. *69*: 5–10.

Fujino, H., Salvi, S., and Regan, J.W. (2005). Differential Regulation of Phosphorylation of the cAMP Response Element-Binding Protein after Activation of EP 2 and EP 4 Prostanoid Receptors by Prostaglandin E 2. Mol. Pharmacol. *68*: 251–259.

Gold, M.S., Levine, J.D., and Correa, A.M. (1998). Modulation of TTX-R INa by PKC and PKA and their role in PGE2-induced sensitization of rat sensory neurons in vitro. J. Neurosci. *18*: 10345–10355.

Harding, S., Sharman, J., Faccenda, E., Southan, C., Pawson, A., Ireland, S., et al. (2018). The IUPHAR/BPS Guide to PHARMACOLOGY in 2018: updates and expansion to encompass the new guide to IMMUNOPHARMACOLOGY. Nucleic Acids Res. *46*: D1091–D1106.

Hétu, P.-O., and Riendeau, D. (2005). Cyclo-oxygenase-2 contributes to constitutive prostanoid production in rat kidney and brain. Biochem. J. *391*: 561–566.

Hill, J.W., Williams, K.W., Ye, C., Luo, J., Balthasar, N., Coppari, R., et al. (2008). Acute

effects of leptin require PI3K signaling in hypothalamic proopiomelanocortin neurons in mice. J. Clin. Invest. *118*: 1796–1805.

Hohenegger, M., Waldhoer, M., Beindl, W., Bing, B., Kreimeyer, A., Nickel, P., et al. (1998). G salpha-selective G protein antagonists. Pharmacology *95*: 346–351.

Jolas, T., Nestler, E.J., and Aghajanian, G.K. (2000). Chronic morphine increases GABA tone on serotonergic neurons of the dorsal raphe nucleus: Association with an up-regulation of the cyclic AMP pathway. Neuroscience *95*: 433–443.

Jones, R.L., Wan Ahmad, W.A.N., Woodward, D.F., and Wang, J. (2013). Nature of the slow relaxation of smooth muscle induced by a EP2 receptor agonist with a non-prostanoid structure. Prostaglandins Leukot. Essent. Fat. Acids *88*: 321–330.

Kay, L.J., Gilbert, M., Pullen, N., Skerratt, S., Farrington, J., Seward, E.P., et al. (2013). Characterization of the EP receptor subtype that mediates the inhibitory effects of prostaglandin E2 on IgE-dependent secretion from human lung mast cells. Clin. Exp. Allergy *43*: 741–751.

Kenakin, T., Jenkinson, S., and Watson, C. (2006). Determining the potency and molecular mechanism of action of insurmountable antagonists. J. Pharmacol. Exp. Ther. *319*: 710–723.

Kenakin, T.P. (1982). The Schild regression in the process of receptor classification. Can. J. Physiol. Pharmacol. *60*: 249–265.

Kilkenny, C., Browne, W., Cuthill, I.C., Emerson, M., and Altman, D.G. (2010). Animal research: Reporting in vivo experiments: The ARRIVE guidelines. Br. J. Pharmacol. *160*: 1577–1579.

Kurowski, P., Gawlak, M., and Szulczyk, P. (2015). Muscarinic receptor control of pyramidal neuron membrane potential in the medial prefrontal cortex (mPFC) in rats. Neuroscience *303*: 474–488.

Lazareno, S., and Birdsall, N.J.M. (1993). Estimation of competitive antagonist affinity from functional inhibition curves using the Gaddum Schild and Cheng-Prusoff equations. Br. J. Pharmacol. *109*: 1110–1119.

Leduc, M., Breton, B., Gouill, C. Le, Bouvier, M., Chemtob, S., and Heveker, N. (2009). Functional Selectivity of Natural and Synthetic Prostaglandin EP 4 Receptor Ligands. Pharmacology *331*: 297–307.

Lin, C.R., Amaya, F., Barrett, L., Wang, H., Takada, J., Samad, T. a, et al. (2006). Prostaglandin E2 Receptor EP4 Contributes to Inflammatory Pain Hypersensitivity. J. Pharmacol. Exp. Ther. *319*: 1096–1103.

Ma, W., and St-Jacques, B. (2018). Signalling transduction events involved in agonist-induced PGE2/EP4 receptor externalization in cultured rat dorsal root ganglion neurons. Eur. J. Pain *22*: 845–861.

Machwate, M., Harada, S., Leu, C.T., Seedor, G., Labelle, M., Gallant, M., et al. (2001). Prostaglandin receptor EP(4) mediates the bone anabolic effects of PGE(2). Mol. Pharmacol. *60*: 36–41.

Malty, R.H., Hudmon, A., Fehrenbacher, J.C., and Vasko, M.R. (2016). Long-term exposure to PGE2 causes homologous desensitization of receptor-mediated activation of protein kinase A. J. Neuroinflammation *13*: 181.

Matsumoto, S., Ikeda, M., Yoshida, S., Tanimoto, T., Takeda, M., and Nasu, M. (2005). Prostaglandin E2-induced modification of tetrodotoxin-resistant Na+ currents involves activation of both EP2 and EP4 receptors in neonatal rat nodose ganglion neurones. Br. J. Pharmacol. *145*: 503–13.

McGrath, J.C., and Lilley, E. (2015). Implementing guidelines on reporting research using animals (ARRIVE etc.): New requirements for publication in BJP. Br. J. Pharmacol. *172*: 3189–3193.

Medrano, M.C., Santamarta, M.T., Pablos, P., Aira, Z., Buesa, I., Azkue, J.J., et al. (2017). Characterization of functional μ opioid receptor turnover in rat locus coeruleus: an electrophysiological and immunocytochemical study. Br. J. Pharmacol. *174*: 2758–2772.

Mendiguren, A., and Pineda, J. (2004). Cannabinoids enhance N-methyl-D-aspartate-induced excitation of locus coeruleus neurons by CB1 receptors in rat brain slices. Neurosci. Lett. *363*: 1–5.

Mendiguren, A., and Pineda, J. (2007). CB1 cannabinoid receptors inhibit the glutamatergic component of KCl-evoked excitation of locus coeruleus neurons in rat brain slices. Neuropharmacology *52*: 617–625.

Miura, A., Kawatani, M., Maruyama, T., and Groat, W.C. de (2002). Effect of prostaglandins

on parasympathetic neurons in the rat lumbosacral spinal cord. Neuroreport *13*: 1557–1562.

Moriyama, T., Higashi, T., Togashi, K., Iida, T., Segi, E., Sugimoto, Y., et al. (2005). Sensitization of TRPV1 by EP1 and IP reveals peripheral nociceptive mechanism of prostaglandins. Mol. Pain *1*: 1–13.

Parent, A.J., Beaudet, N., Beaudry, H., Bergeron, J., Bérubé, P., Drolet, G., et al. (2012). Increased anxiety-like behaviors in rats experiencing chronic inflammatory pain. Behav. Brain Res. *229*: 160–167.

Pineda, J., Kogan, J.H., and Aghajanian, G.K. (1996). Nitric oxide and carbon monoxide activate locus coeruleus neurons through a cGMP-dependent protein kinase: involvement of a nonselective cationic channel. J. Neurosci. *16*: 1389–99.

Pineda, J., Ugedo, L., and García-Sevilla, J. a (1997). Enhanced alpha2A-autoreceptor reserve for clonidine induced by reserpine and cholinomimetic agents in the rat vas deferens. Br. J. Pharmacol. *122*: 833–840.

Poppe, H., Rybalkin, S.D., Rehmann, H., Hinds, T.R., Tang, X.-B., Christensen, A.E., et al. (2008). Cyclic nucleotide analogs as probes of signaling pathways. Nat. Methods *5*: 277–278.

Sachs, D., Villarreal, C., Cunha, F., Parada, C., and Ferreira, S. (2009). The role of PKA and PKCε pathways in prostaglandin E2-mediated hypernociception. Br. J. Pharmacol. *156*: 826–834.

Shi, J., Johansson, J., Woodling, N.S., Wang, Q., Montine, T.J., and Andreasson, K. (2010). The prostaglandin E2 E-prostanoid 4 receptor exerts anti-inflammatory effects in brain innate immunity. J. Immunol. *184*: 7207–7218.

Shibuya, I., Setiadji, S. V, Ibrahim, N., Harayama, N., Maruyama, T., Ueta, Y., et al. (2002). Involvement of postsynaptic EP4 and presynaptic EP3 receptors in actions of prostaglandin E2 in rat supraoptic neurones. J. Neuroendocrinol. *14*: 64–72.

Su, X., Leon, L. a, Wu, C.W., Morrow, D.M., Jaworski, J.-P., Hieble, J.P., et al. (2008). Modulation of bladder function by prostaglandin EP3 receptors in the central nervous system. Am. J. Physiol. Renal Physiol. *295*: F984-94.

Sugimoto, Y., and Narumiya, S. (2007). Prostaglandin E receptors. J. Biol. Chem. *282*: 11613–11617.

Wang, Y.Y., and Aghajanian, G.K. (1987). Excitation of Locus Coeruleus Neurons by an Adenosine 3′,5′-Cyclic Monophosphate-Activated Inward Current: Extracellular and Intracellular Studies in Rat Brain Slices. Synapse *1*: 481–487.

Wang, Y.Y., and Aghajanian, G.K. (1990). Excitation of locus coeruleus neurons by vasoactive intestinal peptide: role of a cAMP and protein kinase A. J. Neurosci. *10*: 3335–3343.

Wise, H. (2006). Lack of interaction between prostaglandin E2 receptor subtypes in regulating adenylyl cyclase activity in cultured rat dorsal root ganglion cells. Eur. J. Pharmacol. *535*: 69–77.

Xu, S., Guo, S., Jiang, X., Yin, Q., Umezawa, T., and Hisamitsu, T. (2003). Effect of indomethacin on the c-fos expression in AVP and TH neurons in rat brain induced by lipopolysaccharide. Brain Res. *966*: 13–8.

Yamaguchi, N., and Okada, S. (2009). Cyclooxygenase-1 and -2 in spinally projecting neurons are involved in CRF-induced sympathetic activation. Auton. Neurosci. Basic Clin. *151*: 82–89.

Yasojima, K., Schwab, C., McGeer, E.G., and McGeer, P.L. (1999). Distribution of cyclooxygenase-1 and cyclooxygenase-2 mRNAs and proteins in human brain and peripheral organs. Brain Res. *830*: 226–236.

Yoshida, K., Oida, H., Kobayashi, T., Maruyama, T., Tanaka, M., Katayama, T., et al. (2002). Stimulation of bone formation and prevention of bone loss by prostaglandin E EP4 receptor activation. Proc. Natl. Acad. Sci. *99*: 4580–4585.

Young, R.N., Billot, X., Han, Y., Slipetz, D.A., Chauret, N., Belley, M., et al. (2004). Discovery and synthesis of a potent, selective and orally bioavailable EP4 receptor agonist. Heterocycles *64*: 437–446.

Zhang, J., and Rivest, S. (1999). Distribution, regulation and colocalization of the genes encoding the EP 2 - and EP 4 -PGE 2 receptors in the rat brain and neuronal responses to systemic inflammation. Eur. J. Neurosci. *11*: 2651–2668.

Tables

Table 1.

Basal firing rate and concentration-effect curve parameters for the excitatory action of the EP4 receptor agonists rivenprost and TCS 2510 on LC neurons in the absence (control) or in the presence of the EP4 (L-161,982) or a combination of the EP2 (PF-04418948) and EP3 (L-798,106) receptor antagonists.

			Concentration-effect curves[1]				
Drugs	Concentration	Basal firing rate (Hz)	Emax (%)	pEC_{50} (M)	(EC_{50}, nM)	Slope factor	*n*
Rivenprost							
Control		0.70 ± 0.09	83.7 ± 13.3	8.84 ± 0.10	(1.43)	0.70 ± 0.17	6
+L-161,982	3 nM	0.80 ± 0.12	67.3 ± 14.2	8.43 ± 0.13	(3.72)	1.43 ± 0.43	5
	30 nM	0.70 ± 0.07	62.2 ± 5.0	8.23 ± 0.08*	(5.92)	0.97 ± 0.15	5
	300 nM	0.82 ± 0.05	62.5 ± 7.5	7.93 ± 0.12*	(11.8)	0.83 ± 0.10	5
+L-798,106	300 nM						
PF-04418948	300 nM	0.75 ± 0.09	80.6 ± 13.0	8.47 ± 0.16	(3.38)	0.81 ± 0.11	5
TCS 2510							
Control		0.78 ± 0.07	98.4 ± 8.1	7.74 ± 0.19	(18.0)	0.67 ± 0.05	6
+L-161,982	300 nM	0.94 ± 0.08	61.0 ± 6.9*	7.43 ± 0.11	(37.5)	1.29 ± 0.25*	5

[1]Values are expressed as mean ± SEM obtained by nonlinear regression of *n* cells. Emax is the maximal excitatory effect, and pEC_{50} is the negative logarithm of the concentration needed to elicit 50% of the Emax. *$P < 0.05$ when compared to the control group of rivenprost (one-way

ANOVA followed by a Dunnett's *post hoc* test) or TCS 2510, respectively (unpaired Student's t-test).

Figure legends

Figure 1. Effect of the EP4 receptor agonist rivenprost on the firing rate of LC neurons in the absence or presence of the EP4 receptor antagonist L-161,982 or a combination of the EP2 receptor antagonist PF-04418948 and EP3 receptor antagonist L-798,106. **(A, B, C)** Representative examples of firing rate recordings of two LC neurons showing the effect of increasing concentrations of rivenprost in the absence **(A)** and presence of L-161,982 (300 nM) **(B)** or presence of PF-04418948 and L-798,106 (300 nM each) **(C)**. The vertical lines represent the number of spikes recorded every 10 s and the horizontal bars the period of drug application. **(D)** Concentration-effect curves for rivenprost in control (filled circles) and in the presence of L-161,982 (3 nM, open circles; 30 nM, full triangles; and 300 nM, open triangles) (left) or in the presence of PF-04418948 and L-798,106 (300 nM each, filled squares) (right). The horizontal axis shows the rivenprost concentration on a semi-logarithmic scale. The vertical axis expresses the increase in firing rate of LC neurons as the percentage of the baseline. Data points are the mean ± SEM at each rivenprost concentration obtained from *n* number of experiments (see Table 1). The lines through the data are the theoretical curves in each group constructed from the mean of the individual concentration-effect curve parameters, as estimated by nonlinear regressions. Note that the concentration-effect curve for rivenprost is shifted to the right by the EP4 receptor antagonist.

Figure 2. Effect of the EP4 receptor agonist TCS 2510 on the firing rate of LC neurons in the absence or presence of the EP4 receptor antagonist L-161,982. (A, B) Representative examples of firing rate recordings of two LC neurons showing the effect of increasing concentrations of TCS 2510 in the absence (A) and presence of L-161,982 (300 nM) (B). The vertical lines represent the number of spikes recorded every 10 s and the horizontal bars the period of drug application. (C) Concentration-effect curves for TCS 2510 in control (filled circles) and in the presence of L-161,982 (300 nM, open triangles). The horizontal axis shows the TCS 2510 concentration on a semi-logarithmic scale. The vertical axis expresses the increase in firing rate of LC neurons as the percentage of the baseline. Data points are the mean ± SEM at each TCS 2510 concentration obtained from n number of experiments (see Table 1). The lines through the data are the theoretical curves in each group constructed from

the mean of the individual concentration-effect curve parameters, as estimated by nonlinear regressions. Note that the Emax of TCS 2510 decreases in the presence of the EP4 receptor antagonist.

Figure 3. Effect of blocking a sodium current and the cAMP/PKA pathway on the rivenprost-induced excitatory effect on LC neurons. **(A)** Representative example of the firing rate recording of an LC neuron showing the effect of rivenprost (30 nM, 10 min) in the presence of low-sodium aCSF (TRIS 80%, 5 min). The vertical lines represent the number of spikes recorded every 10 s and the horizontal bars the period of drug application. Note that TRIS 80% abolishes the stimulatory effect of rivenprost. **(B)** Bar graph showing the increase in the number of spikes per 10 s caused by rivenprost (30 nM) in the absence (control, $n = 6$) and in the presence of TRIS 80% (black bar, $n = 6$) or 2-APB (30 μM, hatched bar, $n = 5$). **(C)** Bar graph showing the increase in the number of spikes per 10 s by rivenprost (30 nM, white bar, $n = 6$), 8-Br-cAMP (1 mM, black bar, $n = 5$), rivenprost in the presence of 8-Br-cAMP (hatched bar, $n = 5$), and the arithmetic sum of the effects of rivenprost and 8-Br-cAMP (black and white bar). Application of rivenprost in the presence of 8-Br-cAMP further increased the excitatory effect caused by 8-Br-cAMP (paired Student's t-test). Note that 8-Br-cAMP does not occlude the excitatory response to rivenprost since no difference was found between the effect of rivenprost in the presence of 8-Br-cAMP and the arithmetic sum of effects (unpaired Student's t-test). **(D)** Bar graph showing the excitatory effect of rivenprost (30 nM, $n = 6$) in the presence of the PKA inhibitor H-89 (10 μM, $n = 5$) compared to control. Bars are the mean ± SEM of n experiments. $^{*}P < 0.05$ when compared to the control group (unpaired Student's t-test).

Figure 4. Effect of butaprost and effect of blocking the $G_{\alpha s}$ and $G_{\beta\gamma}$-dependent signaling, and the PI3K and PKC enzymes on the rivenprost-induced excitatory effect on LC neurons. **(A)** Representative example of the firing rate recording of an LC neuron showing the effect of rivenprost (30 nM, 10 min) in the presence of butaprost (1 μM, 15 min). The vertical lines represent the number of spikes recorded every 10 s and the horizontal bars the period of drug application. **(B)** Bar graph showing the increase in the number of spikes per 10 s caused by rivenprost (30 nM, white bar, $n = 6$), butaprost (1 μM, black bar, $n = 5$), rivenprost in the presence of butaprost (hatched bar, $n = 5$), and the arithmetic sum of the effects of rivenprost and butaprost (black and white bar). Application of rivenprost in the presence of butaprost

further increased the excitatory effect caused by butaprost (paired Student's t-test). Note that application of butaprost does not occlude the excitatory response to rivenprost since no difference was found between the effect of rivenprost in the presence of butaprost and the arithmetic sum of effects (unpaired Student's t-test). **(C, D)** Bar graphs showing the increase in the number of spikes per 10 s caused by rivenprost (30 nM, 10 min) in the absence (control, $n = 6$) or in the presence of NF449 (10 μM, black bar, $n = 6$) or gallein (20 μM, hatched bar, $n = 5$) **(C)** or the PI3K inhibitor wortmannin (100 nM, black bar, $n = 5$) or the PKC inhibitor chelerythrine (10 μM, hatched bar, $n = 5$) **(D)**. Bars are the mean ± SEM of n experiments. *$P < 0.05$ when compared to the control group (unpaired Student's t-test).

Figure 1

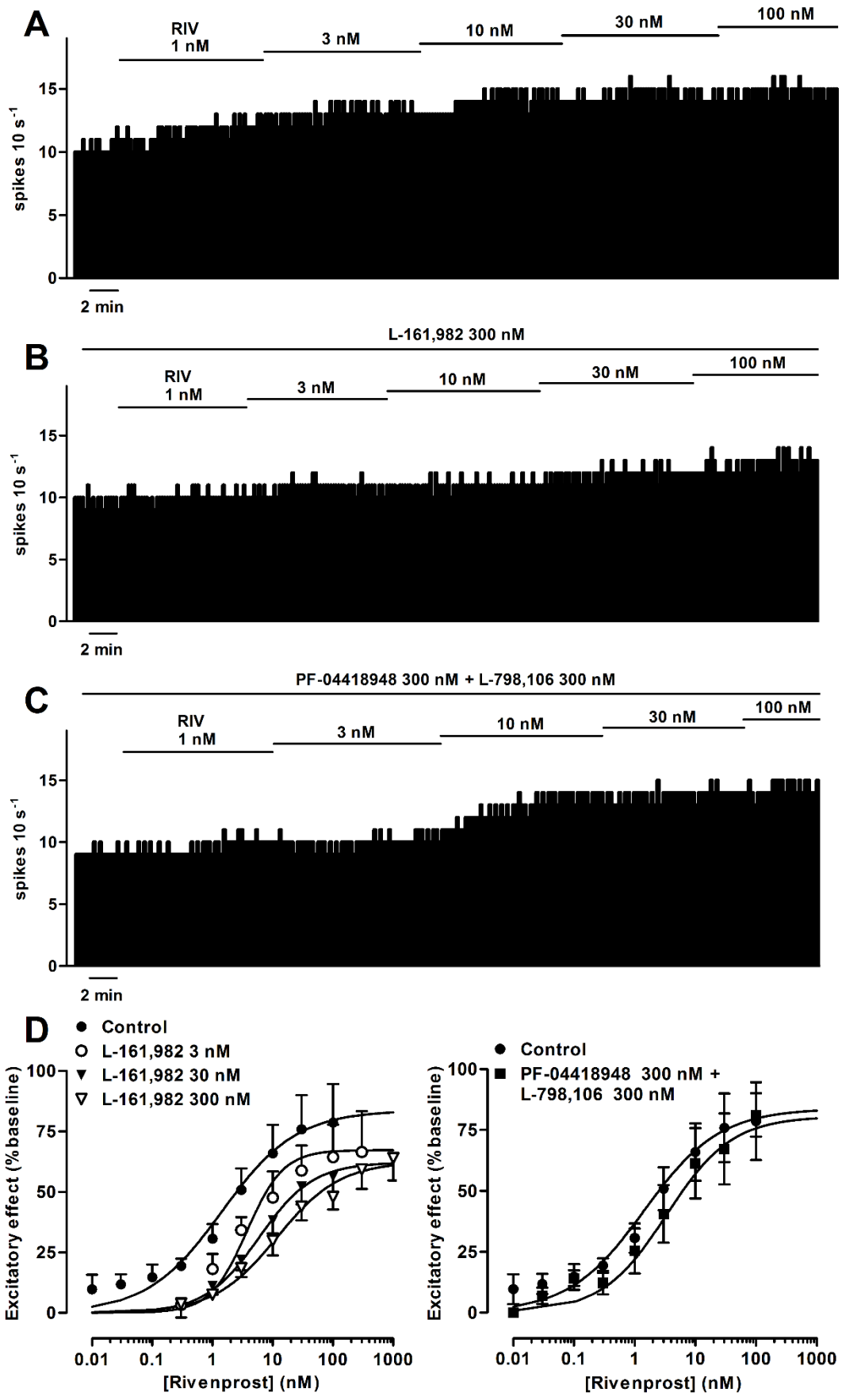
A
RIV
1 nM
3 nM
10 nM
30 nM
100 nM
spikes 10 s-1
2 min
B
L-161,982 300 nM
C
PF-04418948 300 nM + L-798,106 300 nM
D
Control
L-161,982 3 nM
L-161,982 30 nM
L-161,982 300 nM
PF-04418948 300 nM +
L-798,106 300 nM
Excitatory effect (% baseline)
[Rivenprost] (nM)

Figure 2

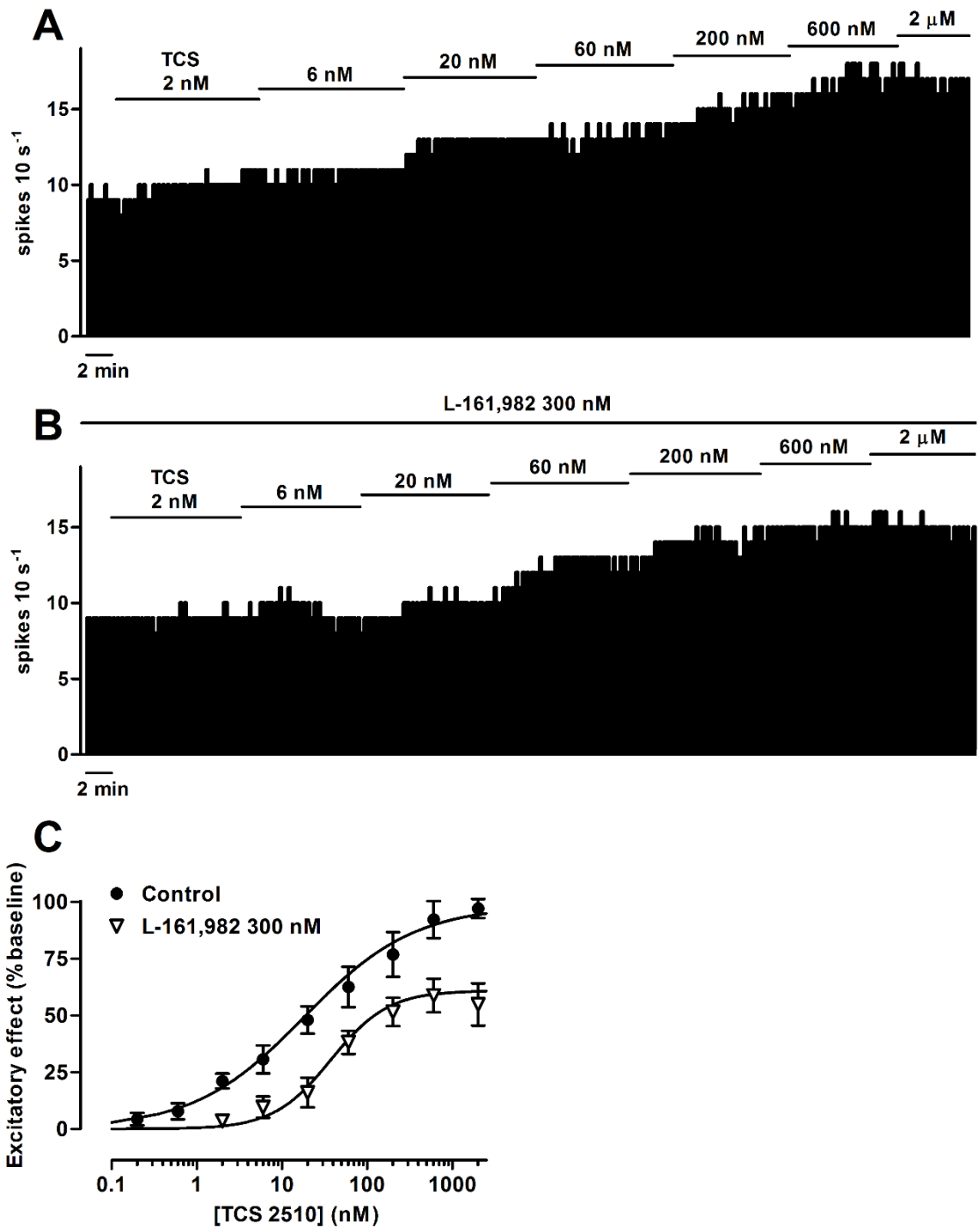
A
TCS
2 nM
6 nM
20 nM
60 nM
200 nM
600 nM
2 μM
spikes 10 s-1
0
5
10
15
2 min
B
L-161,982 300 nM
TCS
2 nM
6 nM
20 nM
60 nM
200 nM
600 nM
2 μM
spikes 10 s-1
0
5
10
15
2 min
C
Control
L-161,982 300 nM
Excitatory effect (% baseline)
0
25
50
75
100
0.1
1
10
100
1000
[TCS 2510] (nM)

Figure 3

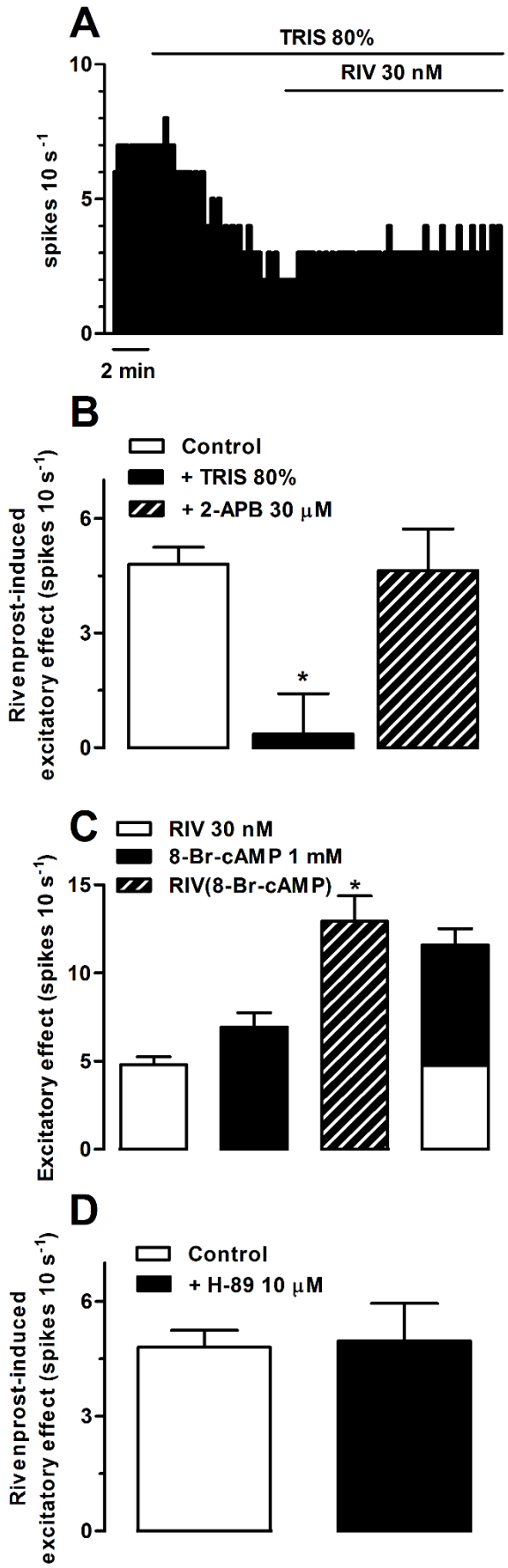
A
TRIS 80%
RIV 30 nM
spikes 10 s-1
10
5
0
2 min
B
Control
+ TRIS 80%
+ 2-APB 30 μM
Rivenprost-induced excitatory effect (spikes 10 s-1)
6
3
0
*
C
RIV 30 nM
8-Br-cAMP 1 mM
RIV(8-Br-cAMP)
*
Excitatory effect (spikes 10 s-1)
15
10
5
0
D
Control
+ H-89 10 μM
Rivenprost-induced excitatory effect (spikes 10 s-1)
6
3
0

Figure 4

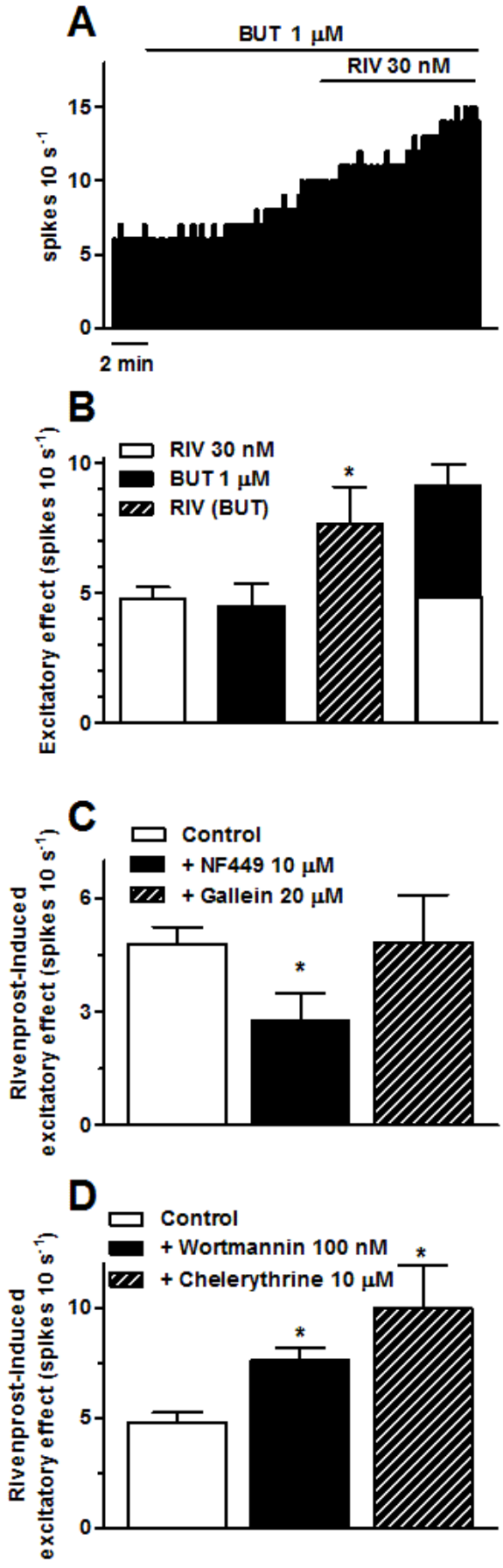
A
BUT 1 µM
RIV 30 nM
spikes 10 s-1
15
10
5
0
2 min
B
RIV 30 nM
BUT 1 µM
RIV (BUT)
Excitatory effect (spikes 10 s-1)
10
5
0
*
C
Control
+ NF449 10 µM
+ Gallein 20 µM
Rivenprost-Induced excitatory effect (spikes 10 s-1)
6
3
0
*
D
Control
+ Wortmannin 100 nM
+ Chelerythrine 10 µM
Rivenprost-Induced excitatory effect (spikes 10 s-1)
10
5
0
*
*

To be submitted to *The Journal of Physiology*

TITLE:

Interaction between opioids and prostaglandin E_2 in the inspiration-generating preBötzinger complex

RUNNING TITLE:

Opioids and PGE_2 in the preBötzinger complex

AUTHORS:

Amaia Nazabal[1,2], David Forsberg[2], Aitziber Mendiguren[1], Joseba Pineda[1], and Eric Herlenius[2*]

[1] Department of Pharmacology, Faculty of Medicine and Nursing, University of the Basque Country (UPV/ EHU), E-48940 Leioa, Bizkaia, Spain. [2]Department of Women's and Children's Health, Karolinska Institutet, Sweden.

***Corresponding author:**

Eric Herlenius, MD, PhD

Department of Women's and Children's Health

Karolinska Institutet

17176 Sweden

E-mail address: eric.herlenius@ki.se

Tel: 0046 (0) 5177 5004

Orcid ID: 0000-0002-6859-0620

Abstract

Prostaglandin E_2 (PGE_2), an inflammatory mediator, depresses breathing movements seemingly from the pre-Bötzinger Complex (preBötC), the brainstem central pattern generator. This inhibitory effect on breathing is mediated by $G_{i/o}$-coupled EP3 receptors and may have serious complications, particularly in neonates; such as apneas, sudden unexpected postnatal collapse or sudden infant death syndrome. PreBötC inspiratory neurons also express μ-opioid receptors and mediate opioid-induced respiratory depression. However, the possible interaction between PGE_2 and opioids to induce major respiratory disruption, e.g., during infections and surgery, remains unknown. Therefore, we performed live time-lapse calcium imaging on organotypic brainstem slices of wild-type mice (WT) and mice lacking the EP3 receptor ($Ptger3^{-/-}$). DAMGO (0.5 and 5 μM) or PGE_2 (10 and 100 nM) reduced Ca^{2+} transient frequency of the whole population and respiratory neurons. Notably, in $Ptger3^{-/-}$, PGE_2-induced effect was absent, and that of DAMGO was delayed on time. Application of DAMGO after PGE_2 did not further reduce the oscillatory Ca^{2+} frequency, suggesting a signaling pathway convergence. Indeed, the phosphodiesterase 4 blocker rolipram and the GIRK channel blocker SCH-23390 prevented both DAMGO- and PGE_2-induced reduction in Ca^{2+} oscillatory activity. Finally, DAMGO and PGE_2 reduced the cellular connectivity and synchronicity and increased the segregation into local cell clusters. This effect of DAMGO was abolished by rolipram and SCH-23390, whereas that of PGE_2 was partially hindered by rolipram. Overall, DAMGO and PGE_2 reduce the respiratory-related frequency and cellular interconnectivity of the preBötC *in vitro* through a supposedly common signaling pathway, which seems to modulate the cAMP and GIRK channels.

Keywords*:* PGE_2; EP3 receptor; opioid; respiratory depression; preBötzinger complex

Non-approved abbreviations

- aCSF: artificial cerebrospinal fluid
- MOR: μ-opioid receptor
- PGE_2: prostaglandin E_2
- PGE1: prostaglandin E_1
- preBötC: preBötzinger complex
- Ptger3: eicosanoid prostanoid receptor 3 gene

Introduction

Breathing is a complex mechanism that requires the assembly of numerous processes, including the rhythmic inspiratory drive. This inspiratory pattern is generated by the preBötzinger complex (preBötC), located in the ventrolateral medulla. The preBötC is a highly heterogeneous region comprised by glycinergic, GABAergic, and particularly, glutamatergic respiratory neurons (Koizumi *et al.*, 2013) whose activity needs to be orchestrated to drive a single inspiratory movement. Thus, the majority of preBötC respiratory neurons are inspiratory, implying that they fire in phase with the population activity (Zavala-Tecuapetla *et al.*, 2014), which is in turn synchronized with the inspiratory motor output in slices (Lieske *et al.*, 2000). Consequently, selective ablation of preBötC inspiratory neurons results in disrupted breathing rhythm in slices (Wang *et al.*, 2014) and *in vivo* (Gray *et al.*, 2001). Furthermore, preBötC neurons are interconnected into clusters (Hartelt *et al.*, 2008) and resembling a small-world architecture (Watts & Strogatz, 1998; Forsberg *et al.*, 2016) that allows efficient information transfer within the network at low wiring costs (Achard & Bullmore, 2007).

Opioids are potent analgesics widely used in the clinic, with the major drawback of producing potentially lethal respiratory depression (Niesters *et al.*, 2013). In the breathing brainstem, the preBötC has been considered crucial in the opioid-induced respiratory depression (Montandon & Horner, 2014). In fact, preBötC inspiratory neurons express μ-opioid receptor (MOR) (Gray *et al.*, 1999) and κ-opioid receptor (KOR) RNA (Hayes *et al.*, 2017), and thus, opioids decrease the inspiratory frequency (Gray *et al.*, 1999). The underlying mechanism involves a $G_{i/o}$ protein-dependent (Johnson *et al.*, 1996) decrease of cAMP formation (Ruangkittisakul & Ballanyi, 2010) and opening of GIRK channels (Montandon *et al.*, 2016*b*), which leads to neuronal hyperpolarization (Gray *et al.*, 1999).

On the other hand, prostaglandins are inflammatory mediators synthesized on demand during inflammatory states or at birth (Mitchell *et al.*, 1978; Beiche *et al.*, 1996) by the rate-limiting COX enzyme, which is constitutively found in human and animal brain (Yasojima *et al.*, 1999; Hétu & Riendeau, 2005). The main final product is the prostaglandin E_2 (PGE_2), which mediates pain, fever, and inflammation, but also produces respiratory disorders as demonstrated by several pieces of evidence. First, PGE_2 metabolite concentration in neonatal

cerebrospinal fluid correlates positively with asphyxia and the outcome of hypoxic-ischemic encephalopathy (Björk *et al.*, 2013). Second, the central administration of PGE_2 produces irregular breathing and apneas (Siljehav *et al.*, 2012, 2014). Moreover, PGE_2 microinjection into the preBötC increases the frequency of sighs *in vivo* and aggravates the gasping response to hypoxia in preBötC slices (Koch *et al.*, 2015). PGE_2 exerts its effects by activating G protein-coupled EP receptors: EP1-EP4. Specifically, the PGE_2-induced respiratory disruption *in vivo* seems to be mediated by the EP3 receptor (Hofstetter *et al.*, 2007). Further, recent work from our laboratory has shown that PGE_2 reduces calcium (Ca^{2+}) transient frequency in preBötC organotypic slices via the EP3 receptor (Forsberg *et al.*, 2016). The underlying mechanism may involve the cAMP pathway, as it has been previously suggested for the PGE_1- and opioid-mediated respiratory depression in brainstem-spinal cord preparations (Ballanyi *et al.*, 1997). However, little is known about the possible interaction between PGE_2 and opioids in the preBötC to cause major respiratory disruption, e.g., during infections and surgery. Thus, we aimed to elucidate whether the opioid-induced respiratory depression would be potentiated under inflammatory conditions by testing the effect of the MOR agonist DAMGO in conjunction with PGE_2 on the network activity and connectivity by time-lapse Ca^{2+} imaging on preBötC organotypic slices.

Methods

Animals and ethics statement

C57 black (C57BL/6J) inbred mice (Charles River, Wilmington, MA) were utilized in the experiments. The eicosanoid prostanoid 3 receptor gene (Ptger3) was selectively deleted in knockout mice ($Ptger3^{-/-}$) with a C57BL/6J background, as described previously (Fleming *et al.*, 1998). C57BL/6J mice were then used as experimental controls for $Ptger3^{-/-}$ mice. All mice were reared by their mothers under standardized conditions with a 12:12-hr light-dark cycle. Food and water were provided *ad libitum*. The studies were performed in accordance with European Community Guidelines and approved by the regional ethic committee. The animals were reared and kept at the Department of Comparative Medicine, Karolinska Institutet, Stockholm, Sweden.

Brainstem organotypic cultures

As previously described in detail (Forsberg *et al.*, 2016), P2-P5 mice pups were used for the organotypic brainstem slice cultures. Briefly, the pups were decapitated at the cervical C3–C4 level. The heads were washed with cold dissection medium and the brain was dissected. The brain was sectioned into 300-µm-thick transverse slices by using a McIlwain Tissue Chopper (Ted Pella, Inc., Redding, CA, USA). Slices were selected by using anatomical landmarks, such as the shape and size of the entire slice and the fourth ventricle, according to online references (Ruangkittisakul *et al.*, 2006, 2011, 2014). On the slices, the preBötC is located within ventrolateral regions. Selected slices were washed by moving them to brain slice medium (55% Dulbecco's modified Eagle's medium, 32.5% Hank's balanced salt solution, 0.3% glucose, 10% fetal bovine serum, 1% HEPES buffer and 1% Antibiotic-Antimycotic [Invitrogen, UK]), after which they were carefully placed on insert membranes (Millicell Culture Plate Inserts; Millipore, Billerica, MA, USA) in six-well plates. The membranes were coated in advance with poly-L-lysine (0.3 ml; 0.1 mg/ml, Sigma- Aldrich, St. Louis, MO, USA). Brain slice medium (1 ml) was placed underneath the membrane, and all fluid on top of the membrane was removed in order to avoid impaired oxygenation (Frantseva *et al.*, 1999). The brainstem slice cultures were maintained in an incubator (37˚C, 5% CO2), and the medium was changed every second day. The brainstem slices were kept in culture for 7–21 days in vitro (DIV) before live imaging experiments.

Ca^{2+} time-lapse imaging

For Ca^{2+} imaging, Fluo-8 AM (AAT Bioquest, Inc., USA) was added to a solution of pluronic acid 1% in DMSO (Invitrogen, UK) and was used at 10 µM in artificial cerebrospinal fluid (aCSF, containing in mM: 151.1 Na^+, 3 K^+, 2 Ca^{2+}, 2 Mg^{2+}, 135 Cl^-, 1.1 $H_2PO_4^-$, 25 HCO_3^- and 10 glucose). To localize the preBötC, tetramethylrhodamine-conjugated Substance P (TMR-SP; Biomol, Oakdale, NY, USA) was used at a final concentration of 3 µM aCSF. The TMR-SP solution was placed on top of the brainstem slice and incubated for 10 min at 37˚C in an atmosphere of 5% CO_2. The TMR-SP solution was then replaced with 1 ml of 10 µM Fluo-8 solution. The Fluo-8 solution was incubated for 30 min (37˚C, 5% CO_2). Before imaging, the slice was washed with aCSF for 1-5 min (37˚C, 5% CO_2). During time-lapse imaging, slices were kept in an open chamber perfused with aCSF (1.5 ml/min) by using a peristaltic pump. A Chamlide Inline Heater (Live Cell instruments, Seoul, Korea, cat no. IL-H-10) was used for temperature control, and a Chamlide AC-PU perfusion chamber for 25-mm coverslips (Live

Cell instruments, Seoul, Korea, cat no. ACPU25) was used for perfusion. The aCSF was constantly bubbled with 5% CO_2 and 95% O_2. The temperature of the chamber was set to 32˚C. Images were captured by using a Zeiss AxioExaminer D1 microscope equipped with 20x and 40x water immersion objectives (N.A. 1.0), a Photometrics eVolve EMCCD-camera and filter sets 38HE (Zeiss) and et560/hq605 (Chroma, Bellows Falls, VT, USA). For live imaging, a frame interval of 0.5 s was used. Exposure time was set to 100 ms. Substances added during imaging were [D-Ala2, N-Me-Phe4, Gly5-ol]-enkephalin (DAMGO, 0.5 – 5 µM; Sigma-Aldrich, St. Louis, MO, USA, cat no. E7384), naloxone hydrochloride dihydrate (naloxone, 5 µM; Sigma-Aldrich, St. Louis, MO, USA, cat no. N7758), R(+)-SCH-23390 hydrochloride (SCH-23390 15 µM; Sigma-Aldrich, St. Louis, MO, USA, cat no. D054), prostaglandin E_2 (PGE_2, 10 – 100 nM; Sigma-Aldrich, St. Louis, MO, USA, cat no. P5640), and rolipram (5 µM; Sigma-Aldrich, St. Louis, MO, USA, cat no. R6520). All substances were dissolved in aCSF prior to experimentation and added to the chamber by using a continuous flow system. SCH-23390 was added to the Fluo-8 solution for the 30-minute incubation. For each experiment, a control or baseline period with aCSF was followed by drug application. The drug concentrations employed in this investigation are in accordance to those used in previous studies in slices (Zamalloa *et al.*, 2009; Ruangkittisakul & Ballanyi, 2010; Chee *et al.*, 2011; Forsberg *et al.*, 2016).

Data analysis and statistics

Ca^{2+} imaging time traces were analyzed with a recently published method (Malmersjo *et al.*, 2013; Smedler *et al.*, 2014). Regions of interest (ROI) were marked for all cells based on the standard deviation of fluorescence intensity over time, using a semiautomatic, adapted ImageJ script kindly provided by Dr. John Hayes (The College of William and Mary, Williamsburg, VA, USA, http://physimage.sourceforge.net/). For each frame, the mean intensity value within each ROI was measured using ImageJ, along with their coordinates. Then, the fluorescence signals were normalized to baseline values. Synchronized activity between cells was measured by the Pearson correlation with a custom-made script in MATLAB (version 9.2.0.538062 R2017a; MathWorks, Natick, MA, USA) and by the mic2net toolbox (Smedler *et al.*, 2014) (version 6.12; MathWorks). The calculated pair-wise correlation coefficients resulted in a correlation matrix that was converted to an adjacency matrix by applying a cut-off level. The cut-off level was selected by calculating the mean of the 99th percentile of correlation coefficients for a set of experiments with scrambled signals. Scrambling was performed by

randomly translating all traces in the time-domain. The network structure was visualized by plotting a line between pairs of cells, where the color of the lines was proportionate to the correlation coefficient. The degree of connections within a network (connectivity) was defined as the number of cell pairs with a correlation coefficient larger than the cut-off value divided by the total number of cell pairs. PreBötC cells are organized in a small-world structure (Forsberg *et al.*, 2016) formed by hubs or nodes connected in clusters and allowing high connectivity efficiency with a minimal connection cost (Achard & Bullmore, 2007). The information travels from one node to another, so that the parameter mean shortest path length (λ) could be defined as the minimum number of nodes that must be passed in between. In addition, the mean clustering coefficient (σ) is the number of neighbors of a node that are also neighbors of each other. Finally, as the small-world parameter (γ) equals σ/λ (Smedler *et al.*, 2014) these networks are defined by short distance λ and high σ (For further details see figure 1.11 in the introduction section). The parameters were calculated by using the MATLAB BGL library (http://www.mathworks.com/matlabcentral/fileexchange/10922) and compared to the corresponding randomized networks. For each ROI a baseline fluorescence was determined (F0), which was used to normalize the change in fluorescence as $\Delta F/F0$, where $\Delta F=F1-F0$, being F1 is the specific fluorescence intensity at a specific time point, and F0 is the average intensity of 30 s before and after F1. A previously published toolbox was used for the frequency analysis of time traces by the Fourier transform (Uhlén, 2004). Data were further processed in GraphPad Prism 5.01 (GraphPad Software, Inc., USA) to create the figures.

A heterogeneous population of cells constitutes the preBötC, and some of them were found insensitive to DAMGO (Barnes *et al.*, 2007). Thus, the cells were sorted out into two groups depending on their behavior within the first 5 minutes of drug application. The behavior was defined as either decreased or increased Ca^{2+} oscillation frequency compared to control. This analysis allowed the proportion of cells that were affected by the drug in a certain way to be calculated. Then, the behavior of single cells could be followed.

Experiments were excluded based on the following criteria: low dye loading, the total number of cells per slice less than 20, standard deviation (SD) at the control period higher than the 50% of the mean frequency, and peaks of maximum amplitude in the Fourier transform of calcium oscillation signal above 200 mHz.

Statistical analysis of paired comparisons was performed by two-sided Student's t-test. Comparisons among more than two experimental conditions by one-way analysis of variance

(ANOVA) followed by a Dunnett's *post hoc* for comparison with a control group and only if F achieved the necessary level of statistical significance (i.e. $P < 0.05$) and there was no significant variance inhomogeneity. All calculations for the statistical tests were conducted with Microsoft Excel 2016 (16.0.4639.1000 for Windows), LibreOffice Calc (6.0.7.3 for Ubuntu), and GraphPad Prism (5.01 for Windows). In all cases, $P < 0.05$ was considered statistically significant. Data are presented as mean ± SD.

Results

Effect of the MOR agonist DAMGO on the cellular activity and network connectivity of the preBötC in vitro

The rhythmic cellular activity of the preBötC is directly related to the respiratory frequency (Alsahafi *et al.*, 2015), so its neuronal hyperpolarization can lead to apneas *in vivo* (Huckstepp *et al.*, 2016). Moreover, it is considered indispensable for the opioid-induced respiratory depression (Montandon & Horner, 2014), as the majority of the $NK1R^+$ cells (i.e., respiratory neurons) in the preBötC co-express MOR (Gray *et al.*, 1999). Therefore, to determine the effect of opioids in preBötC cells *in vitro*, we applied the high-affinity MOR agonist DAMGO (0.5 – 5 μM) for 15 min to organotypic slices and measured Ca^{2+} fluctuations. DAMGO (0.5 μM) did not modify the Ca^{2+} transient amplitude or frequency at any time (n = 7) but the highest concentration of DAMGO (5 μM) reduced by 17.2 ± 7.8% the relative amplitude and by 21.7 ± 6.8% the frequency of Ca^{2+} transients within 5 min (n = 7, P < 0.05 compared to baseline; Figures 1A, B, C, and D, Table 1). Furthermore, within the first 5 min of recording, the effect of the highest concentration of DAMGO (5 μM) was greater than that of DAMGO 0.5 μM (n = 7, P < 0.05 compared to DAMGO 0.5 μM; Figures 1B and C) and more cells were inhibited (75.3 ± 11.0% *vs.* 46.9 ± 14.5%, respectively; n = 7 each, P < 0.05; Figure 1D). The inhibitory effect of DAMGO (5 μM) persisted throughout the experiment (15 min) (Figures 1B and C) showing a small recovery in the Ca^{2+} oscillatory frequency during the last 5 min of application (n = 7, P < 0.05 when compared to the previous 5 min period; Figure 1C), possibly due to MOR desensitization (Lowe *et al.*, 2013). Furthermore, $NK1R^+$ neurons showed a similar inhibition in the Ca^{2+} transient relative amplitude and frequency to the whole cell population (Figure 1A, Table 1), and possibly suggesting that the effect on respiratory neurons might define the behavior of the whole network. In light of these results, the opioid agonist DAMGO reduced the Ca^{2+} oscillatory activity of respiratory neurons in preBötC organotypic cultures.

During an inflammatory state or at birth, there is an endogenous release of PGE_2 (Mitchell *et al.*, 1978), which has been shown to increase the frequency of gasps and sighs at low concentrations (Koch *et al.*, 2015) via activation of the $G_{i/o}$-coupled EP3 receptor in the preBötC (Forsberg *et al.*, 2016). Furthermore, a mutual dependency on the cAMP pathway has been suggested for both opioids and prostanoids (Ballanyi *et al.*, 1997). Thus, to study the possible interaction between the prostanoid and the opioid systems, we analyzed the effect of DAMGO in mice genetically modified to lack the PGE_2-EP3 receptor ($Ptger3^{-/-}$) and compared

them to wild-type mice (WT). Administration of DAMGO (5 μM) in Ptger3$^{-/-}$ mice did not inhibit Ca^{2+} transient amplitude and produced a delayed effect on the oscillatory frequency, as it did not change within the first 10 min, and required 15 min to inhibit to the same extent than WT mice did within 5 min (17.0 ± 13.4% reduction within 15 min in Ptger3$^{-/-}$ mice; $n = 8$, $P < 0.05$ compared to baseline; Figures 1B and C). This result means that the DAMGO-induced reduction in Ca^{2+} transient frequency was more gradual in mice lacking the EP3 receptor, but equal in magnitude as in WT mice. Furthermore, this trend held for respiratory neurons, which showed a decrease in Ca^{2+} signaling frequency only within 15 min of DAMGO (5 μM) administration. Thus, showing that the modification in Ca^{2+} transient amplitude induced by DAMGO (5 μM) was hindered in Ptger3$^{-/-}$. Overall, this delayed effect of opioids in mice lacking the EP3 receptor suggests an interaction between the opioid and the prostanoid systems.

PreBötC pacemaker neurons have synchronized activity mediated by gap junctions and excitatory synaptic interactions (Koshiya & Smith, 1999; Rekling *et al.*, 2000). This synchronized activity between interconnected cells is crucial for driving the inspiratory output (Koshiya & Smith, 1999). According to the algorithm employed, two cells are defined as connected if their correlation coefficient exceeds the set cut-off (Smedler *et al.*, 2014). Administration of DAMGO (5 μM) reduced the mean correlation above cut-off values in WT mice (from 0.74 ± 0.06 to 0.59 ± 0.07; $n = 7$, $P < 0.05$; Figure 1E) thus suggesting a reduced interconnectivity among cells. Furthermore, DAMGO (5 μM) administration reduced the number of correlations per active cell (from 33 ± 21 to 6 ± 3; $n = 7$, $P < 0.05$), suggesting a reduced functional coupling. Likewise, Ptger3$^{-/-}$ mice displayed similar reductions in the mean correlation above cut-off (from 0.86 ± 0.04 to 0.67 ± 0.10; $n = 8$, $P < 0.05$) and the number of correlations per active cell (from 61 ± 35 to 28 ± 18; $n = 8$, $P < 0.05$) upon DAMGO (5 μM) application. These results suggest that the opioid receptor agonist DAMGO reduced the network synchronization of preBötC cells in organotypic slices and that this effect was not altered in mice lacking the EP3 receptor.

Synchronized bursting activity depends on the network topology (Gaiteri & Rubin, 2011) and preBötC neurons are organized into clusters interconnected by hubs resembling the small-world architecture (Hartelt *et al.*, 2008; Forsberg *et al.*, 2016). Thereby, neighboring cells in a network are wired with a few migratory outputs that reduce the average path length between nodes (Watts & Strogatz, 1998; Smedler *et al.*, 2014), and thus providing efficient transmission

of information (Achard & Bullmore, 2007). These networks are defined by the parameters: mean clustering coefficient (σ), mean shortest path length (λ), and small-world parameter (γ= σ/λ). DAMGO (0.5 – 5 μM) increased the σ within 5 min in WT mice (n = 7, both $P < 0.05$ compared to baseline; Figure 1F) and then it returned back to baseline, suggesting increased segregation into clusters and tendency towards local connections during the first 5 min. Similarly, DAMGO (0.5 – 5 μM) increased the γ parameter (n = 7, both $P < 0.05$ compared to baseline; Figure 1F), indicating an enhancement of small-world features. Furthermore, the highest concentration of DAMGO (5 μM) increased λ by 11.8 ± 6.7% (n = 7, $P < 0.05$ compared to baseline; Figure 1F) and produced a higher increase in σ and γ than with DAMGO (0.5 μM) (n = 7, both $P < 0.05$; Figure 1F). Likewise, DAMGO (5 μM) increased σ and γ in Ptger3$^{-/-}$ mice within the same time span (5 min) (Figure 1F) and did not change any further afterward. However, the DAMGO-induced effect on σ and γ was lower in Ptger3$^{-/-}$ than in WT mice (σ by 71.7% and γ by 75.5%; n = 8, both $P < 0.05$ compared to WT; Figure 1F). This result suggests that the effect of DAMGO on the network parameters may be hindered in mice lacking the EP3 receptor. Overall, these data insinuate that DAMGO reduced the synchronicity of the network by promoting segregation and local connections within a cluster with a reduction in the outgoing information.

Finally, to ascertain whether the observed effects induced by DAMGO were mediated by MOR activation, we tested the effect of DAMGO (5 μM) in the presence of the MOR antagonist naloxone. Administration of naloxone (5 μM) for 10 min did not change the Ca^{2+} signaling activity but completely abolished the DAMGO-induced reduction in Ca^{2+} transient frequency or relative amplitude in the whole network and respiratory neurons ($P < 0.05$ compared to control in the absence of naloxone; Table 1). Furthermore, naloxone blocked the DAMGO-induced modifications of the network parameters and connectivity. These results suggest that MOR activation mediates the inhibitory effect induced by DAMGO in preBötC cellular activity and connectivity *in vitro*.

Effect of PGE_2 and its interaction with DAMGO on the cellular activity and network connectivity of the preBötC in vitro

Prostaglandins have been reported to inhibit the inspiratory nerve discharge in brainstem-spinal cord preparations (Ballanyi *et al.*, 1997) and to increase the frequency of sighs *in vivo* (Forsberg *et al.*, 2016). This effect may be particularly threatening in neonates, as high levels of PGE_2

metabolite in neonatal cerebrospinal fluid has been associated with severe perinatal asphyxia (Björk *et al.*, 2013). Furthermore, activation of EP3 receptors in the preBötC has been shown to decrease the Ca^{2+} transient frequency (Forsberg *et al.*, 2016). Here, we aimed to understand whether prostaglandins and opioids may interact to produce major respiratory depression. Thus, we examined the effect of PGE_2 in preBötC organotypic cultures and then tested the effect of DAMGO in the presence of PGE_2. Administration of PGE_2 (10 – 100 nM) for 5 min did not modify the relative Ca^{2+} transient amplitude but reduced the Ca^{2+} transient frequency in WT mice (n = 12 and n = 10, respectively, both $P < 0.05$ compared to baseline; Table 2; Figures 2A and B). This PGE_2-induced inhibitory effect was not observed in Ptger3$^{-/-}$ mice (n = 9 and n = 10, respectively, both $P < 0.05$ compared to WT; Table 2; Figure 2A), which suggests that EP3 receptor activation mediates the inhibition of network activity caused by PGE_2 in the preBötC *in vitro*, as already described(Forsberg *et al.*, 2016). Further, the effect of the highest concentration of PGE_2 (100 nM) was greater than that of PGE_2 (10 nM) (n = 10 and n = 12, respectively, $P < 0.05$; Table 2; Figures 2A and B) and more cells were inhibited (72.3 ± 8.5% *vs*. 58.3 ± 13.8%; n = 10 and n = 12, respectively, $P < 0.05$; Figure 2B). Notably, during PGE_2 (100 nM) administration, the Ca^{2+} transient frequency reduction in $NK1R^+$ cells was similar to the whole cell population (Table 2), thus suggesting that preBötC respiratory neurons were sensitive to PGE_2, in accordance with previous studies(Forsberg *et al.*, 2016).

Next, we assessed the possible interaction between opioids and prostaglandins by applying DAMGO in the presence of PGE_2. Thus, the lowest concentration of DAMGO (0.5 µM) in the presence of PGE_2 (10 nM) did not further change Ca^{2+} transient amplitude or frequency (from 53.5 ± 5.8 mHz to 51.8 ± 5.1 mHz in WT, before and after DAMGO administration; n = 12, $P > 0.05$ compared to the frequency during PGE_2 administration; Figures 2A and B). Similarly, bath perfusion with the highest concentration of DAMGO (5 µM) in the presence of PGE_2 (100 nM) did not further inhibit the Ca^{2+} transient frequency, but decreased the amplitude of the whole network and $NK1^+$ cells (n = 10, $P < 0.05$ compared to baseline; Table 2, Figures 2A and B). Furthermore, the DAMGO-induced reduction in Ca^{2+} transient frequency was smaller in the presence of PGE_2 than in the absence in WT but not in Ptger3$^{-/-}$ ($P < 0.05$ compared to controls in the absence of PGE_2), which suggest that the inhibitory effect of DAMGO was prevented by prior administration of PGE_2 in an EP3 receptor-dependent manner. Overall, these data indicate that the onset of PGE_2-induced inhibitory effect on Ca^{2+} oscillatory activity prevented any further reduction caused by DAMGO. Thus, EP3 receptor activation apparently

occluded the effect of DAMGO and therefore, both EP3 and MOR receptor activation seems to share a similar signaling pathway, as elsewhere mentioned (Ballanyi *et al.*, 1997).

Analysis of the network Ca^{2+} activity revealed that PGE_2 (10 nM) did not modify any parameter, but PGE_2 (100 nM) decreased the mean correlation above cut-off values in WT (from 0.74 ± 0.13 to 0.62 ± 0.10; $n = 10$, $P < 0.05$ compared to baseline; Figure 2C) and Ptger3$^{-/-}$ mice (from 0.77 ± 0.14 to 0.59 ± 0.15; $n = 10$, $P > 0.05$ compared to WT). These results suggest a decreased network synchronicity induced by PGE_2, which was not apparently mediated by the EP3 receptor. However, PGE_2 (100 nM) reduced the number of correlations per active cell in WT (from 36 ± 16 to 21 ± 17; $n = 10$, $P < 0.05$ compared to baseline) but not in Ptger3$^{-/-}$ mice, which implies that EP3 receptor activation may reduce the functional interconnectivity among cells. Overall, these data indicate that PGE_2 reduces the network connectivity and synchronicity of preBötC cells and that this effect may be partly mediated by EP3 receptor activation.

Intriguingly, DAMGO (5 μM) in the presence of PGE_2 (100 nM) increased the mean correlation above cut-off values (from 0.62 ± 0.10 to 0.82 ± 0.09; $n = 10$, $P < 0.05$ compared to the decrease observed during PGE_2 administration; Figure 2C) in WT but not in Ptger3$^{-/-}$ mice. Additionally, DAMGO (5 μM) administration in the presence of PGE_2 (100 nM) reversed the number of correlations per active cell to baseline conditions (from 21 ± 17 to 34 ± 26; $n = 10$, $P < 0.05$ compared to the decrease observed during PGE_2 administration) in WT but not in Ptger3$^{-/-}$ mice. These data suggest that DAMGO in the presence of PGE_2 increased the cellular activity synchronization, which was exactly the opposite behavior than in the absence of PGE_2 (see above). These could be due to an inhibitory effect of DAMGO on a broader number of cells, and then a network resynchronization (see discussion).

Finally, regarding the small-world topology, PGE_2 (100 nM) increased σ and γ in WT mice ($n = 10$, $P < 0.05$ compared to baseline; Figure 2D), suggesting segregation into stronger local connections and small-worldness. On the other hand, this effect was not observed in Ptger3$^{-/-}$ mice or with the lowest concentration of PGE_2 (10 nM) ($n = 12$, $P > 0.05$ compared to baseline; Figure 2D). Thus, suggesting that activation of EP3 receptors mediated the increase of segregation and small-world properties caused by PGE_2 application. In addition, subsequent administration of DAMGO (0.5 – 5 μM) in the presence of PGE_2 (10 – 100 nM) did not change any further the network parameters in WT ($n = 10$, $P < 0.05$ compared to baseline; Figure 2D)

and Ptger3$^{-/-}$ mice. This result suggests that activation of EP3 receptors mediated by PGE_2 occluded the following modification of the small-world network features caused by DAMGO.

Involvement of the cAMP/PKA pathway in the inhibitory effect caused by PGE_2 and DAMGO on the cellular activity and network connectivity of the preBötC in vitro

Both MOR and EP3 receptor activation has been described to couple to $G_{i/o}$ protein (Johnson *et al.*, 1996; Ikeda-Matsuo *et al.*, 2010), which is known to decrease the production of cAMP. Further, a previous study made in isolated brainstem-spinal cord preparations has reported that pharmacological elevation of cAMP levels reversed the PGE_1- and opioid-induced inhibition of the respiratory nerve discharge (Ballanyi *et al.*, 1997). To assess whether the proposed common mechanism converges on the cAMP pathway in the preBötC, we utilized the phosphodiesterase 4 (PDE4) inhibitor rolipram (5 μM), which potentially increases cAMP pathway signaling by blocking cAMP degradation. Then, we tested the effect of DAMGO (5 μM) and PGE_2 (100 nM) in the presence of rolipram. Bath perfusion of rolipram (5 μM) for 10 min increased relative Ca^{2+} transient amplitude within the first 5 min ($n = 8$, $P < 0.05$ compared to baseline), returning back to baseline levels after these 5 min (Figures 3A and B) and decreased the Ca^{2+} transient frequency within 10 min ($n = 8$, $P < 0.05$ compared to baseline; Table 3, Figures 3A and B). On the other hand, upon rolipram administration, respiratory neurons showed a similar tendency in the Ca^{2+} oscillatory activity than the whole network, but it did not reach statistical significance ($P > 0.05$ compared to baseline; Table 3, Figure 3B). Given that a low number of slices were dyed for the NK1R in this group (Table 3), we pooled the NK1R$^+$ data of rolipram administration from before PGE_2 and DAMGO to test whether the respiratory neurons would reflect the response observed in the whole network. Thus, pooling the NK1R$^+$ data resulted in significant changes in Ca^{2+} transient relative amplitude within 5 min (from 26.5 ± 3.8 to 30.6 ± 4.4; $n = 12$, $P < 0.05$ compared to baseline) and frequency within 10 min (from 57.7 ± 6.0 to 51.1 ± 7.2; $n = 12$, $P < 0.05$ compared to baseline). This result indicates that blocking the degradation of cAMP increased the relative Ca^{2+} transient amplitude, but decreased the Ca^{2+} transient frequency of preBötC cells and respiratory neurons *in vitro*.

Next, we tested the effect of DAMGO after these modifications in Ca^{2+} oscillatory relative amplitude and frequency induced by rolipram. Administration of rolipram (5 μM) completely blocked the DAMGO (5 μM)-induced changes in Ca^{2+} transient relative amplitude and

frequency in the whole network ($n = 8$, $P < 0.05$ compared to control in the absence of rolipram, Table 3; Figures 3A, B, and C) and $NK1R^+$ cells ($n = 5$, $P < 0.05$ compared to control in the absence of rolipram) (Figures 3A and B; Table 3). These results indicate that the cAMP pathway may have a role in the inhibitory effect caused by DAMGO in the cellular activity of the respiratory network and respiratory neurons of the preBötC.

Likewise, rolipram (5 μM) prevented the reduction in Ca^{2+} transient frequency induced by PGE_2 (100 nM) in the whole network ($P < 0.05$ compared to control in the absence of rolipram; Table 3, Figures 3A, B, and C). Further, this blockade was also observed in respiratory neurons, which did not display any further decrease in the Ca^{2+} transient frequency upon PGE_2 administration ($P > 0.05$ compared to the previous 5 min period in the presence of rolipram; Table 3; Figure 3B). However, this effect was not different from $NK1R^+$ cells in controls ($P > 0.05$ compared to control in the absence of rolipram). These results indicate that inhibition of the cAMP degradation reverted the modification in the respiratory network activity induced by PGE_2, but not that observed in respiratory neurons. Overall, these data suggest that the levels of cAMP may modulate the respiratory depression observed with opioids and prostaglandins, as previously suggested (Ballanyi *et al.*, 1997), and thus, that the cAMP pathway may be the endpoint of the presumed common signaling mechanism.

Regarding the network circuitry, administration of rolipram (5 μM) reduced the mean correlation above cut-off within 10 min (from 0.74 ± 0.04 to 0.65 ± 0.08; $n = 8$, $P < 0.05$ compared to baseline; Figure 3D) and hindered the DAMGO (5 μM)-induced modification in the mean correlation above cut-off (from 0.65 ± 0.08 to 0.68 ± 0.06; $n = 8$, $P < 0.05$ compared to control in the absence of rolipram; Figure 3D). These results suggest that rolipram may reduce the interconnectivity among cells but prevented that caused by DAMGO. Furthermore, rolipram administration did not change the number of correlations per active cell but blocked the reduction caused by DAMGO (from 14 ± 14 to 12 ± 15; $n = 8$, $P > 0.05$ compared to baseline before DAMGO). However, this effect was not different from that observed under control conditions ($n = 8$, $P > 0.05$ compared to control in the absence of rolipram), possibly due to the high variability. These data suggest that inhibition of cAMP degradation partially hampered the effect of DAMGO on the network configuration. Furthermore, administration of rolipram (5 μM) for 10 min did not modify σ, γ or λ, but abolished the DAMGO-induced changes in small-world features ($n = 8$, $P < 0.05$ compared to control in the absence of rolipram;

Figure 3E). Thus, these results suggest that the cAMP pathway seems to mediate the decrease in network synchronicity and connectivity caused by DAMGO in the preBötC.

Furthermore, bath perfusion of rolipram (5 μM) reduced the mean correlation above cut-off within 10 min (from 0.80 ± 0.06 to 0.71 ± 0.11; $n = 8$, $P < 0.05$ compared to baseline; Figure 3D) and blocked the reduction in the mean correlation above cut-off induced by PGE_2 (100 nM) (from 0.71 ± 0.11 to 0.68 ± 0.11; $n = 8$, $P < 0.05$ compared to control in the absence of rolipram; Figure 3D). Additionally, PGE_2 in the presence of rolipram did not alter the number of correlations per active cell (from 12 ± 13 to 5 ± 5; $n = 8$, $P > 0.05$ compared to baseline before PGE_2) but this effect was not different from that observed under control conditions ($n = 8$, $P > 0.05$ compared to control in the absence of rolipram). These data suggest that the cAMP pathway seems to be partially involved in the effect of PGE_2 on the network configuration. Further, PGE_2 (100 nM) in the presence of rolipram did not change σ or γ ($n = 8$, $P > 0.05$ compared to baseline before PGE_2; Figure 3E). However, this effect was not different from that observed in controls ($n = 8$, $P > 0.05$ compared to control in the absence of rolipram), possibly due to the high variability. Thus, these data reveal that blockade of cAMP degradation with rolipram hindered the inhibitory effect of PGE_2 on Ca^{2+} transient frequency and network synchronicity, but it did not seem to intervene in the small-world topology modification caused by PGE_2. As a whole, the cAMP pathway seemed to be involved in both MOR and EP3 receptor activation in the preBötC organotypic cultures.

Involvement of GIRK channel activation in the inhibitory effect caused by PGE_2 and DAMGO on the cellular activity of the preBötC in vitro

Opioid-induced respiratory depression *in vivo* is thought to be mediated by GIRK channels (Montandon *et al.*, 2016*b*). Thus, to verify the involvement of GIRK channels in the inhibitory effect caused by DAMGO or PGE_2 *in vitro*, we incubated the organotypic slices with the GIRK channel blocker SCH-23390 (15 μM) for 30 min during Fluo-8 loading, and then, we tested the effect of DAMGO (5 μM) or PGE_2 (100 nM) by time-lapse Ca^{2+} imaging. Incubation with SCH-23390 (15 μM) did not alter the basal Ca^{2+} transient amplitude (baseline $\Delta F/F_0$ without SCH-23390 = 31.3 ± 3.0 *vs.* with SCH-23390 = 27.5 ± 3.4; $n = 8$, $P > 0.05$) nor frequency (baseline without SCH-23390 = 55.6 ± 3.6 mHz *vs.* with SCH-23390 = 57.3 ± 5.5 mHz; $n = 8$, $P > 0.05$) compared to baseline values before DAMGO (5 μM) administration in controls. However, GIRK channel blockade with SCH-23390 completely prevented the inhibitory effect

of DAMGO (5 μM) on Ca^{2+} transient amplitude and frequency in the whole network and $NK1R^{+}$ cells (n = 8, P < 0.05 compared to control in the absence of SCH-23390; Table 4, Figures 4A and B). This result indicates that GIRK channel activation is involved in the opioid-induced inhibition of respiratory network and respiratory neurons *in vitro*.

Next, we determined whether SCH-23390 would hinder as well the PGE_2-induced inhibition in Ca^{2+} oscillatory frequency. Thus, upon SCH-23390 (15 μM) incubation, PGE_2 (100 nM) did not reduce the Ca^{2+} transient frequency in the whole network and respiratory neurons (P < 0.05 compared to control in the absence of SCH-23390; Table 4, Figures 4A and B). This result suggests that GIRK channel activation seemed to participate in both the opioid- and PGE_2-induced inhibition of cellular calcium activity and respiratory neurons in preBötC organotypic cultures.

Regarding the network connectivity, slice incubation with SCH-23390 (15 μM) did not change the baseline values of mean correlation above cut-off (without SCH-23390: 0.74 ± 0.06 *vs*. 0.80 ± 0.09 with SCH-23390; n = 8, P > 0.05 compared to baseline values before DAMGO 5 μM administration in controls). However, SCH-23390 hampered DAMGO (5 μM)-induced reduction in the mean correlation above cut-off (from 0.80 ± 0.09 to 0.70 ± 0.09; n = 8, P < 0.05 compared to control in the absence of SCH-23390; Figure 4C) and the number of correlations per active cell (from 23 ± 15 to 16 ± 15; n = 8, P < 0.05 compared to control in the absence of SCH-23390). Therefore, GIRK channel activation seemed to contribute to the asynchronous network activity caused by DAMGO in the preBötC. Further, incubation with SCH-23390 (15 μM) did not change the σ, γ or λ parameters compared to control (n = 8, P < 0.05 compared to control in the absence of SCH-23390). However, SCH-23390 blocked the DAMGO (5 μM)-induced modification of small-world features, as it prevented the increase in σ and γ parameters caused by DAMGO (n = 8, P < 0.05 compared to control in the absence of SCH-23390; Figure 4D). Therefore, in view of these data, GIRK channel activation was involved in the reduction of cellular calcium activity produced by DAMGO, and also in the modification of the network synchronicity and small-world topology of preBötC cells *in vitro*.

On the other hand, after slice incubation with SCH-23390 (15 μM), PGE_2 (100 nM) did not significantly reduce the mean correlation above cut-off (from 0.79 ± 0.08 to 0.75 ± 0.09; n = 9, P > 0.05 compared to baseline; Figure 4C) but this effect was not different from that observed under control conditions (n = 9, P > 0.05 compared to control in the absence of SCH-23390).

Furthermore, GIRK channel blockade with SCH-23390 did not prevent the reduction in the number of correlations per active cell caused by PGE_2 (100 nM) (from 30 ± 23 to 4 ± 2; $n = 9$, $P < 0.05$ compared to baseline and $P > 0.05$ *vs.* control in the absence of SCH-23390). Thus, GIRK channel activation was not apparently involved in the PGE_2-induced reduction of the network synchronicity. Further, PGE_2 (100 nM) administration after slice incubation with SCH-23390 did not increase the σ and γ parameters (Figure 4D), and this effect was not different from control in the absence of SCH-23390 ($n = 9$; $P > 0.05$ compared to control). Thus, blocking the GIRK channel activation did not seem to prevent the asynchronous network activity and small-world topology caused by PGE_2 in preBötC organotypic cultures. Overall, these data indicate that GIRK channel activation seems to mediate the opioid- and PGE_2-induced inspiratory frequency inhibition, but it does not apparently intervene in the network rewiring induced by the latter.

Discussion

The purpose of this study was to assess whether the opioid-induced respiratory depression was intensified under inflammatory conditions (i.e., those caused by PGE_2) by time-lapse calcium imaging in brainstem organotypic cultures. In the preBötC cellular network, we found that both MOR agonist DAMGO and EP3 receptor agonist PGE_2 reduced Ca^{2+} oscillatory activity. The effect of DAMGO was blocked by naloxone, whereas deletion of the EP3 receptor abolished the PGE_2-induced effect and delayed that of DAMGO. The reduction in Ca^{2+} oscillatory activity caused by DAMGO was occluded by prior administration of PGE_2, which suggested a common signaling pathway. Indeed, both DAMGO and PGE_2-induced modification in Ca^{2+} activity was prevented by blocking cAMP degradation and GIRK channel activation. Furthermore, both DAMGO and PGE_2 reduced the number of connections among cells and the synchronicity.

Recently, we have developed brainstem organotypic slice cultures containing the preBötC that allow the study of the respiratory brainstem activity *in vitro* (Forsberg *et al.*, 2016). These cultured slice preparations maintain the respiratory-related rhythm (Forsberg *et al.*, 2016; Phillips *et al.*, 2016) identical to acute slices (Phillips *et al.*, 2016) while preserving the cytoarchitecture (Forsberg *et al.*, 2016). These features along with the tissue flattening over time (Forsberg *et al.*, 2016; Phillips *et al.*, 2016) create an optimal model for the activity

evaluation of a broad population of cells by calcium imaging techniques and their synchronicity by means of cross-correlation analysis (Smedler *et al.*, 2014). Furthermore, preBötC respiratory neurons *in vitro* preserve rhythmic Ca^{2+} transients in phase with the inspiratory motor output measured on the hypoglossal XII nerve (Koizumi *et al.*, 2013), and therefore, the observed calcium oscillatory activity in our study is representative of the respiratory rhythm. The PreBötC was identified in our slices with the fluorescent ligand TMR-SP, which labels the NK1R-positive cells and thereby, the respiratory neurons (Gray *et al.*, 1999). In our study, we measured the effect of DAMGO as MOR agonist since it has high affinity and selectivity for the MOR (Raynor *et al.*, 1993). The effect of DAMGO was antagonized by using naloxone, which shows high affinity for all opioid receptors, but especially for the MOR (Raynor *et al.*, 1993). The endogenous inflammatory response was mimicked by using PGE_2, a non-selective EP receptor agonist that shows high affinity for the EP3 receptor (Abramovitz *et al.*, 2000). Finally, the fluorescent dye employed here was non-ratiometric, so the described amplitude data is relative to its baseline, and no intracellular Ca^{2+} concentration could be inferred.

In the current study, DAMGO and PGE_2 reduced Ca^{2+} transient frequency in what seemed a concentration-dependent fashion, as we tested two different concentrations of each and the highest concentration produced a greater inhibition in the frequency than the lowest. Furthermore, the DAMGO (5 μM)-induced reduction in Ca^{2+} transient frequency of the whole population (22%) was similar to that observed with PGE_2 (100 nM) (19%), and further, similar to the breathing frequency reduction (18%) *in vivo* caused by microinjection of DAMGO into the preBötC described elsewhere (Qi *et al.*, 2017). An improvement in the data analysis allowed us to know how single cells behaved over time and how many of them varied their frequency compared to their baseline. By using this script, 75% of the cells showed a marked frequency reduction of 34% upon DAMGO, and similarly, 72% of the cells displayed a frequency reduction with PGE_2 of 32%. Moreover, $NK1R^+$ data revealed that the reduction in Ca^{2+} transient frequency in respiratory neurons upon DAMGO and PGE_2 is representative of the whole population, which may suggest that the respiratory neurons define the activity of the entire network. This result agrees with previous reports in similar brainstem slice culture preparations, which observed Ca^{2+} oscillatory activity only from neurons and not from glial cells (Phillips *et al.*, 2016). Furthermore, previous data from our laboratory demonstrated that $NK1R^+$ cells respond to PGE_2 in the preBötC (Forsberg *et al.*, 2016) and co-express EP3 receptor in medullary sections at the preBötC level (Hofstetter *et al.*, 2007). In line, other

studies showed a co-expression of MOR and NK1R in the preBötC (Gray *et al.*, 1999; Qi *et al.*, 2017) and accordingly, preBötC respiratory neurons have been considered fundamental for the opioid-induced respiratory depression (Montandon *et al.*, 2011).

In our study, the DAMGO-induced reduction in Ca^{2+} transient frequency was prevented by the application of the MOR antagonist naloxone and delayed by deleting the EP3 receptor. Thus, in Ptger3$^{-/-}$ mice, DAMGO (5 μM) needed 15 min instead of 5 min to cause the same magnitude of effect as in WT mice, suggesting a hindered effect of DAMGO in Ptger3$^{-/-}$ mice. Interestingly, this late effect was similar to that observed with the lowest concentration of DAMGO (0.5 μM) in WT mice. Furthermore, the PGE_2-induced frequency decrease was absent in mice lacking the EP3 receptor, in agreement with previous results from our laboratory (Forsberg *et al.*, 2016). These results highlight the functional relevance of the EP3 receptor in the preBötC. Similarly, activation of the EP3 receptor has been shown to have inhibitory actions in other brain regions, for example, it inhibits the network frequency in the neocortex (Koch *et al.*, 2010) and the neuronal activity of the central chemosensitive LC cells (Nazabal et al., unpublished results). In contrast with our study, PGE_2 has shown to increase the fictive sigh frequency in preBötC acute slices, and even increase the eupnoeic frequency at higher concentrations than those employed in our study (Koch *et al.*, 2015). These differences could be due to a loss of selectivity at higher concentrations of PGE_2, given that it has a high affinity for many other prostanoid receptors, and the receptor mediating this effect was not determined in that study.

In the present work, the onset of the PGE_2-induced inhibitory effect occluded any further reduction in Ca^{2+} oscillatory activity caused by DAMGO. Furthermore, this result is congruent with the attenuation of the morphine-induced respiratory depression observed in a neuropathic pain model (Kamei *et al.*, 2011), where the involvement of PGE_2 is widely known (Ma & Quirion, 2008). This occlusion could be caused by the reach of a maximum reduction in Ca^{2+} transient frequency, considering the ongoing Ca^{2+} dynamics that are partly regulated by intracellular stores, and thus a basal Ca^{2+} fluctuation. However, a common signaling pathway was elsewhere mentioned (Ballanyi *et al.*, 1997), so we tested whether it would be plausible. The nature of the proposed common mechanism would be the result of a signaling pathway convergence in either the cAMP or the GIRK channels, based on previous data (Ballanyi *et al.*,

1997; Montandon *et al.*, 2016*b*). In our study, administration of the blocker of cAMP degradation rolipram prevented the DAMGO- and PGE_2-induced reduction in Ca^{2+} oscillatory activity. This result is in consonance with previous studies showing that rolipram restores the inspiratory-related rhythm after DAMGO-induced inhibition in acute slices (Ruangkittisakul & Ballanyi, 2010) and that high cAMP levels reverse the DAMGO- and PGE_1-induced respiratory depression in brainstem-spinal cord preparations (Ballanyi *et al.*, 1997). On the other hand, incubation with the GIRK channel blocker SCH-23390 prevented the reduction in Ca^{2+} transient frequency caused by both DAMGO and PGE_2 in our study. These data agree with previous reports *in vivo*, describing that the respiratory rate decrease produced by microperfusion of DAMGO into the preBötC is blocked by a GIRK channel inhibitor (Montandon *et al.*, 2016*b*). Furthermore, immunohistochemical techniques have demonstrated that $NK1R^+$ cells in the preBötC co-express GIRK channels (Montandon *et al.*, 2016*a*), which suggests that these channels are present in respiratory neurons, and thus, that may intervene in the opioid- and PGE_2-induced respiratory depression. Overall, the inhibitory actions of PGE_2 and DAMGO on the cellular Ca^{2+} transient frequency seems to be mutually dependent on cAMP levels and GIRK channels.

The respiratory rhythmogenesis is thought to be driven by preBötC cellular activity coordination into a group pacemaker mediated by glutamatergic transmission and electrical coupling (Koshiya & Smith, 1999; Rekling *et al.*, 2000). Thus, the study of the network synchronization may be key for understanding the mechanism of opioid- and prostaglandin-induced respiratory depression. Herein, both DAMGO and PGE_2 reduced the mean correlation above cut-off and the number of correlations per active cell, suggesting a reduction in the network circuitry and synchronization. In line with our results, elimination of correlated population activity and desynchronization of Ca^{2+} activity have been observed in the preBötC *in vitro* after blockade of gap junctions (Forsberg *et al.*, 2016) and glutamatergic synaptic transmission (Koshiya & Smith, 1999). It is therefore tempting to speculate that the DAMGO- and PGE_2-induced respiratory depression may be caused by the lack of integrated group pacemaker activity. Intriguingly, in our results, DAMGO restored the baseline values of mean correlation and number of correlations per active cell after the reduction caused by PGE_2. This means that the effect of DAMGO in the presence of PGE_2 was the opposite than in the absence, suggesting that DAMGO administration might affect a broader number of cells that reconfigure the circuit, possibly through an additional mechanism. Furthermore, synchronized bursting

activity depends on the network topology(Gaiteri & Rubin, 2011) and the preBötC is organized into a small-world architecture (Hartelt *et al.*, 2008; Forsberg *et al.*, 2016), where the neuronal connections are favored within clusters, in comparison with across clusters (Hartelt *et al.*, 2008). In fact, in our work, both DAMGO and PGE_2 increased the clustering coefficient and small-world parameter, suggesting segregation into local clusters and a shift towards a more regular topology, which is less synchronizable than the small-world composition (Watts & Strogatz, 1998). Similar alterations of small-world structures have been observed in patients with Alzheimer's disease and neuromyelitis optica (He *et al.*, 2008; Liu *et al.*, 2012), where the global activity integration may be compromised, leading to a weaker population bursting in a computational model (Gaiteri & Rubin, 2011). Overall, the opioid-induced asynchronous network seems to be mediated by MOR activation with the involvement of the cAMP pathway and GIRK channels; while the PGE_2-induced asynchrony seemed to be partly mediated by the EP3 receptor and the cAMP pathway. These results may suggest a different mechanism for PGE_2-induced disruption of network organization, possibly mediated by persistent sodium current and gap junctions as previously suggested for other effects caused by PGE_2 in the preBötC (Koch *et al.*, 2015; Forsberg *et al.*, 2016).

In conclusion, PGE_2 modulates preBötC activity *in vitro* and it seems to interact with the opioid-induced inhibitory effect, so a common signaling pathway was proposed, with the apparent involvement of the cAMP pathway and GIRK channels. Furthermore, both opioids and prostaglandins seem to disrupt the structural integrity of the network, leading to less wiring and synchronicity. Thus, the current study supports that preBötC inspiratory neurons mediate the opioid- and PGE_2-induced respiratory depression by reducing their activity and synchronization. However, it remains unknown the possible implication of other areas of the breathing brainstem (Lalley *et al.*, 2014; Levitt *et al.*, 2015), such as the recently discovered postinspiratory complex (PiCo) (Anderson *et al.*, 2016), that may shape the *in vivo* opioid response into a quantal slowing of the respiratory rhythm (Mellen *et al.*, 2003). The endogenous release of PGE_2 during the course of inflammation and the concurrent treatment with opioids may condition the ventilatory behavior, which may be of relevance in post-operative states. Moreover, the pediatric population should receive special consideration in view of the endogenous release of PGE_2 at birth (Mitchell *et al.*, 1978) and the implication of PGE_2 in neonatal breathing disorders (Siljehav *et al.*, 2014, 2015), which may ultimately lead to apneas during infections by attenuating the hypercapnic and hypoxic response (Siljehav *et al.*, 2014).

Acknowledgments

This work was supported by the Ministerio de Ciencia e Innovación [Grant SAF2008-03612] and the University of the Basque Country (UPV/EHU) [Grant GIU14/29]. Pineda´s research group takes part in a network unit supported by the University of the Basque Country [UFI 11/35]. A. Nazabal was supported by predoctoral fellowships from the Basque Government. The experiments comply with the current laws of Spain.

Conflict of interest

EH: employed at the Karolinska Institutet and the Karolinska University Hospital and is a Co-inventor of a patent application regarding biomarkers and their relation to breathing disorders, WO2009063226. The other authors declare that they have no conflict of interest.

References

Abramovitz M, Adam M, Boie Y, Carrière MC, Denis D, Godbout C, Lamontagne S, Rochette C, Sawyer N, Tremblay NM, Belley M, Gallant M, Dufresne C, Gareau Y, Ruel R, Juteau H, Labelle M, Ouimet N & Metters KM (2000). The utilization of recombinant prostanoid receptors to determine the affinities and selectivities of prostaglandins and related analogs. *Biochim Biophys Acta - Mol Cell Biol Lipids* **1483,** 285–293.

Achard S & Bullmore E (2007). Efficiency and cost of economical brain functional networks. *PLoS Comput Biol* **3,** 0174–0183.

Alsahafi Z, Dickson CT & Pagliardini S (2015). Optogenetic excitation of preBotzinger complex neurons potently drives inspiratory activity in vivo. *J Physiol* **593,** 3673–3692.

Anderson TM, Garcia AJ, Baertsch NA, Pollak J, Bloom JC & Wei AD (2016). A novel excitatory network for the control of breathing. *Nature* **536,** 76–80.

Ballanyi K, Lalley PM, Hoch B & Richter DW (1997). cAMP-dependent reversal of opioid- and prostaglandin-mediated depression of the isolated respiratory network in newborn rats. *J Physiol* **504,** 127–134.

Barnes BJ, Tuong C-M & Mellen NM (2007). Functional imaging reveals respiratory network activity during hypoxic and opioid challenge in the neonate rat tilted sagittal slab preparation. *J Neurophysiol* **97,** 2283–2292.

Beiche F, Scheuerer S, Brune K, Geisslinger G & Goppelt-Struebe M (1996). Up-regulation of cyclooxygenase-2 mRNA in the rat spinal cord following peripheral inflammation. *FEBS Lett* **390,** 165–169.

Björk L, Leifsdottir K, Saha S & Herlenius E (2013). PGE2 - Metabolite levels in CSF correlate to HIE score and outcome after perinatal asphyxia. *Acta Paediatr Int J Paediatr* **102,** 1041–1047.

Chee MJ, Price CJ, Statnick M a & Colmers WF (2011). Nociceptin/orphanin FQ suppresses the excitability of neurons in the ventromedial nucleus of the hypothalamus. *J Physiol* **589,** 3103–3114.

Fleming EF, Athirakul K, Oliverio MI, Key M, Goulet J, Koller BH & Coffman TM (1998). Urinary concentrating function in mice lacking EP3 receptors for prostaglandin E2. *Am J*

Physiol **275,** F955–F961.

Forsberg D, Horn Z, Tserga E, Smedler E, Silberberg G, Shvarev Y, Kaila K, Uhlén P & Herlenius E (2016). CO2-evoked release of PGE2 modulates sighs and inspiration as demonstrated in brainstem organotypic culture. *Elife* **5,** 1–41.

Frantseva M V., Carlen PL & El-Beheiry H (1999). A submersion method to induce hypoxic damage in organotypic hippocampal cultures. *J Neurosci Methods* **89,** 25–31.

Gaiteri C & Rubin JE (2011). The Interaction of Intrinsic Dynamics and Network Topology in Determining Network Burst Synchrony. *Front Comput Neurosci* **5,** 10.

Gray PA, Janczewski WA, Mellen N, McCrimmon DR & Feldman JL (2001). Normal breathing requires preBötzinger complex neurokinin-1 receptor-expressing neurons. *Nat Neurosci* **4,** 927–930.

Gray PA, Rekling JC, Bocchiaro CM & Feldman JL (1999). Modulation of respiratory frequency by peptidergic input to rhythmogenic neurons in the preBötzinger complex. *Science (80-)* **286,** 1566–1568.

Hartelt N, Skorova E, Manzke T, Suhr M, Mironova L, Kügler S & Mironov SL (2008). Imaging of respiratory network topology in living brainstem slices. *Mol Cell Neurosci* **37,** 425–431.

Hayes JA, Kottick A, Picardo MCD, Halleran AD, Smith RD, Smith GD, Saha MS & Del Negro CA (2017). Transcriptome of neonatal preBötzinger complex neurones in Dbx1 reporter mice. *Sci Rep* **7,** 8669.

He Y, Chen Z & Evans A (2008). Structural Insights into Aberrant Topological Patterns of Large-Scale Cortical Networks in Alzheimer's Disease. *J Neurosci* **28,** 4756–4766.

Hétu P-O & Riendeau D (2005). Cyclo-oxygenase-2 contributes to constitutive prostanoid production in rat kidney and brain. *Biochem J* **391,** 561–566.

Hofstetter AO, Saha S, Siljehav V, Jakobsson P-J & Herlenius E (2007). The induced prostaglandin E2 pathway is a key regulator of the respiratory response to infection and hypoxia in neonates. *Proc Natl Acad Sci U S A* **104,** 9894–9899.

Huckstepp RTR, Henderson LE, Cardoza KP & Feldman JL (2016). Interactions between

respiratory oscillators in adult rats. *Elife* **5,** 1–22.

Ikeda-Matsuo Y, Tanji H, Ota a., Hirayama Y, Uematsu S, Akira S & Sasaki Y (2010). Microsomal prostaglandin e synthase-1 contributes to ischaemic excitotoxicity through prostaglandin E 2 EP 3 receptors. *Br J Pharmacol* **160,** 847–859.

Johnson SM, Smith JC, Feldman JL, Smith C, Feldman JL, Smith JC & Jack L (1996). Modulation of respiratory rhythm in vitro : role of Gi / o protein-mediated mechanisms. *J Appl Physiol* **80,** 2120–2133.

Kamei J, Ohsawa M, Hayashi SS & Nakanishi Y (2011). Effect of chronic pain on morphine-induced respiratory depression in mice. *Neuroscience* **174,** 224–233.

Koch H, Caughie C, Elsen FP, Doi A, Garcia AJ, Zanella S & Ramirez JM (2015). Prostaglandin E2 differentially modulates the central control of eupnoea, sighs and gasping in mice. *J Physiol* **593,** 305–319.

Koch H, Huh S-E, Elsen FP, Carroll MS, Hodge RD, Bedogni F, Turner MS, Hevner RF & Ramirez J-M (2010). Prostaglandin E2-Induced Synaptic Plasticity in Neocortical Networks of Organotypic Slice Cultures. *J Neurosci* **30,** 11678–11687.

Koizumi H, Koshiya N, Chia JX, Cao F, Nugent J, Zhang R & Smith JC (2013). Structural-Functional Properties of Identified Excitatory and Inhibitory Interneurons within Pre-Botzinger Complex Respiratory Microcircuits. *J Neurosci* **33,** 2994–3009.

Koshiya N & Smith JC (1999). Neuronal pacemaker for breathing visualized in vitro. *Nature* **400,** 360–363.

Lalley PM, Pilowsky PM, Forster H V. & Zuperku EJ (2014). CrossTalk opposing view: The pre-Bötzinger complex is not essential for respiratory depression following systemic administration of opioid analgesics. *J Physiol* **592,** 1163–1166.

Levitt ES, Abdala AP, Paton JF, Bissonnette JM & Williams JT (2015). Mu opioid receptor activation hyperpolarizes respiratory-controlling Kölliker-Fuse neurons and suppresses post-inspiratory drive. *J Physiol* **19,** 4453–4469.

Lieske SP, Thoby-Brisson M, Telgkamp P & Ramirez JM (2000). Reconfiguration of the neural network controlling multiple breathing patterns: eupnea, sighs and gasps. *Nat Neurosci* **3,** 600–607.

Liu Y, Duan Y, He Y, Wang J, Xia M, Yu C, Dong H, Ye J, Butzkueven H, Li K & Shu N (2012). Altered Topological Organization of White Matter Structural Networks in Patients with Neuromyelitis Optica. *PLoS One*; DOI: 10.1371/journal.pone.0048846.

Lowe JD, Kelly E & Henderson G (2013). Desensitization of Mu opioid receptors in the preBötzinger complex. *Proc Br Pharmacol Soc*; DOI: 10.1111/j.1476-5381.1981.tb10708.x.

Ma W & Quirion R (2008). Does COX2-dependent PGE2 play a role in neuropathic pain? *Neurosci Lett* **437,** 165–169.

Malmersjo S, Rebellato P, Smedler E, Planert H, Kanatani S, Liste I, Nanou E, Sunner H, Abdelhady S, Zhang S, Andang M, El Manira A, Silberberg G, Arenas E & Uhlen P (2013). Neural progenitors organize in small-world networks to promote cell proliferation. *Proc Natl Acad Sci* **110,** E1524–E1532.

Mellen NM, Janczewski WA, Bocchiaro CM & Feld JL (2003). Opioid-induced quantal slowing reveals dual networks for respiratory rhythm generation. *Neuron* **37,** 821–826.

Mitchell MD, Brunt J, Bibby J, Flint APF, Anderson ABM & Turnbull AC (1978). Prostaglandins in the Human Umbilical Circulation At Birth. *BJOG An Int J Obstet Gynaecol* **85,** 114–118.

Montandon G & Horner R (2014). CrossTalk proposal: The preBotzinger complex is essential for the respiratory depression following systemic administration of opioid analgesics. *J Physiol* **592,** 1159–1162.

Montandon G, Liu H & Horner RL (2016*a*). Contribution of the respiratory network to rhythm and motor output revealed by modulation of GIRK channels, somatostatin and neurokinin-1 receptors. *Sci Rep* **6,** 32707.

Montandon G, Qin W, Liu H, Ren J, Greer JJ & Horner RL (2011). PreBotzinger Complex Neurokinin-1 Receptor-Expressing Neurons Mediate Opioid-Induced Respiratory Depression. *J Neurosci* **31,** 1292–1301.

Montandon G, Ren J, Victoria NC, Liu H, Wickman K, Greer JJ & Horner RL (2016*b*). G-protein-gated Inwardly Rectifying Potassium Channels Modulate Respiratory Depression by Opioids. *Anesthesiology* **124,** 641–650.

Niesters M, Overdyk F, Smith T, Aarts L & Dahan A (2013). Opioid-induced respiratory depression in paediatrics: A review of case reports. *Br J Anaesth* **110,** 175–182.

Phillips WS, Herly M, Del Negro CA & Rekling JC (2016). Organotypic slice cultures containing the preBötzinger complex generate respiratory-like rhythms. *J Neurophysiol* **115,** 1063–1070.

Qi J, Li H, Zhao TB, Lu YC, Zhang T, Li JL, Dong YL & Li YQ (2017). Inhibitory Effect of Endomorphin-2 Binding to the μ-Opioid Receptor in the Rat Pre-Bötzinger Complex on the Breathing Activity. *Mol Neurobiol* **54,** 461–469.

Raynor K, Kong H, Chen Y, Yasuda K, Yu L, Bell G & Reisine T (1993). Pharmacological Characterization of the Cloned kappa-, delta-, and mu-Opioid Receptors. *Mol Pharmacol* **45,** 330–334.

Rekling JC, Shao XM & Feldman JL (2000). Electrical Coupling and Excitatory Synaptic Transmission between Rhythmogenic Respiratory Neurons in the PreBötzinger Complex. *J Neurosci* **20,** RC113.

Ruangkittisakul A & Ballanyi K (2010). Methylxanthine reversal of opioid-evoked inspiratory depression via phosphodiesterase-4 blockade. *Respir Physiol Neurobiol* **172,** 94–105.

Ruangkittisakul A, Kottick A, Picardo MCD, Ballanyi K & Del Negro CA (2014). Identification of the pre-Bötzinger complex inspiratory center in calibrated "sandwich" slices from newborn mice with fluorescent Dbx1 interneurons. *Physiol Rep* **2,** 1–16.

Ruangkittisakul A, Panaitescu B & Ballanyi K (2011). K+ and Ca2+ dependence of inspiratory-related rhythm in novel " calibrated" mouse brainstem slices. *Respir Physiol Neurobiol* **175,** 37–48.

Ruangkittisakul A, Schwarzacher SW, Secchia L, Poon BY, Ma Y, Funk GD & Ballanyi K (2006). High Sensitivity to Neuromodulator-Activated Signaling Pathways at Physiological [K+] of Confocally Imaged Respiratory Center Neurons in On-Line-Calibrated Newborn Rat Brainstem Slices. *J Neurosci* **26,** 11870–11880.

Siljehav V, Hofstetter AM, Leifsdottir K & Herlenius E (2015). Prostaglandin E2 Mediates Cardiorespiratory Disturbances during Infection in Neonates. *J Pediatr* **167,** 1207–1213.

Siljehav V, Olsson Hofstetter A, Jakobsson P-J & Herlenius E (2012). mPGES-1 and

prostaglandin E2: vital role in inflammation, hypoxic response, and survival. *Pediatr Res* **72,** 460–467.

Siljehav V, Shvarev Y & Herlenius E (2014). Il-1β and prostaglandin E2 attenuate the hypercapnic as well as the hypoxic respiratory response via prostaglandin E receptor type 3 in neonatal mice. *J Appl Physiol* **117,** 1027–1036.

Smedler E, Malmersjö S & Uhlén P (2014). Network analysis of time-lapse microscopy recordings. *Front Neural Circuits* **8,** 1–10.

Uhlén P (2004). Spectral Analysis of Calcium Oscillations. *Sci STKE* **258,** 1–13.

Wang X, Hayes JA, Revill AL, Song H, Kottick A, Vann NC, LaMar MD, Picardo MC ristina D, Akins VT, Funk GD & Del Negro CA (2014). Laser ablation of Dbx1 neurons in the pre-Bötzinger complex stops inspiratory rhythm and impairs output in neonatal mice. *Elife* **3,** e03427.

Watts DJ & Strogatz SH (1998). Collective dynamics of "small-world" networks. *Nature* **393,** 440–442.

Yasojima K, Schwab C, McGeer EG & McGeer PL (1999). Distribution of cyclooxygenase-1 and cyclooxygenase-2 mRNAs and proteins in human brain and peripheral organs. *Brain Res* **830,** 226–236.

Zamalloa T, Bailey CP & Pineda J (2009). Glutamate-induced post-activation inhibition of locus coeruleus neurons is mediated by AMPA/kainate receptors and sodium-dependent potassium currents. *Br J Pharmacol* **156,** 649–661.

Zavala-Tecuapetla C, Tapia D, Rivera-Angulo AJ, Galarraga E & Peña-Ortega F (2014). Morphological characterization of respiratory neurons in the pre-bötzinger complex. *Prog Brain Res* **209,** 39–56.

Tables

Table 1. Inhibitory effect of DAMGO (5 μM) within 5 min on the Ca^{2+} transient frequency and amplitude of preBötC cells (network) and respiratory neurons ($NK1R^+$) *in vitro* in the absence and presence of naloxone (5 μM). N: number of slices, n: number of cells. Data are presented as mean ± SD. **P* < 0.05 when compared to their respective baseline values. Note that the effect on the respiratory networks resembled the effect of the whole network.

			Relative amplitude ($\Delta F/F_0$)		**Mean frequency (mHz)**	
	Cells	Sample size	Baseline	+DAMGO (5 μM)	Baseline	+DAMGO (5 μM)
Control	network	N=7, n=977	31.1 ± 3.0	25.6 ± 1.2*	55.6 ± 3.6	43.3 ± 2.9*
	$NK1R^+$	N=7, n= 110	32.6 ± 6.4	25.4 ± 1.9*	54.8 ± 3.9	43.1 ± 2.5*
Naloxone (5 μM)	network	N=8, n=1300	31.1 ± 3.9	30.7 ± 5.2	56.0 ± 7.3	54.7 ± 5.9
	$NK1R^+$	N=6, n=95	30.3 ± 4.4	29.3 ± 6.8	55.4 ± 7.5	50.3 ± 9.3

Table 2. Inhibitory effect of PGE_2 (100 nM) within 5 min on the Ca^{2+} transient frequency of preBötC cells (network) and respiratory neurons ($NK1R^+$) *in vitro* and effect of subsequent DAMGO (5 μM) administration in the presence of PGE_2 (100 nM). N: number of slices, n: number of cells. Data are presented as mean ± SD. * *P* < 0.05 when compared to their respective baseline values. Note that the effect on the respiratory networks resembled the effect of the whole network and that the inhibitory effect of PGE_2 was absent in slices from $Ptger3^{-/-}$ mice.

			Mean frequency (mHz)		
	Cells	Sample size	Baseline	+ PGE_2 (100 nM)	+ DAMGO (5 μM)
WT	network	N=10, n=1460	59.9 ± 5.2	48.2 ± 6.1*	50.9 ± 7.4*
	$NK1R^+$	N=8, n= 43	59.2 ± 7.4	51.6 ± 8.6*	52.6 ± 5.7
$Ptger3^{-/-}$	network	N=10, n=1938	55.1 ± 5.3	50.9 ± 9.5	47.8 ± 5.1*
	$NK1R^+$	N=9, n=288	53.8 ± 6.8	53.5 ± 15.1	46.6 ± 5.6*

Table 3. Inhibitory effect of rolipram (5 µM) within 10 min on the Ca^{2+} transient frequency of preBötC cells (network) and respiratory neurons ($NK1R^+$) *in vitro* and effect of subsequent DAMGO (5 µM) or PGE_2 (100 nM) administration in the presence of rolipram (5 µM). N: number of slices, n: number of cells. Data are presented as mean ± SD. * $P < 0.05$ when compared to their respective baseline values. N.S.: not significant when the group of DAMGO or PGE_2 was compared to the previous 5 min period in the presence of rolipram. Note that once rolipram had decreased the Ca^{2+} transient frequency, neither DAMGO nor PGE_2 induced any further modification.

			Mean frequency (mHz)			
	Cells	Sample size	Baseline	+ rolipram (5 µM)	+ DAMGO or PGE_2	
DAMGO	network	N=8, n=1943	57.3 ± 4.6	52.8 ± 3.1*	50.9 ± 2.7*	N.S.
(5 µM)	$NK1R^+$	N=5, n= 78	52.2 ± 3.7	46.3 ± 4.6	49.2 ± 5.4	N.S.
PGE_2	network	N=8, n=1796	57.3 ± 3.1	53.3 ± 3.4*	52.0 ± 5.2*	N.S.
(100 nM)	$NK1R^+$	N=7, n=98	61.6 ± 3.6	53.7 ± 6.8*	50.0 ± 7.0*	N.S.

Table 4. Effect of SCH-23390 (15 µM) incubation on the Ca^{2+} transient frequency of preBötC cells (network) and respiratory neurons ($NK1R^+$) *in vitro* and effect of subsequent DAMGO (5 µM) or PGE_2 (100 nM) administration in the presence of SCH-23390 (15 µM). N: number of slices, n: number of cells. Data are presented as mean ± SD. N.S.: not significant when the group of DAMGO or PGE_2 was compared to their respective baseline.

			Mean frequency (mHz)		
	Cells	Sample size	Baseline	+ DAMGO or PGE_2	
DAMGO	network	N=8, n=755	57.3 ± 5.5	55.2 ± 7.6	N.S.
(5 µM)	$NK1R^+$	N=5, n=72	54.6 ± 7.4	55.9 ± 4.6	N.S.
PGE_2	network	N=9, n=1000	59.0 ± 6.8	53.8 ± 5.2	N.S.
(100 nM)	$NK1R^+$	N=4, n=83	59.0 ± 6.2	60.1 ± 5.6	N.S.

Figure legends

Figure 1. DAMGO modulates preBötC network activity and connectivity. **(A)** Localization of the preBötC in a sagittal drawing of the brainstem and in the coronal slice, which also contains the nucleus ambiguus (NA), the nucleus tractus solitarius (NTS), and the nucleus hypoglossus (XII) (Adapted from Forsberg et al., 2016). Effect of DAMGO (5 μM) administration on representative Ca^{2+} traces as $\Delta F/F_0$ from regular cells (black; #1 and 2) and $NK1R^+$ cells (respiratory neurons; #3 and 4 in blue) and their localization in a single frame of the Ca^{2+} signaling recording from a WT mouse (top right). **(B)** Inhibitory effect of DAMGO (0.5 – 5 μM) on Ca^{2+} transient relative amplitude and frequency **(C)** as a percentage of the baseline value in WT (circles) and $Ptger3^{-/-}$ (diamonds). **(D)** Cells that showed a decrease in Ca^{2+} transient frequency within 5 min of DAMGO (5 μM) administration as a percentage (gray filled circles) and their subsequent behavior over time, in comparison with the non-sensitive cells. Note that sensitive cells displayed a higher baseline frequency. **(E)** Graphical depiction of the network structure on top of NK1R-labelled cells. Each line represents the correlation coefficient above the set cut-off for the cell pairs, and warmer colors are a stronger correlation between the cells connected by the line. Administration of DAMGO (5 μM) decreased the number of correlated cells and the correlation coefficient. **(F)** Network parameter values revealing a small-world topology during baseline and upon DAMGO (0.5 – 5 μM) administration in WT and $Ptger3^{-/-}$ mice. Note that the highest concentration of DAMGO caused more effect than the lowest. Data are presented as means ± SD. * $P < 0.05$ compared to baseline (paired Student's t-test) and # $P < 0.05$ when compared among groups (paired Student's t-test in D and ANOVA followed by a Dunnett's *post hoc* test in the rest). A.U.: arbitrary units. Scale bars: 100 μm.

Figure 2. PGE_2 (10 – 100 nM) reduces preBötC network activity and connectivity in WT but not in $Ptger3^{-/-}$ mice and occludes the subsequent inhibitory effect induced by DAMGO (0.5 – 5 μM). **(A)** Representative Ca^{2+} traces as $\Delta F/F_0$ from regular cells (top black) and $NK1R^+$ cells (respiratory neurons, bottom blue) in WT (left) and $Ptger3^{-/-}$ mice (right). **(B)** Effect of PGE_2 (10 and 100 nM) and DAMGO (0.5 and 5 μM) administration on Ca^{2+} transient amplitude (left) and frequency (center) as a percentage of the baseline value in WT. Note that DAMGO in the presence of PGE_2 did not produce a further inhibitory effect on the Ca^{2+} transient frequency. At the right: cells that showed a decrease in Ca^{2+} transient frequency within 5 min of PGE_2 (100 nM) administration as a percentage (gray filled circles) and their subsequent behavior over

time, in comparison with the non-sensitive cells. Note that PGE_2-sensitive cells displayed a higher baseline frequency and that DAMGO administration did not change the Ca^{2+} transient frequency in those cells, but decreased that of the PGE_2 non-sensitive cells. **(C)** Graphical depiction of the network structure on top of NK1R-labelled cells. Each line represents the correlation coefficient above the set cut-off for the cell pairs, and warmer colors are a stronger correlation between the cells connected by the line. Administration of PGE_2 (100 nM) decreased the number of correlated cells and the correlation coefficient in WT mice, and this effect was reversed by DAMGO (5 μM). **(F)** Network parameter values revealing a small-world topology during baseline and upon PGE_2 (10 – 100 M) administration in WT. Note that the highest concentration of PGE_2 produced a greater effect. Subsequent administration of DAMGO (5 μM) in the presence of PGE_2 (100 nM) did not change the network parameters any further. Data are presented as means ± SD. * $P < 0.05$ compared to baseline (paired Student's t-test) and # $P < 0.05$ when compared among groups (paired Student's t-test in A and unpaired in D). A.U.: arbitrary units. Scale bars: 100 μm.

Figure 3. Administration of rolipram (5 μM) prevented both DAMGO (5 μM)- and PGE_2 (100 nM)-induced reduction in preBötC network activity and connectivity. **(A)** Effect of rolipram (5 μM) and subsequent administration of DAMGO (5 μM) or PGE_2 (100 nM) on Ca^{2+} transient relative amplitude (top) and frequency (bottom). Note that neither DAMGO nor PGE_2 modified the Ca^{2+} transient relative amplitude or frequency after administration of rolipram. **(B)** Representative Ca^{2+} traces showing the effect of rolipram and subsequent DAMGO or PGE_2 administration as $\Delta F/F_0$ from regular cells (top black) and $NK1R^+$ cells (respiratory neurons, bottom blue). **(C)** Effect of DAMGO (5 μM) or PGE_2 (100 nM) in the presence of rolipram (5 μM) on Ca^{2+} transient frequency compared to their respective control in the absence of rolipram. The effects were normalized to their baseline in control or baseline in the presence of rolipram). **(D)** Graphical depiction of the network structure. Each line represents the correlation coefficient above the set cut-off for the cell pairs, and warmer colors are a stronger correlation between the cells connected by the line. Administration of rolipram (5 μM) decreased the correlation coefficient in WT mice and subsequent application of DAMGO (5 μM) (top) or PGE_2 (100 nM) (bottom) did not decrease the mean correlation any further. **(E)** Rolipram (5 μM) prevented the increase in network parameter values induced by DAMGO (5 μM), but not that of PGE_2 (100 nM). The experimental values were normalized to their

respective baseline. Data are presented as means ± SD. * $P < 0.05$ compared to baseline (paired Student's t-test) and # $P < 0.05$ when compared among groups (unpaired Student's t-test).

Figure 4. Administration of SCH-23390 (15 μM) prevented both DAMGO (5 μM)- and PGE_2 (100 nM)-induced reduction in preBötC network activity. **(A)** Representative Ca^{2+} traces showing the effect of SCH-23390 and subsequent DAMGO or PGE_2 administration as $\Delta F/F_0$ from regular cells (top black) and $NK1R^+$ cells (respiratory neurons, bottom blue). Note that neither DAMGO nor PGE_2 modified the Ca^{2+} transient relative amplitude or frequency after administration of rolipram. **(B)** Effect of DAMGO (5 μM) or PGE_2 (100 nM) after incubation SCH-23390 (15 μM) on Ca^{2+} transient frequency compared to their respective control in the absence of SCH-23390. The effects were normalized to their respective baseline. **(C)** Graphical depiction of the network structure. Each line represents the correlation coefficient above the set cut-off for the cell pairs, and warmer colors are a stronger correlation between the cells connected by the line. Incubation with SCH-23390 (15 μM) prevented the decrease in the number of correlated cells and the correlation coefficient induced by DAMGO (5 μM), but not that induced by PGE_2 (100 nM). **(D)** SCH-23390 (15 μM) prevented the increase in network parameter values induced by DAMGO (5 μM), but not that of PGE_2 (100 nM). The experimental values were normalized to their respective baseline. Data are presented as means ± SD. * $P < 0.05$ compared to baseline (paired Student's t-test) and # $P < 0.05$ when compared among groups (unpaired Student's t-test).

Figure 1

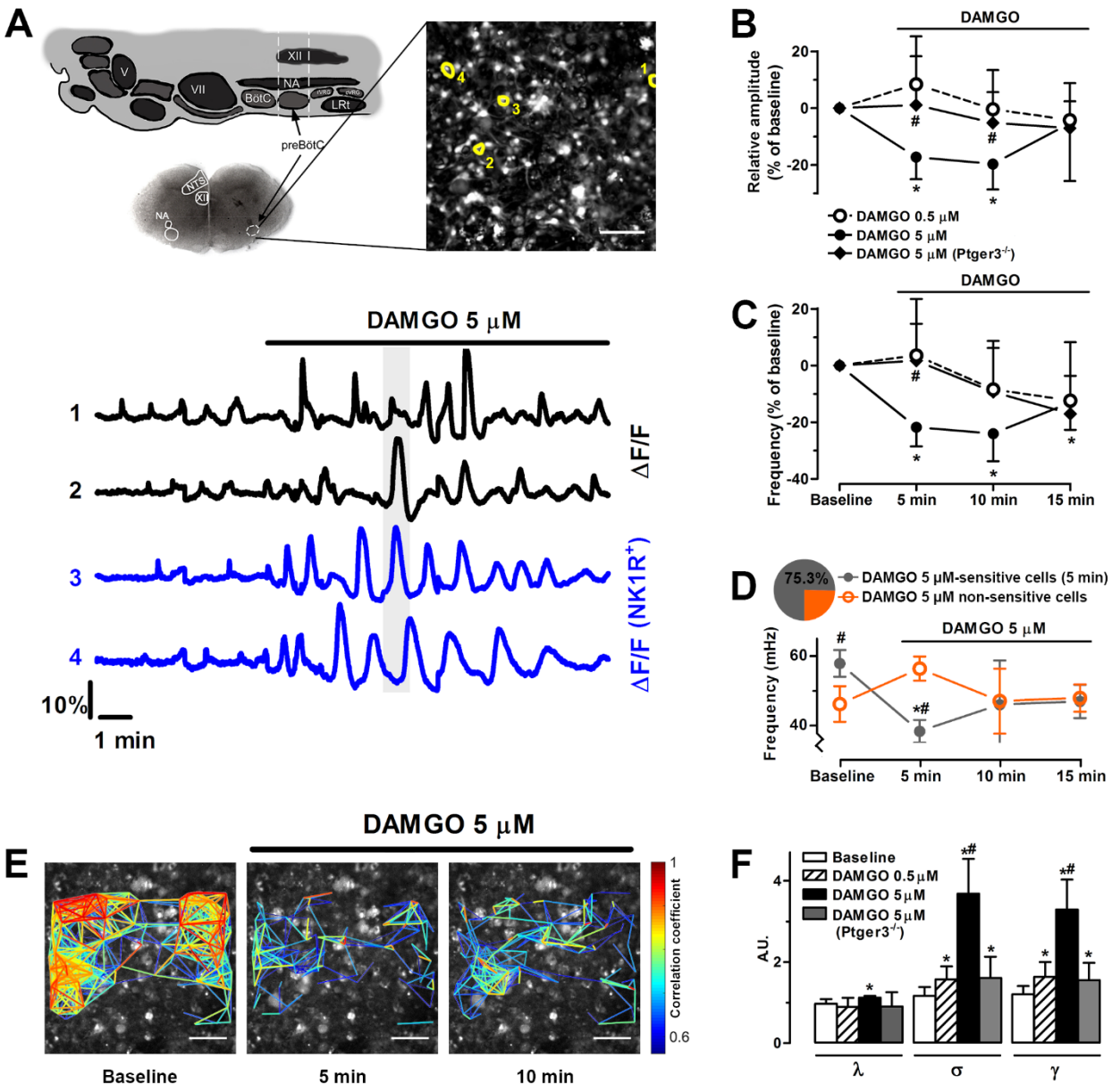
A
V
VII
XII
NA
BötC
LRt
preBötC
NA
XII
1
2
3
4
DAMGO 5 μM
ΔF/F
ΔF/F (NK1R+)
10%
1 min
B
DAMGO
Relative amplitude (% of baseline)
DAMGO 0.5 μM
DAMGO 5 μM
DAMGO 5 μM (Ptger3-/-)
C
DAMGO
Frequency (% of baseline)
Baseline
5 min
10 min
15 min
D
75.3%
DAMGO 5 μM-sensitive cells (5 min)
DAMGO 5 μM non-sensitive cells
DAMGO 5 μM
Frequency (mHz)
Baseline
5 min
10 min
15 min
E
DAMGO 5 μM
Correlation coefficient
Baseline
5 min
10 min
F
Baseline
DAMGO 0.5 μM
DAMGO 5 μM
DAMGO 5 μM (Ptger3-/-)
A.U.
λ
σ
γ

Figure 2

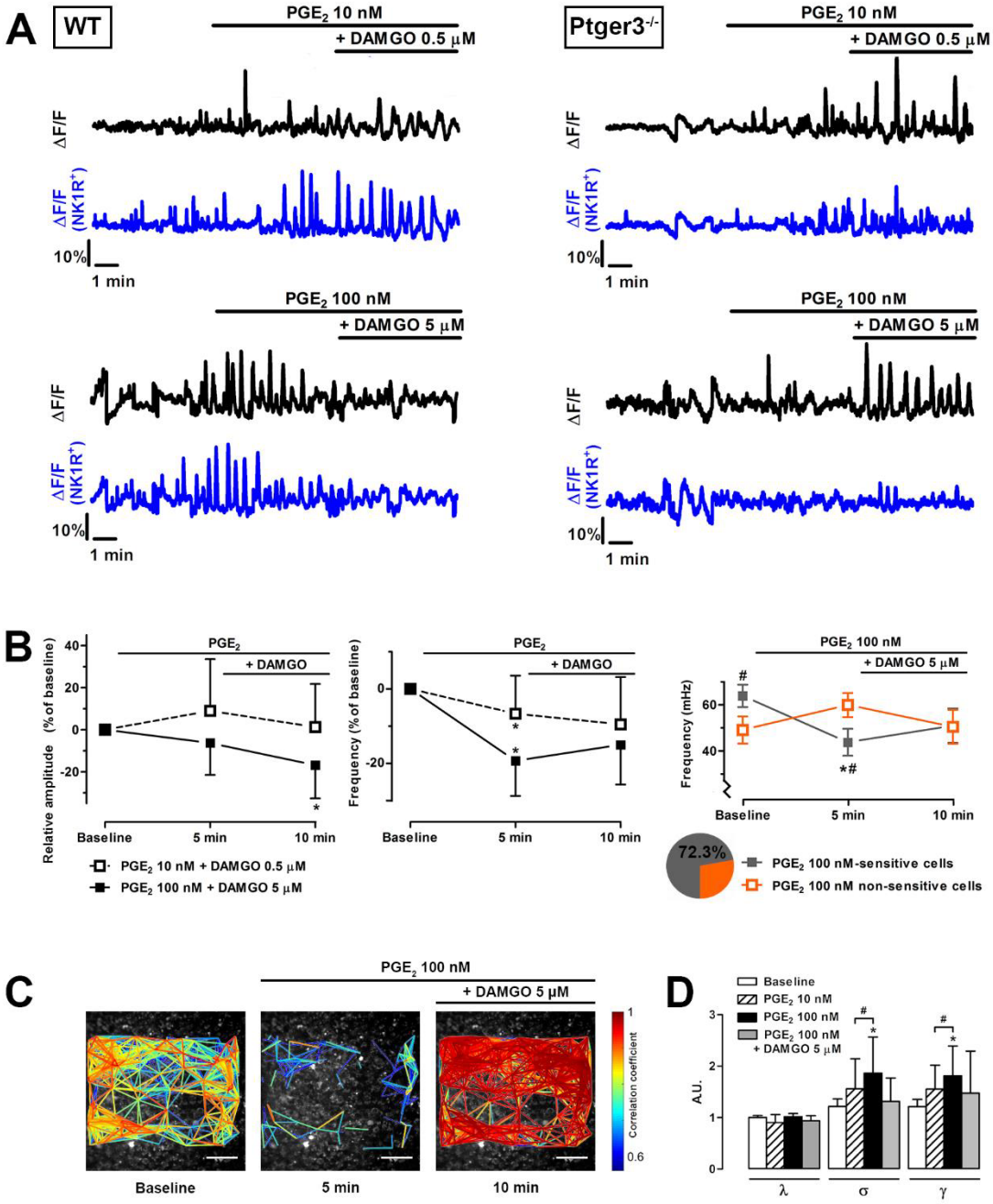
A
WT
PGE2 10 nM
+ DAMGO 0.5 μM
ΔF/F
ΔF/F (NK1R+)
10%
1 min
PGE2 100 nM
+ DAMGO 5 μM
Ptger3-/-
B
PGE2
+ DAMGO
Relative amplitude (% of baseline)
Frequency (% of baseline)
Baseline
5 min
10 min
PGE2 10 nM + DAMGO 0.5 μM
PGE2 100 nM + DAMGO 5 μM
PGE2 100 nM + DAMGO 5 μM
Frequency (mHz)
72.3%
PGE2 100 nM-sensitive cells
PGE2 100 nM non-sensitive cells
C
PGE2 100 nM
+ DAMGO 5 μM
Correlation coefficient
1
0.6
Baseline
5 min
10 min
D
Baseline
PGE2 10 nM
PGE2 100 nM
PGE2 100 nM + DAMGO 5 μM
A.U.
λ
σ
γ

Figure 3

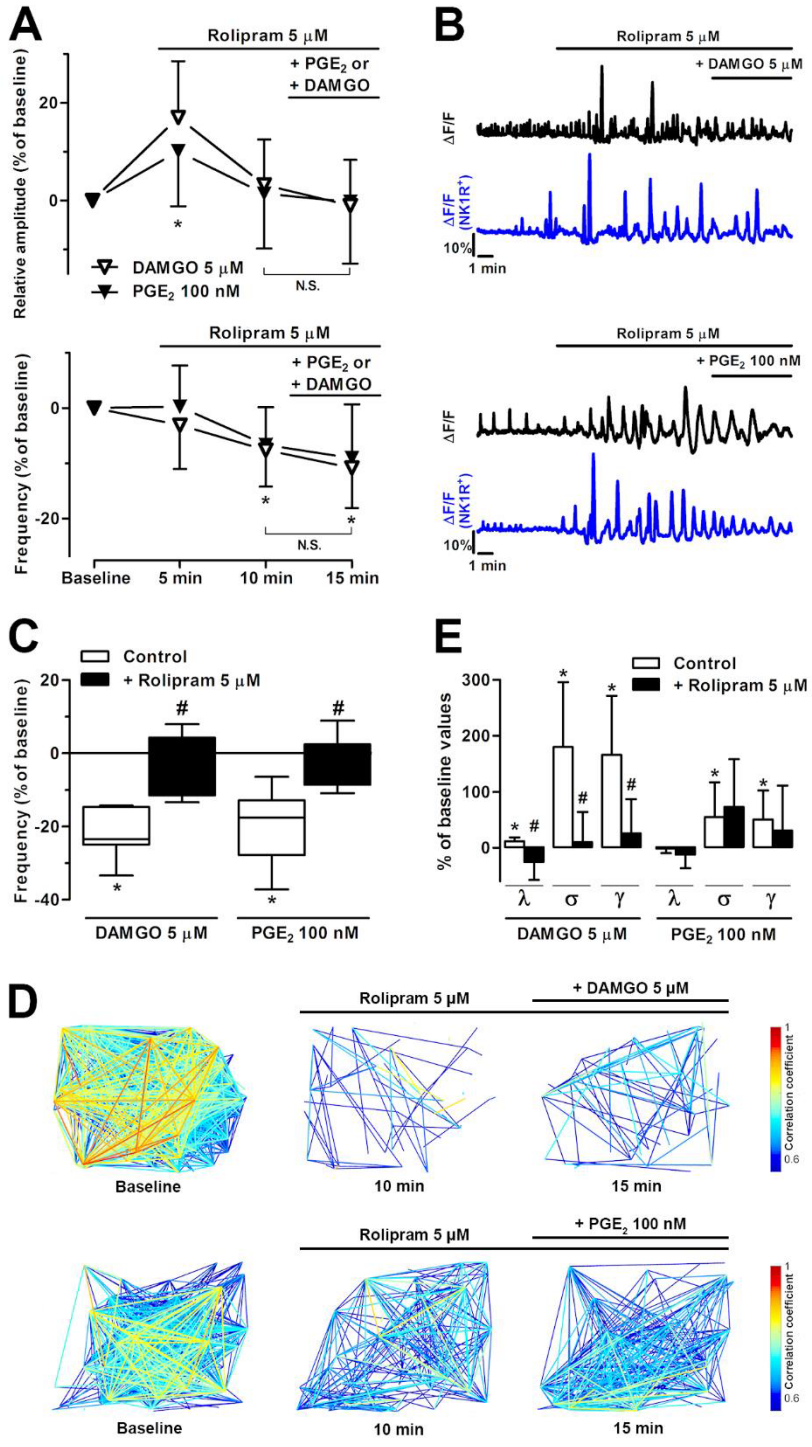
A
Rolipram 5 μM
+ PGE2 or
+ DAMGO
Relative amplitude (% of baseline)
20
0
*
DAMGO 5 μM
PGE2 100 nM
N.S.
Rolipram 5 μM
+ PGE2 or
+ DAMGO
Frequency (% of baseline)
0
-20
*
*
N.S.
Baseline
5 min
10 min
15 min
B
Rolipram 5 μM
+ DAMGO 5 μM
ΔF/F
ΔF/F (NK1R+)
10%
1 min
Rolipram 5 μM
+ PGE2 100 nM
ΔF/F
ΔF/F (NK1R+)
10%
1 min
C
Control
+ Rolipram 5 μM
Frequency (% of baseline)
20
0
-20
-40
#
#
*
*
DAMGO 5 μM
PGE2 100 nM
E
Control
+ Rolipram 5 μM
% of baseline values
300
200
100
0
*
#
*
#
*
#
*
*
*
λ
σ
γ
λ
σ
γ
DAMGO 5 μM
PGE2 100 nM
D
Rolipram 5 μM
+ DAMGO 5 μM
Baseline
10 min
15 min
Correlation coefficient
1
0.6
Rolipram 5 μM
+ PGE2 100 nM
Baseline
10 min
15 min
Correlation coefficient
1
0.6

Figure 4

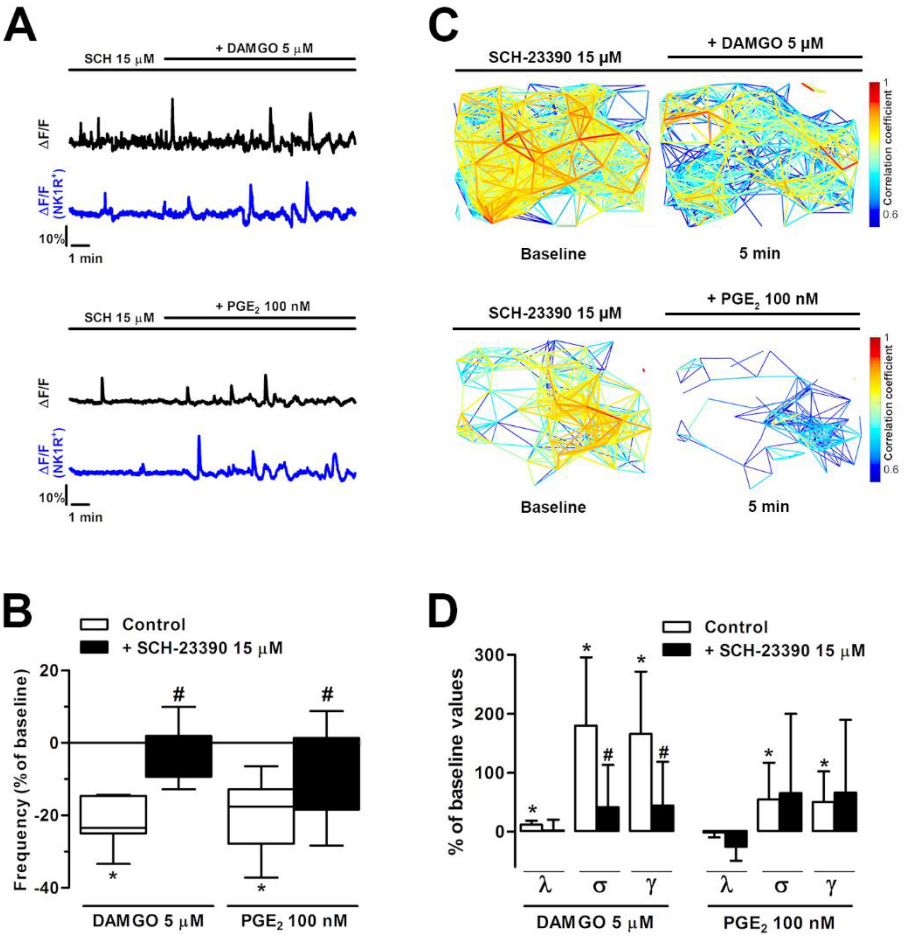
A
SCH 15 μM
+ DAMGO 5 μM
ΔF/F
ΔF/F (NK1R+)
10%
1 min
SCH 15 μM
+ PGE2 100 nM
ΔF/F
ΔF/F (NK1R+)
10%
1 min
C
SCH-23390 15 μM
+ DAMGO 5 μM
Correlation coefficient
1
0.6
Baseline
5 min
SCH-23390 15 μM
+ PGE2 100 nM
Correlation coefficient
1
0.6
Baseline
5 min
B
Control
+ SCH-23390 15 μM
Frequency (% of baseline)
20
0
-20
-40
DAMGO 5 μM
PGE2 100 nM
D
Control
+ SCH-23390 15 μM
% of baseline values
300
200
100
0
λ
σ
γ
λ
σ
γ
DAMGO 5 μM
PGE2 100 nM